



Programme, annonces et livre des résumés

Avec le soutien de



Préambule

Didier Lasseux, Président du FIC, France Interpore Chapter

Les Journées d'Etude des Milieux Poreux (JEMP) sont, depuis maintenant 30 ans, un moment phare de rassemblement bisannuel de la communauté travaillant sur les milieux poreux en France dans l'environnement académique, avec une très large ouverture sur le monde industriel concerné. Ces journées offrent une occasion privilégiée pour des échanges riches sur les derniers travaux de recherche conduits dans cette thématique. Depuis 2014, les JEMP sont placées sous l'égide du France InterPore Chapter (FIC), antenne française de la société savante InterPore, société internationale co-fondée avec la participation de membres de la communauté française. Dans ce contexte, les JEMP constituent une excellente plateforme pour promouvoir l'activité de la communauté française dans le domaine à l'international.

Le FIC souhaite remercier et féliciter chaleureusement l'IFPEN qui accueille cette 16ème édition des journées, et tout particulièrement les organisateurs ainsi que toute l'équipe rassemblée autour de cet évènement pour en faire un réel succès. Nous sommes particulièrement reconnaissants envers les sociétés TOTALENERGIES (Sponsoring Or) SERLABO Technologies, TESCAN (sponsoring argent), le CEA et STORENGY (sponsoring bronze), qui, par leur soutien financier, ont significativement contribué à la réussite de ce colloque. Le FIC remercie également vivement tous les participants pour leur contribution et leur présence à ces journées. En souhaitant de nombreux échanges, cordiaux et enrichissants, à toutes et tous. Belles JEMP 2023 !

Mme Olga Vizika-Kavvadias, Directrice scientifique IFPEN

La tenue des JEMP sur notre site de Rueil est un formidable sujet de satisfaction pour notre organisme de recherche et d'innovation, membre et partenaire de longue date d'Interpore. Tout d'abord, c'est un honneur d'avoir été retenu pour accueillir cette édition anniversaire des 30 ans des JEMP. Ensuite c'est pour nous l'occasion de marquer notre attachement à cette communauté des milieux poreux et d'entretenir notre lien avec elle. Enfin, c'est l'opportunité de partager nos nouveaux enjeux et actions de recherche, les problématiques scientifiques qui en découlent tout comme les visées applicatives multiples qui motivent tous nos travaux dans ce domaine.

L'étude des milieux poreux, naturels comme artificiels, est une composante historique de notre maison, qui a marqué des décennies de recherche dans le contexte de l'O&G, et qui aujourd'hui conserve toute sa pertinence pour préparer les innovations de demain au service de la transition énergétique et écologique. Qu'il s'agisse des problématiques des énergies décarbonées, du stockage d'énergie électrochimique, de la gestion de la ressource en eau ou de la préservation des milieux naturels, les nouvelles problématiques sur lesquelles IFPEN travaille depuis maintenant des années ont toujours à voir avec les milieux poreux. Leur caractérisation, leur simulation numérique, ou encore la compréhension des mécanismes physico-chimiques et la modélisation des écoulements de fluides en leur sein sont autant de sujets dans lesquels les besoins de recherche fondamentale n'ont pas faibli. Bien au contraire, et c'est pourquoi nous y maintenons et enrichissons des compétences multiples et des approches à fort caractère interdisciplinaire. Ainsi, plus de la moitié des compétences présentes à IFPEN sont impliquées dans des travaux de recherche en lien avec les milieux poreux. Sur ces sujets, nous nous appuyons sur les progrès les plus récents dans les méthodes et les outils (par exemple dans le numérique

et le digital) et c'est pour cela que nous souhaitons multiplier les échanges avec la communauté d'Interpore et partager le meilleur état des connaissances et des techniques.

C'est dans cet esprit que nous accueillons ces 16èmes journées du FIC et nous vous souhaitons qu'elles soient riches en échanges et fécondes en collaborations futures.

Comité local d'organisation

Pour cette édition qui coïncide avec les 30 ans des JEMP (encore jeunes mais atteignant leur pleine maturité !), nous sommes très honorés d'accueillir dans nos locaux de Rueil-Malmaison la communauté d'Interpore, si importante pour nous au regard de nos travaux de recherche et d'innovation dans de multiples domaines.

Un grand merci au FIC de nous avoir confié cette organisation, ainsi qu'à la Direction scientifique et à la Direction de la communication de IFPEN qui nous ont soutenu pour honorer cet engagement.

En trente ans, bien des choses se sont passées dans notre communauté et sont devenues possibles par rapport aux débuts des JEMP, sur le plan scientifique, citons

- la possibilité de « voir » l'espace des pores d'une roche naturelle
- la fabrication de micro-modèles de très fine résolution
- la meilleure accessibilité d'outils de caractérisation à l'échelle microscopique, comme la RMN ou le Synchrotron
- l'avènement de méthodes pour la simulation numérique (PNM, LBM, VoF parmi d'autres) permettant d'en saisir les conséquences macroscopiques

Enfin, l'essor d'une communauté « Milieu poreux », structurée et active à l'échelle nationale et internationale, propice à des échanges et des synergies fructueuses, n'est pas le moindre bénéfice de ces rencontres régulières, dynamiques et chaleureuses.

Votre présence en nombre à ces 16-èmes journées du JEMP en atteste pleinement.

Bon anniversaire aux JEMP, et nous vous souhaitons une excellente conférence !

Mardi 17 octobre - Matin

08h15 – 09h15 – Accueil

09h15 – 09h45 – Séance d'ouverture – *Amphi Dahlias*

09h45 -10h30 – Conférence plénière – *Amphi Dahlias*

Sophie Roman, Institut des Sciences de la Terre d'Orléans

[Microfluidics for geosciences to unravel reactive transport processes in porous media](#)

10h30 – 11h00 – Pause-café

11h00 – 12h15 – Sessions en parallèle

	<i>Amphi Dahlias</i>	<i>Amphi Séquoia</i>	<i>Amphi Hortensias</i>
Session	Modélisation numérique des écoulements en milieux poreux	Systèmes multiphases - multicomposants	Couplages mécaniques, chimiques et thermiques entre fluides et matrice dans les milieux poreux
11h00–11h25	Physics-informed neural networks for modelling groundwater flow in unconfined aquifers <i>Adhish Guli Virupaksha, ITES</i>	Non-Fickian dispersion in unsaturated porous media, influence of the Peclet number <i>Ollivier-Triquet, IFPEN</i>	Coupled numerical modeling of multiphase reactive transport and geomechanics <i>Anthony Michel, IFPEN</i>
11h25–11h50	Physics informed neural network for modelling flow in porous media: First order formulation <i>Marwan Fahs, ITES</i>	Imbibition dynamics including corner film flow in a spiral-grooved channel <i>Christian Kankolongo, I2M</i>	Meso-scale analysis of precipitation-induced damage in limestone using 4D X-ray tomographic imaging <i>Syrine Ben Elhadj Hamida, UPPA</i>
11h50–12h15	Weakly monotone finite volume scheme for parabolic and diffusion equations in strongly anisotropic porous media <i>Moha Aberrah, Moulay Ismail University</i>	Fragmentation and coalescence dynamics of non-wetting blobs during immiscible two-phase flows in porous media <i>Laurent Talon, FAST</i>	Carbon rich materials for solar evaporation: a critical perspective on performance measurement <i>Romain Fillet, Institut Jean Lamour</i>

12h15 – 14h00 – Déjeuner



Partenaire or



Partenaires argent



Partenaires bronze

Mardi 17 octobre – Après-midi

14h00 – 14h45 – Conférence plénière – *Amphi Dahlias* <https://jemp2023.sciencesconf.org/file/968074>

Adrian Bejan, Duke university, USA, Perfection is the Enemy of Evolution

14h45 – 15h30 – Pitch Poster : synthèse en 1 min

	Amphi Dahlias	Amphi Séquoia	Amphi Hortensias
Session	Modélisation numérique des écoulements en milieux poreux	Stockage du CO₂	Couplages mécaniques, chimiques et thermiques entre fluides et matrice dans les milieux poreux
15h30–15h55	Sensitivity analysis for rainfall-induced landslide models Rashad Abbasov, ITES	Capillary trapping mechanisms for CO₂ geological storage: experimental and computational microfluidic Nathan Bernard, ISTO	An efficient Crouzeix-Raviart Finite Element model for coupled hydro-mechanical processes in variably saturated porous media Lingai Guo
15h55–16h20	A finite element solver for modeling coupled heat transfers in architected porous media up to very high temperature Salih Ouchtout, IFPEN	Wettability alteration of microfluidic devices using plasma and its influence on trapping mechanisms in geological reservoirs Viktor Gredičak, ISTO	Application of the volume averaging method to the problem of a moving granular porous medium driven by a multi-phase flow Rémi Clavier, CEA
16h20–16h45	Numerical study and inverse analysis of a non destructive measurement method for oxygen diffusivity in partially carbonated concrete Oujidane Qacami, Lafarge	Microwave Treatment of Shales for Carbon Capture and Enhanced Oil Recovery Anuka Agnes, University of Nottingham	Thermal performance assessment in a porous media for a vented enclosure with hot obstacle Raoudha Chaabane, Monastir University

16h45 –17h15 – Pause-café

	Amphi Dahlias	Amphi Séquoia	Amphi Hortensias
Session	Comportement des fluides complexes en milieux poreux	Systèmes multiphases - multicomposants	Stockage d'énergie électrochimique
17h15–17h40	Swelling and maturity effects on adsorption in organic source rocks' organic matter by molecular simulations Amael Obliger, ISM	Surfactant-enhanced remediation of LNAPL contaminated porous medium Diana Kerimbekova, Université de Lorraine	Geometric optimization of a Lithium-ion battery model Richard Joly, TotalEnergies OneTech,
17h40–18h05	Droplets flow in a micromodel porous network Elliot Speirs, IFPEN	Averaged model for mass and momentum transport in porous media with evolving heterogeneities Morgan Chabanon, LEMMC	Two-phase Flow Through the PTL of PEM Water Electrolyzer: MRI Experiments and Numerical Modeling Using Phase-Field Theory Bilal Amoury, EMTA
18h05–18h30	Bubble nucleation in liquids confined in nanopores Joel Puibasset, ICMN	Model of water drop infiltration in amphiphilic porous media Florian Cajot, EMMAH	Unlocking Insights in Battery Research with Digital Twin-driven Data Augmentation Sonia Ait Hamouda, LFC



Partenaire or



Partenaires argent



storengy

Partenaires bronze

Mercredi 18 octobre - Matin

09h00 - 9h45 – Conférence plénière– *Amphi Dahlias*
Philippe Coussot, Laboratoire Navier
[Features of transports in nano-porous media - Contribution of NMR and MRI](#)

	Amphi Dahlias	Amphi Séquoia	Amphi Hortensias
Session	Comportement des fluides complexes en milieux poreux	Caractérisation, imagerie, génération numérique de milieux poreux	A la mémoire de M. Panfilov
9h50–10h15	Pore-scale modeling of pore-clogging by aggregation of particles Laurez Maya Fogouang, ISTO	Analysis of evaporation in a hydrophobic micro-model Nour Sghaier, LESTE-ENIM	Numerical simulation of reactive single phase multicomponent flows in porous media: a sequential coupling between DuMuX and PHREEQC Sara Tabriznejadas, UPPA
10h15–10h40	Clogging of a 2D-porous medium: effects of main operating parameters on particle deposition and permeability reduction under geothermal conditions Anne-Sophie Esneu, IFPEN	Dispersion, stretching and direct visualization in 3D porous media Mathieu Souzy, Université de Rennes	An efficient deterministic forward modelling tool for the simulation of water flow and electrical current in fractured porous media Behshad Koohbor, GeoResources

10h40 – 11h10 – Pause-café

	Amphi Dahlias	Amphi Séquoia	Amphi Hortensias
Session	Comportement des fluides complexes en milieux poreux	Mécanique des milieux poreux : déformation, rupture, endommagement	A la mémoire de M. Panfilov
11h10–11h35	Viscoelastic flow in porous media -- a web of sticky strands Yohan Davit, IMFT	Transmissivité d'une fracture et perméabilité d'un milieu poreux en régime glissant Tony Zaouter, ISEC	Macroscopic dynamic capillary pressure for two-phase flow in porous media Didier Lasseux, Université de Bordeaux
11h35–12h00	Characterization of the first normal stress difference in diluted polymer solutions by tracking particle migration in a microfluidic channel Antoine Naillon, Univ. Grenoble	Induced seismicity due to fluid injection in geological reservoirs: influence of pumping strategies Bérénice Vallier, ITES	Computing the diphasic effective properties on nanoporous clayrock using Direct Numerical Simulation Anne-Julie Tinet, Université de Lorraine
12h00–12h25	Active Viscous Fingering Harold Auradou, FAST	Geothermal induced seismicity: Understanding the 2019 earthquake crises of Strasbourg Arezou Dodangeh, ITES	Large scale numerical simulation of flow in fractured porous media Michel Kern, INRIA

12h25 – 14h00 – Déjeuner



Partenaire or



Partenaires argent



Partenaires bronze

Mercredi 18 octobre – Après-midi

14h00 – 14h45 – Conférence plénière – *Amphi Dahlias*

Linda Luquot, Géosciences Montpellier

[Experimental study on karst formation: role of flow, chemical stress and rock heterogeneities](#)

14h45 – 16h30 – Assemblée générale du FIC, Anniversaire des 30 ans – **Didier Lasseux, président** – *Amphi Dahlias*

16h30 – 17h30 – **Posters avec pause-café** – *Hall Dahlias*

	Amphi Dahlias	Amphi Séquoia	Amphi Hortensias
Session	Modélisation numérique des écoulements en milieux poreux	Stockage du CO2	Structures poreuses réactives
17h30–17h55	Analysis of carbon brush seals with long bristles <i>Ala Souissi, Institut Pprime</i>	CO₂ Hydrate Kinetics for CO₂ Storage in Depleted Gas Reservoirs through Microfluidic Experiments <i>Peyman Dehghani, IFPEN</i>	Reactive transport modelling in porous fractured media: contribution to the understanding of weathering processes <i>Fabrice Golfier, GeoResources</i>
17h55–18h20	Inertial flow in porous media: effect of pressure gradient orientation <i>Yanis Bendali, EM2C</i>	Rayleigh-Taylor convection in a granular porous medium: An experimental study <i>Yves Meheust, Géosciences Rennes</i>	Development of 3D and functionalised electrodes to metal decontamination of polluted water: application to the uranium recovery <i>Florent Belnou, laboratoire d'ingénierie des surfaces et lasers</i>
18h20–18h45	NaCl Salt Crust Dynamics Diagram <i>Glad-Calin Licsandru, IMFT</i>	Microwave Assisted CO₂ Desorption from Solvent Flowing into Hollow Fiber Membrane <i>Ali Hajj, IMT Atlantique</i>	Development of macroporous geopolymer foams functionalized by a photocatalyst <i>Sara Benkhirat, Université de Perpignan</i>
18h45-19h10			Porous On-Demand Wafers for Energy, Environment and a Resilient supply chain <i>Ghadi Dakroub, CEA</i>



Partenaire or



Partenaires argent



storengy

Partenaires bronze

Jeudi 19 octobre - Matin

09h00 - 9h45 – Conférence plénière - *Amphi Dahlias*

Stefania Specchia, Politecnico di Torino

[The role of porosity in platinum-group-metal free electrocatalysts for PEM fuel cells](#)

	<i>Amphi Dahlias</i>	<i>Amphi Séquoia</i>	<i>Amphi Hortensias</i>
Session	Comportement des fluides complexes en milieux poreux	Caractérisation, imagerie, génération numérique de milieux poreux	Mécanique des milieux poreux : déformation, rupture, endommagement
9h50–10h15	Adsorption and desorption surface dynamics of gaseous adsorbate on silicate-1 by molecular dynamics simulation <i>Jean-Marc Simon, ICB</i>	Hydrodynamics in a coarse porous layer above a sandy bed with application to contact erosion in hydraulic structures <i>Pierre Philippe, INRAE</i>	Towards a DFT approach to the Mechanical Properties of Nanoporous Materials <i>Akli Kahlal, UPPA</i>
10h15–10h40	Water absorption of particles immersed in a colloidal suspension: Application to recycled concrete <i>Emmanuel Keita, Laboratoire Navier</i>	Characterization of multiscale porosity in activated carbon by X-ray tomography and FIB-SEM <i>Othmane Darouich, LFCR</i>	Numerical study of the effect of the boundary conditions in DEM modelling on the mechanical behavior of a cemented granular media: application to biocalcified sand <i>Théo Dumas, 3SR</i>

10h40 – 11h10 – Pause-café

	<i>Amphi Dahlias</i>	<i>Amphi Séquoia</i>	<i>Amphi Hortensias</i>
Session	Systèmes multiphases - multicomposants	Caractérisation, imagerie, génération numérique de milieux poreux	Milieux poreux biologiques
11h10–11h35	Analysis of the surface/subsurface coupled evaporation for an energetic system <i>Thomas Doury, IMFT</i>	Open-cell foam ultra-realistic microstructure model: a new generation workflow validated through experimental data and CFD simulations <i>Enrico Agostini, IFEN</i>	Nonlocal dynamics of biofilm clogging in a porous microfluidic device <i>Gabriel Ramos, IMFT</i>
11h35–12h00	Impact of initial air and subsequent H2 gas migration in a radioactive waste repository <i>Mohamed Haythem Bahlouli, IRSN</i>	Analysis of evaporation in a hydrophobic micro-model <i>Mohamed Amine Ben Amara, LESTE-ENIM</i>	Can we control biofilm-induced clogging in porous media? <i>Clara Toulouze, IMFT</i>
12h00–12h25	Gas migration through water-saturated bentonite: laboratory experiments and microstructural analysis <i>Mohammed Zaidi, IRSN</i>	Auto-weighting multitask inverse problems for reactive flows at the pore-scale with evolving fluid-solid interface and related uncertainty quantification <i>Sarah Perez, UPPA</i>	Dynamics and upscaling of porous biofilms with heterogeneous rheology <i>Philippe Poncet UPPA</i>

12h25 – 14h00 – Déjeuner



Partenaire or



Partenaires argent



Partenaires bronze

Jeudi 19 octobre – Après-midi

14h00 – 14h45 – Conférence plénière : Pierre Levitz, Physicochimie des Electrolytes et Nanosystèmes Interfaciaux

[Molecular diffusion in porous media: a multimodal approach coupling 3D imagery, X ray scattering, NMRD and numerical simulations](#) – *Amphi Dahlias*

	<i>Amphi Dahlias</i>	<i>Amphi Séquoia</i>	<i>Amphi Hortensias</i>
Session	Systèmes multiphases - multicomposants	Milieus fibreux multi-échelles, nano et micro poreux	Milieus poreux biologiques
14h50–15h15	Evaluation of electrostatic force in the vicinity of the three-phase contact region <i>Mojtaba Norouziadeh, ISTO</i>	Probing diffusional exchange in mesoporous zeolite by NMR diffusion and relaxation methods <i>Marc Fleury, IFPEN</i>	Hydrodynamic dispersion in porous media enhances reaction in spherical fronts <i>Pratyaksh Karan, Géosciences Rennes</i>
15h15–15h40	Pollutant transport in shallow aquifers <i>Christophe Bourel, LMPA Joseph Liouville</i>	Acid sites confinement in micro/mesoporous Y zeolite revealed from in situ IR monitoring of tri-tert-butylpyridine diffusion <i>Mickael Rivallan, IFPEN</i>	Mechanical properties and durability of a sand cemented by microbially-induced calcite precipitation (MICP) <i>Michela La Bella, Université Grenoble Alpes</i>
15h40–16h05	Use of Oil-in-Water Emulsions to achieve Stable Displacement of Soil Pollution <i>Shuxin Wang, I2M</i>	Porous capsules with liquid core prepared by Pickering emulsion: Understanding of diffusional phenomena for catalyst implementation <i>Rémi Duclos, IFPEN</i>	Insight into the mechanism of malachite green dye adsorption on porous media: Characterization, modeling, and effects of adsorption affinity <i>Fatima Zahra Falah, University of Casablanca</i>

16h10 –16h30 – Clôture des JEMP 2023



Partenaire or



Partenaires argent



Partenaires bronze

École d'hiver APPRISE

Fundamentals of trAnspOrt Phenomena in PoRous media across ScalEs

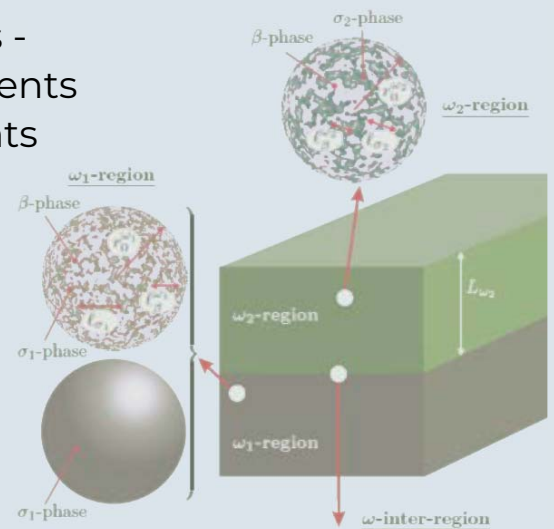
organisée par le FIC (France InterPore Chapter)

<https://apprise.sciencesconf.org/>

D. Lasseux, L. Luquot, S. Roman, B. Rousseau

Thème & Contenu

- **Cours général (9h00) :** Bases physiques - Transferts en milieu poreux – Changements d'échelle – Modélisation des écoulements monophasiques et diphasiques
- **Module thématique (6h00) :** Acquisition et utilisation d'images pour la modélisation des transferts
- **Travaux pratiques numériques (15h00)** (OpenFoam et COMSOL)



Lieu

Centre Paul Langevin - CAES du CNRS - 73500 Aussois

Dates : du 05 au 09 février 2024

Inscriptions sur : <https://apprise.sciencesconf.org/inscriptions>

Participation aux frais (incluant le séjour)

Académiques : 650 € - Etudiants : 500€ - Industriels : 900 €

Limité à 30 places - Date limite d'inscription : 30 décembre 2023



Chers congressistes, chers amis,

Pensez à publier en Open access WOS gratuit via la revue STET supportée par le CEA et IFPEN

<https://www.stet-review.org/>

edpsciences Journals Books Conferences Submit your paper EDPS Account

STET All issues Topical Issues Forthcoming About Search Menu

Vol. 78 (2023)

Science and Technology for Energy Transition (STET)

Formerly Oil & Gas Science and Technology - Revue d'IFP Energies nouvelles

Science and Technology for Energy Transition (STET) is the new name of former OGST (*Oil & Gas Science and Technology*, journal headed by IFPEN).

STET is an international scientific journal supported by IFPEN (IFP Energies nouvelles) and CEA (French Alternative Energies and Atomic Energy Commission), both major French research and technology organizations in energy.

The journal is intended to be a forum for exchanging and sharing scientific results focusing on effective and sustainable energy transition in response to climate change. Submitted articles must be factual and shall not express opinions. Their scientific quality and compliance to the journal's [aims & scope](#) are the main criteria by

- Sign up for Email-alert
- Instructions for Authors
- Author toolkit
- Recommend this journal

Forthcoming topical issues

Calls for papers

Invité

Perfection is the Enemy of Evolution ...

Adrian Bejan * ¹

¹ Duke university [Durham] – États-Unis

You may be familiar with the saying "The best is the enemy of the good" (Voltaire), or "Perfection is the enemy of progress" (Churchill). It sounds counterintuitive. Most of us tend to associate the better performing with the more perfect. Is the saying true? This is a question of physics. I predict in simple terms the 'enemy' relationship between performance and perfection (access to movement, space, and time). It is natural. Everywhere we see it, in vascular designs, human movement (life) in the city, animal design, athletics evolution, business, and diversity on the globe and in universities. From cause to effect, nature 'happens' in this direction, not the other way around: Freedom to change → evolution → performance (access) → diversity.

*Intervenant

Features of transports in nano-porous media - Contribution of NMR and MRI

Philippe Coussot * ¹

¹ Laboratoire Navier – Ecole des Ponts ParisTech, Centre National de la Recherche Scientifique,
Université Gustave Eiffel – France

Many porous materials such as concretes, soils, wood, etc, contain at least a fraction of nanopores. The transports in these nanopores play an important role for various energy transfers (osmotic transport, energy storage, hygrothermal behavior of bio-based materials, etc). However, the flow properties at this scale, even in straight channels, are complex (1), in particular as the continuum assumption may be invalid, and the interactions of molecules with solid surfaces can play a major role. We can therefore expect original transport properties in non-model porous media, possibly multi-scale, with also the possibility of exchanges between the different pore sizes, but observations or measurements at this scale are tricky. NMR relaxometry offers the possibility to obtain precise quantitative (statistical) information concerning the liquid distribution in the different pore types. Moreover, this technique makes it possible to follow the evolutions of pore size, surface wetting, or even exchanges between different porous phases (2). In addition, the spatial distribution of liquid in the different types of pores can be measured using appropriate MRI sequences (3).

It is thus shown that the desaturation of a silica glass (Vycor) results from a vapor pressure gradient associated with local saturation and inducing a pressure gradient in the liquid, leading globally to a diffusion mechanism (4). In a "bi-porous" material formed of nanoporous inclusions and micrometric pores, it is shown that the liquid contained in the large pores is drained in depth and transported through the nanopores, which are therefore emptied last (2). NMR also makes it possible to measure the distribution of bound water absorbed in the form of nanometric inclusions in the amorphous regions of the cellulose of bio-sourced materials. It can then be observed that the drying of wood relies on the diffusion of bound water, which first extracts the free water from the fibers, vessels or tracheids, and transports it to the free surface (3). Finally, this bound water appears to be very mobile: its diffusion coefficient, which can be directly measured by blocking the transport of free water, is higher than the self-diffusion coefficient of water.

References

(1) Kakovine et al, Fluids at the Nanoscale: From Continuum to Subcontinuum Transport, *Annual Review of Fluid Mechanics*, 53, 377-410 (2021)

(2) Maillet et al, Diffusion-like drying of a nanoporous solid as revealed by Magnetic Resonance Imaging, *Physical Review Applied* 18, 054027 (2022)

(3) Cocusse et al, Two-step diffusion in cellular hygroscopic (plant-like) materials, *Science Advances*, 19, eabm7830 (2022)

*Intervenant

(4) Maillet et al, "Dynamic NMR relaxometry" as a simple tool for measuring liquid transfers and characterizing surface and structure evolution in porous media, *Langmuir*, 38, 15009–15025 (2022)

Molecular diffusion in porous media: a multimodal approach coupling 3D imagery, X ray scattering, NMRD and numerical simulations

Pierre Levitz * ¹, Anne-Laure Rollet ¹

¹ PHysicochimie des Electrolytes et Nanosystèmes Interfaciaux – Institut de Chimie du CNRS, Sorbonne Université, Centre National de la Recherche Scientifique – France

1 Introduction Diffusive transport of confined fluid in disordered porous media raise some challenging questions related to fluid dynamics inside these materials, at different time and length scales. Some examples can be mentioned such as the life cycle of building materials associated to concrete durability (water and ion long term diffusion) (1,2), the degradation of porous media belonging to the cultural heritage (3), the long-term confinement of nuclear wastes in geological horizons (clays) and the optimal design of catalyst supports (4). Molecular diffusion dynamics inside nanoporous and meso porous materials follows an intermittent dynamic (5-7) involving adsorption, surface diffusion and relocation inside the pore space. This coupling between dynamics and interfacial confinement, contributes to constraint the molecular diffusion inside pore network. In order to quantify this coupling, some parameters need to be measured such as the molecular surface diffusion coefficient, the average residence time on the pore surface, the time delay between two consecutive adsorptions where molecule diffuses inside the bulky part of the pore network (6). In the case of hierarchical disordered porous material such as soil, and mesoporous catalysts, molecular exchange between two or more pore networks, organized at different length scale, generalizes and extend molecular intermittent dynamics toward larger time. In both cases, the pore network organization on a length-scale ranging from nanometers to some micrometers is a cornerstone to properly understand diffusion-permeation properties. A strong need to a bottom-up approach mixing X-ray scattering (SAXS, SANS, 2D-3D imagery technics and numerical simulations is highly suitable for these types of multiscale complex systems (1,2,3,6). This multimodal structural analysis offers the possibility to use 3D reconstructions and to build constrained models mimicking geometrical features observed experimentally (6,8). These models can then be used to compute transport properties, allowing comparison with experimental determinations. In this presentation, we attempt to illustrate these topics and focus on two specific examples. 2 Molecular diffusion in a mesoporous material This first example concerns the water interfacial dynamics inside a mesoporous precursor of a catalytic support, the boehmite. As Al₂O₃ catalyst support inherits most of morphological properties of this precursor, understanding and optimizing molecular transport inside a boehmite pore network is a key parameter to improve molecular accessibility to a specific pore surface location. 3D morphology and topology of a commercial sample from was first investigated by electron tomography (8) and small angle scattering, providing a reliable 3D representation of the pore network at the nanometer scale. At the mesoscopic time scale (from 1ns to 10 ms), water dynamics was probed by NMRD (8) of

*Intervenant

1H and 2H at different levels of water saturation of the pore network. In all cases, dispersion curves $R_1(\omega)$ follow a very similar algebraic law, highlighting the determinant contribution of the water dynamics on surface. In order to decipher different contributions of interfacial molecular dynamics, numerical simulations are conducted using the 3D reconstruction of the pore network, as it was formerly done in the case of the Vycor glass (6). Respective role of surface interaction and surface geometry on water dynamics were analyzed. Comparison with NMRD experimental data has allowed determining two important surface descriptors: First, the escaping time and/or the adsorption time found to be rather long: $8 \cdot 10^{-6}$ s; second, the surface self-diffusion of the proton inside the surface layer estimated on the order of 10^{-10} m²/s. More technically, it was also concluded that the interfacial geometry and its curvature properties plays an important role to understand water proton diffusing on the surface of this porous material and its NMRD signature.

3 Bridging scales in hierarchical pore networks

In the second part of this presentation, more numerical oriented, we propose some possible ways to upscale the analysis of fluid dynamics, allowing decoupling the scale of the so-called "elementary pore" (which involves adsorption and relocation dynamics) and the long-range exploration, sensitive to the porous network structure. More specifically, in the case of a multiscale pore network and using first passage statistics, we analyze the possibility to quantify the molecular exchange between two pore networks organized at different length scales, Kinetics of a first encounter with a reactive site, located inside one specific pore network of a multiscale porous material is also discussed. References (1) Soft X-ray Ptychographic Imaging and Morphological Quantification of Calcium Silicate Hydrates (C-S-H). S. Bae, R. Taylor, D.Shapiro, P. Denes, J. Joseph, R. Celestre, S. Marchesini, H. Padmore, T. Tyliczszak, T. Warwick, D. Kilcoyne, P. Levitz and P.J.M Monteiro. *J. Am. Ceram. Soc.*, 98, 4090-4095 (2015) (2) S. Brisard, C. A. Davy, L. Michot, D.Troadec, P. Levitz, Mesoscale pore structure of a high-performance concrete by coupling focused ion beam/scanning electron microscopy and small angle X-ray scattering.. *J Am Ceram Soc.*102:2905–2923 (2019) (3) G.P. Odin, V. Rouchon, F. Ott, N. Malikova, P. Levitz, L.J. Michot, Neutron imagi investigation f fossil woods: non-destructive characterization of microstructure and detection of in situ changes as occurring in museum cabinets, *Fossil record*, 20, 95-103, (2017) (4) J-B Pigot, Dynamique multi-échelle et échange inter-porosité par relaxométrie RMN au sein de zéolithes mésoporisées, PhD Thesis of Sorbonne-universite, <https://www.theses.fr/2020SORUS424> (2020) (5) P. Levitz, Random flights in confining interfacial systems, *J. Phys. Cond. Mat.* 17, S4059 (2005) (6) P. Levitz, Probing interfacial dynamics of water in confined nanoporous systems by NMRD. *Molecular Physics*, 117 (7- 8),952-959 (2018) (7) Colin Bousige, Pierre Levitz and Benoit Coasne, Bridging scales in disordered porous media by mapping molecular dynamics onto intermittent Brownian motion, *Nature Comm*, 12, Article Number1043, (2021) (8) Z. Gu, R. Goulet, P. Levitz, D. Ihiawakrim, O. Ersen, and M. Z. Bazant, Mercury cyclic porosimetry: Measuring pore-size distributions corrected for both pore-space accessivity and contact-angle hysteresis, *J. Colloid Interface Sci.*, vol. 599, pp. 255– 261, (2021) (9) Field-cycling NMR Relaxometry; New Developments in NMR Serie, editor R Kimmich, RSC, (2018)

Experimental study on karst formation: role of flow, chemical stress and rock heterogeneities

Linda Luquot * ¹

¹ Geosciences Montpellier – Université de Montpellier, Centre National de la Recherche Scientifique – France

The formation of underground cavities, called karsts, resulting from carbonate rock dissolution, is at stake in many environmental and societal issues, notably through risk management and the administration and quality of drinking water resources. Facing natural environment complexity, we propose a laboratory study combining hydro-chemical monitoring, 3D imaging, and non-invasive observation of electrical properties, showing the benefits of geoelectrical monitoring to map karst formation. The present study predominantly focuses on the differences in dissolution patterns depending on the mineralogy and on the structure of different carbonate rock types, as well as on the experimental hydrodynamic conditions. To this end, three distinct carbonate rock types are selected for their differences in structure and mineralogy: chalk, crinoidal limestone and dolomite. Acid injections are conducted on samples cored from these three rock types at atmospheric conditions. With the same acidic fluid, four Péclet conditions, associated to different flow rates depending on the rock type, were applied to the samples. Samples are characterized with laboratory and images methods before and after these experiments, during which chemical, hydraulic and electric properties are recorded. The rock properties evolution, associated with the initial structural and mineral differences between the three rock types and the experimental conditions, is analyzed in order to determine the influence of each of these parameters on the dissolution patterns induced by the acid injection.

*Intervenant

Microfluidics for geosciences to unravel reactive transport processes in porous media

Sophie Roman * ¹

¹ Institut des Sciences de la Terre d'Orléans - UMR 7327 – Univ. Orléans, CNRS, BRGM, ISTO, UMR 7327, F-45071, Orléans, France : UMR7327 – France

There is a strong interest in imaging and numerical modeling of reactive flow at the pore scale applied to reservoir engineering, subsurface hydrology, soil remediation, and CO₂ sequestration. The dynamics at the pore-scale, however, remain relatively unknown but influence macroscale behaviors considerably. In particular, an in-depth understanding of dissolution and precipitation of minerals in porous media and the complex feedback on the transport of fluids and colloids is essential for various subsurface applications.

Using state-of-the-art microfluidic experiments, we explore pore-scale mechanisms and their consequences on the upscaling of rock and fluid properties. Such micromodels have the pore network pattern and pore sizes of a real rock or idealized medium. Importantly, these micromodels permit direct, high-magnification, time-lapse observations of fluid movement through pores, as well as visualization of the evolution of the pore space due to dissolution or precipitation. We combine microfluidic experiments, high-resolution imaging, chemical and geo-electrical characterization, and numerical simulations to understand the microdynamics of reactive flow in geological porous media.

In this work, we will describe and discuss the current possibilities and challenges associated with microfluidics for reactive transport processes in geosciences, as well as how these experimental datasets are used to provide data to verify and complete numerical models, to gain a better understanding of the mechanisms at the pore-scale, and to improve large scale models.

*Intervenant

The role of porosity in platinum-group-metal free electrocatalysts for PEM fuel cells

Stefania Specchia * ¹

¹ Politecnico di Torino = Polytechnic of Turin – Italie

Polymer electrolyte membrane fuel cells (PEMFCs) are one of the solutions for the transition towards an emission-free way of producing energy. PEMFCs in fact, are electrochemical devices which transform chemical energy into electrical energy without harmful emissions, if hydrogen is used as a fuel. However, the cathodic reaction, namely the oxygen reduction reaction (ORR), is sluggish. The best activities so far are yet assured by platinum-based electrocatalysts, which suffer of stability problems. Moreover, Pt is scarce and expensive, its price being linked to the stock exchange (1).

Non-noble transition metals such as Fe and Co, with nitrogen and carbon, in the shape of M-N-C, are the most promising alternative to Pt-based electrocatalysts. Transition metal is the heart of the electrocatalytic site for ORR, while nitrogen coordinates the transition metal atoms linking them to the carbon-based structure. Carbon has the purpose of conducting electrons and providing high specific surface area and porous structure (2). The porous structure, in particular the microporous surface, is believed to provide a role in the formation of active sites for ORR (3), while the mesoporous structure plays a fundamental role in the working functioning on a PEMFC, favouring the transport of oxygen (reactant) and water (reaction product) (4). In fact, the microporosity of the carbon material has a great impact on flooding of the cathodic catalytic layer, limiting the performance of the PEMFC. If water is not properly removed, its accumulation into the pores leads to a decreasing fuel cell performance due to pore clogging and subsequent oxygen deficiency.

*Intervenant

Session

A la mémoire de M. Panfilov

Macroscopic dynamic capillary pressure for two-phase flow in porous media

D. Lasseux^a, F.J. Valdés-Parada^b

^a*I2M, UMR 5295, CNRS, Université de Bordeaux, 351 Cours de la Libération, 33405 Talence CEDEX, France*

^b*División de Ciencias Básicas e Ingeniería, Universidad Autónoma Metropolitana-Iztapalapa, Avenida Ferrocarril San Rafael Atlixco, Número 186, Iztapalapa C.P. 09310, CDMX, Mexico*

Keywords: Two-phase flow, dynamic capillary pressure, upscaling

1. Introduction

A closed predictive model for the macroscopic pressure difference, often referred to as the *macroscopic capillary pressure*, for two-phase flow in homogeneous porous media is of major importance to form a complete set of governing macroscale equations. This has been a long-lasting subject of research during the past 40 years [1, 3], and the majority of the existing models remain empirical at some level of their derivation. A new closed macroscopic dynamic capillary pressure equation is reported in this work on the basis of the existence of a representative (periodic) unit cell able to locally describe microscale momentum transport in the system. This is carried out with an adjoint method together with a Green's formulation, requiring no other simplifying assumption.

2. Upscaled dynamic capillary pressure

The general framework of the analysis is the incompressible, creeping flow of two Newtonian fluids α and β saturating a homogeneous porous medium whose rigid and spatially homogeneous solid skeleton is the σ -phase.

2.1. Pore-scale and adjoint problems

The pore-scale flow problem can be written in a periodic unit cell representative of the domain as follows ($\alpha = \beta, \gamma$)

$$\nabla \cdot \mathbf{v}_\alpha = 0, \quad \text{in } \mathcal{V}_\alpha, \quad (1a)$$

$$\mathbf{0} = \nabla \cdot \mathbf{T}_{\tilde{p}_\alpha} - \nabla \mathcal{P}_\alpha, \quad \text{in } \mathcal{V}_\alpha, \quad (1b)$$

$$\mathbf{v}_\beta = \mathbf{v}_\gamma, \quad \text{at } \mathcal{A}_{\beta\gamma}, \quad (1c)$$

$$\mathbf{n}_{\beta\gamma} \cdot \mathbf{T}_{\tilde{p}_\beta} = \mathbf{n}_{\beta\gamma} \cdot \mathbf{T}_{\tilde{p}_\gamma} + \mathbf{n}_{\beta\gamma} \left(\langle p_\beta \rangle^\beta - \langle p_\gamma \rangle^\gamma \right)_{\mathbf{r}_{\beta\gamma}} + 2H\gamma \mathbf{n}_{\beta\gamma} + \nabla_s \gamma, \quad \text{at } \mathcal{A}_{\beta\gamma}, \quad (1d)$$

$$\mathbf{v}_\alpha = \mathbf{0}, \quad \text{at } \mathcal{A}_{\alpha\sigma}, \quad (1e)$$

$$\mathbf{v}_\alpha|_{\mathcal{S}_{\alpha i}^-} = \mathbf{v}_\alpha|_{\mathcal{S}_{\alpha i}^+}, \quad i = 1, \dots, N, \quad (1f)$$

$$(\mathbf{n}_\alpha \cdot \mathbf{T}_{\tilde{p}_\alpha})_{\mathcal{S}_{\alpha i}^-} = -(\mathbf{n}_\alpha \cdot \mathbf{T}_{\tilde{p}_\alpha})_{\mathcal{S}_{\alpha i}^+}, \quad i = 1, \dots, N, \quad (1g)$$

$$\langle \tilde{p}_\alpha \rangle^\alpha = 0. \quad (1h)$$

Here, \mathbf{v}_α is the velocity in the α -phase, in which the pressure, p_α , is decomposed as $p_\alpha = \langle p_\alpha \rangle^\alpha + \tilde{p}_\alpha$, $\mathbf{T}_{\tilde{p}_\alpha} = -\tilde{p}_\alpha \mathbf{I} + \mu_\alpha (\nabla \mathbf{v}_\alpha + \nabla \mathbf{v}_\alpha^T)$, $\nabla \mathcal{P}_\alpha = \nabla \langle p_\alpha \rangle^\alpha - \rho_\alpha \mathbf{b}_\alpha$, H is the double mean curvature of the fluid-fluid interface, $\mathcal{A}_{\beta\gamma}$, which unit normal directed from the β phase to the γ phase is $\mathbf{n}_{\beta\gamma}$, μ_α and γ are the dynamic viscosity and interfacial tension and $\nabla_s \gamma$ stands for possible Marangoni effects; $\mathcal{S}_{\alpha i}^\pm$ are the entrances/exits of the α -phase at the i th edge of the periodic unit cell.

For the derivation of the upscaled model, an adjoint problem is now considered that writes

$$\nabla \cdot \mathbf{f}_\beta = \frac{1}{V_\beta}, \quad \text{in } \mathcal{V}_\beta, \quad \nabla \cdot \mathbf{f}_\gamma = -\frac{1}{V_\gamma}, \quad \text{in } \mathcal{V}_\gamma, \quad (2a)$$

$$\mathbf{0} = \nabla \cdot \mathbf{T}_{f_\alpha}, \quad \text{in } \mathcal{V}_\alpha, \quad (2b)$$

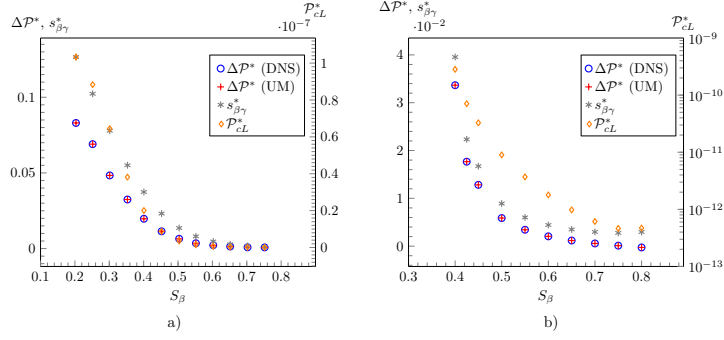


Figure 1: $\Delta\mathcal{P}^*$, obtained from direct numerical simulation (DNS) and predicted from the upscaled equation (3) (UE), along with the interfacial term contribution, $s_{\beta\gamma}^*$, and classical Laplace capillary pressure, \mathcal{P}_{cL}^* (see text), versus the wetting phase saturation, S_β . a) $\mu^* = 0.1$, $Ca = 10$; b) $\mu^* = 10$, $Ca = 0.1$. $\varepsilon = 0.8$.

$$\mathbf{f}_\beta = \mathbf{f}_\gamma, \quad \mathbf{n}_{\beta\gamma} \cdot \mathbf{T}_{f_\beta} = \mathbf{n}_{\beta\gamma} \cdot \mathbf{T}_{f_\gamma}, \quad \text{at } \mathcal{A}_{\beta\gamma}, \quad (2c)$$

$$\mathbf{f}_\alpha = \mathbf{0}, \quad \text{at } \mathcal{A}_{\alpha\sigma}, \quad (2d)$$

$$\mathbf{f}_\alpha|_{\mathcal{G}_{\alpha i}^-} = \mathbf{f}_\alpha|_{\mathcal{G}_{\alpha i}^+}, \quad (\mathbf{n}_\alpha \cdot \mathbf{T}_{f_\alpha})_{\mathcal{G}_{\alpha i}^-} = -(\mathbf{n}_\alpha \cdot \mathbf{T}_{f_\alpha})_{\mathcal{G}_{\alpha i}^+}, \quad i = 1, \dots, N, \quad (2e)$$

$$f_\alpha = 0, \quad \text{at } \mathbf{r}_\alpha^0. \quad (2f)$$

2.2. Macroscopic capillary pressure

Following the procedure detailed in [2], a Green's formula can be used to combine the physical flow problem and the adjoint (closure) problem that leads to the following macroscopic equation for the dynamic capillary pressure

$$\Delta\mathcal{P} = \langle p_\gamma \rangle^\gamma|_{\mathbf{x}_\gamma} - \langle p_\beta \rangle^\beta|_{\mathbf{x}_\beta} = -\boldsymbol{\psi}_\beta \cdot \nabla \langle p_\beta \rangle^\beta + \rho_\beta \mathbf{b}_\beta \cdot \boldsymbol{\varphi}_\beta - \boldsymbol{\psi}_\gamma \cdot \nabla \langle p_\gamma \rangle^\gamma + \rho_\gamma \mathbf{b}_\gamma \cdot \boldsymbol{\varphi}_\gamma + s_{\beta\gamma}, \quad (3)$$

where $\boldsymbol{\varphi}_\alpha = \int_{\mathcal{V}_\alpha} \mathbf{f}_\alpha dV$, $\boldsymbol{\psi}_\alpha = \boldsymbol{\varphi}_\alpha - \int_{\mathcal{A}_{\beta\gamma}} \mathbf{n}_{\alpha\kappa} \cdot \mathbf{f}_\alpha \mathbf{z}_\alpha dA$, and $s_{\beta\gamma} = \int_{\mathcal{A}_{\beta\gamma}} (2H\gamma \mathbf{n}_{\beta\gamma} + \nabla_s \gamma) \cdot \mathbf{f}_\beta dA$. Here, \mathbf{z}_α denotes the position of a point located at $\mathcal{A}_{\beta\gamma}$ relative to the α -phase barycenter in the unit cell.

3. Results

This predictive equation is tested in the simple case of two-phase flow within a square pattern of parallel cylinders of circular cross section (see figure 1 in [2]) with flow along a principal axis of the structure orthogonal to the cylinders axes. The wetting fluid flows under the form of sheets aligned with the mean flow and attached to the cylinders, whereas the non-wetting phase flows in the core, between the wetting fluid sheets. The test consists in comparing the results on the dimensionless macroscopic dynamic capillary pressure $\Delta\mathcal{P}^*$ obtained from the solution of the pore-scale flow problem (DNS), on the one hand, and from the upscaled equation (3) (UE), on the other hand. Results are reported in figure 1 versus the wetting fluid saturation S_β for a porosity $\varepsilon = 0.8$, two viscosity ratios $\mu^* = \mu_\beta/\mu_\gamma$ and two values of the capillary number $Ca = h\ell^2/\gamma$, h being the pressure gradient magnitude in both phases and ℓ the periodic unit cell size. No volume force and no Marangoni effect are considered. The classical Laplace pressure $\mathcal{P}_{cL}^* = 2\langle H^* \rangle_{\beta\gamma}/Ca$, where $\langle H^* \rangle_{\beta\gamma} = \frac{1}{A_{\beta\gamma}^*} \int_{\mathcal{A}_{\beta\gamma}^*} H^* dA^*$ and $A_{\beta\gamma}^*$ is the dimensionless measure of $\mathcal{A}_{\beta\gamma}$, is also reported in these figures. These results show the excellent agreement between DNS and the upscaled equation, and highlight the fact that the classical Laplace relationship cannot represent a satisfactory estimate of $\Delta\mathcal{P}^*$. The influence of the pressure gradient in each phase (dynamic effects) is also pinpointed.

References

- [1] HASSANIZADEH, S. M. & GRAY, W. G. 1990 Mechanics and thermodynamics of multiphase flow in porous media including interphase boundaries. *Advances in Water Resources* **13** (4), 169–186.
- [2] LASSEUX, D. & VALDÉS-PARADA, F. J. 2023 Upscaled dynamic capillary pressure for two-phase flow in porous media. *Journal of Fluid Mechanics* **959**, R2.
- [3] MARLE, C.-M. 1981 From the pore scale to the macroscopic scale: equations governing multiphase fluid flow through porous media. *Flow and transport in porous media. Proc. Euromech 143, Delft, 1981* pp. 57–61.

Large scale numerical simulation of flow in fractured porous media

M. Kern^{a,b}, G. Pichot^{a,b}, D. Zegarra Vasquez^{a,b}

^a*Inria, 2 rue Simone Iff, 75012, Paris, France*

^b*Université Paris-Est, CERMICS (ENPC), 77455 Marne-la-Vallée, France*

Keywords: Fractured media, subsurface flow, mixed-finite element, linear solvers

1. Introduction

This paper deals with the numerical simulation of flow and transport in a fractured porous medium. We are particularly interested in the simulation of *very large* fracture networks (several thousands of fractures in a porous medium), and how numerical methods must be adapted to scale-up to such large systems. We consider one phase Darcy flow of water. Following the work of Martin et al. [1], fractures are represented as co-dimension one interfaces, and the conservation law in the fracture is modified to include a source term representing the exchange with the porous matrix. We assume the pressure is continuous across the matrix–fracture interface, and the model is closed by adding a zero total flux along fracture intersections.

2. Numerical methods

A first step is to obtain realistic large scale networks. We rely on networks obtained from the DFN.Lab software [2]. A dedicated mesh generation code MODFRAC¹ is then used to mesh the resulting network, and this is used as input to a 3D mesh generation software (see figure 1).

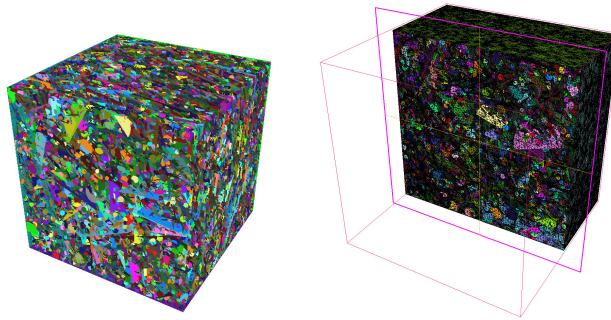


Figure 1: Geometry (left) and mesh (right) for a fractured porous medium, with 87 00 fractures and 16M cells

The discretization is based on mixed-hybrid finite element [3, 4]. This choice presents several advantages: the method is conservative by construction, and is robust with respect to heterogeneous or anisotropic media. Hybridization leads to a symmetric and positive definite matrix with one unknown on each face of the mesh, but its main interest is to give a very natural way of coupling the 3D and 2D models: the pressure at the center of triangular fracture elements coincides with the Lagrange multiplier (or pressure trace) on the faces or tetrahedra in the porous matrix.

¹MODFRAC is a proprietary software owned by Inria and the University of Technology of Troyes (UTT)

The code has been validated on the “Field case” example from the benchmark proposed in [5]. We note that results from the participants are available on a dedicated GitHub server, which enabled us to validate the results.

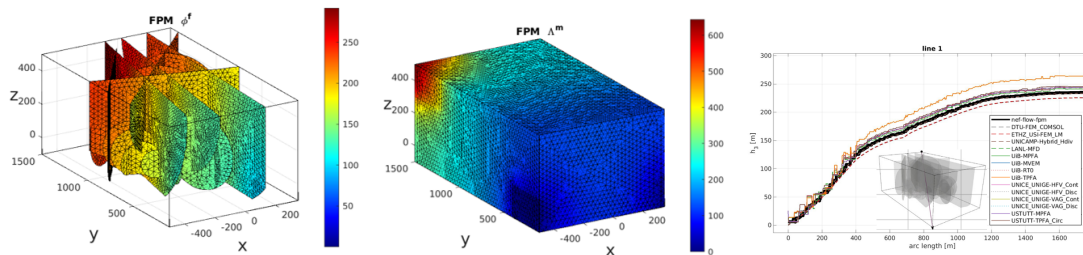


Figure 2: Flow in the fractures (left) and in the matrix (right), and comparison along a line for the “Field” benchmark test case

The last, but crucial, step is to solve the resulting linear system. It is both large, because of the large number of unknowns in the porous matrix, and may be highly ill-conditioned because the 3D mesh is constrained by the geometry of the fractures, and may become quite distorted. Direct methods worked well for fracture networks (whose topology remains two-dimensional) or smaller examples like that shown on Figure 2 but become impractical for large 3D meshes. One must turn to iterative methods, such as conjugate gradient or GMRES. The critical ingredient in ensuring the success of an iterative method is the choice of a preconditioner. We compare the performance of a sparse direct solver with that of a conjugate gradient with an algebraic multigrid preconditioner in Table 1. The iterative method reduces the memory usage, but the number of iterations remains very high.

Test case	Fractures	3D cells	DOFs	Cond. number	UMFPACK	PCG + AMGCL
L40 geo	12.4 k	3.57 M	8.27 M	$6.46 \cdot 10^{12}$	1h 50 mn 183 GB	2h 47mn (5 941 it) 3.55 GB
L60 geo	39.5 k	7.87 M	18.6 M	$5.35 \cdot 10^{12}$	16h 25 mn 2 TB	6h 47mn (5 736 it) 8 GB

Table 1: Solver performance for test cases of increasing complexity

An interesting alternative to algebraic multigrid is afforded by domain decomposition methods, in particular the recently developed multilevel spectral domain decomposition methods based on the GenEO framework [6, 7]. We report a preliminary performance result: on a model with 87 000 fractures, 16 million cells and 37 millions unknowns (shown in Figure 1), AMG did not converge to a tolerance of 10^{-12} after 50 000 iterations, while the HPDDM preconditioner used from PETSc converged in 131 iterations, and 8 minutes on 1024 cores.

References

- [1] V. Martin, J. Jaffré, and J. E. Roberts. Modeling fractures and barriers as interfaces for flow in porous media. *SIAM J. Sci. Comp.*, 26(5):1667–1691, 2005.
- [2] R. Le Goc, B. Pinier, C. Darcel, E. Lavoine, D. Doolaeghe, S. de Simone, J.-R. de Dreuzy and Ph. Davy DFN. lab: software platform for Discrete Fracture Network models. *American Geophysical Union Fall Meeting*, 2019, H41H-1778
- [3] G. Pichot, J. Erhel, and J.-R. de Dreuzy A Generalized Mixed Hybrid Mortar Method for Solving Flow in Stochastic Discrete Fracture Networks *SIAM J. Sci. Comp.*, vol. 34 (1), 2012, 10.1137/100804383
- [4] L. Amir, M. Kern, Z. Mghazli and J. E. Roberts Intersecting fractures in porous media: theoretical and numerical analysis *Applicable Analysis*, 2021, (10.1080/00036811.2021.1981878)
- [5] I. Berre, W. M. Boon, B. Flemisch et al. Verification benchmarks for single-phase flow in three-dimensional fractured porous media *Adv. Wat. Res.*, 147, 2021, 103759
- [6] V. Dolean, P. Jolivet, and F. Nataf, An Introduction to Domain Decomposition Methods, *Society for Industrial and Applied Mathematics*, Philadelphia, 2015.
- [7] P. Jolivet, J. E. Roman and S. Zampini, KSPHPDDM and PCHPDDM: Extending PETSc with advanced Krylov methods and robust multilevel overlapping Schwarz preconditioners, *Computers & Mathematics with Applications*, Vol. 84, 2021, pp. 277-295,

Computing the diphasic effective properties on nanoporous clayrock using Direct Numerical Simulation

A.-J. Tinet ^a, F. Golfier ^a, A. Pazdniakou ^{a,b}, M. Dymitrowska ^b, M. Prat ^c, J. Vicente ^d

^a *Université de Lorraine, CNRS, GeoRessources, F-54000, Nancy, France*

^b *IRSN, PRP-DGE/SRTG/LETIS, BP 17, 92260 Fontenay-aux-Roses, France*

^c *Institut de Mécanique des Fluides de Toulouse (IMFT), Université de Toulouse, CNRS, Toulouse, France*

^d *Aix Marseille University, CNRS, IUSTI UMR 7343, 13013 Marseille, France*

Keywords: Direct Numerical Simulation, Multiphase flow, Nanoporous

1 Introduction

The low permeability of sedimentary clays as well as their chemical characteristics make them particularly suitable to serve as a natural barrier for radioactive waste geological storage. Due to the low permeability, the gas, mainly the hydrogen, originating from the bacterial corrosion of the metallic parts of the facility can be accumulated through time causing significant pressure rise at the interface between sedimentary clay and the facility components. Depending on the pressure, gas is transported through the clayrock with different mechanisms (with increasing pressure: diffusion, visco-capillary flow, dilatant flow and fracturing) [1]. In this work, we will focus on the intermediate multiphase flow without structure evolution.

2 Material and methods

In the present work, we will use different approaches (Direct Numerical Simulations (DNS) (using Lattice Boltzmann Method (LBM) [2] and Smooth Particle Hydrodynamics (SPH) [3]), Pore Network Models (PNM)) and protocols (drainage simulation and co-current simulations) to assess the capacity of such methods to correctly predict the retention curve. Drainage simulations are performed with LBM using inlet and outlet reservoirs and pressure boundary conditions, and PNM. The co-current flow simulations, which consists in setting an initial phase distribution for a given saturation and the performing co-current with periodic boundaries, is performed using LBM and SPH.

The image data used in this study corresponds to an illite sample from Le Puy en Velay basin. Details on the sample, image acquisition and image segmentation may be found in [4]. We use the image segmented by the watershed-based method developed by [4] (Figure 1). There are 180 images of 1096 x 1095 pixels in total, with pixel size 5 x 5 nm. Since the distance between the consecutive images is also 5 nm, the voxel is a cube with 5 nm side. The DNS are performed on a sub-sample extracted from the original image. The sub-sample size is 101 x 101 x 102 voxels. PNM are performed on samples of various sizes. Experimental measurement of the retention curve is obtained using gravimetric water vapour adsorption-desorption isotherms.

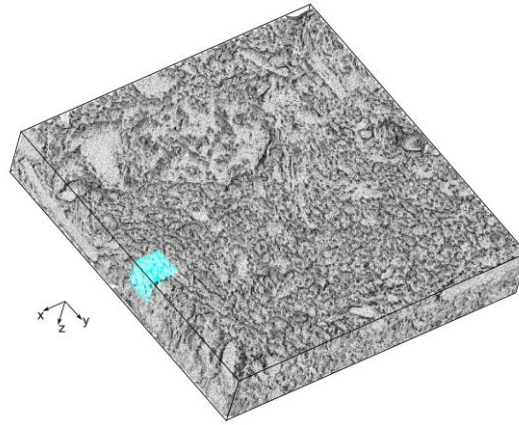


Figure 1: Pore space of the illite sample from FIB-SEM imaging [4].

3 Results

The simulation results will be compared to experimental data and discussed in regards to parametrization, cut length, pore pressure distribution and representativity. We demonstrated the challenges relating to using pore-scale simulations on low resolution data, the discrepancy between a drainage and a co-current approach. We show that despite such limitations, the DNS drainage simulation gives satisfying results for the higher saturation values (Figure 2).

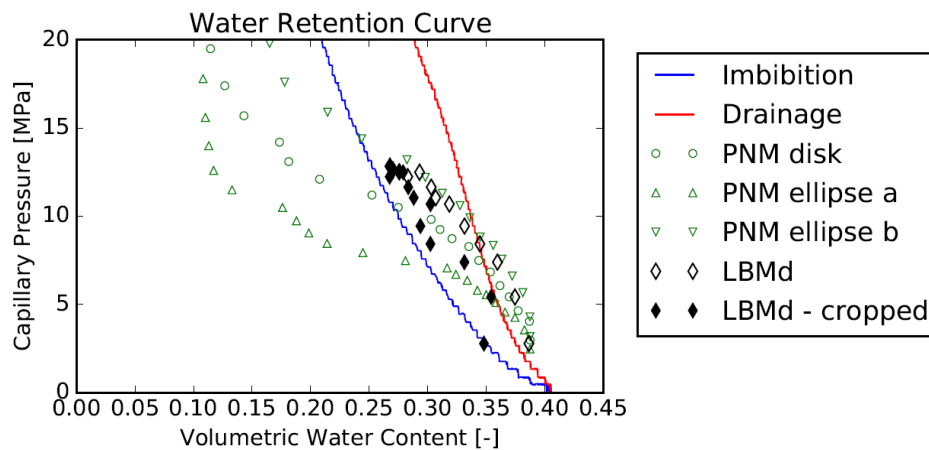


Figure 2: Results from the drainage simulations using LBM and PNM, comparison with experimental data

References

- [1] Kim, K. et al., Discrete dilatant pathway modeling of gas migration through compacted bentonite clay, *International Journal of Rock Mechanics and Mining Sciences*, 137, 104569 (2021).
- [2] Tinet, A.-J. et al., Comparison of various 3d pore space reconstruction methods and implications on transport properties of nanoporous rocks, *Advances in Water Resources*, 141, 103615 (2020).
- [3] Pazdniakou, A. and Dymitrowska, M., Migration of gas in water saturated clays by coupled hydraulicmechanical model, *Geofluids*, (2018)
- [4] Gaboreau, S. et al., Optimization of pore-network characterization of a compacted clay material by tem and FIB/SEM imaging, *Microporous and Mesoporous Materials*, 224, 116-128 (2016)

Computing the diphasic effective properties on nanoporous clayrock using Direct Numerical Simulation

A.-J. Tinet ^a, F. Golfier ^a, A. Pazdniakou ^{a,b}, M. Dymitrowska ^b, M. Prat ^c, J. Vicente ^d

^a *Université de Lorraine, CNRS, GeoRessources, F-54000, Nancy, France*

^b *IRSN, PRP-DGE/SRTG/LETIS, BP 17, 92260 Fontenay-aux-Roses, France*

^c *Institut de Mécanique des Fluides de Toulouse (IMFT), Université de Toulouse, CNRS, Toulouse, France*

^d *Aix Marseille University, CNRS, IUSTI UMR 7343, 13013 Marseille, France*

Keywords: Direct Numerical Simulation, Multiphase flow, Nanoporous

1 Introduction

The low permeability of sedimentary clays as well as their chemical characteristics make them particularly suitable to serve as a natural barrier for radioactive waste geological storage. Due to the low permeability, the gas, mainly the hydrogen, originating from the bacterial corrosion of the metallic parts of the facility can be accumulated through time causing significant pressure rise at the interface between sedimentary clay and the facility components. Depending on the pressure, gas is transported through the clayrock with different mechanisms (with increasing pressure: diffusion, visco-capillary flow, dilatant flow and fracturing) [1]. In this work, we will focus on the intermediate multiphase flow without structure evolution.

2 Material and methods

In the present work, we will use different approaches (Direct Numerical Simulations (DNS) (using Lattice Boltzmann Method (LBM) [2] and Smooth Particle Hydrodynamics (SPH) [3]), Pore Network Models (PNM)) and protocols (drainage simulation and co-current simulations) to assess the capacity of such methods to correctly predict the retention curve. Drainage simulations are performed with LBM using inlet and outlet reservoirs and pressure boundary conditions, and PNM. The co-current flow simulations, which consists in setting an initial phase distribution for a given saturation and the performing co-current with periodic boundaries, is performed using LBM and SPH.

The image data used in this study corresponds to an illite sample from Le Puy en Velay basin. Details on the sample, image acquisition and image segmentation may be found in [4]. We use the image segmented by the watershed-based method developed by [4] (Figure 1). There are 180 images of 1096 x 1095 pixels in total, with pixel size 5 x 5 nm. Since the distance between the consecutive images is also 5 nm, the voxel is a cube with 5 nm side. The DNS are performed on a sub-sample extracted from the original image. The sub-sample size is 101 x 101 x 102 voxels. PNM are performed on samples of various sizes. Experimental measurement of the retention curve is obtained using gravimetric water vapour adsorption-desorption isotherms.

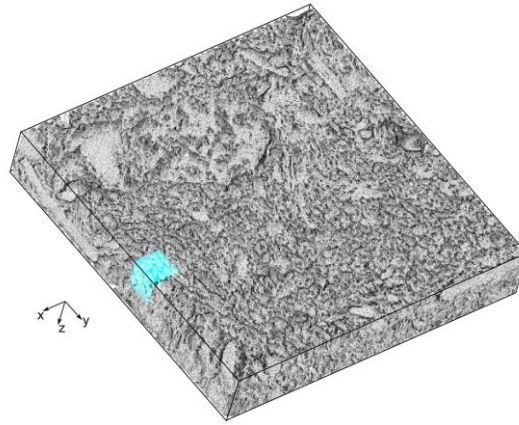


Figure 1: Pore space of the illite sample from FIB-SEM imaging [4].

3 Results

The simulation results will be compared to experimental data and discussed in regards to parametrization, cut length, pore pressure distribution and representativity. We demonstrated the challenges relating to using pore-scale simulations on low resolution data, the discrepancy between a drainage and a co-current approach. We show that despite such limitations, the DNS drainage simulation gives satisfying results for the higher saturation values (Figure 2).

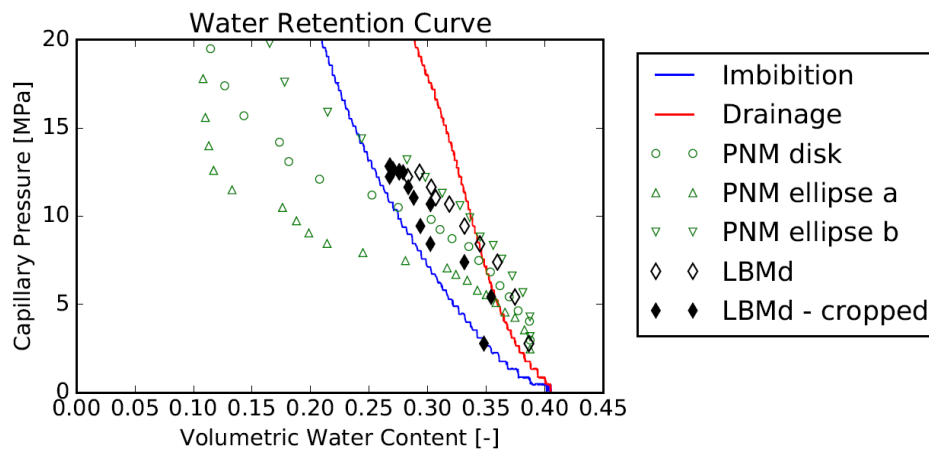


Figure 2: Results from the drainage simulations using LBM and PNM, comparison with experimental data

References

- [1] Kim, K. et al., Discrete dilatant pathway modeling of gas migration through compacted bentonite clay, *International Journal of Rock Mechanics and Mining Sciences*, 137, 104569 (2021).
- [2] Tinet, A.-J. et al., Comparison of various 3d pore space reconstruction methods and implications on transport properties of nanoporous rocks, *Advances in Water Resources*, 141, 103615 (2020).
- [3] Pazdniakou, A. and Dymitrowska, M., Migration of gas in water saturated clays by coupled hydraulicmechanical model, *Geofluids*, (2018)
- [4] Gaboreau, S. et al., Optimization of pore-network characterization of a compacted clay material by tem and FIB/SEM imaging, *Microporous and Mesoporous Materials*, 224, 116-128 (2016)

Macroscopic dynamic capillary pressure for two-phase flow in porous media

D. Lasseux^a, F.J. Valdés-Parada^b

^a*I2M, UMR 5295, CNRS, Université de Bordeaux, 351 Cours de la Libération, 33405 Talence CEDEX, France*

^b*División de Ciencias Básicas e Ingeniería, Universidad Autónoma Metropolitana-Iztapalapa, Avenida Ferrocarril San Rafael Atlixco, Número 186, Iztapalapa C.P. 09310, CDMX, Mexico*

Keywords: Two-phase flow, dynamic capillary pressure, upscaling

1. Introduction

A closed predictive model for the macroscopic pressure difference, often referred to as the *macroscopic capillary pressure*, for two-phase flow in homogeneous porous media is of major importance to form a complete set of governing macroscale equations. This has been a long-lasting subject of research during the past 40 years [1, 3], and the majority of the existing models remain empirical at some level of their derivation. A new closed macroscopic dynamic capillary pressure equation is reported in this work on the basis of the existence of a representative (periodic) unit cell able to locally describe microscale momentum transport in the system. This is carried out with an adjoint method together with a Green's formulation, requiring no other simplifying assumption.

2. Upscaled dynamic capillary pressure

The general framework of the analysis is the incompressible, creeping flow of two Newtonian fluids α and β saturating a homogeneous porous medium whose rigid and spatially homogeneous solid skeleton is the σ -phase.

2.1. Pore-scale and adjoint problems

The pore-scale flow problem can be written in a periodic unit cell representative of the domain as follows ($\alpha = \beta, \gamma$)

$$\nabla \cdot \mathbf{v}_\alpha = 0, \quad \text{in } \mathcal{V}_\alpha, \quad (1a)$$

$$\mathbf{0} = \nabla \cdot \mathbf{T}_{\tilde{p}_\alpha} - \nabla \mathcal{P}_\alpha, \quad \text{in } \mathcal{V}_\alpha, \quad (1b)$$

$$\mathbf{v}_\beta = \mathbf{v}_\gamma, \quad \text{at } \mathcal{A}_{\beta\gamma}, \quad (1c)$$

$$\mathbf{n}_{\beta\gamma} \cdot \mathbf{T}_{\tilde{p}_\beta} = \mathbf{n}_{\beta\gamma} \cdot \mathbf{T}_{\tilde{p}_\gamma} + \mathbf{n}_{\beta\gamma} \left(\langle p_\beta \rangle^\beta - \langle p_\gamma \rangle^\gamma \right)_{\mathbf{r}_{\beta\gamma}} + 2H\gamma \mathbf{n}_{\beta\gamma} + \nabla_s \gamma, \quad \text{at } \mathcal{A}_{\beta\gamma}, \quad (1d)$$

$$\mathbf{v}_\alpha = \mathbf{0}, \quad \text{at } \mathcal{A}_{\alpha\sigma}, \quad (1e)$$

$$\mathbf{v}_\alpha|_{\mathcal{S}_{\alpha i}^-} = \mathbf{v}_\alpha|_{\mathcal{S}_{\alpha i}^+}, \quad i = 1, \dots, N, \quad (1f)$$

$$(\mathbf{n}_\alpha \cdot \mathbf{T}_{\tilde{p}_\alpha})_{\mathcal{S}_{\alpha i}^-} = -(\mathbf{n}_\alpha \cdot \mathbf{T}_{\tilde{p}_\alpha})_{\mathcal{S}_{\alpha i}^+}, \quad i = 1, \dots, N, \quad (1g)$$

$$\langle \tilde{p}_\alpha \rangle^\alpha = 0. \quad (1h)$$

Here, \mathbf{v}_α is the velocity in the α -phase, in which the pressure, p_α , is decomposed as $p_\alpha = \langle p_\alpha \rangle^\alpha + \tilde{p}_\alpha$, $\mathbf{T}_{\tilde{p}_\alpha} = -\tilde{p}_\alpha \mathbf{I} + \mu_\alpha (\nabla \mathbf{v}_\alpha + \nabla \mathbf{v}_\alpha^T)$, $\nabla \mathcal{P}_\alpha = \nabla \langle p_\alpha \rangle^\alpha - \rho_\alpha \mathbf{b}_\alpha$, H is the double mean curvature of the fluid-fluid interface, $\mathcal{A}_{\beta\gamma}$, which unit normal directed from the β phase to the γ phase is $\mathbf{n}_{\beta\gamma}$, μ_α and γ are the dynamic viscosity and interfacial tension and $\nabla_s \gamma$ stands for possible Marangoni effects; $\mathcal{S}_{\alpha i}^\pm$ are the entrances/exits of the α -phase at the i th edge of the periodic unit cell.

For the derivation of the upscaled model, an adjoint problem is now considered that writes

$$\nabla \cdot \mathbf{f}_\beta = \frac{1}{V_\beta}, \quad \text{in } \mathcal{V}_\beta, \quad \nabla \cdot \mathbf{f}_\gamma = -\frac{1}{V_\gamma}, \quad \text{in } \mathcal{V}_\gamma, \quad (2a)$$

$$\mathbf{0} = \nabla \cdot \mathbf{T}_{f_\alpha}, \quad \text{in } \mathcal{V}_\alpha, \quad (2b)$$

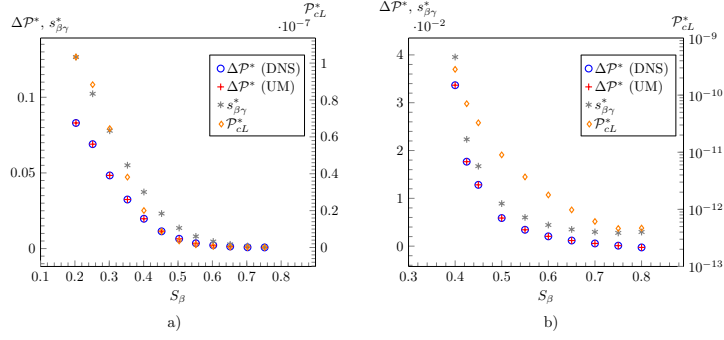


Figure 1: $\Delta\mathcal{P}^*$, obtained from direct numerical simulation (DNS) and predicted from the upscaled equation (3) (UE), along with the interfacial term contribution, $s_{\beta\gamma}^*$, and classical Laplace capillary pressure, \mathcal{P}_{cL}^* (see text), versus the wetting phase saturation, S_β . a) $\mu^* = 0.1$, $Ca = 10$; b) $\mu^* = 10$, $Ca = 0.1$. $\varepsilon = 0.8$.

$$\mathbf{f}_\beta = \mathbf{f}_\gamma, \quad \mathbf{n}_{\beta\gamma} \cdot \mathbf{T}_{f_\beta} = \mathbf{n}_{\beta\gamma} \cdot \mathbf{T}_{f_\gamma}, \quad \text{at } \mathcal{A}_{\beta\gamma}, \quad (2c)$$

$$\mathbf{f}_\alpha = \mathbf{0}, \quad \text{at } \mathcal{A}_{\alpha\sigma}, \quad (2d)$$

$$\mathbf{f}_\alpha|_{\mathcal{G}_{\alpha i}^-} = \mathbf{f}_\alpha|_{\mathcal{G}_{\alpha i}^+}, \quad (\mathbf{n}_\alpha \cdot \mathbf{T}_{f_\alpha})_{\mathcal{G}_{\alpha i}^-} = -(\mathbf{n}_\alpha \cdot \mathbf{T}_{f_\alpha})_{\mathcal{G}_{\alpha i}^+}, \quad i = 1, \dots, N, \quad (2e)$$

$$f_\alpha = 0, \quad \text{at } \mathbf{r}_\alpha^0. \quad (2f)$$

2.2. Macroscopic capillary pressure

Following the procedure detailed in [2], a Green's formula can be used to combine the physical flow problem and the adjoint (closure) problem that leads to the following macroscopic equation for the dynamic capillary pressure

$$\Delta\mathcal{P} = \langle p_\gamma \rangle^\gamma|_{\mathbf{x}_\gamma} - \langle p_\beta \rangle^\beta|_{\mathbf{x}_\beta} = -\boldsymbol{\psi}_\beta \cdot \nabla \langle p_\beta \rangle^\beta + \rho_\beta \mathbf{b}_\beta \cdot \boldsymbol{\varphi}_\beta - \boldsymbol{\psi}_\gamma \cdot \nabla \langle p_\gamma \rangle^\gamma + \rho_\gamma \mathbf{b}_\gamma \cdot \boldsymbol{\varphi}_\gamma + s_{\beta\gamma}, \quad (3)$$

where $\boldsymbol{\varphi}_\alpha = \int_{\mathcal{V}_\alpha} \mathbf{f}_\alpha dV$, $\boldsymbol{\psi}_\alpha = \boldsymbol{\varphi}_\alpha - \int_{\mathcal{A}_{\beta\gamma}} \mathbf{n}_{\alpha\kappa} \cdot \mathbf{f}_\alpha \mathbf{z}_\alpha dA$, and $s_{\beta\gamma} = \int_{\mathcal{A}_{\beta\gamma}} (2H\gamma \mathbf{n}_{\beta\gamma} + \nabla_s \gamma) \cdot \mathbf{f}_\beta dA$. Here, \mathbf{z}_α denotes the position of a point located at $\mathcal{A}_{\beta\gamma}$ relative to the α -phase barycenter in the unit cell.

3. Results

This predictive equation is tested in the simple case of two-phase flow within a square pattern of parallel cylinders of circular cross section (see figure 1 in [2]) with flow along a principal axis of the structure orthogonal to the cylinders axes. The wetting fluid flows under the form of sheets aligned with the mean flow and attached to the cylinders, whereas the non-wetting phase flows in the core, between the wetting fluid sheets. The test consists in comparing the results on the dimensionless macroscopic dynamic capillary pressure $\Delta\mathcal{P}^*$ obtained from the solution of the pore-scale flow problem (DNS), on the one hand, and from the upscaled equation (3) (UE), on the other hand. Results are reported in figure 1 versus the wetting fluid saturation S_β for a porosity $\varepsilon = 0.8$, two viscosity ratios $\mu^* = \mu_\beta/\mu_\gamma$ and two values of the capillary number $Ca = h\ell^2/\gamma$, h being the pressure gradient magnitude in both phases and ℓ the periodic unit cell size. No volume force and no Marangoni effect are considered. The classical Laplace pressure $\mathcal{P}_{cL}^* = 2\langle H^* \rangle_{\beta\gamma}/Ca$, where $\langle H^* \rangle_{\beta\gamma} = \frac{1}{A_{\beta\gamma}^*} \int_{\mathcal{A}_{\beta\gamma}} H^* dA^*$ and $A_{\beta\gamma}^*$ is the dimensionless measure of $\mathcal{A}_{\beta\gamma}$, is also reported in these figures. These results show the excellent agreement between DNS and the upscaled equation, and highlight the fact that the classical Laplace relationship cannot represent a satisfactory estimate of $\Delta\mathcal{P}^*$. The influence of the pressure gradient in each phase (dynamic effects) is also pinpointed.

References

- [1] HASSANIZADEH, S. M. & GRAY, W. G. 1990 Mechanics and thermodynamics of multiphase flow in porous media including interphase boundaries. *Advances in Water Resources* **13** (4), 169–186.
- [2] LASSEUX, D. & VALDÉS-PARADA, F. J. 2023 Upscaled dynamic capillary pressure for two-phase flow in porous media. *Journal of Fluid Mechanics* **959**, R2.
- [3] MARLE, C.-M. 1981 From the pore scale to the macroscopic scale: equations governing multiphase fluid flow through porous media. *Flow and transport in porous media. Proc. Euromech 143, Delft, 1981* pp. 57–61.

Numerical simulation of reactive single phase multicomponent flows in porous media: a sequential coupling between DuMu^X and PHREEQC

S. Tabrizinejadas¹, E. Ahusborde¹, B. Amaziane¹

¹ *Universite de Pau et des Pays de l'Adour, E2S UPPA, CNRS, LMAP, Pau, France.*

Keywords: Reactive transport, Coupled processes, DuMu^X, PHREEQC

1. Introduction

Reactive transport modeling is widely used in several environmental applications such as CO₂ sequestration and nuclear waste disposal. Significant efforts are made to improve the capacity of the models in comprehensively representing the reactive transport processes. Among these efforts, DuMu^X [1] with a modular-based structure allows for efficient modeling of the multi-physical processes in porous media and implementing constitutive relations. Despite the capacity of DuMu^X in integrating the full complexity of hydraulic and chemical coupled processes on a reservoir scale, its use is still relatively limited due to the constraints in integrating with realistic chemical descriptions of fluids and rocks. Therefore, the aim of this study is to decouple the hydraulic and chemical sub-problems and solve the latter with a geochemical code for handling complex chemical systems. Among the variety of geochemical codes, the software package PHREEQC [2], a code for simulating aqueous speciation and reaction path, has obtained popularity due to the convenience of defining and solving the desired geochemical system via basic scripts. Coupling DuMu^X with PHREEQC brings the convenience of efficient modeling of the multi-physical processes together with access to the rich chemical database of PHREEQC and flexibility in defining the chemical system.

2. Mathematical model and numerical scheme

A reactive single phase multicomponent flow process in porous media is considered. Chemical reactions can involve solutes, sorbed species, and minerals. The problem is modeled by Darcy's law for the conservation of momentum and a mass conservation law is written in an element-based approach. The system is closed by a mass action law for each equilibrium reaction and an ordinary differential equation for each kinetic reaction. The coupling between the hydraulic transport part in DuMu^X and the chemical reaction part in PHREEQC has been done through a sequential non-iterative approach (SNIA) using PhreeqcRM [3]. PhreeqcRM is called in each time step as the reaction engine for updating the values of element concentrations which are given by DuMu^X after a transport step. Precisely, the concentration of each element participating in the reactive transport is governed by a mass conservation law that writes:

$$\phi \frac{\partial(u_m + u_f)}{\partial t} + \mathbf{L}(u_m) = r_{kin}, \quad (1)$$

where, ϕ is the porosity, u_m and u_f are mobile and fixed total concentration vectors of all elements in the system, respectively. \mathbf{L} is the diffusion-advection operator. The right-hand side term r_{kin} is the kinetic reaction rate which is a nonlinear function of the concentrations. As an example, following [4], one time step of size Δt_n from t_n to t_{n+1} using SNIA for solving the system (1) can be summarized as:

- Hydraulic transport step (DuMu^X): $\phi \frac{v_m^{n+1} - v_m^n}{\Delta t_n} + \mathbf{L}(v_m^{n+1}) = 0$, $v_m^n = u_m^n$, provided with boundary conditions,

- Chemical reactive step (PHREEQC) with f as the set of equations used in the chemical system:

$$\begin{cases} \phi \frac{d(w_m + u_f)}{dt} = r_{kin} \text{ in } [t_n, t_{n+1}], & w_m(t_n) = v_m^{n+1}, \\ f(w_m, u_f, r_{kin}) = 0, \end{cases}$$

- Update solution $u_m^{n+1} = w_m^{n+1}$.

For the spatial discretization, we used a cell-centered finite volume method combining an upwind scheme for the convective terms and a two-point flux approximation for the diffusive terms. An implicit Euler scheme is used for time discretization.

3. Numerical results

Firstly, we validated our coupling approach on a 1D single phase reactive flow and a calcite dissolution benchmark which is proposed in [5]. Figure 1 compares the concentration of mobile elements as well as minerals obtained with coupled DuMu^X-PHREEQC and the reference solution given by PHREEQC. Calcium and carbonate are initially at equilibrium in the solution. With the progressive introduction of magnesium, calcite mineral starts to dissolve and dolomite precipitates. A very good accordance between results is observed. The extension of this sequential coupling to deal with multiphase reactive flows is in progress. The first results obtained by coupling the two platforms are encouraging and promising, and open up new prospects for efficient modeling of multiphase reactive transport for a variety of realistic applications in the subsurface.

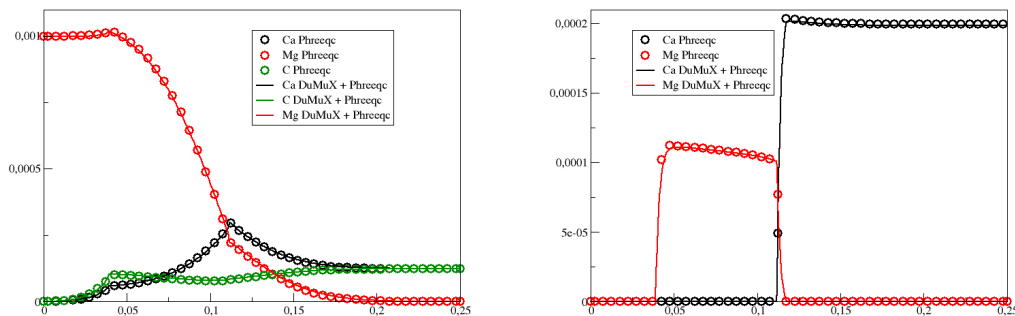


Figure 1: Profiles for total mobile concentrations of elements and concentrations of minerals at $t = 10000$ s for the test case presented in [5].

4. Acknowledgements

This project has received funding from the European Union’s Horizon 2020 research and innovation program under grant agreement 28467 No 847593 (WP DONUT).

References

- [1] T. Koch *et al.* DuMu^X 3 - an open-source simulator for solving flow and transport problems in porous media with a focus on model coupling, *Computers & Mathematics with Applications*, 81, 423-443 (2021).
- [2] D. L. Parkhurst, C.A.J Appelo. Description of input and examples for PHREEQC version 3-A computer program for speciation, batch-reaction, one-dimensional transport, and inverse geochemical calculations, U.S. Geological Survey Techniques and Methods (2013).
- [3] D. Parkhurst, L. Wissmeier. PhreeqcRM: A reaction module for transport simulators based on the geochemical model PHREEQC. *Advances in Water Resources*, 83, 176-189 (2015).
- [4] A. Nardi, A. Idiart, P. Trinchero, L.M. de Vries, J. Molinero. Interface COMSOL-PHREEQC (iCP), an efficient numerical framework for the solution of coupled multiphysics and geochemistry, A reaction module for transport simulators based on the geochemical model PHREEQC, *Computers & Geosciences*, 69, 10-21 (2014).
- [5] J. Daniel, J. de Dreuzy, B. Cochevin. TReacLab: An object-oriented implementation of non-intrusive splitting methods to couple independent transport and geochemical software, *Computers & Geosciences*, 109, 281-294 (2017).

Session
Caractérisation, imagerie,
génération numérique de milieux poreux

Analysis of evaporation in a hydrophobic micro-model

M.A.Ben Amara^a, N. Sghaier^a, M. Prat^b

^a *Laboratoire d'Etudes des Systèmes Thermiques et Energétiques de Monastir, Tunisia*

^b *Université de Toulouse, INPT, UPS, IMFT, Avenue Camille Soula, F-31400 Toulouse, France and CNRS, IMFT, F-31400 Toulouse, France*

Keywords: Evaporation pattern, micro-model, drying, image processing.

1 Introduction

Numerous engineering and environmental applications involve evaporation from a porous medium. In the present work, evaporation is studied in a quasi-two-dimensional micro-model composed of spherical hydrophobic beads of 1 mm in diameter sandwiched between two hydrophobic glass plates with the lower plate coated by a polymeric film (RTV). The study is based on two visualization experiments. In the first experiment, the micro-model is held horizontally and filled with a NaCl aqueous solution at 5% in NaCl mass fraction. In the second experiment, the micromodel is vertical and filled with a solution at 25%. The consideration of a saline solution is motivated by the study of salt crystallization induced by the evaporation process. However, the focus here is on the drying pattern prior to the occurrence of crystallization.

2. Results

As illustrated in Fig.1, the micromodel orientation, i.e. vertical or horizontal, leads to two markedly different drying patterns. In the horizontal case, invasion by the air as the result of evaporation occurs preferentially in the central region of the micromodel with a well-defined boundary between the gaseous region and the liquid region. In the vertical case, the pattern is characterized by an almost flat travelling front separating the gas region (on top) from the liquid region.

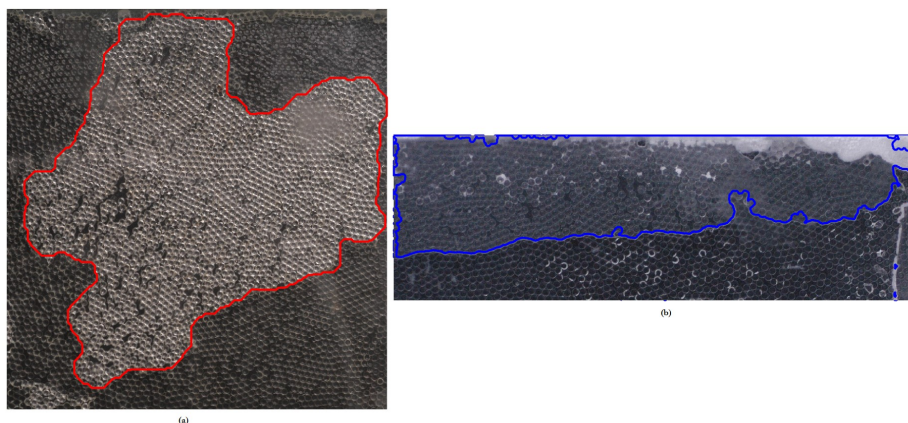


Figure 1: Drying pattern: on the left: horizontal micro-model (gas region in light grey, liquid region in dark grey, the red line corresponds to the boundary between both regions), on the right: vertical micro-model (the blue line corresponds to the boundary between the gas region (lighter grey) and the liquid region (darker grey)).

2 Analysis

The almost flat front in the vertical case is consistent with the expected combined effects of capillarity and gravity in a hydrophobic system. The puzzling pattern is the one observed in the horizontal case. From previous works on drying in hydrophobic systems [1, 2], it is indeed expected that an almost flat travelling front also forms in the horizontal case. In order to explain the observed unexpected pattern, the micromodel is partitioned in eight regions of interest. The porosity, pore body distribution (PSD) and pore

throat distribution (TSD) are determined in each region of interest thanks to image processing techniques based on the identification of the Delaunay and Voronoi diagram from the centres of the beads in the micro-model (Fig.2).

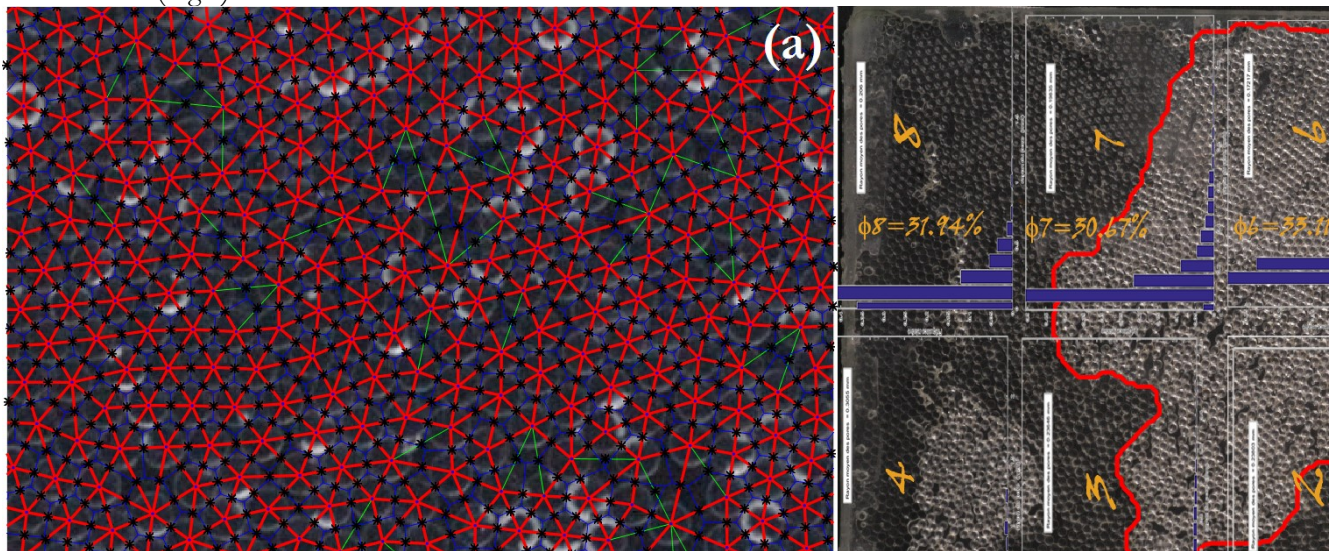


Figure 2: (a) Zoom of Voronoi tessellation (in blue) and Delaunay triangulation (in red) from beads centres in the micromodel. (b) PSD in the eight regions of interest in the micromodel.

3 Conclusion

This investigation leads to the conclusion that the preferential invasion seen in the experiment is due to a different arrangement of the beads in the region preferentially invaded leading to different pore body and throat size distribution compared to the adjacent regions. In other words, a heterogeneity at larger scale than the bead scale disorder is responsible for the observed pattern in the horizontal case. Thus, the present investigation sheds light on the combined effects of hydrophobicity, gravity, capillarity and large scale disorder on evaporation in porous media. This situation is currently further investigated from pore network simulations on a two-dimensional network.

References

- [1] O.Chapuis, M.Prat, Influence of wettability conditions on slow evaporation in two-dimensional porous media, Phys. Rev. E, 75, 046311 (1-11)(2007)
- [2] H.Chraïbi, M.Prat, O.Chapuis, Influence of contact angle on slow evaporation in two dimensional porous media, Phys. Rev. E, 79, 026313 (2009)

Auto-weighting multitask inverse problems for reactive flows at the pore-scale with evolving fluid-solid interface and related uncertainty quantification

Sarah Perez^{*1} and Philippe Poncet¹

¹Laboratoire de Mathématiques et de leurs Applications [Pau] – Université de Pau et des Pays de l'Adour, Centre National de la Recherche Scientifique – France

Résumé

Pore-scale modelling of reactive flows in porous media is intrinsically related to X-ray microtomography experiments. Advances in this imaging technique coupled with efficient numerical simulation offer a valuable opportunity to investigate dynamical processes and study their impact on the macro-scale properties such as the upscaled porosity and permeability. This is of great importance in risk management from the perspective of CO₂ storage in natural underground reservoirs. Ensuring the reliability of pore-scale modelling and simulation is, therefore, crucial and it requires embedding uncertainty quantification concerns. Uncertainties arise from the microtomography imaging process itself where artefacts, noise and unresolved morphological features are intrinsic limitations inducing important deviations in the estimation of petrophysical properties (1). In addition, proper assessment of the kinetic parameters in dissolution processes also raises challenges. Mineral reactivities are critical parameters to account though they commonly suffer from discrepancies of several orders of magnitude (2). Therefore, we aim to quantify both morphological uncertainties due to unresolved features in X-ray microtomography and kinetic parameter uncertainties for reactive processes in porous media.

In this presentation, we focus on a multitask inverse problem for reactive flows at the pore scale through a data assimilation approach that incorporates uncertainty quantification by means of a Bayesian Physics-Informed Neural Network (BPINN). This novel approach combines dynamical imaging data and physics-based regularization induced by the PDE model of calcite dissolution. This PDE model is a two-scale porosity formulation, similar to the benchmark introduced in (3).

We build the present technique upon the efficient data-assimilation framework developed in (4), which robustly addresses multi-objective and multiscale Bayesian inverse problems including latent field reconstruction. The strategy relies on an adaptive and automatic weighting of the target distribution parameters and objectives. It benefits from enhanced convergence and stability compared to conventional formulations and reduces sampling bias by avoiding manual tuning of critical weighting parameters (5). The adjusted weights bring information on the task uncertainties, improve the reliability of the noise-related and model adequacy estimates and ensure unbiased uncertainty quantification.

^{*}Intervenant

Finally, we present posterior distributions on the chemical inverse parameters in addition to local morphological uncertainties on the micro-porosity field for pore-scale imaging on calcite dissolution.

References:

- (1) S. Perez, P. Moonen, and P. Poncet, On the Deviation of Computed Permeability Induced by Unresolved Morphological Features of the Pore Space, *Transport in Porous Media*, 141:151-184 (2022).
- (2) C. Noiriél, M. Oursin, G. Saldi, and D. Haberthür, Direct determination of dissolution rates at crystal surfaces using 3D X-Ray microtomography, *ACS Earth and Space Chemistry*, 3(1):100-108 (2019).
- (3) S. Molins, C. Soullaine, N.I. Prasianakis, A. Abbasi, P. Poncet, A.J.C Ladd, V. Starchenko, S. Roman, D. Trebotich, H.A. Tchelepi, and C.I Steefel, Simulation of mineral dissolution at the pore scale with evolving fluid-solid interfaces: review of approaches and benchmark problem set, *Computational Geosciences*, 25(4):1285-1318 (2021).
- (4) S. Perez, S. Maddu, I.F. Sbalzarini, and P. Poncet, Adaptive weighting of Bayesian physics informed neural networks for multitask and multiscale forward and inverse problems, *under revision for Journal of Computational Physics* (2023).
- (5) S. Maddu, D. Sturm, C. L Müller, and I. F Sbalzarini, Inverse Dirichlet weighting enables reliable training of physics informed neural networks, *Machine Learning: Science and Technology*, 3(1):015026 (2022).

Dispersion, stretching and direct visualization in 3D porous media

M. Souzy^{a,b,c}, T. Leborgne^b, Y. Méheust^b, H. Lhuissier^a, B. Metzger^a

^aIUSTI-CNRS, Marseille, France

^bOSUR-CNRS Rennes, France

^cINRAE RECOVER, Le Tholonet, France

Keywords: Porous media, direct visualization, dispersion, mixing, transport process, experimental

1 Introduction

Geomaterial are complex porous material presenting a wide diversity of structures, which set the flow kinematic of any fluid through it. When rainwater flow through soils, it flows through an interconnected network of pores of various sizes. This leads to complex transport processes which occur redundantly within these tortuous geometries: for instance when expansive resin is injected to stabilize a soil and reinforce its mechanical properties to prevent cracks [1], during pollutant transport in soils and aquifer [2], or during bacteria injection for bio-cementation to reinforce hydraulic structures and prevent catastrophic landslides or dam failure. In a context of climate change, unprecedented solicitations (e.g. an increase in the frequency of extreme events such as heavy precipitations, or sea level rise) will be applied to materials and hydraulic infrastructures, increasing the occurrence of transport processes which may damage infrastructures and cause severe inconveniences to entire communities. Therefore, the stabilization and reinforcement of soils could prevent catastrophic events in the incoming years, implying that we must deepen our understanding of the mechanisms at play to optimize such processes. **The understanding of the mechanisms controlling the flow kinematics at the pore scale** is therefore decisive to predict and control the transport processes (dispersion and mixing).

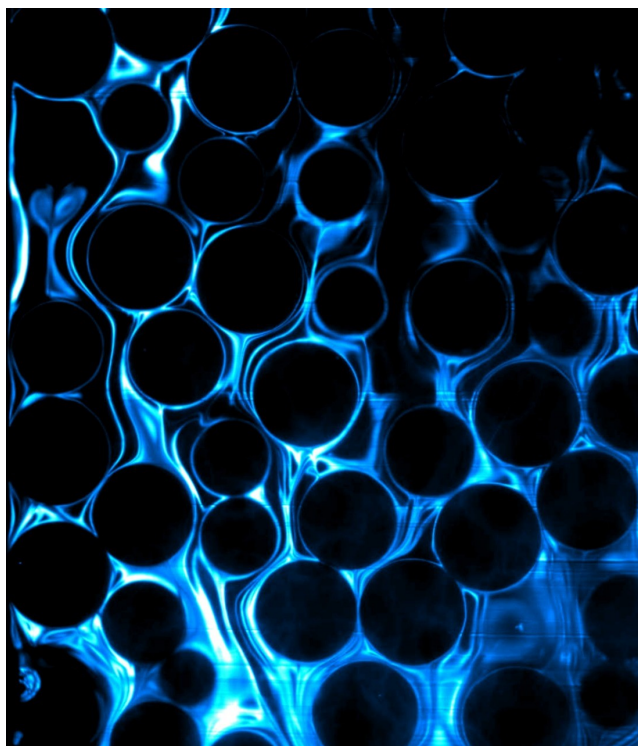


Figure 1: A layer of fluorescent dye is injected in a 3D transparent porous media and visualized using a laser sheet. The blob of dye is heterogeneously elongated while flowing through the pore network, leading to a complex mixing process.

Because of the opaque nature of geomaterial, direct visualizations are particularly challenging in porous material such as soils. However, recent development of experimental techniques including index matching [3], allow to develop transparent porous media to perform direct visualization of the flow in these artificial materials.

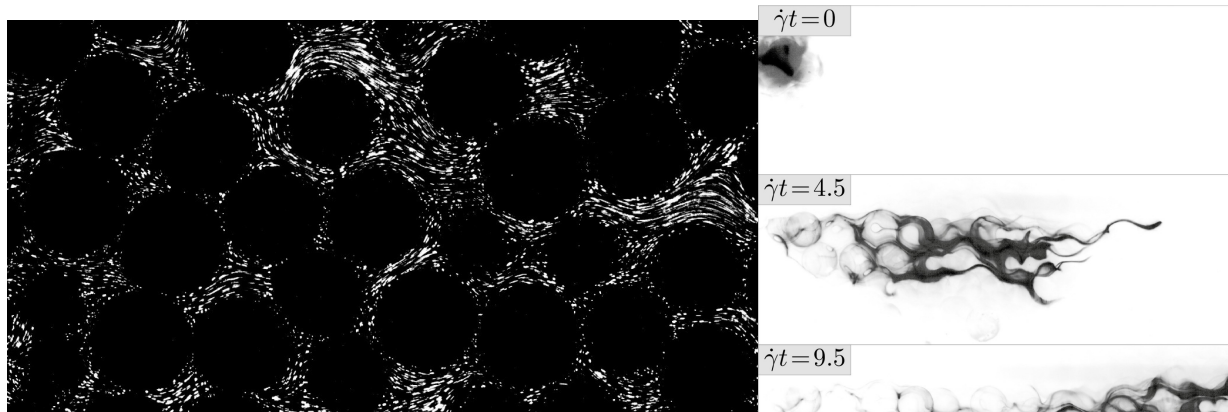


Figure 2: (Left) Long time exposure picture of PIV experiment in a 3D porous media highlighting the wide distribution of velocity in such complex flow. (Right) Successive images of a blob of dye injected in the bulk of a 3D porous media. The blob tends to form elongated lamellae structures which get stretched while being advected, thus leading to a complex homogenization process of the dye concentration distribution.

I will here discuss about how such approach allows to study porous media composed of randomly packed solid monodisperse spheres, allowing to directly visualize the flow within the bulk of the 3-D media, and to investigate how a blob of dye stretches and get mixed when injected within such 3-D porous media. Using Particle Image Velocimetry techniques (PIV), successive scans of the velocity field are used to provide highly resolved experimental reconstruction of the 3-D Eulerian fluid velocity field in the bulk of the porous media. From the experimentally measured 3D velocity field, the stretching process (how fluid material line gets elongated within the flow) and the dispersion process (how a blob of dye explores its surrounding media) are characterized, and an explanation for the reported anomalous dispersion will be discussed [4].

References

- [1] Dei Svaldi A., Favaretti M., Paschetto A., Vinco G. «Analytical modelling of the soil improvement by injections of high expansion pressure resin.» *Bulletin für angewandte Geologie*, 10(2), 71-81 (2005).
- [2] Dentz M., Le Borgne T., Lester D. R., and de Barros F. P. «Mixing in groundwater.» *The Handbook of Groundwater Engineering*, pp. 401-430 (2016).
- [3] Dijkstra J. A., Rietz F., Lorincz K. A., van Hecke M., and Losert W. «Invited article : Refractive index matched scanning of dense granular materials.» *Review of Scientific Instruments*, vol. 83, no. 1, pp. 011301–011301 (2012).
- [4] Souzy M., Lhuissier H., Méheust Y., Le Borgne T., and Metzger B. «Velocity distributions, dispersion and stretching in three-dimensional porous media.» *Journal of Fluid Mechanics*, vol. 891 (2020).

Hydrodynamics in a coarse porous layer above a sandy bed with application to contact erosion in hydraulic structures

P. Philippe^a, R. Béguin^b

^aRECOVER, INRAE, Aix-Marseille University – Aix-en-Provence, 13100 France

^bgeophyConsult, 73000 Chambéry, France

Keywords : porous flow, refractive index matching, particle image velocimetry, contact erosion

1 Introduction

Many natural or industrial processes take place within a porous medium subject to flow, and it is essential to characterise this type of flow as accurately as possible. Applications include the transport of particles of all types, the diffusion of chemical compounds, depth filtration and some of the mechanisms of internal erosion of soils. Of particular interest here is contact erosion where porous flow along a coarse layer induces erosion of particles from a finer soil layer in contact. Once eroded, the fine particles are transported through the pores and constrictions of the coarse material. This phenomenon is often suspected in river embankments. The present work provides a better understanding of flow at the pore scale through the use of an experimental model system based on an optical technique combining refractive index matching with plane laser-induced fluorescence. Pore flow can then be measured by particle image velocimetry within a granular layer in contact with an underlying fine sand layer, in a situation where erosion of the sand layer is not active. The results demonstrate in particular that correct modelling of such flows cannot be satisfied solely with average values, as is often suggested in the literature, but must take account of the variability of porous flow, in time for turbulent flow or in space in the present porous geometry case. With this in mind, statistical modelling of contact erosion is proposed and compared with previous sample-scale contact erosion tests, with satisfactory agreement.

2 Methodology and results

2.1 Experimental device and techniques

The set-up is presented in Figure 1 and consists of a cell containing a layer of fine sand topped by a layer of larger spherical beads within which a liquid flow is imposed at a controlled constant rate.

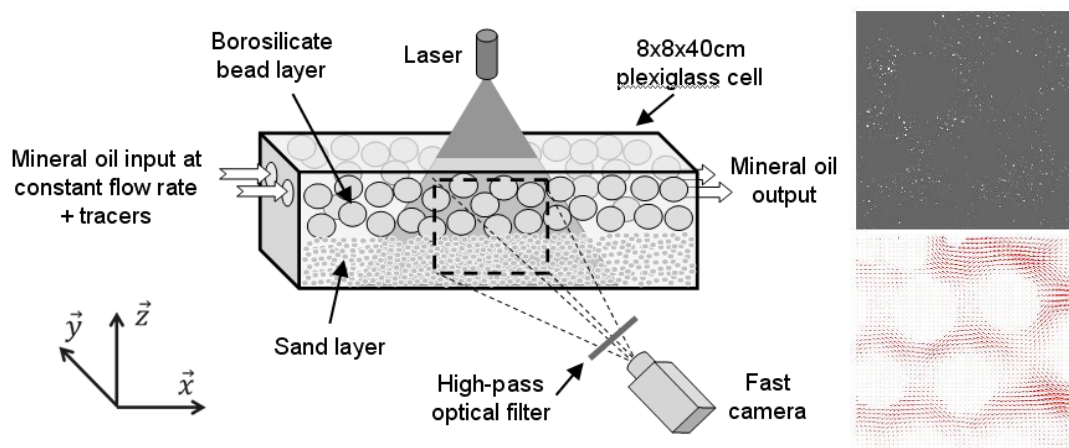


Figure 1: Experimental device with typical images of tracers and deduced velocity field after PIV processing.

The liquid is a mixture of mineral oils whose refractive index is precisely matched to that of the borosilicate glass of the beads. The top layer is thus transparent, and illumination by a vertical laser sheet activates the fluorescence of tracers seeded in the liquid. Using a fast camera, a high-pass optical filter is used to collect only the light re-emitted by fluorescence and eliminate any spurious reflections of the laser. The images obtained over a short exposure time (see top right picture) are analysed in pairs by a PIV algorithm to provide, after averaging over a large series, the stationary velocity field in the illuminated 2D plane (see bottom right picture). In addition, a very long exposure time provides an image of the internal structure of the section and allows porosity in particular to be deduced.

2.2 Hydrodynamics of the coarse layer

Mean vertical profiles of velocity and porosity are obtained, where a transition zone near the sand bed is clearly observed and characterised. Then, we calculate first the distribution of the longitudinal velocity, which is consistent with previous experimental and numerical studies, and second the distribution of the shear stress as presented in Figure 2 (left graph). Both distributions exhibit large tails towards the higher values reflecting the spatial variability of the flow, with a clear distinction between the bulk and the transition zone.

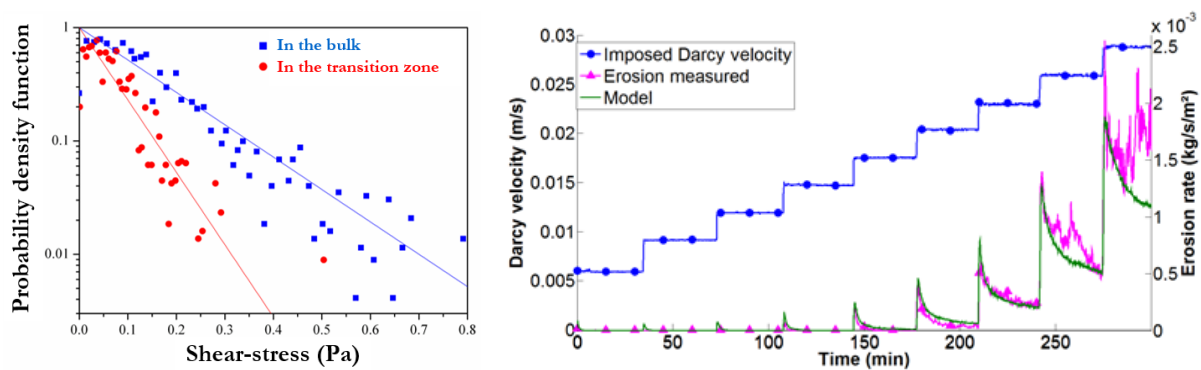


Figure 2: Shear-stress distribution with distinction between bulk and transition zone; Calibration of our statistical model on a typical contact-erosion test [3].

2.3 Application to contact erosion

The above results show that an approach limited solely to mean hydrodynamic quantities, as is frequently done in the literature, will be far too limiting. It is important to include the variability aspect when modelling an erosive flow, particularly because of the threshold effect associated with sediment erosion. This variability can be temporal, as in turbulent flows, or spatial, in the present case of laminar porous flow. Here, with this specific geometry of contact erosion, we were able to build a probabilistic model based on the exponential distribution of the shear stress exerted in the transition zone. A calibration with only two adjustable parameters gives very good agreement with a typical macroscopic contact erosion test, as shown in Figure 2 (right graph).

References

- [1] Hlushkou and Tallarek, Transition from creeping via viscous-inertial to turbulent flow in fixed beds, *Journal of Chromatography A*, 1126 (1-2), 70-85 (2006).
- [2] Bonelli (Ed.), *Erosion of Geomaterials*. Wiley-ISTE, New-York (2012).
- [3] Béguin et al., Pore-scale flow measurements at the interface between a sandy layer and a model porous medium: Application to statistical modeling of contact erosion, *Journal of Hydraulic Engineering ASCE*, 139, 1-11 (2013).

Open-cell foam ultra-realistic microstructure model: a new generation workflow validated through experimental data and CFD simulations

E. Agostini^{a,b}, M. Moreaud^a, G. Boccardo^b, Y. Haroun^a, D. Marchisio^b

^aIFP Energies Nouvelles, Rond-point de l'échangeur de Solaise BP3, 69360 Solaise, France

^bDISAT, Politecnico di Torino, Corso Duca degli Abruzzi 24, 10128, Torino, Italy

Keywords: Open-cell Foams, stochastic microstructure model, Porous Media, CFD

1 Introduction

Over the past thirty years, the use of open-cell foams has increased significantly in many domains of the process industry, from catalyst support in fixed bed reactors to particulate filters for molten metals. Their characteristic high porosity and large specific surface are appreciated to reduce pressure drops and high mass transfer coefficients. Commercially available foams are usually labelled by their *pore per inch* (PPI) value, an approximation of the average pore diameter size, and porosity ε . Few information is available regarding other key geometric parameters, such as Specific surface S_V , or tortuosity τ , yet necessary to attempt to link macroscopic geometric descriptors to performance.

The objective of this abstract is to introduce an ultra-realistic microstructure foam model and its digital workflows tested and validated to reproduce a great variety of geometries. Macro-geometric characteristics can be computed from these virtual microstructures, to investigate the relationship between macro-descriptors and foams performances and optimize the geometric structure according to the different application areas.

2 Materials and Methods

Several models have been proposed to represent the geometry of open-cell foams with random Voronoi tessellations, allowing to generate objects with similar levels of complexity [1]. Starting from an initial set of random points called *seeds*, the Voronoi algorithm generates open cellular structures closely resembling those of ceramic or metallic foams. The aim of this workflow is to create realistic foam structures, with geometric features comparable to those of real foams. To achieve this result, the workflow uses morphological modifications of three-dimensional binary volumes composed of voxels, using the free software plug im! (<https://plugim.fr>). The seeds are generated using the sphere aggregation model proposed by [2], which allows to control the compactness and repulsion of the aggregated spheres. This procedure allows the creation of a huge variety of foam structures with similar macroscopic characteristics (ε , S_V and τ) originated from different spheres aggregates. The flowchart in Fig. 1 show the steps composing the workflow and leading to the generation of an open-cell foam geometry.

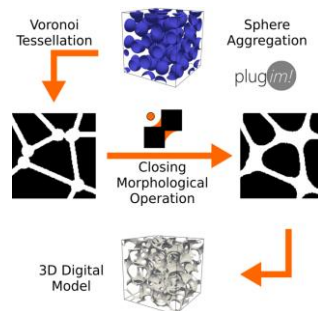


Figure 1: A schematic representation of the workflow.

Real foams samples were used to carry out experimental measurements and to extract information regarding micro- and macroscopic geometric descriptors, analysing the image obtained from the x-rays tomography. The validation of the open-cell foams obtained from our workflow was carried out both in terms of macroscopic geometric descriptors and in terms of fluid flow, comparing pressure drops measurements obtained experimentally as well as from the fluid flow numerical simulations with CFD. Measurements of pressure drops were carried out on a vertical custom-built column packed with foam

pellets in which distilled water was circulated. Four foams were considered: two Al_2O_3 ceramic foams, 20 and 40 PPI, and two NiCr metallic foams, 14 and 30 PPI. Tab. 1 report values of ε , S_V and τ for each foam.

Foam type	Porosity ε (%)	Spec. Surface S_V (m^2/m^3)	Tortuosity τ	$e_{r,\varepsilon}$ (%)	e_{r,S_V} (%)	$e_{r,\tau}$ (%)
Al_2O_3 20 PPI	75.9	852	1.2	0.9	0.3	0.1
Al_2O_3 40 PPI	75.7	1715	1.17	2	1	0.9
NiCr 14 PPI	91.9	1054	1.24	0.6	3	5.6
NiCr 30 PPI	92.1	3091	1.22	0.1	4.7	4

Table 1: Geometrical macro-descriptors of the foam investigated, and the relative error for their digital replica.

3 Results and Conclusions

The workflow presented in Section 2 was used to generate a digital replica of real foams investigated previously. The generation parameters were fixed to obtain foam structures such that their macroscopic descriptors (ε , S_V and τ) will have a relative error compared to the data extracted from the tomography images, no greater than 10%. The relative error with respect to the original geometry is reported in Tab. 1. The comparison of the pressure drops values measured experimentally, calculated from the CFD simulations and from two well known correlations from literature, shows that there is good agreement between the real foam geometries and their digital replica, validating the proposed workflow. This shows how the generation procedure can be fine-tuned to create the digital foam that replicates the desired descriptors with great accuracy. An example of these results is reported in Fig. 2, where Fig. 2a and 2b show the structure of the real NiCr foam and its replica, whereas Fig. 2c report the results of the pressure drops comparisons.

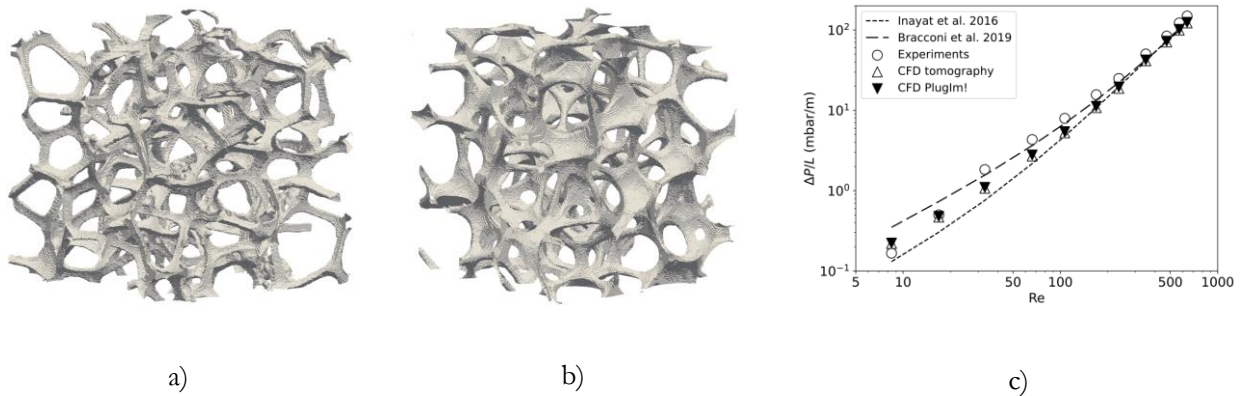


Figure 2: Results for a) NiCr 14 PPI real foam (tomography images), b) its digital replica and c) the comparison of pressure drops from real/virtual replica and literature correlations.

In conclusion, the presented workflow correctly describes foam structures and reproduces their performances in terms of pressure drops, at a limited computational cost, while still allowing the generation of a wide spectrum of digital structures. Using this realistic foam microstructure model, future perspectives will be to improve the understanding of the transport phenomena occurring inside open-cell foams, by exploring, in-silico, a wider number of cases discerning impacts of geometrical descriptors like porosity or tortuosity.

References

- [1] Agostini, E., Boccardo, G., Marchisio, D., An open-source workflow for open-cell foams modelling: Geometry generation and CFD simulations for momentum and mass transport, *Chemical Engineering Science*, Volume 255, 117583, ISSN 0009-2509 (2022).
- [2] G. Ferri, S. Humbert, M. Digne, J.-M. Schweitzer, M. Moreaud. Simulation of Large Aggregate Particles System with a New Morphological Model. *Image Anal Stereol*, 40- 2 (2021).

Characterization of multiscale porosity in activated carbon by X-ray tomography and FIB-SEM

O. Darouich ^{a,b}, P. Sénéchal ^c, D. Barresi ^b, P. Moonen ^{a,c}

^aLFCR, E2S UPPA, CNRS, TOTAL, Université de Pau et Pays de l'Adour - Pau, France

^bTESCAN France - Fuveau, France

^cDMEX, E2S UPPA, CNRS, Université de Pau et Pays de l'Adour - Pau, France

Keywords: Multiscale porous materials, Activated carbon, X-ray tomography, FIB-SEM

1 Introduction

Many natural and man-made porous media exhibit pore sizes covering a wide range of length scales. This so-called multi-scale porosity greatly impacts key-properties such as the material's reactivity and permeability and are of interest in areas including energy storage, adsorption, and catalysis.

Activated carbon features an exceptional porosity, a high specific surface area, and a remarkable adsorption capacity. Furthermore, the porous structure of activated carbon enables selective interactions with diverse substances, facilitating efficient removal of pollutants and enabling specific chemical reactions, which render the material ideal for applications in fields such as catalysis, water purification, air decontamination, and energy production [1][2].

The characterization of the multiscale porosity in activated carbon is challenging due to its wide range of pore sizes. Conventional characterization techniques such as mercury porosimetry, X-ray tomography or Scanning Electron Microscopy (SEM), when used independently, offer limited insights into the complete range of pore sizes present in these materials [3]. Consequently, there is a need to develop combined approaches that enable a more comprehensive characterization of multiscale porosity.

2 Methodology

In this study, we propose the combined use of X-ray tomography and FIB-SEM as a promising approach to visualize and quantify the pore system at different scales, aiming to achieve a better understanding of the pore structure and properties of multiscale porous activated carbon samples (Figure 1). By integrating these techniques, we can obtain a more comprehensive characterization of multiscale porosity, incorporating fine resolution information and an extended field of view.

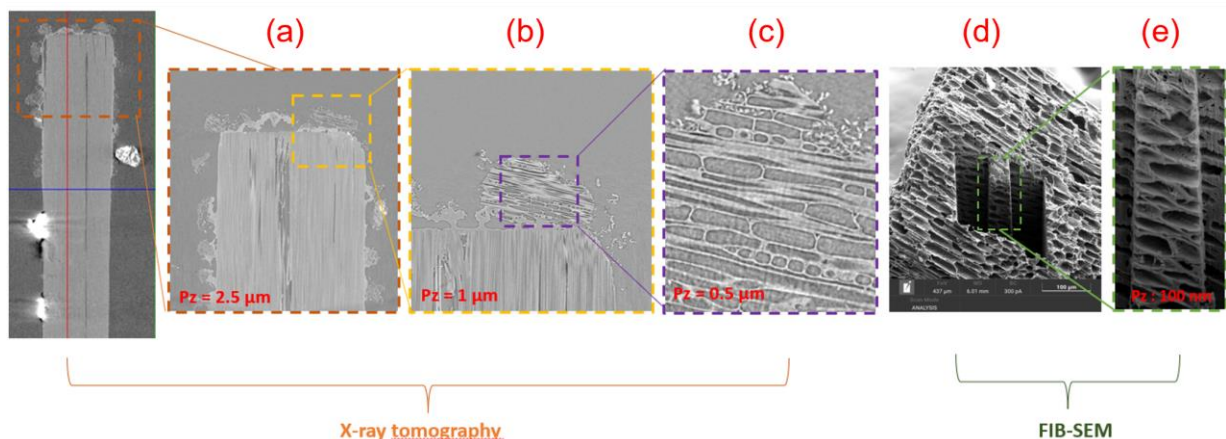


Figure 1: Coupling X-ray tomography and FIB-SEM to characterize activated carbon.

A large number of activated carbon grains were fixed on a carbon rod by means of x-ray transparent varnish. A first X-ray tomography was performed with a Zeiss Xradia Versa 510 at a resolution of 2.5 $\mu\text{m}/\text{voxel}$ and allowed for the localization of the different grains as well as an initial impression of their

shape (Figure 1a). A grain was selected and imaged in more detail, first at 1 $\mu\text{m}/\text{voxel}$ to capture the full grain (1b), and then at 0.5 $\mu\text{m}/\text{voxel}$ (1c) providing more precise information about the macro-scale porosity and its associated morphological and topological parameters. Next the carbon rod was positioned in a FIB-SEM (Tescan Amber X) and a 10 nm conductive carbon coating was applied. The FIB enabled cutting a trench around the region of interest (1d). By intermittently removing material with the FIB and taking images at 100nm/px with the SEM, a 3D stack of the volume of interest was obtained (1e). The latter enabled quantifying the part of the pore system invisible by X-ray tomography. This combination of techniques provided a comprehensive view of the pore structure of the seeds, offering valuable insights into pore sizes and shapes (Figure 2) as well as their connectivity (not shown).

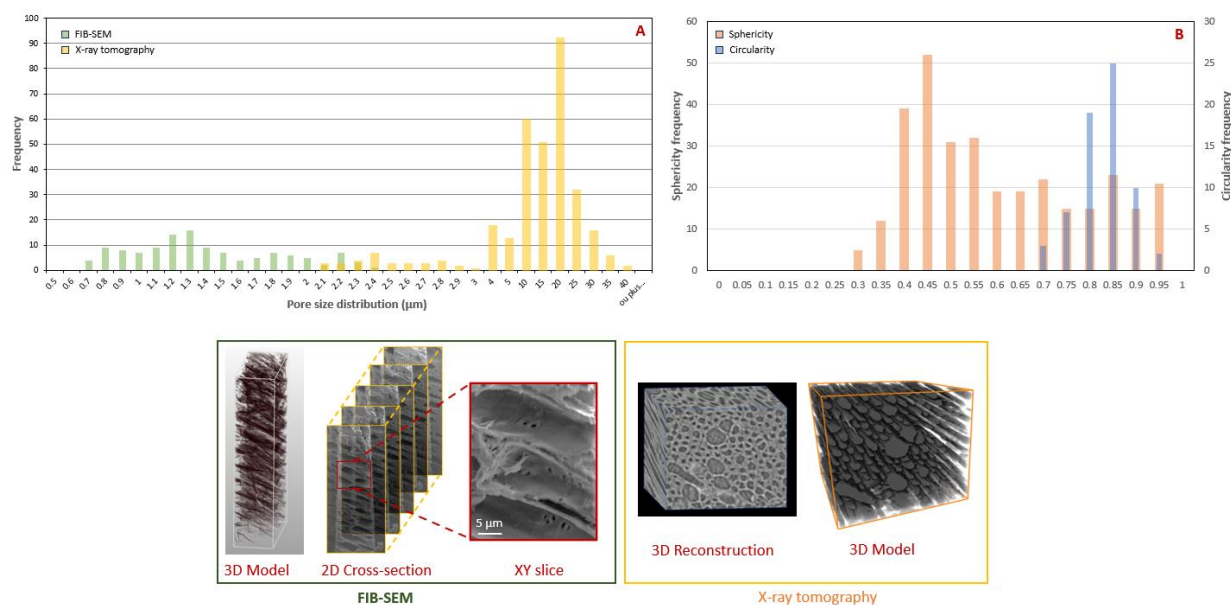


Figure 2: (A) Pore size distribution and (B) sphericity and circularity for the multi-scale porosity present on activated carbon and obtained by combining FIB-SEM and X-ray tomography.

3 Conclusion

In this work, we showed a successful application of true correlative imaging involving both X-ray tomography and FIB-SEM. An activated carbon bead acted as a vehicle to demonstrate how the proposed approach enables to characterise the multi-scale pore system from nanometre up to the millimetre scale. We showed the successful determination of the pore size and shape distribution, yet the methodology is applicable to other morphological parameters as well. The proposed innovative methodology provides a deeper understanding of pore structure and properties, opening up new opportunities for optimizing and utilizing multi-scale porous materials in various industrial applications, including in catalysis, adsorption, energy storage, water remediation and many others.

Acknowledgements: The authors acknowledge funding of the ASN through grant ANR-21-PRRD-0059-01 and Tescan France for financial support of this research. P. Moonen acknowledges intellectual support by the Electron, and X-ray microscopy Community for structural, and chemical Imaging Techniques for Earth materials (EXCITE) community. This project has received funding from the European Union's Horizon 2020 research and innovation programme under grant agreement No 101005611.

References

- [1] H. Jüntgen, Activated carbon as catalyst support: A review of new research results, *Fuel*, 65, 1436-1446 (1986).
- [2] N. Maximoff et al., Performance evaluation of activated carbon sorbents for indoor air purification during normal and wildfire events, *Chemosphere*, 304, (2022).
- [3] A.C.Alvarez et al., Determination of the textural characteristics of carbon samples using scanning electronic microscopy images: Comparison with mercury porosimetry data, *Adsorption*, 19, 841-850 (2013).

Session

Couplages mécaniques, chimiques et thermiques entre
fluides et matrice dans les milieux poreux

Thermal performance assessment in a porous media for a vented enclosure with hot obstacle

Raoudha Chaabane, Nejia Khoudi

*Laboratory of Thermal and Energetic Systems Studies (LESTE) at the National School of Engineering of Monastir,
University of Monastir, Tunisia*

Keywords: LBM, vented, porous media, Block, convection, thermally, Darcy–Forchheimer–Brinkman model.

Abstract

In the present paper, thermal and dynamic assessment is highlighted in a vented fluid saturated porous media with hot obstacle. A mesoscopic approach based on D2Q9 Thermal Lattice Boltzmann Method (TLBM) by using the Darcy–Forchheimer model is applied. A laminar, two dimensional and incompressible flow is considered. The goal in this paper is to investigate the effect of the presence of the porous medium on the convective heat transfer in a given obstructed vented cavity. The numerical simulations are conducted for various Richardson numbers and porosities. The cold entering fluid temperature is of constant velocity. After having passed over the hot obstacle block, the fluid leaves the cavity with a moderate high temperature. Moreover, the no-slip hydrodynamic is also used at the solid boundaries. Besides, zero gradient is used at the outlet wall. The bottom and the top sides of the porous enclosure are thermally isolated. A partially thermally isolated vertical wall facing the partially opening sidewall is considered. The partial slice of left and the right wall of the cavity are with a fixed length as $(H/11)$, is fixed at a hot and cold temperature, respectively. The partial right side is open to the ambient physical conditions. The influences of Richardson number and porosities on convection characteristics, namely isotherms, streamlines, centerline variations of horizontal and vertical, average and local Nusselt numbers are explored for a fixed Darcy number and Prandtl number.

Application of the volume averaging method to the problem of a moving granular porous medium driven by a multi-phase flow

R. Clavier^a, N. Seiler^a, C. Treol^a, B. Goyeau^b

^aCEA, DES, IRESNE, DTN, SMTA, LMAG, Cadarache, 13108 Saint Paul-lez-Durance, France

^bEcole Centrale-Supélec, EM2C, UPR CNRS 188, Université Paris-Saclay, Bâtiment Eiffel – 8-10 rue Joliot Curie, 91192 Gif sur Yvette, France

Keywords: Volume averaging, Granular flow, SFR, Severe accident, Debris bed

1. Introduction

The *Volume Averaging method* has been successfully applied to the macroscopic description of various multi-phase media including fluid flows in fixed porous media [6, 7, 4], convection and boiling in fixed porous media [2], or particle suspension [3] and solidification [5]. On the basis of these previous works, this work is an attempt to extend the method to the problem of a moving granular porous medium with internal heat release, driven by a flow of gas and liquid. This situation is typically expected during a severe accident in a Sodium-cooled Fast neutron Reactor (SFR), when a bed of solidified debris of molten nuclear fuel and steel settles down on the Core catcher at the bottom of the primary vessel (Figure 1). The intense boiling of the sodium, induced by the radioactive decay of the fission products in the debris, drags the debris at the upper parts of the heap. This leads to the *self-levelling* of the debris bed, which has a significant impact on both its coolability and its neutron reactivity.

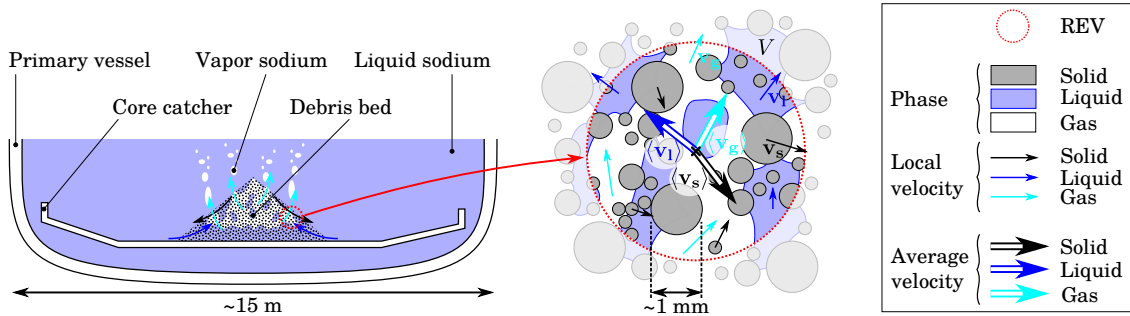


FIGURE 1: Debris bed under self-levelling on the core catcher

2. Local problem

Combining the vision proposed by Ni and Beckermann [5] to account for the motion of the solid phase s , the one of Whitaker [6, 7] to describe the fluid phases l and g , and the one of Duval *et al.* [2] to treat the energy conservation equation and phase change, a boundary-value problem at the pore-scale accounting for all the physics of interest has been proposed. This problem includes the mass momentum and energy conservation for each phase ($k = l, g, s$) :

$$\nabla \cdot \mathbf{v}_k = 0 \quad (1)$$

$$\frac{\partial \mathbf{v}_k}{\partial t} + \nabla \cdot (\mathbf{v}_k \mathbf{v}_k) = (1 - \beta_k \theta_k) \mathbf{g} - \frac{1}{\rho_k} \nabla P_k + \frac{\eta_k}{\rho_k} \nabla^2 \mathbf{v}_k \quad (2)$$

$$\frac{\partial \theta_k}{\partial t} + \nabla \cdot (\theta_k \mathbf{v}_k) = \frac{\dot{q}_k}{c_{p,k}} + \alpha_k \nabla^2 \theta_k \quad (3)$$

where \mathbf{v}_k , P_k and θ_k respectively stand for the local velocity, pressure and temperature of phase k , the temperature θ_k being expressed relatively to the saturation temperature of the liquid phase ($\theta_k = T_k - T_l^{sat}$). The physical properties of interest for the phase k are the density (ρ_k), the thermal dilatation coefficient (β_k), the dynamic viscosity (η_k), the heat capacity ($c_{p,k}$), and the thermal diffusivity (α_k).

The boundary conditions of the local problem (not provided here for the sake of conciseness) express the no-slip at the solid phase boundary (no mass transfer with phase s), the vaporization at the $l - g$ interface, the continuity of the temperature and the conservation of heat fluxes on both sides of all interfaces, and the continuity of tangential stress and discontinuity of normal stress (due to surface tension) at all interfaces.

3. Macroscopic problem

The application of the Volume averaging method [6] to the local boundary value problem is a relatively long process leading to two kinds of problems, coupled with each other but acting at different scales : the *macroscopic problem* (below) exclusively implying the average variables and effective properties of the medium ; and the *closure problems* (not given there) at the pore-scale. The effective properties are derived the resolution of the closure problems at the pore-scale on a Representative Elementary Volume.

The macroscopic conservation equations for each phase $k = l, g, s$ are the following :

$$\frac{\partial \varepsilon_k}{\partial t} + \nabla \cdot (\varepsilon_k \langle \mathbf{v}_k \rangle^k) = \sum_{\substack{j=l,g,s \\ j \neq k}} \frac{\dot{m}_{kj}}{\rho_k} \quad (4)$$

$$\begin{aligned} \varepsilon_k \frac{\partial \langle \mathbf{v}_k \rangle^k}{\partial t} + (\varepsilon_k \langle \mathbf{v}_k \rangle^k \cdot \nabla) \langle \mathbf{v}_k \rangle^k &= \varepsilon_k (1 - \beta_k \langle \theta_k \rangle^k) \mathbf{g} - \frac{\varepsilon_k}{\rho_k} \nabla \langle P_k \rangle^k + \frac{\eta_k}{\rho_k} \nabla^2 (\varepsilon_k \langle \mathbf{v}_k \rangle^k) - \frac{\eta_k}{\rho_k} \nabla \langle \mathbf{v}_k \rangle^k \cdot \nabla \varepsilon_k \\ &+ \frac{\eta_k}{\rho_k} \sum_{j=l,g,s} \langle \mathbf{v}_j \rangle^j \cdot \mathbf{A}_{kj} + \sum_{j=l,g,s} \langle \mathbf{v}_j \rangle^j \cdot \mathbf{B}_{kj} \end{aligned} \quad (5)$$

$$\begin{aligned} \varepsilon_k \frac{\partial \langle \theta_k \rangle^k}{\partial t} + \varepsilon_k \langle \mathbf{v}_k \rangle^k \cdot \nabla \langle \theta_k \rangle^k &= - \sum_{\substack{j=l,g,s \\ j \neq k}} \frac{\dot{m}_{kj}}{\rho_k} \langle \theta_k \rangle^k + \frac{\varepsilon_k \dot{q}_k}{c_{p,k}} + \alpha_k \nabla^2 (\varepsilon_k \langle \theta_k \rangle^k) - \alpha_k \nabla \langle \theta_k \rangle^k \cdot \nabla \varepsilon_k \\ &+ \alpha_k \sum_{j=l,g,s} \langle \theta_j \rangle^j C_{kj} + \alpha_k \sum_{j=l,g,s} \nabla \langle \theta_j \rangle^j \cdot \mathbf{D}_{kj} \end{aligned} \quad (6)$$

where $\langle \Phi_k \rangle^k$ stands for the *phase average* of the property Φ of phase k (velocity \mathbf{v}_k , pressure P_k or temperature θ_k) and ε_k is the volume fraction of phase k . The volumic mass transfer rate from phase k to phase j is \dot{m}_{kj} . Since there is no mass transfer with the solid phase, $\dot{m}_{ks} = \dot{m}_{sj} = 0$. Furthermore, the mass conservation implies that $\dot{m}_{lg} = -\dot{m}_{gl}$.

Finally, the macroscopic equations exhibit four kinds of effective properties for the medium : \mathbf{A}_{kj} and \mathbf{B}_{kj} are 2nd-order tensors, while C_{kj} is scalar and \mathbf{D}_{kj} is vectorial. Since there are 3 phases in the system ($j, k = l, g, s$), there are 9 effective properties of each kind.

The properties \mathbf{A}_{kj} concern the momentum diffusion from phase k to another. Following the interpretation proposed by Lasseux *et al.* [4] and Clavier *et al.* [1], the \mathbf{A}_{kk} term is the *intrinsic term*, representing the momentum diffusion from phase k when the other phases are static. In the case of a single-phase viscous flow in a fixed porous medium, it typically corresponds to the Darcy term. The \mathbf{A}_{kj} terms, with $j \neq k$, are the *crossed terms* and account for the effect of the motion of phase j on the momentum diffusion from or to phase k .

The properties \mathbf{B}_{kj} concern the transfer of momentum from phase k due to the mass transfer of phase k . Since there is no mass transfer from phase s , $\mathbf{B}_{sj} = 0 \forall j$. However, nothing imposes *a priori* that $\mathbf{B}_{ks} = 0$, but it is not possible at present time to estimate the importance of these terms.

The properties C_{kj} and \mathbf{D}_{kj} concern the transfer of enthalpy from phase k . These terms have been obtained in previous similar works in fixed porous media, for example by Duval *et al.* [2]. Their analysis could be extended to the present modelling with a mobile solid phase in the future.

4. Perspectives

The main purpose of the present work is to derive analytically, using the volume averaging method, the structure of the macroscopic conservation equations that describe a debris bed expected in case of severe accident in a SFR : 3-phase porous system (l, g, s) , with moving particles and heat and mass transfer between the liquid and the gas phases. An original macroscopic equation structure has been obtained, exhibiting new effective properties under analysis. The corresponding closure problems have been formulated, and their resolution on relevant pore-scale geometries and physical conditions will be investigated in the near future. In the meantime, the derived structure is under implementation in a new Open-FOAM solver.

Références

- [1] R. Clavier, N. Chikhi, F. Fichot, and M. Quintard. Modeling of Inertial Multi-phase Flows through High Permeability Porous Media : Friction Closure Laws. *International Journal of Multiphase Flow*, 91 :243–261, 2017.
- [2] F. Duval, F. Fichot, and M. Quintard. A local thermal non-equilibrium model for two-phase flows with phase-change in porous media. *International Journal of Heat and Mass Transfer*, 47(3) :613–639, 2004.
- [3] R. Jackson. Locally averaged equations of motion for a mixture of identical spherical particles and a Newtonian fluid. *Chemical Engineering Science*, 52(15) :2457–2469, 1997.
- [4] D. Lasseux, A. Ahmadi, and A. Arani. Two-phase inertial flow in homogeneous porous media : A theoretical derivation of a macroscopic model. *Transport in Porous Media*, 75 :371–400, 2008.
- [5] J. Ni and C. Beckermann. A volume-averaged two-phase model for transport phenomena during solidification. *Metallurgical Transactions B*, 22B :349–361, 1991.
- [6] S. Whitaker. Flow in porous media I : a theoretical derivation of Darcy’s law. *Transport in Porous Media*, 1 :3–25, 1986.
- [7] S. Whitaker. The Forchheimer equation : a theoretical development. *Transport in Porous Media*, 25 :27–61, 1996.

Meso-scale analysis of precipitation-induced damage in limestone using 4D X-ray tomographic imaging

S. Ben Elhadj Hamida^{a,b}, M.A. Boone^c, V. Cnudde^{d,e}, P. Moonen^{a,b}, H. Derluyn^{a,b}

^aUniversité de Pau et des Pays de l'Adour, E2S UPPA, CNRS, TotalEnergies, LFCR, Pau, France

^bUniversité de Pau et des Pays de l'Adour, E2S UPPA, CNRS, DMEX, Pau, France

^cTESCAN XRE, Ghent, Belgium

^dProGRess/UGCT, Department of Geology, Ghent University, Ghent, Belgium

^eEnvironmental hydrogeology, Utrecht University, The Netherlands

Keywords: Salt precipitation, Crystallization-induced damage, 4D X-ray imaging

1 Introduction

Salt precipitation may yield material degradation in a wide field of applications, ranging from underground aquifers used for seasonal gas storage up to the weathering of landscapes and built structures. Typically salts enter the natural building stones or geologic formations under the form of saline solutions. Examples are salt spraying in coastal environments, infiltration of contaminated irrigation water in soils or groundwater flow originating from saltwater-bearing bedrock formations. Each time salts precipitate in the material's pore space, mechanical stresses accumulate, potentially leading to fracturing of the material matrix. Hereby new pathways for fluid transfer are created while simultaneously decreasing the load-bearing capacity of the material, paving the way for an intensification of the degradation process during successive precipitation-dissolution cycles.

2 Methodology and results

Advancing our understanding of the complex interaction among transport phenomena, salt precipitation, crack initiation, and propagation in natural porous media remains a crucial research area. To unravel these interconnected processes, it is imperative to conduct experiments enabling simultaneous investigations of transport, precipitation, and fracture kinetics.

In this study, we analyse a 4D micro-tomographic dataset obtained from a Savonnières limestone plug subjected to NaCl precipitation and dissolution. The specimen consists of distinct regions with differing wettability, comprising a hydrophobic and a hydrophilic part. Initially saturated with a brine solution, the plug experiences precipitation induced by drying of the hydrophobized region, resulting in crystallization-induced fractures at the hydrophobic-hydrophilic interface. Subsequently, dissolution occurs by exposing the sample to a highly humid environment surpassing the deliquescence point of NaCl. This induces rewetting of the sample, dissolution of salt crystals, and partial closure of fractures.

The acquired dataset has a voxel size of 9 μm enabling direct visualization of over 50% of the pore volume. Imaging was performed every 30 minutes over the first 24h of drying and hourly intervals were applied during subsequent drying and deliquescence. Data analysis using a customized Python script revealed that the hydrophobic part of the sample exhibits volumetric changes during drying (figure 1, left). Digital volume correlation using the SPAM software [1] allowed to determine local displacement fields, enabling the identification of local strain bands within the deforming sample (Figure 1, right). As the grey tones of the images vary as function of the local moisture and salt crystal content, a systematic analysis of grey tones made it possible to relate the observed deformations to moisture content and crystal content variations.

To further enhance our comprehensive understanding of the relationship between the pore structure and precipitation, dissolution, and fracture kinetics, we employed an advanced deep learning-based segmentation method. This technique enables accurate classification and segmentation of diverse pore

families, particularly those that are inadequately resolved under the given scanning conditions. At JEMP we will show how this advanced segmentation approach, helps to gain deeper insights into the communication between and behaviour of different pore families during drying and dissolution.

Our work shows that combining experimental observations with advanced imaging techniques and segmentation methods, advances our knowledge of the interconnected phenomena and their implications for the deterioration of natural stone materials, as well as the effectiveness of energy transition strategies.

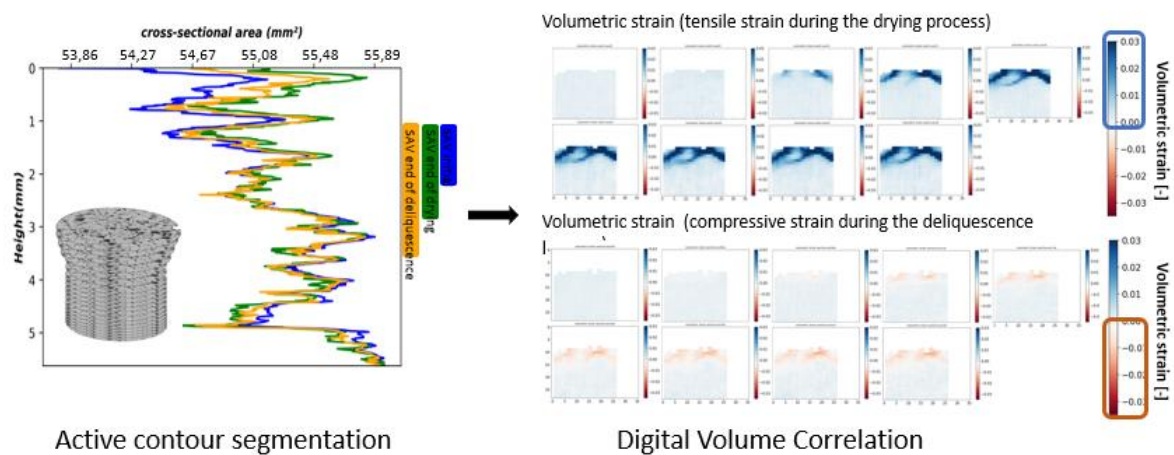


Figure 1: global (left) and local (right) deformation in a sample during drying and subsequent rewetting.

The authors acknowledge the support from the Research Foundation – Flanders (FWO grants 1276814N and 1521815N) and from the European Research Council (ERC) under the European Union’s Horizon 2020 research and innovation programme (grant agreement No 850853).

References

- [1] O. Stamati *et al.*, “spam: Software for Practical Analysis of Materials,” *J. Open Source Softw.*, vol. 5, no. 51, p. 2286, 2020, doi: 10.21105/joss.02286.

Carbon rich materials for solar evaporation : a critical perspective on performance measurement

R. Fillet¹, V. Nicolas^{*1}, A. Celzard^{1,2}, V. Fierro¹

¹Université de Lorraine, CNRS, IJL, F-88000 Epinal, France

²Institut Universitaire de France (IUF)

^{*}(Corresponding author : vincent.nicolas@univ-lorraine.fr)

Keywords: Biosourced material, Carbon, Solar energy, Water evaporation, Heat and mass transfers

1 Introduction

Due to global warming, population growth and pollution, water supply is becoming an important, urgent and global issue. By 2050, it is likely that 3.9 billion people, or more than 40% of the world's population, will be living in river basins subject to high water stress [1]. In France, the water situation is also deteriorating, with increasingly noticeable effects such as early droughts and fires. The beginning of 2023 was marked by a winter drought with 32 days without precipitation. Another example is the predicted reduction of 10% to 40% in average annual river flows in mainland France by 2050 [2,3]. One of the key measures in the "water" plan proposed by the government in March 2023 concerns the recovery of unconventional water, such as wastewater and grey water.

One method of water purification is solar evaporation, which harnesses the energy of solar radiation to vaporise water, subsequently condensing and recovering it for human consumption. The process involves placing a material on the water's surface to accelerate evaporation. This material needs to efficiently capture solar radiation while allowing water to diffuse towards the evaporation surface [4]. In addition, it should minimize heat transfer to the liquid water to maintain energy at the surface. To meet these requirements, an insulating foam is combined to facilitate water diffusion to the material on the surface [5]. Characterisation of the six carbon rich materials is carried out, and a critical assessment is provided for the performance measurement using 2D and 3D evaporators.

2 Evaporation material exploration

Six carbon rich materials are chosen for their specific properties. Two activated carbon (PAC and KAC), a tannin foam (TF), a PTFE-activated carbon paste (PTFE-PAC), ordered mesoporous carbons (OMC) and graphite deposited on a cellulose film (GL). The activated carbons (ACs) are commercially available, as well as the graphite spray and the cellulose film. The PTFE is mixed with PAC using ethanol and ground to form the paste. TF is formed by foaming a tannin thermosetting resin during its polymerisation, as described elsewhere [6]. The OMC are prepared through a 60 min mecanochemical synthesis using 2g of mimosa tannin (*Acacia Mearnsii*), 0.75g of Pluronic® F127 and 1.75g of water. Further information regarding the synthesis process can be found elsewhere [7].

The temperature of both dry and humid materials under solar illumination is measured, as well as hydrophilicity with a sessile drop test. Also, water adsorption and nitrogen adsorption isotherms were measured. The performance of evaporation is then measured for each material under an illumination of 1 kW.m⁻². Results showed that little variation was observed as long as water was supplied to the evaporator surface (Figure 1a).

3 Critical assessment of the evaporation performance measurement

In the existing literature, the evaporation performance results are currently presented as the mass rate of evaporated water per projected surface area. The maximum theoretical amount of water that can evaporate from a surface exposed to $1 \text{ kW}\cdot\text{m}^{-2}$ illumination is $1.47 \text{ kg}\cdot\text{m}^{-2}\cdot\text{h}^{-1}$. It is expected that the results obtained would align with this value, except in the case of 3D materials where the structure can receive additional energy from the surrounding air, as only the illuminated area becomes hotter than the air.

Initially, the focus is on the case of 2D materials, where measurements are taken by gradually reducing the surface area using the same measurement system consisting of a beaker and an insulation layer. It is important to take precautions, such as using a film to prevent unintended evaporation or limiting the solar input to the material surface, as without these measures, the results can be artificially increased by 326%. Next, the focus shifts to the examination of 3D materials is investigated. In the literature, shafts have been utilized resulting in remarkably high values of evaporation performance. A shaft comprises a small surface area that receives direct sunlight, while its larger side surface area leads to a significant additional evaporation. When compared to a material with a wider projected area (referred to here as a pillar), the actual amount of water evaporated is lower. However, since the evaporation rate is calculated based on the projected surface area, the numerical value is increased. Moreover, when shafts are used in arrays as part of a complete system that includes water condensation, the projected surface area is increased. To investigate the effect of such geometries, a shaft and a pillar of equal height are 3D-printed to allow for a direct comparison with cotton and PAC. Results show that when the evaporation rate numbers are considered, the shaft outperforms the pillar by 1256%, However, in reality, the shaft evaporates 64% less water, as illustrated in Figure 1b, and even less than a 2D material.

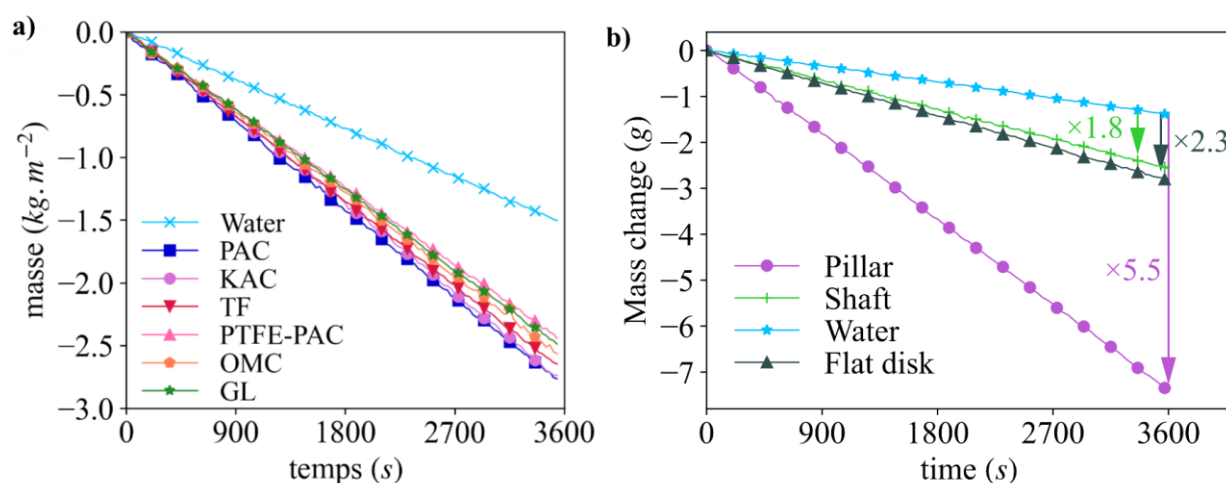


Figure 1: a) Pictures of the different 2D carbon rich evaporators and b) mass of water over time for the carbon rich materials under $1 \text{ kW}\cdot\text{m}^{-2}$ illumination.

References

- [1] C. Chen, Y. Kuang, L. Hu, Challenges and Opportunities for Solar Evaporation, *Joule*. 3 (2019) 683–718. <https://doi.org/10.1016/j.joule.2018.12.023>.
- [2] Plan d'action pour une gestion résiliente et concertée de l'eau, (2023). <https://www.ecologie.gouv.fr/plan-action-gestion-resiliente-et-concertee-eau> (accessed May 16, 2023).
- [3] BRGM, Explore 2070, (2012). <https://professionnels.ofb.fr/fr/node/44> (accessed May 16, 2023).
- [4] Fillet R, Nicolas V, Fierro V, Celzard A. A review of natural materials for solar evaporation. *Sol Energy Mater Sol Cells* 2021;219:110814. <https://doi.org/10.1016/j.solmat.2020.110814>.
- [5] Fillet R, Nicolas V, Fierro V, Celzard A. Modelling heat and mass transfer in solar evaporation systems. *Int J Heat Mass Transf* 2021;181:121852. <https://doi.org/10.1016/j.ijheatmasstransfer.2021.121852>.
- [6] Tondi G, Fierro V, Pizzi A, Celzard A. Tannin-based carbon foams. *Carbon* 2009;47:1480–92. <https://doi.org/10.1016/j.carbon.2009.01.041>.
- [7] Castro-Gutiérrez J, Sanchez-Sanchez A, Ghanbaja J, Díez N, Sevilla M, Celzard A, et al. Synthesis of perfectly ordered mesoporous carbons by water-assisted mechanochemical self-assembly of tannin. *Green Chem* 2018;20:5123–32. <https://doi.org/10.1039/C8GC02295J>.

An efficient Crouzeix-Raviart Finite Element model for coupled hydro-mechanical processes in variably saturated porous media

L. Guo^{a,b}, A. Younes^a, M. Fahs^a, H. Hoteit^b

^a Institut Terre et Environnement de Strasbourg, Université de Strasbourg, CNRS, ENGEEES, Strasbourg, France.

^b Physical Science and Engineering Division, King Abdullah University of Science and Technology, Thuwal, Saudi Arabia

Keywords: Poroelasticity, Biot model, Unsaturated porous media, Richards equation, Nonconforming Finite Elements

Abstract

In this paper, we consider coupled hydro-mechanical processes in variably saturated porous media governed by the coupled nonlinear partial differential equations:

- Fluid mass conservation equation

$$\left[S_w S_s + c(h) \right] \frac{\partial H}{\partial t} + \alpha S_w \frac{\partial}{\partial t} (\nabla \cdot \mathbf{u}) + \nabla \cdot \mathbf{q} = q_s \quad (1)$$

- Darcy's law

$$\mathbf{q} = -k_r \mathbf{K} \nabla H \quad (2)$$

- Equilibrium equation

$$\nabla \cdot (\boldsymbol{\sigma}_e - \alpha \chi \mathbf{P} \mathbf{I}) + \rho_b g \nabla z = 0 \quad (3)$$

- Generalized Hooke's law

$$\boldsymbol{\sigma}_e = \mu (\nabla \mathbf{u} + (\nabla \mathbf{u})^t) + \lambda (\nabla \cdot \mathbf{u}) \mathbf{I} \quad (4)$$

- Van Genuchten (1980) water content - pressure head relationship

$$S_e = \frac{\theta(h) - \theta_r}{\theta_s - \theta_r} = \begin{cases} \frac{1}{\left(1 + |\alpha_v h|^{n_v}\right)^{m_v}} & h < 0 \\ 1 & h \geq 0 \end{cases} \quad (5)$$

- Mualem (1976) conductivity-saturation relationship

$$k_r = S_e^{1/2} \left[1 - \left(1 - S_e^{1/m_v}\right)^{m_v} \right]^2 \quad (6)$$

with $S_w = \theta/\theta_s$ the saturation [-], θ the current water content [L^3L^{-3}], θ_s the saturated water content [L^3L^{-3}], S_e [-] the effective saturation, θ_r the residual water content [L^3L^{-3}], S_s the specific mass storativity related to head changes [L^{-1}], $H = h + z$ the hydraulic head [L], $h = \frac{P}{\rho_w g}$ the pressure head, P the pressure [Pa], ρ_w the fluid density [ML^{-3}], g the gravity acceleration [LT^{-2}], z the upward vertical coordinate [L], $c(h) = \partial\theta/\partial h$ the specific moisture capacity [L^{-1}], \mathbf{q} the Darcy velocity [LT^{-1}], q_s the sink term [T^{-1}], $\mathbf{K} = \frac{\rho_w g}{\mu_w} \mathbf{k}$ the hydraulic conductivity [LT^{-1}], \mathbf{k} the permeability tensor [L^2], μ_w the fluid dynamic viscosity [$ML^{-1}T^{-1}$], k_r the relative conductivity [-], α_v [L^{-1}] and n_v [-] the van Genuchten parameters, $m_v = 1 - 1/n_v$, α the Biot coefficient, $\rho_b = \rho_s (1 - \theta_s) + \theta \rho_w$ the bulk density, ρ_s the density

of the solid [ML⁻³], σ_e the effective stress tensor, χ the Bishop's function typically set equal to S_w , \mathbf{u} the displacement field [L], λ and μ the Lamé coefficients.

Several challenges emerge from the nonlinear character and the high coupling between the equations when solving the system (1)-(6). In this work, the equations are solved simultaneously using the method of lines (MOL) which avoids operator-splitting errors. The MOL is an efficient procedure for solving highly nonlinear systems of equations (Miller *et al.*, 2006). With MOL, all the spatial derivatives are discretized while the time derivatives are kept in their continuous form.

For practical reasons, related to the computational burden of the system (1)-(6), the spatial discretization is often limited to low-order approximation methods, such as standard Galerkin Finite Elements (GFE). However, the standard GFE method can produce unstable and oscillatory pressure results, which is known as locking.

In this work, we use the low-order Crouzeix-Raviart (CR) finite elements for both the hydraulic head of the fluid phase and the displacement of the solid phase. The CR method uses P1 linear test functions with the degrees of freedom allocated to center of the edges, rather than to the vertices. Contrarily to the standard GFEs, the CR method is locally conservative. Further, using the connection between the Discontinuous Galerkin method and the CR method, Hansbo and Larson (2003) developed a locking-free CR formulation for elasticity. This formulation is employed here for poroelasticity in unsaturated porous media.

For the fluid flow, the nonlinear Richard's equation is also discretized in space using the CR method which is equivalent to the Lumped Raviart-Thomas Mixed Finite Element Method developed in Younes et al. (2006). The time discretization of the obtained system is performed using high-order integration methods and an efficient adaptive time stepping scheme with the DASPCK time solver.

Numerical results in saturated and unsaturated conditions are presented to validate the new model and to show the effectiveness of the model to overcome nonphysical pressure oscillations.

References

- [1] Miller, Cass T., Abhishek, C., Farthing, M.W. A Spatially and Temporally Adaptive Solution of Richards' Equation. *Advances in Water Resources.*, 29, no. 4: 525–45 (2006).
- [2] Hansbo, P., Larson, M.G. Discontinuous Galerkin and the Crouzeix–Raviart element: Application to elasticity. *ESAIM Math. Model. Numer. Anal.*, 37 (1), pp. 63-72 (2003)
- [3] Younes, A., Ackerer, P., Lehmann, F. A new mass lumping scheme for the mixed hybrid finite element method. *Int. J. Num. Meth. Eng.*, 67, 89-107 (2006).

Coupled numerical modeling of multiphase reactive transport and geomechanics

Anthony Michel, Axelle Alavoine, Guillaume Enchéry, Audrey Estublier, Isabelle Faille, Eric Flauraud, Jérémy Frey, Raphaël Gayno, Thomas Guignon^a

^aIFP Energies nouvelles, 1-4 avenue de Bois-Preau, 92852 Rueil-Malmaison Cedex

Keywords: multi-physics coupling, reactive transport, geomechanics, virtual-element-method

During the last few years, we have developed a prototype software coupling multiphase reactive transport in porous media and geomechanics.

The multiphase reactive transport model implements a fully implicit formulation for flow and transport equations with different levels of coupling for chemistry. Simple water-rock interactions such as salt precipitation or hydrate kinetics can be added directly to the global implicit system. Complex chemistry problems with water speciation and detailed mineralogy are solved in a separate reactive transport model coupled with the multiphase flow model by an iterative sequential splitting approach [1].

The geomechanical model, solving the poro-elasticity equations, is based on the virtual element method VEM. This method is an extension of finite element methods that can be used on distorted and degenerated grids, which is particularly interesting for complex geological structures [2]. It can be easily combined with standard finite volume methods on corner point geometry grids without the need for grid transfer operations.

The mechanical material properties are tightly coupled with reactive transport results by using a flexible physical law system. This system allows the user to freely define its own physical laws functions depending on any available physical properties at run time. Starting from a test case with constant material properties, one can then easily update it to study the effects of fluid replacement and mineralogy changes on mechanics.

In our talk, we will outline the features of the different models and recall the principle of the VEM method. We will then present our coupling approach and discuss its advantages and limitations. As an illustration, we will present numerical simulations of gas injection and storage operations at field scale and reactive plug flow experiments at the laboratory scale [3].

Références

- [1] Trenty, L. and Michel, A. and Tillier, E. and Le Gallo, Y., A Sequential Splitting Strategy for CO2 Storage Modelling, *ECMOR Conference*, (2006).
- [2] Coulet, Julien and Faille, Isabelle and Girault, Vivette and Guy, Nicolas and Nataf, Frédéric, A fully coupled scheme using virtual element method and finite volume for poroelasticity, *Computational Geosciences*, Volume 24, page 381–403 (2020).
- [3] Bemer, Elisabeth and Nguyen, Minh Tuan and Dautriat, Jérémie and Adelinet, Mathilde and Fleury, Marc and Youssef, Souhail, Impact of chemical alteration on the poromechanical properties of carbonate rocks, *Geophysical Prospecting*, Volume 64, page 810–827 (2016).

Session
Stockage d'énergie électrochimique

Geometric optimization of a Lithium-ion battery model.

Richard Joly^{a,b}, Grégoire Allaire^a, Romain de Loubens^b

^a*CMAP, Ecole Polytechnique, Institut Polytechnique de Paris, 91120 Palaiseau, France*

^b*TotalEnergies OneTech, 3 Boulevard Thomas Gobert, 91120 Palaiseau, France*

Keywords: Lithium-ion battery, Shape optimization, FreeFem++

Abstract

The homogenized model known as the Newman model [2,3] - or more precisely, the Doyle Fuller and Newman model (DFN) - serves as the foundation for numerous academic [4, 5] and industrial softwares used to simulate the operation of lithium-ion batteries during charging and discharging. Its multiscale equations, derived from the theory of porous electrodes, form a coupled system of two unsteady diffusion equations for the concentration of lithium in the solid phase and the concentration of ions in the liquid phase,

$$\epsilon_e \frac{\partial c_e}{\partial t} = \nabla \cdot (\mathbf{D}_{e,\text{eff}} \nabla c_e) - \frac{t_+^0}{F} \nabla \cdot \mathbf{i}_e + \frac{a_s i_{se}}{F} \quad \text{in } \Omega \quad (1)$$

$$\frac{\partial c_s}{\partial t} = \frac{1}{r^2} \frac{\partial}{\partial r} \left(D_s r^2 \frac{\partial c_s}{\partial r} \right) \quad \text{in } B_R \quad (2)$$

along with two steady-state elliptic equations for the electric and ionic potentials,

$$-\mathbf{\Lambda}_{e,\text{eff}} \nabla \varphi_e + \frac{2RT(1-t_+^0)(1+\delta_e)}{F} \mathbf{\Lambda}_{e,\text{eff}} \nabla \ln c_e = \mathbf{i}_e, \quad -\nabla \cdot \mathbf{i}_e + a_s i_{se} = 0 \quad (3)$$

$$\nabla \cdot (\mathbf{\Lambda}_{s,\text{eff}} \nabla \phi_s) = a_s i_{se} \quad (4)$$

- \mathbf{i}_e : superficial average of ionic current density (units : V),
- i_{se} : macroscopic average of current density at solid-electrolyte interfaces (units : A.m⁻²),
- c_e : macroscale lithium-ion molar concentration in electrolyte (units : mol.m⁻³),
- c_s : microscale solid-phase lithium concentration (units : mol.m⁻³),
- φ_e : macroscale ionic potential of electrolyte (units : mol.m⁻².s⁻¹),
- ϕ_s : macroscale solid-phase electric potential (units : mol.m⁻².s⁻¹).

To these equations, boundary conditions [3] are added, as well as continuity conditions at the interfaces. Macroscale variables are either defined on the entire battery cell domain Ω or on the domains of both porous electrodes -cf. Figure 1 -. Finally, $a_s, D_s, \epsilon_e, t_+^0$ and δ_e are parameters of the model, and $\mathbf{\Lambda}_{e,\text{eff}}, \mathbf{\Lambda}_{s,\text{eff}}$ and $\mathbf{D}_{e,\text{eff}}$ the homogenized coefficients of the model.

The ultimate objective of our work is to apply geometric and topological optimization tools [1] to the electrode interfaces in order to optimize a performance function calculated using the DFN model. Thus, within this context, we propose here an implementation of the so-called pseudo-3D (P3D) version of the DFN model, which combines finite element and finite difference methods using the FreeFem++ and C++ languages. We discuss the validation methods for our implementation, explain the application of shape optimization tools with interfaces developed in recent years [1] to this model, and present an initial result of geometric optimization of the interfaces between the separator and electrodes during discharge.

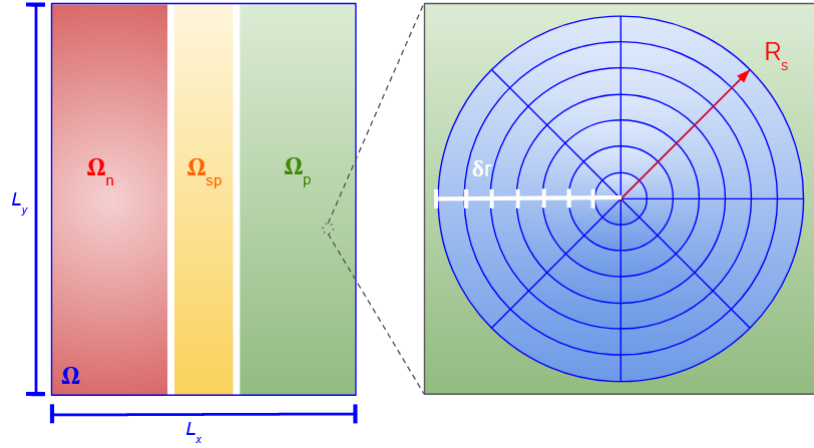


FIGURE 1: Domain $\Omega = \Omega_n \cup \Omega_{sp} \cup \Omega_p$ of the lithium-ion battery numerical model. On the right is drawn an active material particle B_R .

Références

- [1] ALLAIRE, Grégoire, DAPOGNY, Charles, et JOUVE, François. Shape and topology optimization. In : Handbook of Numerical Analysis. Elsevier, 2021. p. 1-132.
- [2] EFENDIEV, Yalchin, ILIEV, Oleg, et TARALOVA, Vasilena. Upscaling of an isothermal Li-ion battery model via the Homogenization Theory. Fraunhofer Inst. für Techno-und Wirtschaftsmathematik, ITWM, 2013.
- [3] FULLER, Thomas F., DOYLE, Marc, et NEWMAN, John. Simulation and optimization of the dual lithium ion insertion cell. Journal of the electrochemical society, 1994, vol. 141, no 1, p. 1.
- [4] KOROTKIN, Ivan, SAHU, Smita, O'KANE, Simon EJ, et al. Dandelion v1 : An extremely fast solver for the Newman model of lithium-ion battery (dis) charge. Journal of The Electrochemical Society, 2021, vol. 168, no 6, p. 060544.
- [5] TORCHIO, Marcello, MAGNI, Lalo, GOPALUNI, R. Bhushan, et al. Lionsimba : a matlab framework based on a finite volume model suitable for li-ion battery design, simulation, and control. Journal of The Electrochemical Society, 2016, vol. 163, no 7, p. A1192.

Two-phase Flow Through the PTL of PEM Water Electrolyzer: MRI Experiments and Numerical Modeling Using Phase-Field Theory

B. Amoury^a, T.D. Le^a, J. Dillet^a, S. Leclerc^a, G. Maranzana^a, S. Didierjean^a

^aLaboratory of Energies and Mechanical Engineering, University of Lorraine, CNRS, 54000 Nancy

Keywords: PEM electrolysis, porous transport layer, two-phase flow, magnetic resonance imaging, Phase-field theory

1 Introduction

In 2021, estimation shows that the worldwide annual hydrogen production is around 94 Mt. Exploitation of native hydrogen being not mature, it is obtained by its separation from other elements by different methods such as steam methane reforming, and electrolysis of water. The latter supplied by a renewable power source will take part in the development of a green hydrogen economy [1]. In this context, Proton Exchange Membrane (PEM) Electrolyzer is a promising technology due to its flexibility and very quick adaptation to load variations. However, its current development still confronts some limitations at a large industrial scale. For instance, efficiency and durability are directly impacted by the mass transport and electrical transfer within the porous materials at the anode side. Limitation of the water supply to the catalyst layer happens once there is a poor oxygen evacuation which decreases the performance of the device by inducing high overpotential. Furthermore, the PTL has an important role as an electrical conductor for charge transfer from the catalyst layer [1]. The efficiency of all the transport phenomena through the PTL and porous electrode assembly depends on their transport properties which are related to their microstructure and operating conditions. For instance, PTL with a large pore size allows good water and gas transport, while produced electrons choose a long-distance path generating an electrical resistance higher than that in the case of PTL with a small pore size [1]. So, controlled and optimum porosity and pore size could contribute to efficient water, gas, and electron transport. To overcome the above-mentioned issues and to define the best porous layers morphologies, an extensive analysis was performed by integrating both experimental research and modeling to investigate gas invasion patterns and saturation profiles across samples with varying PTL properties.

2 MRI experimental application to PTL

Magnetic resonance imaging (MRI) technique which is based on NMR (Nuclear magnetic resonance spectroscopy), was used for the measurement of hydrogen nuclei affiliated to water molecules present or moving inside the porous layer during the two-phase flow. The amount of target fluid (water intensity) inside the porous medium is determined by the signal strength of the MRI intensity. Instead of the real PTL made of titanium which is paramagnetic and cannot be used in the MRI, borosilicate filters with thickness, porosity, and pore size similar to PTL were used. After positioning the sample in the 600 MHz vertical imager (Figure 1-A), a constant water flow rate is introduced while the gas flow rate is varied. Each flow rate corresponds to a specific current density. A variation can be observed from 0.43 A/cm² at a flow rate of 0.15 ln/hr to 2.65 A/cm² at 0.9 ln/hr. The saturation profiles measured through the porous material depend on the gas flow rate and a semi-dryness of the sample occurs (Figure 1-B) with a residual quantity trapped between pores (minimum stable water content). The water flow rate variation in the channel does not affect saturation, but a higher gas flow rate is needed to reach a minimum stable water content for a higher water flow rate. The gas pressure drop through the porous medium was measured and bubble formation in the channel was also analyzed. The results show that the pressure drops

and types of flow (slug, annular, and bubble flow) depend on the orientation of the water channel (horizontally and vertically) and flow direction (up or downward), and on the water and gas flow rates.

3 Multiphase flow modeling in PTL

To reach a better understanding of the dynamic characteristics of water and oxygen transport over the PTL, the phase-field model based on the Cahn-Hilliard theory was used to simulate the two-phase flow through a porous medium [2]. In this model, the modified Navier-Stokes equations for two phases are coupled with a phase field equation for describing the diffuse interface. Numerical simulations performed in the COMSOL® Multiphysics software were carried out on 2D geometries composed of spherical solid grains (white region) of different sizes, having properties similar to the PTL used in the MRI experiments. To mimic the multiphase flow patterns in PTL, gas injection is considered at CL as represented in Figure 1-C. The figure presents the basic understanding of invasion pattern (IP) during gas (blue) percolation process where it flows through the porous medium initially saturated with water (red) and evacuated on another side in contact with the water channel. Gas flow in the porous medium and bubble formation in the water channel are studied while varying the gas and water flow rates. The simulation results give information about the gas pathways within the porous medium and the saturation profiles over time, depending on the gas/water flow rates, which will be compared with experimental results.

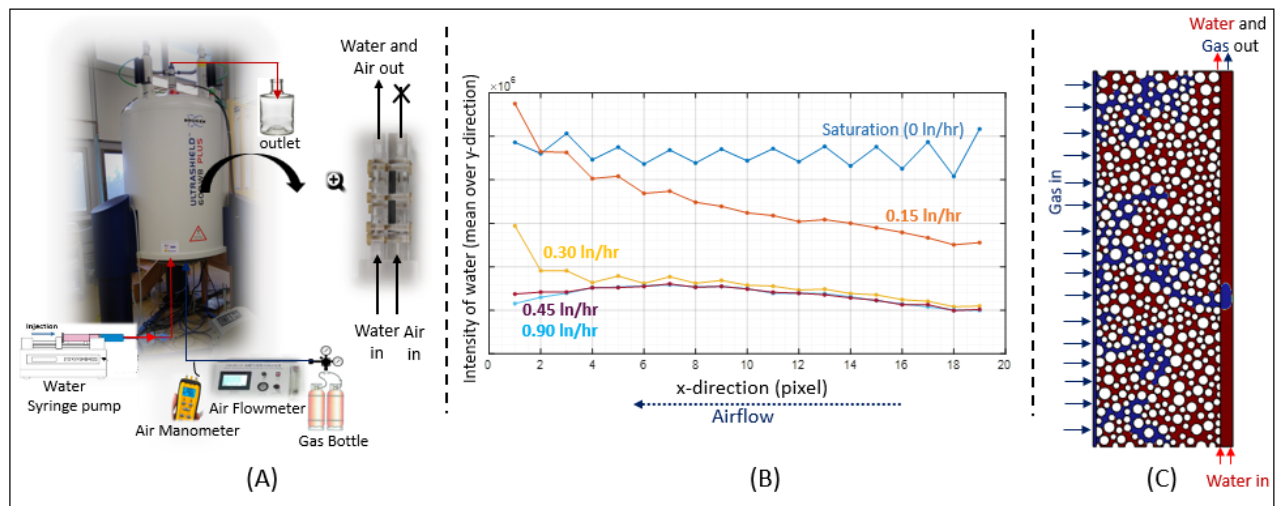


Figure 1:(A) Sample positioning in MRI-setup with the necessary connections (B) Water signal intensity vs position through the porous sample in airflow direction for different gas flow rates for a Borosilicate sample with pore diameter ranging from 10 to 16 μm (C) Gas distribution through the porous medium and bubble formation in the channel obtained by numerical simulations

References

- [1] J. Parra-Restrepo, “Caractérisation des hétérogénéités de fonctionnement et de dégradation au sein d’un électrolyseur à membrane échangeuse de protons (PEM)”, Université de Lorraine, (2020).
- [2] J. W. Cahn and J. E. Hilliard, “Free Energy of a Nonuniform System. I. Interfacial Free Energy,” *The Journal of Chemical Physics*, vol. 28, no. 2, pp. 258–267 (Feb. 1958).

Unlocking Insights in Battery Research with Digital Twin-driven Data Augmentation

S. Ait Hamouda^a, P. Moonen^{a,b}

^aLFCR, E2S UPPA, CNRS, TotalEnergies, Université de Pau et Pays de l'Adour - Pau, France

^bDMEX, E2S UPPA, CNRS, Université de Pau et Pays de l'Adour - Pau, France

Keywords: Battery degradation, Thermo-elasticity, Inverse problem, Finite Element Method, PDE-constrained optimization, Image registration.

1 Introduction

Increasing both the amount of charge a battery can hold and the total number of times a battery can be charged are two of the key challenges that the battery sector is facing [1]. Among the many strategies to achieve this goal, dynamic experiments with X-ray tomography or Transmission Electron Microscopy (TEM) are of particular interest. Both techniques enable to non-destructively observe the ongoing processes in the interior of a battery cell while it degrades during successive charging and discharging cycles and to distil lessons to iteratively improve the design [2]. However, while they do provide morphological -and sometimes electrochemical- information, other quantities of interest, such as the internal pressure and temperature distribution, are invisible. The current study tackles this challenge by creating a digital twin of the cell to provide the missing quantities. As will be shown, the proposed methodology is generic and can be used in a wide range of applications to fill in missing data.

2 Methodology

The method was developed and tested based on a synthetic dataset mimicking the temporal evolution of a symmetric Li-Li solid-state battery cell. When such cell is charging or discharging, the chemical reactions that take place are respectively endothermic or exothermic. The local temperature variation associated with the absorption or generation of heat causes the cell to locally deform, and these geometric variations can be observed using X-ray tomography or TEM.

For testing purposes, we have generated a number of synthetic datasets that differ in the amount of heat that is locally absorbed or released, and we varied the image resolution and the image quality. In the current study we focus on a two-dimensional cross section through the cell and its evolution over time, yet the method can also be used to investigate the full cell in three-dimensions. The entire workflow is developed in Python.

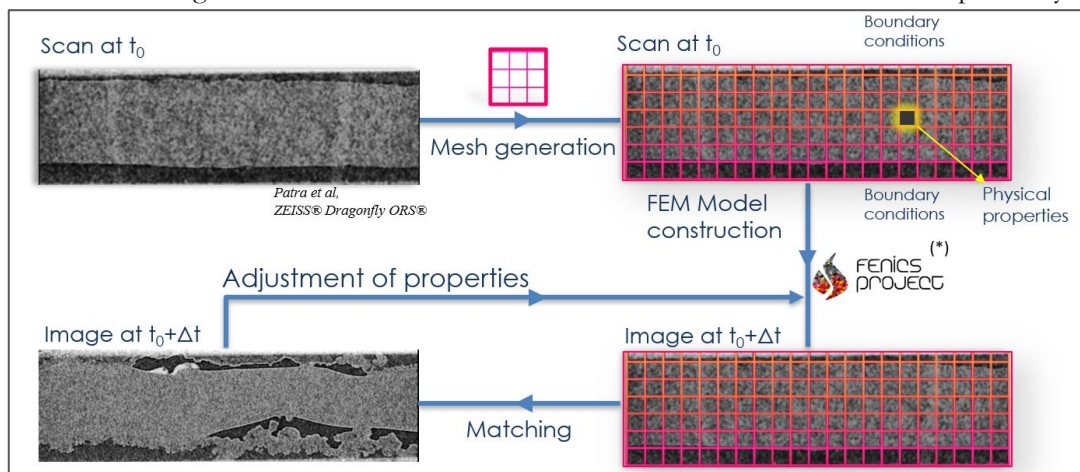


Figure 1: Schematic of the developed workflow

The first image of the sequence is automatically segmented by means of grey-tone thresholding into three phases, i.e., the electrode, the electrolyte and the surrounding air. Next, a finite element grid is constructed on top of it and physical properties are assigned to each element, corresponding to the underlying material phases. At the macroscale, the thermal deformation of the cell can be regarded as a thermo-elasticity problem, whereby an unknown heat source or sink mimics the energy exchange by the electrochemical processes during

battery cycling. Complemented with initial and boundary conditions, the governing equations are solved using *FEniCS* [3], a software package that enables scientific models to be efficiently translated into a finite element code, and yield the displacement and temperature fields inside the battery cell, as well as their corresponding evolution over time. The resulting displacement field is used to warp the initial image. The latter is then compared to the next image in the sequence and the difference is iteratively minimised by adjusting the unknown heat source. The iterative optimisation procedure relies on the COBYLA-algorithm[4][5], which was found to offer consistent performance in a wide range of test cases. Once the differences between the warped and the real image are smaller than a user-defined tolerance, the algorithm moves to the next time point. The final result consists of a series of displacement fields consistent with the input image sequence, as well as temperature and heat source fields that are compatible with both the displacement field and the test conditions (i.e. initial and boundary conditions).

3 Results

The model was thoroughly tested to evaluate its robustness in the case of low-quality images i.e. exhibiting a low signal-to-noise ratio. Furthermore, we studied the impact of scale and resolution changes in the image. This evaluation allowed us to have a better insight into the robustness of the model as well as its limitations. In the case of low-resolution images, results revealed that the model showed accurate predictions (<10% error) over a range of heat source intensities between 500 and 20 000 W/kg. At higher image resolution, this reliable range extends towards smaller heat source intensities. The performance was found to degrade with increasing noise level, yet even under high noise levels (4x higher than typical tomography datasets) the predicted values do not deviate more than 20% from reality. Overall, these results demonstrate the robustness of the model and highlight the importance of both image resolution and image quality in its implementation.

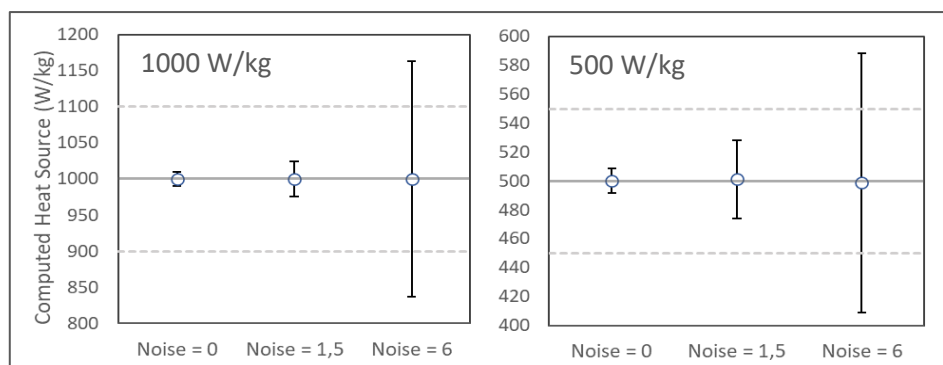


Figure 2: Sensitivity to image noise for two different heat sources.

The error bars span the range of predictions over time.

4 Conclusions and perspectives

The results show that the proposed methodology enables augmenting experimental datasets with numerical data. The proposed approach implicitly ensures that the obtained quantities respect the governing equations as well as the initial and boundary conditions. The method was tested for a wide range of heat sources, both constant and variable over time, for different image resolutions and for various image noise levels. As long as the deformations were sufficiently large to be detected at the image resolution, and sufficiently small to remain contained within the borders of the image, accurate results were obtained. Current work focuses on the application of the method on real datasets.

Acknowledgements: This research was financially supported by the European Doctoral program on ENergy and Environment (EDENE) under the European Union's Horizon 2020 research and innovation program (grant agreement No 945416). The authors also thank TotalEnergies for financial support.

References

- [1] N. S. Choi *et al.*, “Challenges facing lithium batteries and electrical double-layer capacitors,” *Angewandte Chemie - International Edition*, vol. 51, no. 40. pp. 9994–10024, Oct. 01, 2012. doi: 10.1002/anie.201201429.
- [2] S. Basak *et al.*, “Characterizing battery materials and electrodes via in situ / operando transmission electron microscopy ,” *Chemical Physics Reviews*, vol. 3, no. 3, p. 031303, Sep. 2022, doi: 10.1063/5.0075430.
- [3] H. P. Langtangen and A. Logg, “SIMULA SPRINGER BRIEFS ON COMPUTING 3 Solving PDEs in Python The FEniCS Tutorial I.” [Online]. Available: <http://www.springer.com/series/13548>
- [4] M. J. D. Powell, “Direct search algorithms for optimization calculations,” *Acta Numerica*, vol. 7, pp. 287–336, 1998, doi: 10.1017/S0962492900002841.
- [5] M. J. D. Powell, “A view of algorithms for optimization without derivatives 1,” 2007.

Session
Comportement des fluides complexes
en milieux poreux

Viscoelastic flow in porous media — a web of sticky strands

O. Mokhtari^{a,b,c}, J.-C. Latché^d, M. Quintard^a, Y. Davit^a

^a*Institut de Mécanique des Fluides (IMFT, UMR 5502), CNRS & Université de Toulouse, Toulouse, France.*

^b*TotalEnergies E&P, CSTJF, 64018 Pau, France.*

^c*Physikalisches Institut, Universität Bern, Gesellschaftsstrasse 6, 3012 Bern.*

^d*Institut de Radioprotection et de Sécurité Nucléaire (IRSN), 13115 Saint-Paul-Lez-Durance, France.*

Keywords: viscoelastic, birefringent strands, stability, elastic turbulence

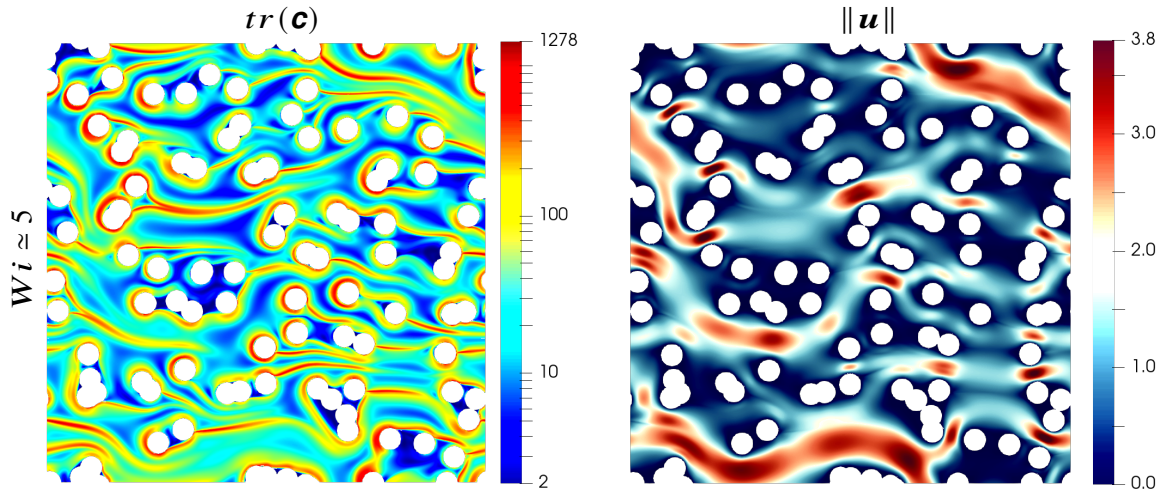


FIGURE 1: HPC simulation of the flow of an Oldroyd-B fluid through an array of obstacles (in white) for a Weissenberg number ($Wi = \frac{Elastic}{Viscous}$) approximately equal to 5. On the right, the trace of the conformation tensor (stretching of the polymer chains) and on the left the magnitude of the velocity field.

The flow of polymer solutions through porous media is a rich problem in fluid mechanics, combining the complexity of flows through porous structures with the viscoelasticity of the fluid. Such flows can display peculiar behaviors, including : instabilities at low Reynolds numbers and “elastic turbulence” ; a strong localization of polymeric stress in specific zones at pore-scale ; or an increase of flow resistance at Darcy-scale, even for a fluid that is shear-thinning in a rotational rheometer. Despite continuous efforts, a clear picture of the small-scale mechanisms involved and their link with larger scale phenomena are still lacking.

To better understand this problem, we first developed a code to simulate the flow of viscoelastic fluids through model porous structures [1]. This code is based upon a new staggered projection scheme for viscoelastic flows, with some unique properties. It shows good accuracy, even for relatively large Weissenberg numbers (ratio of elastic to viscous forces). It verifies important mathematical properties – the conformation tensor remains symmetric positive definite and the space semi-discretization is consistent with a free-energy estimate. It is well suited to high-performance computing (HPC) and can be readily used for a variety of viscoelastic constitutive laws such as Oldroyd or FENE-type models. It is also implemented for HPC in the CALIF3S open-source platform developed at the Institut de Radioprotection et de Sécurité Nucléaire (IRSN).

Our first step was to simulate steady-state flows through 2D arrays of cylinders [2]. We showed that localized zones of large polymeric stress, known as birefringent strands, guide the flow of an Oldroyd-B fluid through the porous structures. We found that these strands form a web (Fig 1) through the

porous structure that generates a complete reorganization of the flow with an increase of stagnation zones, a reinforcement of preferential paths and a splitting of flow channels. We also found that this reorganization is the source of an increase in global dissipation that can be directly linked with the increase of flow resistance. Our results demonstrate that the birefringent strands – not the elongational viscosity – control the flow of viscoelastic fluids through porous media and that the increase of flow resistance can occur even at steady-state, before the transition to elastic turbulence.

Recent microfluidic experiments [3, 4] have studied the transition to unsteady flow in 2D lattices of hexagonal cylinders and have evidenced complex spatiotemporal fluctuations. By randomly displacing the cylinders from their original position, [3] also suggest that disorder suppresses the instability. But [4] found a counterexample showing that disordering the structure can also promote the instability. They propose that the parameter controlling this phenomenon is the number of stagnation points on the surface of the cylinders that are accessible to the main flow, with the idea that stagnation points act as a source of polymeric stress and thus lead to the instability. In geometries where successive obstacles can screen each other, the development of the instability may be delayed. Here, we will detail the nonlinear dynamics of these instabilities using HPC simulations of the flow. We will show that different regimes develop that explain the experimental observations. We will also show that these regimes are all controlled by the dynamics of “sticky” birefringent strands, thus demonstrating that these strands are the key to understanding both steady and unsteady flows of viscoelastic fluids through porous media.

Références

- [1] O. Mokhtari, Y. Davit, J.-C. Latché, and M. Quintard. A staggered projection scheme for viscoelastic flows. *Mathematical Modelling and Numerical Analysis (ESAIM : M2AN)*, 57(3) :1747–1793, 2023.
- [2] O. Mokhtari, J.-C. Latché, M. Quintard, and Y. Davit. Birefringent strands drive the flow of viscoelastic fluids past obstacles. *Journal of Fluid Mechanics*, 948 :A2, 2022.
- [3] D. M. Walkama, N. Waisbord, and J. S. Guasto. Disorder suppresses chaos in viscoelastic flows. *Physical Review Letters*, 124(16) :164501, 2020.
- [4] S. J. Haward, C. C. Hopkins, and A. Q. Shen. Stagnation points control chaotic fluctuations in viscoelastic porous media flow. *Proceedings of the National Academy of Sciences*, 118(38), 2021.

Characterization of the first normal stress difference in diluted polymer solutions by tracking particle migration in a microfluidic channel

A. Naillon^{a*}, X. Salas Barzola^b, C. de Loubens^b, G. Maitrejean^b, H. Bodiguel^b

^a *Univ. Grenoble Alpes, CNRS, Grenoble-INP, 3SR, F-38000 Grenoble*

^b *Univ. Grenoble Alpes, CNRS, Grenoble-INP, LRP, F-38000 Grenoble*

Keywords: Particle migration, Viscoelasticity, Complex fluid, Polymer solution, Rheometry

1 Introduction

Flows of complex liquids in porous media are involved in different fields such as in environmental remediation for removing pollutants from wastewater and soil, as well as in the field of energy with energy storage devices, drilling fluids, and enhanced oil recovery. The characterization of the properties of these complex fluids is essential to understand their behaviour, optimize their performance, and ensure their stability and effectiveness in their applications

Polymer solution belong to the family of complex fluid, usually exhibiting viscoelastic properties. This study aims at characterizing the elastic force in viscoelastic liquids by studying the migration of particles in microfluidic devices. Contrary to Newtonian liquids in which lift forces are negligible at low Reynolds number, in viscoelastic liquids, a transverse force acts on the particles. It is due to the shear rate gradient around the particle and depends strongly on the Weissenberg (Wi) number and the ratio between the particle size and the channel size. Taking advantage on the huge aspect ratio between the length and the height of a microfluidic slit, it is possible to detect very small transverse velocities, by determining the particle trajectory. Previous studies had already shown that this phenomenon was well adapted to low Weissenberg numbers (typically 10^{-3} – 10^{-1}), but were mainly restricted to viscoelastic fluid exhibiting a rate-independent viscosity [1]–[3]. We extended these studies to the common case of shear-thinning polymer solutions.

2 Experimental results

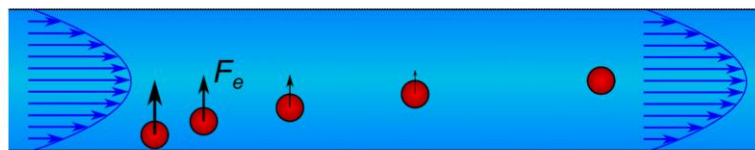
PDFs of the particle position were systematically measured in various solutions, for various pressure drops, particle and channel sizes. For shear-thinning liquids, a less efficient migration was qualitatively evidenced, and as compared to rate-independent solutions, the PDFs exhibited various specific shapes. We also found experimentally that in some cases, when the solvent viscosity is dominant, the migration occurred towards the wall contrary to the most common case where it occurs towards the center of the channel. No accurate theory was available for shear-thinning liquids. We thus derived a model based on the assumption that the viscoelastic lift force is simply proportional to the gradient of the first normal stress difference (N_1) across the particle,

$$F_e = K a^3 \frac{\partial N_1}{\partial z} \quad (1)$$

Assuming additionally that it is balanced by a drag force involving the local (rate-dependent) shear viscosity, one could derived the trajectory of the particles. When both N_1 and the shear viscosity are power law

functions of the shear rate, we found analytical solutions of the model. These allowed us to predict the PDFs of the particle positions along the channel. The solution tested did not always follow power laws on a large range of shear rate, but could be approximated by a power law around the mean shear rate of the

a)



b)

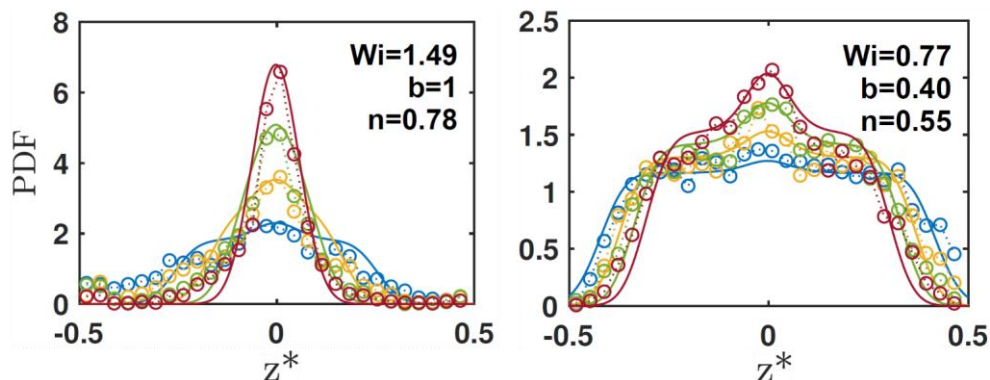


Figure 1: a) Illustration of the transverse viscoelastic migration in a plan-Poiseuille flow. b) Evolution of the experimental PDF of the particle position and theoretical prediction for two different experiments. Wi is the Weissenberg number, b and n refer to the exponent of the local power law for the normal force and the viscosity. z^* is the dimensionless particle position in the transverse direction.

flow. For low solvent viscosity ratios, the model allowed to predict the measured PDFs. By fitting these, we were able to determine the first normal stress difference as a function of shear rate. Importantly, it was in good agreement with measurement performed using standard rheometry techniques.

References

- [1] A. M. Leshansky, A. Bransky, N. Korin, and U. Dinnar, Tunable nonlinear viscoelastic ‘focusing’ in a microfluidic device, *Physical Review Letters*, 98, 1–4 (2007).
- [2] A. Naillon, C. de Loubens, W. Chèvremont, S. Rouze, M. Leonetti, and H. Bodiguel, Dynamics of Particle Migration in Confined ViscoElastic Poiseuille Flows, *Physical Review Fluids*, 4, 053301, (2019).
- [3] G. D’Avino and P. L. Maffettone, Particle dynamics in viscoelastic liquids, *Journal of Non-Newtonian Fluid Mechanics*, 215, 80–104, (2015).

Adsorption and desorption surface dynamics of gaseous adsorbate on silicate-1 by molecular dynamics simulation

J.-M. Simon^a

^aLab. Interdisciplinaire Carnot de Bourgogne, UMR 6303 CNRS-Université de Bourgogne, 9 av A. Savary, Dijon 21000.

Keywords: Adsorption, Simulation, Surface dynamics

1. Introduction

The sticking coefficient, α , is one of the fundamental quantities that quantify the dynamics process at interfaces. It represents the probability that, on approaching the external surface of a particle, a molecule will be captured by the particle and will enter its inner space (for porous solids), rather than being rejected to continue its trajectory in the open space between the particles. Its counterpart from the perspective of the particle is the desorption coefficient, β .

2. Adsorption/desorption dynamics on silicalite-1 external surface

The adsorption/desorption processes of different gaseous molecular species on the zeolite silicalite-1 have been investigated using molecular dynamics simulations. Values of α and β were computed for different temperatures and different loadings for ethylene, n-butane, argon, n-heptane [1] [2]. The results for α are summarized on Figure 1. The values of α and β and the shape of the curves will be discussed in relation with the nature of the interaction between the solid and the guest molecules, in particular the adsorption energy and the isotherm of adsorption. These results will give insights in the kinetic process of adsorption and desorption that occurs at the interface between the solid and the gas phase.

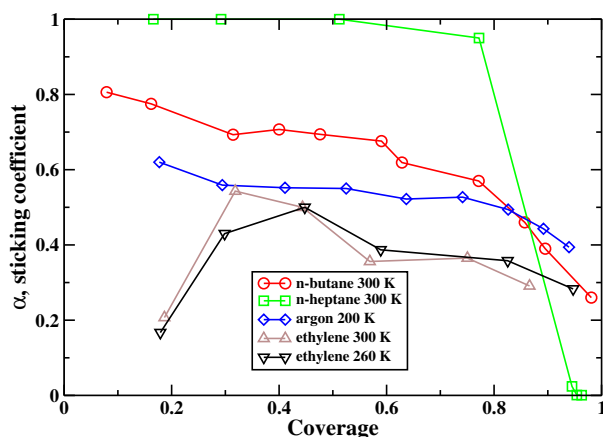


FIGURE 1: Sticking coefficient as a function of the coverage for various molecules on silicalite-1.

Références

- [1] J.-M. Simon, J.-P. Bellat, S. Vasenkov, J. Kärger, Sticking Probability on Zeolites, *J Phys Chem B*, 109, 13523 (2005).
- [2] J.-M. Simon, J.-P. Bellat and J.M. Salazar, Adsorption and desorption surface dynamics of gaseous adsorbate on silicate-1 by molecular dynamics simulation, *Molecular Simulation*, 40, 52-57 (2014).

Active Viscous Fingering

Akash Ganesh^a, Carine Douarche^a, Harold Auradou^a

^aUniversité Paris-Saclay, CNRS, FAST, 91405, Orsay, France.

Keywords: Viscous instability, Saffman-Taylor instability, Bacterial suspension, Miscible fluids, Zero viscosity fluid, Viscosity reduction by active fluid

Adding swimming bacteria to a liquid lowers its viscosity [1, 2, 3, 4, 5]. We study how this phenomenon can lead to the formation of viscous Saffman–Taylor fingers which occurs when a less viscous fluid is injected into a more viscous fluid [6]. To do this, we injected bacterial suspensions into a Hele-Shaw cell containing the suspending fluid to prove that active fluids can induce this instability. The role of the flow velocity, and bacterial volume fraction was then systematically studied. The Saffman-Taylor fingers (See Fig. 1(a,b,c)) observed are identical to those obtained with a pair of Newtonian fluids with different viscosities (See Fig. 1(e)). Quarter five spots experiments were also performed (See Fig. 1(f,g,h)). They demonstrate that the addition of bacteria in the suspension reduces the breakthrough time. These results reproduce what is observed with pairs of Newtonian fluids of different viscosities.

Our study determines the flow conditions and the bacterial volume fraction to observe the Saffman-Taylor instability from an active fluid. For run-and-tumble *E.Coli* bacteria, it requires a flow characterized by a low shear rate ($< 1s^{-1}$) and a suspension of volume fraction ($\Phi > 0.8\%$) greater than the volume fraction for which the zero viscosity regime is observed.

In the conclusion, we will examine the implications of this new instability for flow applications in porous media.

References

- [1] A. Sokolov and I. S. Aranson, Reduction of Viscosity in Suspension of Swimming Bacteria, *Physical Review Letters* **103**, [10.1103/PhysRevLett.103.148101](https://doi.org/10.1103/PhysRevLett.103.148101) (2009)
- [2] J. Gachelin, G. Mino, H. Berthet, A. Lindner, A. Rousselet, and E. Clement, Non-Newtonian Viscosity of Escherichia coli Suspensions, *Physical Review Letters* **110**, 268103 (2013), wOS:000320990800024
- [3] H. M. López, J. Gachelin, C. Douarche, H. Auradou, and E. Clément, Turning Bacteria Suspensions into Superfluids, *Physical Review Letters* **115**, 028301 (2015), publisher: American Physical Society
- [4] Z. Liu, K. Zhang, and X. Cheng, Rheology of bacterial suspensions under confinement, [arXiv:1906.04054](https://arxiv.org/abs/1906.04054) [cond-mat, physics:physics] (2019), arXiv: 1906.04054
- [5] J. Y. Y. Chui, C. Douarche, H. Auradou, and R. Juanes, Rheology of bacterial superfluids in viscous environments, *Soft Matter* **17**, 7004 (2021), publisher: The Royal Society of Chemistry
- [6] P.G.Saffman and G.I.Taylor, The penetration of a fluid into a porous medium or hele-shaw cell containing a more viscous fluid, *Proceedings of Royal Society* (1958)
- [7] P. Petitjeans, C.-Y. Chen, E. Meiburg, and T. Maxworthy, Miscible quarter five-spot displacements in a Hele-Shaw cell and the role of flow-induced dispersion, *Physics of Fluids* **11**, 1705 (1999)

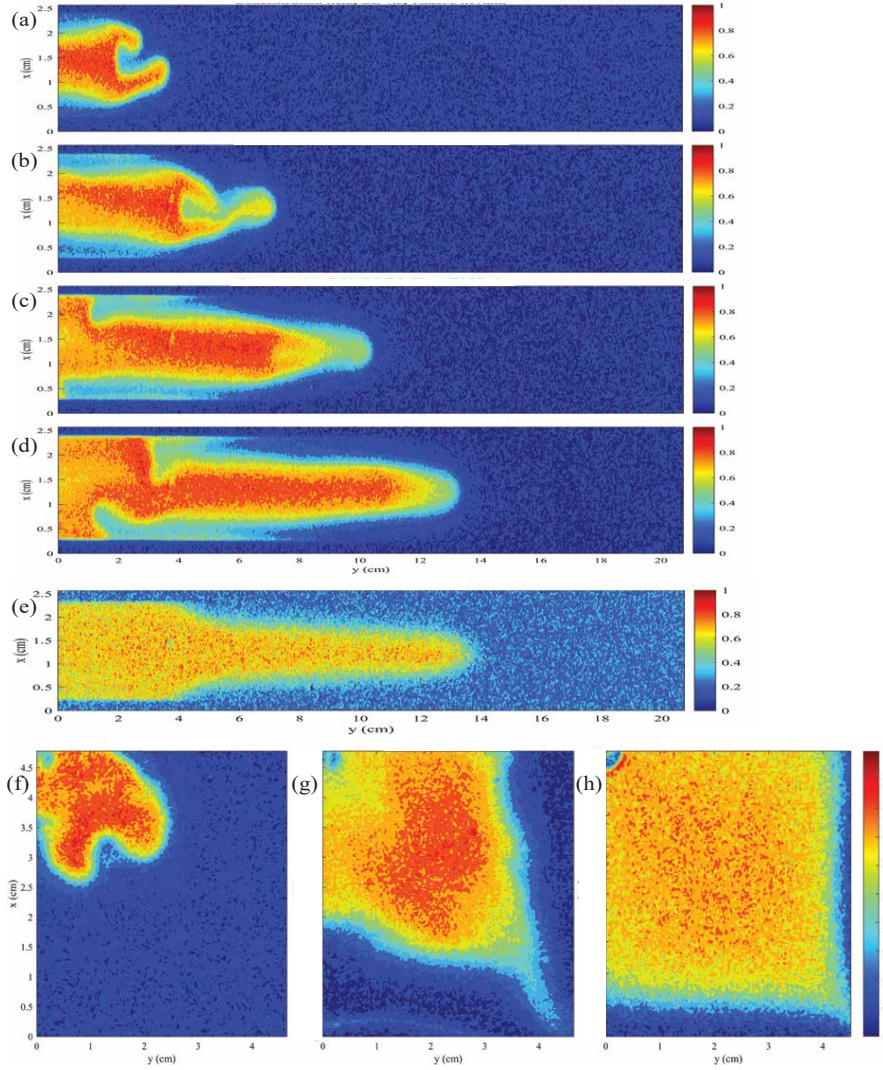


Figure 1: (a)-(d) Bacteria concentration fields for an experiment performed in a channel of width $W = 2$ cm and length $L=20$ cm. The aperture of the Hele Shax cell is $H=500\mu m$. In this experiment, a suspension containing a volume fraction $\Phi \sim 0.8\%$ of bacteria displaces the suspending fluid. (e) Displacement experiment performed with a pair of Newtonian fluids characterized by a viscosity ratio $M = 3.2$. For all experiments, the flow velocity is $U/V_s = 1.5$ where $V_s = 15\mu m.s^{-1}$ is the average bacteria swimming velocity. (f)-(g) Experiment where the suspending fluid displaces the bacteria suspension ($\Phi \sim 0.8\%$) in the quarter five-spot configuration [\[7\]](#). (h) Quarter five-spot configuration experiment performed with bacteria volume fraction ($\Phi \sim 0.1\%$) lower than the critical volume fraction.

Clogging of a 2D-porous medium: effects of main operating parameters on particle deposition and permeability reduction under geothermal conditions.

Anne-Sophie Esneu^{1,2*}, Jalila Boujlel¹, Arnaud Erriguible³ and Samuel Marre²

¹IFP Energies Nouvelles, 1-4 Avenue du Bois Préau, 92852 Rueil-Malmaison, France

²CNRS, Univ. Bordeaux, Bordeaux INP, ICMCB, 87 Avenue du Dr Albert Schweitzer, 33600 Pessac, France

³Univ. Bordeaux, Bordeaux INP, I2M, UMR 5295, 33600 Pessac, France

Keywords: colloids, clogging, microfluidic, porous media

The flow of a suspension of particles through a porous medium occurs in various environmental engineering and process applications. A precise understanding of the transport and interactions of colloidal particles in suspension is necessary to evaluate for example the fate of contaminants or the damage of geological formations. In geothermal energy, the flow of fluids loaded with mineral and organic particles can pose significant problems on the sustainability of production and the maintenance of injectivity in the short term and, in the long term, on the stability and continuity of the resource. To control particle transport, minimize clogging, enhance filtration efficiency, and mitigate potential environmental or health risks associated with colloidal particles, understanding the fate of particles flow in porous media is crucial. Hence, colloidal particle behavior in porous media has been extensively studied, primarily through macroscopic measurements such as corefloods or reconstituted porous media. However, due to the opacity of rocks, information about the mechanisms occurring at the pore scale is lacking.

More recently, progress in understanding colloidal deposition and clogging phenomena has been allowed thanks to microfluidic devices [1-6]. However, these experiments often use simplified pore-network micromodels or microchannels that do not fully replicate real porous media. In this study, we are interested in this issue and therefore use a complex pore-network micromodel. The aim is to describe, based on local information, the characteristics of permeability damage induced by colloidal deposition under conditions similar to those found in geothermal energy systems, such as high flow rates and permeability.

Microfluidics, which allows direct visualization and advanced optical quantification at the pore scale, is used along other measurements (pressure monitoring, concentration, temperature...). Two experimental setups are employed, based on different visualization techniques: optical imaging and laser-induced fluorescence (LIF) imaging. These systems integrate tools for particle concentration monitoring, pressure drop kinetics, and direct visualization of the micromodel during fluid injection. The use of both techniques provides complementary information at various scales, essential to understand the interactions between hydrodynamics (velocity, pore geometry) and DLVO forces (particle-particle and particle-surface interactions).

This experimental study has revealed significant insights into the relationships between velocity fields and deposit characteristics. Various "types" of deposits have been identified, primarily influenced by the porous medium's geometry. While pore-throat clogging plays a crucial role in reducing permeability, pore bodies can also become critical deposition zones under specific conditions and injection stages. Moreover, as the suspension concentration increases, the kinetics of permeability reduction are delayed, and clogging mechanisms, along with deposit types, evolve accordingly. At very high concentrations, hydrodynamic effects have been observed.

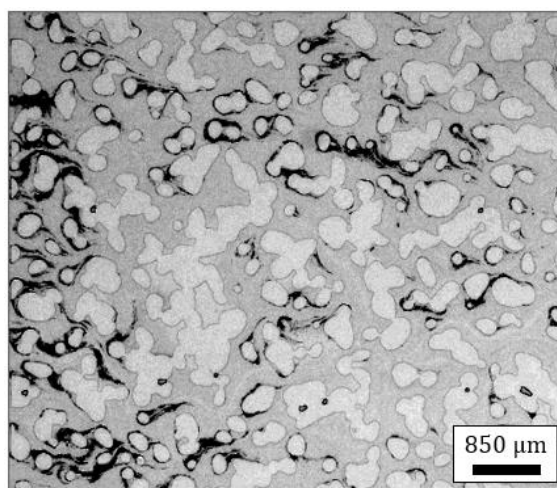


Figure 1 – Deposition of colloidal particles ($d=1\mu\text{m}$) in black in permeable porous medium (grains appear in light gray, porous area with fluid flow in medium gray).

References

- [1] Bacchin, P., Derx, Q., Veyret, D., Glucina, K., & Moulin, P.: Clogging of microporous channels networks: role of connectivity and tortuosity. *Microfluidics and Nanofluidics*, 17(1), 85–96, (2014).
- [2] Delouche, N., Dersoir, B., Schofield, A. B., & Tabuteau, H.: Flow decline during pore clogging by colloidal particles. *Physical Review Fluids*, 7(3), (2022).
- [3] Delouche, N., Schofield, A. B., & Tabuteau, H.: Dynamics of progressive pore clogging by colloidal aggregates. *Soft Matter*, 16(43), 9899–9907, (2020).
- [4] Dincau, B., Tang, C., Dressaire, E., & Sauret, A.: Clog mitigation in a microfluidic array via pulsatile flows. *Soft Matter*, 18(9), 1767–1778, (2022).
- [5] Duchène, C., Filipe, V., Huille, S., & Lindner, A.: Clogging of microfluidic constrictions by monoclonal antibody aggregates: role of aggregate shape and deformability. *Soft Matter*, 16(4), 921–928, (2020).
- [6] Kim, D. Y., Jung, S. Y., Lee, Y. J., & Ahn, K. H.: Effect of colloidal interactions and hydrodynamic stress on particle deposition in a single micropore. *Langmuir: The ACS Journal of Surfaces and Colloids*, 38(19), 6013–6022, (2022).

Droplets flow in a micromodel porous network

E. Speirs^a, C. Brigodiot^a, N. Pannacci^a, M. Moreaud^a, M.-C. Jullien^b

^aIFP Energies nouvelles, 1-4 avenue de Bois-Préau, 92500 Rueil-Malmaison, France

^bIPR - Institut de Physique de Rennes, 263 Avenue Général Leclerc, 35700 Rennes

Keywords: micromodel, complex fluid, droplets flow

Multiphase flow in porous media is encountered in many natural phenomena and industrial processes, such as geologic CO₂ sequestration, water infiltration into soil, and particle filtration. Numerous questions are of interest on this topic, such as to the effect of the confinement and the geometry of the porous medium on the transport of dispersions.

We address these questions experimentally using controlled transparent 2D porous media: micromodels. We used polydimethylsiloxane (PDMS) micromodels consisting of regular networks of vertical cylindrical posts (50 μm in diameter), at the centres of which we injected water droplets in a continuous oil phase (radial flow). In such a geometry of the porous medium, the alignment of the posts, i.e. the tortuosity of the network, varies angularly in a periodic manner. We show that this tortuosity plays a key role in droplet transport by generating reproducible preferential paths. We characterize the droplet flow varying the geometrical configuration of the posts, injection capillary number, droplet size, and droplet concentration. We observe that at low capillary numbers, the droplet transport is homogeneous (isotropic). By increasing the capillary number, droplets initially follow the least tortuous paths before transitioning to a stable flow regime whereby droplets flow in the most tortuous paths. The axes of symmetry observed at a centimetre scale in the flow are found to be the same as the ones at the microscale of the periodic patterns. Through large-scale droplet tracking, we demonstrate the influence of the geometric tortuosity of the media on the resulting droplet flow patterns and the counter-intuitive responses that can arise. We also report observations on droplet rupture and preliminary results on the effect of patterns of wettability in the porous medium.

Water absorption of particles immersed in a colloidal suspension: Application to recycled concrete

F. Théré^a, J. Naël-Redolfi^a, P. Boustingorry^a, N. Roussel^b, E. Keita^b

^a*Chryso, Sermaises du Loiret, France*

^b*Navier Lab, Univ Eiffel/CNRS /ENPC, Champs-sur-Marne, France*

Keywords: Imbibition, Colloidal suspension, Building materials

This study investigates the water transfer dynamics between porous aggregates and fresh cement paste, particularly in the context of generalizing recycled aggregate uses in construction practices. Indeed, the increasing adoption of recycled aggregates is due to limited alluvial resources and the distinct composition and structure of these recycled materials compared to natural aggregates.

This study establishes the relationship between colloidal suspensions (fresh cement paste) and a porous medium (hardened cement paste). Due to its high porosity, the hardened cement paste absorbs a substantial amount of water, despite having smaller pore sizes than the particles suspended in the fluid being absorbed.

To explore water transfer phenomena, we employed sintered glass beads as a model for porous media, and water serves as a substitute for cement paste to better understand the underlying physical processes. The influence of the porous medium's geometry and microstructure on imbibition kinetics during water immersion is investigated, necessitating the development of geometry-specific imbibition models since the traditional Washburn model is insufficient for describing the observed kinetics.

Subsequently, the water transfer between fresh cement paste and the porous aggregates is characterized using advanced Nuclear Magnetic Resonance spectrometry (NMR) techniques. The findings reveal that the absorption of aggregates in fresh cement paste is lower than pure water absorption, primarily attributable to the contraction of the fresh cement paste during the imbibition process. Furthermore, the absorption kinetics in this scenario is notably slower than in pure water.

In conclusion, this study provides valuable insights into the complex interactions between water intake by porous media and compression of colloidal suspensions. Understanding the intricate water transfer dynamics will improve the mix-design of recycled concrete properties and, more generally, may be used to better understand many processes beyond building materials.

Swelling and maturity effects on adsorption in organic source rocks' organic matter by molecular simulations

A. Obliger, K. Potier, J.-M. Leyssale

Institut des Sciences Moléculaires de Bordeaux, UMR 5255, Univ. de Bordeaux – CNRS, F-33400 Talence, France

Keywords: kerogen, maturity, carbon sequestration, adsorption, swelling

The term "kerogen" defines the source rocks' organic matter (OM) that produces oil during the geological process of thermal maturation, in which the OM is progressively exposed to higher temperatures and pressures. Now, kerogen's definition is restricted to the source rocks' OM that is insoluble in the usual organic solvents. The maturity of a kerogen reflects whether it is in a state of oil generation (immature), gas generation (mature), or above its hydrocarbon production stage (overmature). In the so-called van Krevelen diagram, the maturation of kerogen is characterized through a two-dimensional diagram showing the evolution of the atomic H/C and O/C ratios, where three kerogen families are classified according to the origin of the OM: type I kerogen, with the largest H/C and lowest O/C, originates from lacustrine environments, type II kerogen from marine deposits and type III kerogen, with the lowest H/C and largest O/C, from terrestrial plants and animal remains [1]. Kerogen has gained a lot of attention due to the emergence of shales gas because it is the key phase impacting the processes of hydrocarbon recovery or carbon sequestration as the fluid molecules are mainly trapped in the vicinity of its amorphous microporosity (pore size < 20 Å). Owing to the inherent complexity, heterogeneity, and diversity of kerogens, predicting their thermodynamic properties remains challenging.

In the past decade, several atomistic models of kerogen have been proposed [2,3,4] in order to study kerogens' properties through molecular simulations (see [5] for a review). Among such models, those of Ungerer *et al.* [3] have been the most widely used. They are built by packing a number of identical kerogen molecules, that respect the OM chemistry, in a periodic simulation box using annealing and cooling Molecular Dynamics (MD) simulations.

More recently, another strategy based on the Replica Exchange Molecular Dynamics (REMD) method was developed to obtain kerogen's models directly related to their organic precursor [4]. The thermal decomposition of the latter (lignin, cellulose, etc.) is simulated through the REMD technique with the use of a reactive force field (ReaxFF) to allow for chemical bond breaking and formation. The REMD method accelerates the sampling of the full energy landscape over geological timescales by considering the dynamics of the initial precursor at various temperatures (above the geological one) and by allowing exchanges at a constant time interval between configurations of neighboring temperatures according to a Metropolis criterion. In the end, the resulting kerogen structure depends on the precursor considered (type) and the simulation duration (maturity). Ultimately, the fluid generated during the degradation process is removed from the simulation box and the resulting kerogen microstructure is equilibrated at a given pressure and temperature.

Here, based on the REMD technique, we present a new collection of atomistic models of kerogen (REMD models), obtained from a fatty acid precursor (type I), at various maturities (H/C ratio from 1.3 to 0.3). Additionally, the chemical inconsistencies of the obtained models resulting from the inherent approximations in the reactive force field used during the REMD simulations are corrected using a simulated annealing algorithm. Radicals of the kerogen microstructure are first identified, and then a Monte-Carlo method is used to ensure that all atoms satisfy the duet or the octet rules by adding (or removing) hydrogens or transforming a pi (sigma) bond into a sigma (pi) one. A similar procedure can be used to control the quantity of oxygen by functionalizing the microstructure. Once corrected, the kerogens' microstructures can be simulated using the OPLS classical force field, allowing for very efficient molecular simulations. Before turning to their adsorption properties, the evolution of their chemical, structural and mechanical properties (aromatic cluster size, heptagons/pentagons ratio, porosity, bulk modulus, etc..) as function of the H/C ratio is investigated first to notably show that they clearly follow simple trends.

We present a comparative study of CO₂ adsorption in some of our models and those of Ungerer *et al.*, which correspond in terms of H/C and O/C ratios, while accounting for the poromechanical coupling between the adsorbed fluid and the kerogen microstructure, i.e., the ability of the structure to deform and swell upon adsorption. This is achieved by alternating between molecular simulations in the grand-canonical (μVT) and the isobaric-isothermal (NPT) ensemble for a large number of cycles, until both, the volume V and the number of adsorbed molecules N fluctuate around equilibrium values, giving thus access to the adsorption isotherm and the volumetric swelling. The imposed chemical potential of the fluid corresponds to a bulk fluid at the same mechanical pressure P that is imposed on the system (unjacketed or drained condition). Strikingly, we find that for pressures above tens of MPa Ungerer's models start to dissolve in CO₂, unlike the REMD models (see Fig. 1). This is mainly due to the lack of cross-linking between the molecules used to build the models. Even for the most immature REMD model considered here (H/C = 1.53), the low amount of cross-linking in the model ensures its insolubility at large pressures, even though the volumetric swelling is important ($\sim 37\%$). Notably, it is also found that for the slightly more mature case (H/C = 1.12), both models have very similar adsorption isotherms at low pressure, although their accessible porous volumes can differ by 50%. We also note that, with increasing maturity (H/C ratio from 1.53 to 0.59), the porosity of the REMD models at low pressure evolves from roughly 7 to 37%, while it ranges from roughly 1 to 14% for Ungerer's models.

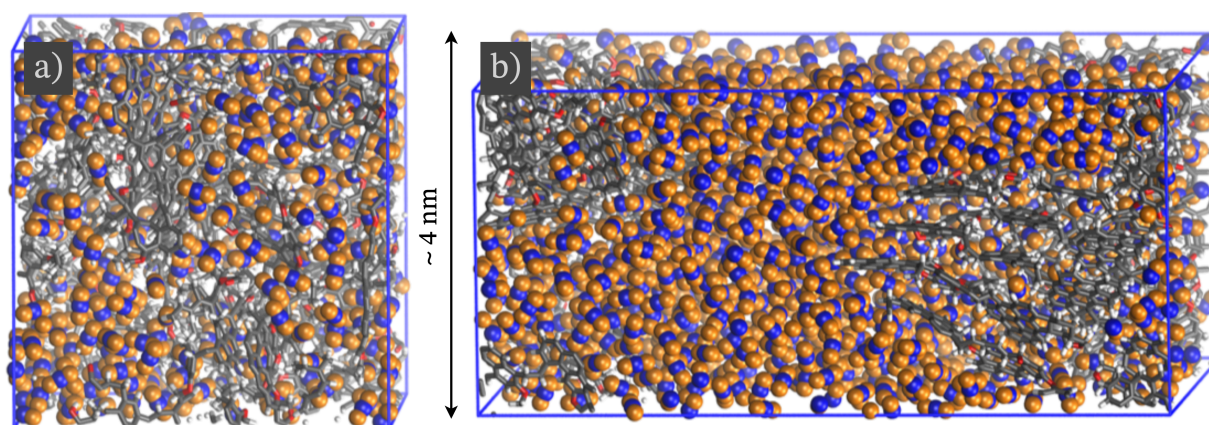


Figure 1: Snapshots of the simulation cell with periodic boundary conditions in all dimensions for our REMD (a) and Ungerer's (b) models, both having an H/C ratio of 0.59, at 300 K and 50 Mpa. The adsorbed CO₂ is represented with blue and orange spheres for the carbon and the oxygens, respectively. The atoms of the kerogen's microstructures and their bonds are in gray, white, and red for the carbons, hydrogens, and oxygens, respectively. We clearly see in b) that the kerogen microstructure has dissolved in the fluid.

Finally, a study of adsorption for CH₄ and CO₂ is presented for nine REMD models corresponding to a fatty acid precursor with maturities ranging from very immature to overmature (H/C from 1.3 to 0.3), so as to unveil the effect of the maturity on the adsorption properties while always accounting for the adsorption-induced swelling, which largely prevails when the H/C ratio is greater than 0.7 for both fluids, even though swelling is more important in the case of CO₂.

References

- [1] Vandenbroucke, M.; Largeau, C., Kerogen origin, evolution and structure, *Organic Geochemistry*, 38, 719–833 (2007).
- [2] Ungerer, P.; Colléll, J.; Yiannourakou, M., Molecular modeling of the volumetric and thermodynamic properties of kerogen: Influence of organic type and maturity, *Energy & Fuels*, 29, 91–105 (2015).
- [3] Bousige, C. *et al.*, Realistic molecular model of kerogen's nanostructure, *Nature Materials*, 15, 576–582 (2016).
- [4] Atmani, L. *et al.*, Simulating the geological fate of terrestrial organic matter: Lignin vs cellulose, *Energy & Fuels*, 34, 1537–1547 (2020).
- [5] Obliger, A. *et al.*, Development of atomistic kerogen models and their applications for gas adsorption and diffusion: A mini-review, *Energy & Fuels*, 37 (3), 1678–1698 (2023).

Pore-scale modeling of pore-clogging by aggregation of particles

L. F. Maya^{a,b}, P. Leroy^b, L. André^{a,b}, C. Soulaïne^a

^a*Institut des Sciences de la Terre d'Orléans (ISTO), UMR7327, F-45071, Orléans, France*

^b*BRGM, F-45060, Orléans, France*

Keywords: Colloid deposition, pore-clogging, CFD-DEM, DLVO Theory

The injection of cold water into the subsurface to recharge the aquifer during the exploitation of geothermal resources mobilizes fine particles (colloids) that can detach, precipitate, or even deposit irreversibly clogging the porous formation in the vicinity of the well. These processes very often lead to a reduction in the operating time of the wells and additional operating costs are required in order to separate and remobilize the aggregates thus formed. At the reservoir scale, these processes are described using CFT (Colloidal Filtration Theory) and the Kozeny-Carman relationship. Such models, however, rely on heuristic parameters that have to be tuned to fit with experimental data, which limits their predictive capabilities. In this work, we use a novel CFD-DEM (Computational Fluid Dynamics - Discrete Element Method) approach for simulating the transport of particles at the pore-scale. Our model includes both resolved and unresolved coupling, meaning that we are limited by the particle-to-cell aspect ratio. The model relies on a four-way CFD-DEM coupling that includes hydro-mechanical interactions (e.g. collision, drag, buoyancy, gravity) and electro-chemical interactions (e.g. van der Waals attraction, electrostatic double layer repulsion commonly known as DLVO (Derjaguin-Landau-Verwey-Overbeek) forces and JKR (Johnson-Kendall-Roberts) adhesive contact) between the particles, the fluid, and the porous formation. The model, implemented within the open-source platform OpenFOAM, has been validated in cases for which reference solutions exist. It is used to investigate the deposition/remobilization kinetics and the permeability/porosity relationship at the pore-scale under various flow, particle size, concentration, pH, and salinity conditions. These new insights into the transport and deposition of colloids in porous media will guide the development of reservoir-scale models rooted in elementary physical principles.

Bubble nucleation in liquids confined in nanopores.

J. Puibasset^a

^aICMN, UMR7374 CNRS - Université d'Orléans, 45071 Orléans, France

Keywords: molecular simulation, nucleation, nanopore

1 Introduction

The extreme confinement of fluids in nanopores strongly affects their properties, which has measurable consequences even at the micrometre scale. One can cite the effect of surface chemistry or corrugation, local curvature, pore morphology, or any other nanometre-scale property of the surface. Molecular simulation is a powerful route to address such issues since it takes into account the relevant fluid/fluid and fluid/substrate interactions at the atomic scale. The present study focuses on cavitation in bulk and confinement.

2 Discussion

An interesting issue is the out-of-equilibrium pore emptying, in particular in the case of the so-called inkbottle pores that are connected to the outside only through narrow channels. Focusing on the molecular simulation of fluids confined in chemically disordered pores, we will show how the heterogeneities induce the appearance of metastable states, and how these states can be used to study cavitation in inkbottle pores. The simulations are compared to the classical nucleation theory, through the direct evaluation of the nucleation rate and the barrier height. The results are relevant to experiments showing that in such pores desorption proceeds via liquid fracture (cavitation).

A second interesting feature concerns the bubble size distribution. From a statistical point of view, the bubble nucleation barrier $W(s)$ is related to the equilibrium bubble size distribution $p(s)$ through the Boltzmann factor $p(s) \sim \text{EXP}(-W(s)/kT)$. In principle, $p(s)$ is measurable in equilibrium molecular simulations. However, we will show that, in practice, the quantity that can be obtained from simulations is the distribution of the *largest* nucleus $p^l(s)$ and not of *all* nuclei $p(s)$. We will show how few mathematics help to rigorously transform $p^l(s)$ into $p(s)$. This opens new routes to the calculation of nucleation barriers in realistic thermodynamic conditions.

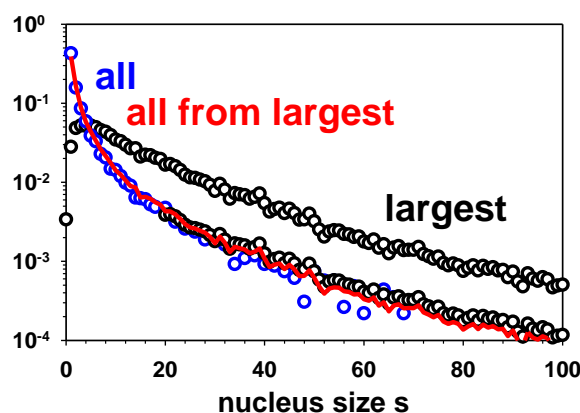


Figure 1: bubble size distributions: black symbols: $p^l(s)$ as given by biased simulations; blue symbols: the expected $p(s)$; red line: mathematic transformation of $p^l(s)$ into $p(s)$.

References

- [1] Puibasset, J., Adsorption/Desorption Hysteresis of Simple Fluids Confined in Realistic Heterogeneous Silica Mesopores of Micrometric Length: A New Analysis Exploiting a Multiscale Monte Carlo Approach, *J. Chem. Phys.* 127, 154701 (2007).
- [2] Puibasset, J., Adsorption-Induced Deformation of a Nanoporous Material: Influence of the Fluid–Adsorbent Interaction and Surface Freezing on the Pore-Load Modulus Measurement, *J. Phys. Chem. C* 121, 18779-18788 (2017).
- [3] Puibasset, J., Cavitation in Heterogeneous Nanopores: The Chemical Ink-Bottle, *AIP Adv.* 11, 095311 (2021).
- [4] Puibasset, J., A General Relation between the Largest Nucleus and All Nuclei Distributions for Free Energy Calculations, *J. Chem. Phys.* 157, 191102 (2022).
- [5] Puibasset, J., Are nucleation bubbles in a liquid all independent?, *J. Mol. Liq.* accepted (2023).

Session
Milieux fibreux multi-échelles,
nano et micro poreux

Probing diffusional exchange in mesoporous zeolite by NMR diffusion and relaxation methods.

M. Fleury^a, G. Pirngruber^b, E. Jolimaître^b

^a IFP Energies nouvelles, 1 et 4 avenue de Bois-Préau, 92852 Rueil-Malmaison, France

^b IFP Energies nouvelles, Rond-point de l'échangeur de Solaize, BP 3, 69360 Solaize, France

Keywords: zeolite, NMR relaxation, diffusion, cryoporometry

1 Introduction

USY zeolites belong to the most frequently used zeolite catalysts. They were historically developed for an application in fluid catalytic cracking and subsequently in hydrocracking. More recently they are also widely applied for the pyrolysis of biomass, for plastic recycling, etc. During the synthesis and shaping processes, the thermal dealumination generates mesopores within the zeolite crystals and the alumina binder. Since these crystals are rather large (cross section in the order of 0.5 μm), the generation of mesopores supposedly favors the transport of reactants and products to and from the acid sites in the crystal.

The approach taken in this work is different from simple or advanced diffusion measurements. Instead, we propose to use relaxation methods to evaluate diffusive exchange between the different porosity compartments in a shaped catalysis support that could be used in industrial processes. Zeolite extrudates were prepared on purpose for the present study, with a very high zeolite content, so as to be as sensitive as possible to the role of zeolite microporosity.

2 Results

1.1 Pore size distribution by NMR cryoporometry, and long range diffusivity by PFG-NMR

The two pore systems were first characterized using NMR cryoporometry in the range 2 nm up to 1 μm (Figure 1). To complement these results in the microporosity range, we measured the amount of unfrozen water using T_2 relaxation data at -29°C , the lowest temperature reached in the cryoporometry experiments at which water located in pores smaller than 2 nm does not freeze. Hence the two pore systems are fully characterized in the entire pore size range of interest (Table 1). CBV400 contains a slightly dealuminated USY zeolite with a fairly low mesopore volume while CBV720 contains a strongly dealuminated form of USY, with a significantly higher internal mesoporosity. Hence the mesoporosity of CBV720 is a combination of the zeolite mesoporosity and the alumina binder.

Diffusional tortuosity was measured using extrudates fully saturated with cyclohexane and standard PFG-NMR techniques. The advantage of using cyclohexane is that T_2 relaxation times are much larger than when saturated with water. The diffusion coefficients are then easily determined at a diffusion time t_d of 29.7 ms, with a corresponding diffusion length $(6Dt_d)^{1/2}$ of about 9.5 μm . Hence, we are measuring a pore diffusivity in which molecular motions are much larger than any pore size in the system (zeolite, mesopores and macropores). CBV720 has a larger tortuosity than CBV400 (Table 1).

	CBV400	CBV720
Microporosity (<2 nm) (ml/g)	0.266	0.244
Mesoporosity (2 – 50 nm) (ml/g)	0.343	0.202
Macroporosity (>50 nm) (ml/g)	0.138	0.239
Porous volume (ml/g)	0.747	0.684
Diffusional tortuosity (cyclohexane)	3.11 ± 0.12	3.55 ± 0.14

Table 1: Combined characterization of the pore systems by cryoporometry and relaxation data for the microporosity.

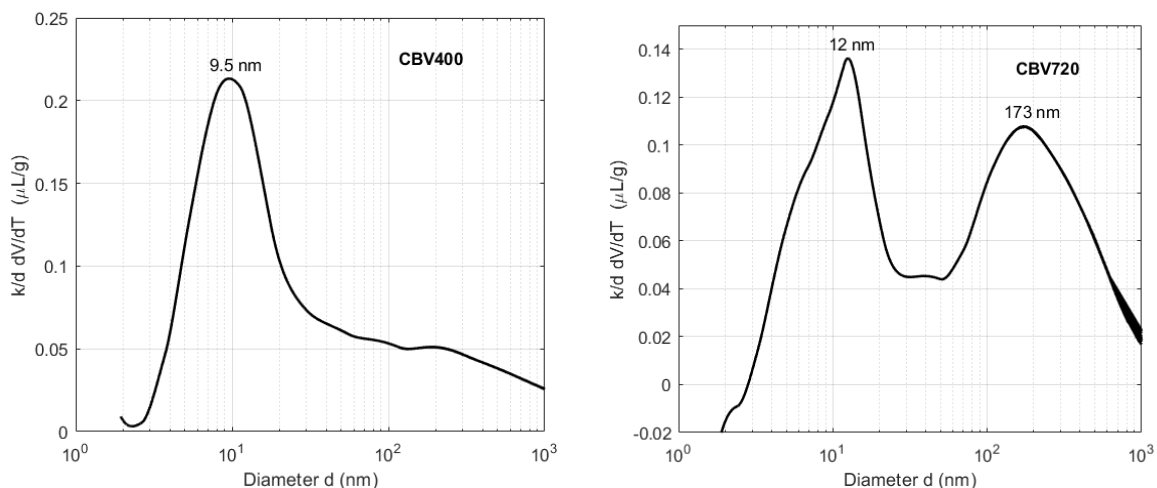


Figure 1: Meso and macropore size distribution by NMR cryoporometry for the two systems studied.

1.2 Short range diffusivity using T2-exchange-T2 experiments with squalane.

The diffusive exchange at short length scales is evidenced by relaxation exchange experiments on the same systems saturated with squalane (Figure 2 left). At 90°C, the bulk diffusion coefficient of squalane is $0.26 \cdot 10^{-9} \text{ m}^2/\text{s}$ and therefore the diffusion length becomes comparable to macropores. The diffusive exchange between the different porosity compartment is quantified by the analysis of the off diagonal peak amplitudes vs. exchange time t_e (Figure 2 right). While the exchange times were found similar for both systems, a larger number of molecules are exchanged for CBV720. We conclude that the mesoporosity of CBV720 has a beneficial effect for the access of molecules to microporosity. More details are given in reference [1].

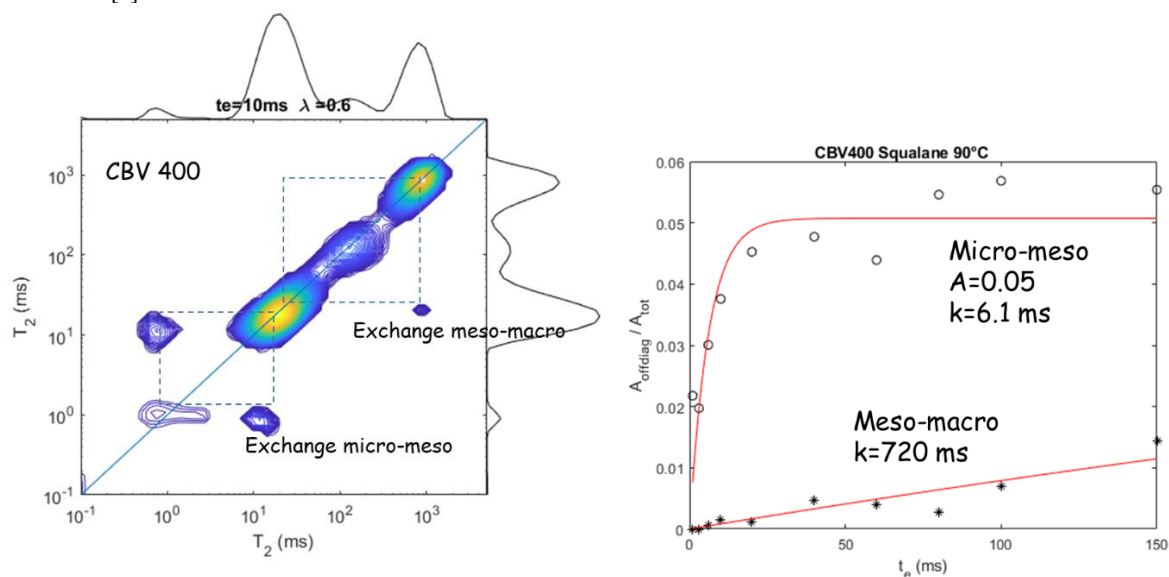


Figure 2: Left: relaxation exchange experiments performed with squalane at 90°C. The off-diagonal amplitudes indicate the diffusive coupling between micro and mesopores, but also between meso and macropores. Right: normalized off diagonal peak amplitudes vs. exchange time.

References

[1] M. Fleury, G. Pirngruber, E. Jolimaître, Probing diffusional exchange in mesoporous zeolite by NMR diffusion and relaxation methods, *Microporous and Mesoporous Materials* 355 (2023) 112575

Acid sites confinement in micro/mesoporous Y zeolite revealed from in situ IR monitoring of tri-tert-butylpyridine diffusion.

Y. Han, I. Clemencon, E. Soyer, M. Rivallan, G. Pirngruber, K. Larmier
IFP Energies nouvelles, Rond-point de l'échangeur de Solaise, BP 3, 69360 Solaise, France

Keywords: FTIR, diffusion, zeolite, catalysis, acid site

1 Introduction

The zeolite faujasite is widely used in catalytic applications. The as-synthesized zeolite must be dealuminated by steaming at high temperatures and/or acid leaching to prepare a more stable form, the so-called ultrastable Y (USY). During this treatment, framework Al atoms responsible for Brønsted acidity are removed and mesoporosity is created. These mesopores are very useful for improving the transport properties within the crystal, but they are generated at the expense of initial micropores, leading to a hierarchical meso/microporous material with diminished acidity. The challenge in catalyst development is to find the best compromise between improving transport within the crystal and preserving acidity. We thought that the best method to characterize at the same time the concentration and the accessibility of acid sites was to use the adsorption of a very bulky base. Its adsorption on the acid sites provides the driving force for diffusion, but the diffusion into the micropores is very slow, if the size of the base exceeds the size of the pore apertures. This perfectly reflects what is happening in the catalytic conversion of bulky molecules. In the present work, we used tri-tert-butylpyridine molecule (TTBPy, kinetic diameter 1.1 nm vs. 0.74 nm pore aperture in the faujasite structure) as a bulky base and followed its adsorption in hierarchical faujasite zeolites by IR spectroscopy [1,2].

2 Experimental section

Hierarchical USY zeolites with very high mesopore volumes were prepared by desilication of commercial USY zeolites (purchased from Zeolyst).

Diffusion of TTBPy was performed in a transmission FTIR coupled reactor at 150°C, after previous thermal activation of self-supported wafer zeolite (~15 mg, 13 mm diameter) at 450°C under vacuum.

3 Results and discussion

The Brønsted acid sites in USY zeolites are bridging Si(OH)Al groups, which have two characteristic IR bands (OH stretching vibrations): at 3625 cm⁻¹ (called high frequency or HF band) and at about 3570 cm⁻¹ (called low frequency or LF band), see Figure 1. Upon adsorption of TTBPy, the intensities of these bands slowly decrease, because the OH groups interact with the base. At the same time, a new NH stretching vibration band appears, due to protonated TTBPy, and increases slowly with time (Figure 1B).

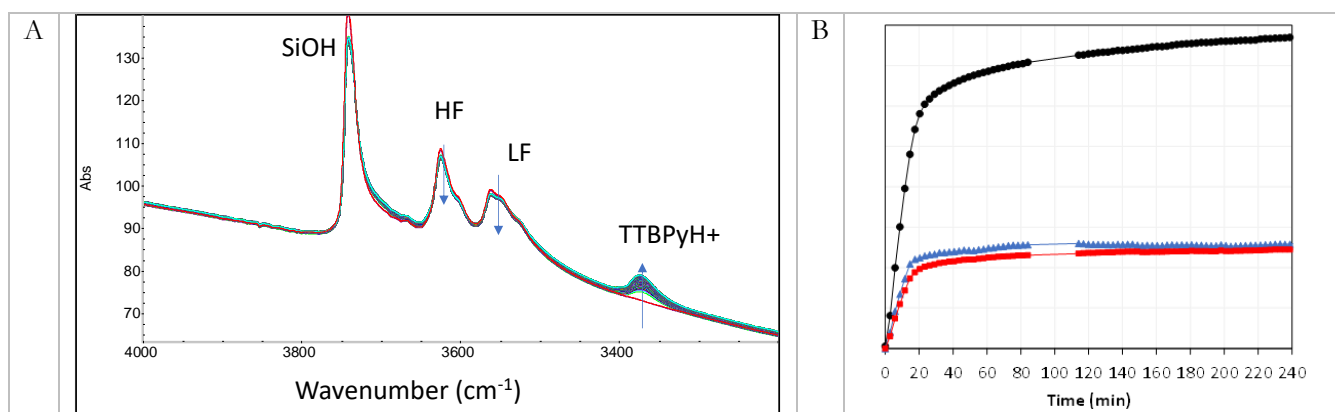


Figure 1A: IR spectra series of CBV720 in contact with TTBPY at 150°C, B: example of a time evolution of the HF band (red), the LF band (blue) and the TTBPYH⁺ band (black).

The diffusion into zeolite micropores is often controlled by surface barriers. We, therefore, fitted the uptake curves by a sum of two terms: (i) a Fickian diffusion term, describing the transport in the mesopores (the fast uptake in Figure 1B) and (ii) an exponential rate equation describing surface barrier controlled diffusion into the micropores (the slow uptake in Figure 1B) [3]. The fit allowed us to determine the concentration of acid sites in the mesopores and in the micropores, as well as the characteristic diffusion times of both processes. The relation of these parameters to the textural characteristics of the samples as well as the impact on the catalytic properties will be discussed in detail in the presentation.

References

- [1] L. Lakiss, Probing the Brønsted Acidity of the External Surface of Faujasite-Type Zeolites, *ChemPhysChem*, 21, 1873 (2020).
- [2] T. W. Beutel, Probing External Brønsted Acid Sites in Large Pore Zeolites with Infrared Spectroscopy of Adsorbed 2,4,6-Tri-tert-butylpyridine, *J. Phys. Chem. C*, 125, 16, 8518–8532 (2021).
- [3] M.R. Bonilla, Diffusion Study by IR Micro-Imaging of Molecular Uptake and Release on Mesoporous Zeolites of Structure Type CHA and LTA, *Materials*, 6(7), 2662 (2013).

Porous capsules with liquid core prepared by Pickering emulsion: Understanding of diffusional phenomena for catalyst implementation.

R. Duclos^{a,b}, D. Loffical^b, C. Dalmazzone^b, D. Proriot^b, S. Humbert^b, S. Parola^a, F. Lerouge^a

^a *Laboratoire de chimie, ENS de Lyon, 46 allée d'Italie, 69342 Lyon Cedex 07, France.*

^b *IFP Energies Nouvelles, Etablissement de Lyon, Rond-point de l'échangeur de Solaize, 69360 Solaize, France.*

Keywords: catalysis, Pickering, emulsion, encapsulation, sol-gel, capsule, core-shell, porous, nanoparticle

The ideal catalyst is likely to merge the advantages of both homogeneous and heterogeneous catalysis. For example, it may exhibit the performance of a homogeneous catalyst in terms of activity and selectivity combined with the ease of use of a heterogeneous catalyst. In that context, the possibility to entrap a homogeneous phase catalytic system within a solid porous capsule would lead to a system that allows the catalytic performances to be maintained under certain conditions [1], with a material that is easy to handle. Therefore, the conditions for maintaining its performances lie partly in the efficiency of diffusional transfers:

- The transfer of reagents from the external medium (phase immiscible with the internal phase of the capsule) to the interior of the capsule. This transfer takes place via a solid medium which constitutes the capsule shell (Figure 1, A and B).
- The transfer of the reaction products from the liquid phase inside the capsule (phase immiscible with the phase outside the capsule) to the outside of the capsule (Figure 1, C).
- The transfer of the catalytic system from a liquid phase inside the capsule to an immiscible phase on the outside via the shell. This phenomenon must be absolutely limited to maintain the catalytic activity.

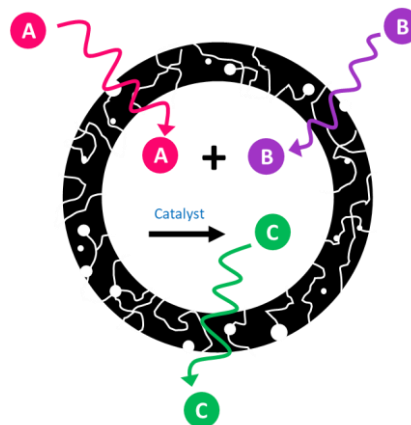


Figure 1 - Diffusions through a capsule

Such type of material can be obtained from a Pickering emulsion [2, 3] (emulsion stabilized with solid nanoparticles), where the dispersed phase is a homogeneous phase catalyst. Then, in order to prepare liquid filled microcapsules, shell consolidation can be achieved by sol-gel process to create a metal oxide (such as SiO₂) porous wall allowing reagents and products to diffuse easily [2, 4].

Here, we describe the design of such material obtained by a Pickering emulsion using hydrophobized silica nanoparticles with ionic liquids ([BMIM][NTf₂] and [BMIM][BF₄]), water and a catalyst (HNTF₂) as the dispersed phase and heptane as the continuous phase. These ionic liquids and this catalyst have been chosen in order to carry out the isobutene dimerization reaction, which is the model reaction chosen for this project because it is well mastered by IFPEN. The final capsules are formed from the emulsion droplets by hydrolysis of alkoxy silanes and polycondensation of the resulting products. Those capsules have been studied using optical microscopy, scanning electron microscopy (SEM), confocal microscopy, nitrogen sorption and mercury porosimetry. The main difficulty lies in characterising the capsules: Indeed, once the sol-gel process is complete, the capsules must remain in suspension to be used for the model reaction. This is a source of concern regarding the evaluation of certain characteristics like textural properties impacting diffusion. Indeed, the material needs to be dried to perform nitrogen sorption or mercury porosimetry. When dried, silica gel is subject to shrinkage, which completely changes its textural properties [5]. The results obtained using mercury porosimetry or nitrogen sorption therefore do not represent the real system. However, it is possible to obtain the real porosity and pore size distribution of capsules still in liquid using a less common method: thermoporometry, which is a calorimetric method for characterizing pore structure from the melting or freezing point depression of a liquid confined in a pore [6].

A washing protocol has been developed to extract all the substances contained in the capsules, particularly the ionic liquids. This included successive washes with methanol and heat treatment at 390°C under nitrogen to decompose the ionic liquids remaining after the washes, while limiting densification of the silica gel due to dehydroxylation and decomposition of silanols, leading to polycondensation. The first capsules synthesised had intermediate type II/type IV isotherms with a hysteresis loop that starts at high pressure (reflecting the presence of large mesopores) and ends at around 0.42 (reflecting the presence of small mesopores) (Figure 2). The BET specific surface area obtained varies between 200 and 250 m²/g, the mesoporous volume between 0.4 and 0.45 cm³/g and the microporous volume between 0.05 and 0.1 cm³/g. The DFT pore size distribution shows peaks in micropores area at 1.4 and 1.7 nm and peaks in mesopores area at 4 and 50 nm (Figure 3). These results were confirmed using the BJH model for mesopores and the HK model for micropores. These capsules have a multiscale porosity: microporosity, mesoporosity and mercury porosimetry confirmed that there is even macroporosity.

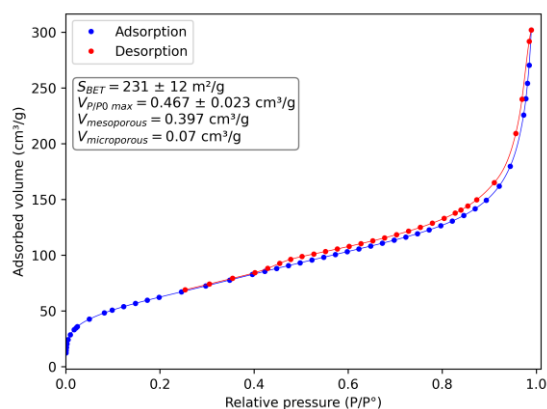


Figure 2 – Nitrogen isotherms of dried capsules

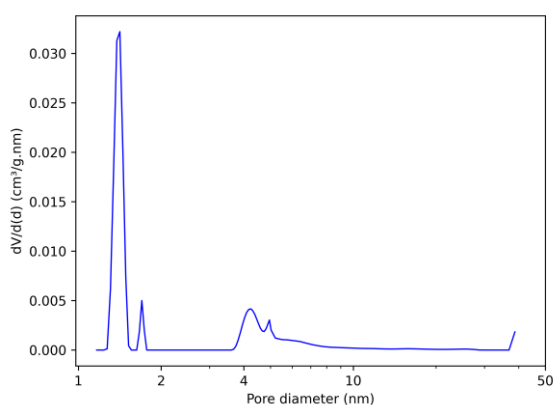


Figure 3 – DFT PSD

However, textural properties of silica gel forming the shell of these capsules are highly dependent on experimental conditions, including pH, molar ratio of water to alkoxy silane, type and functionalisation of the alkoxy silane and temperature.

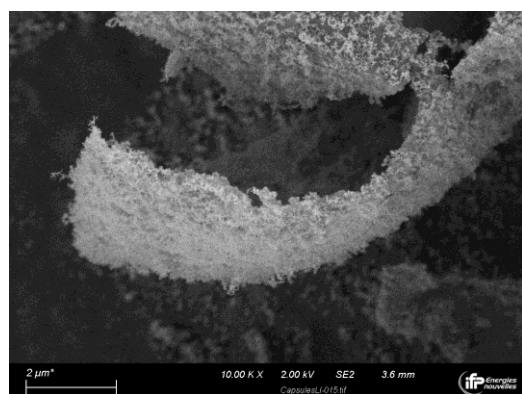


Figure 4 – SEM image of capsule wall

The diameter of the capsules depends on that of the Pickering emulsion droplets which varies according to the speed of agitation during emulsification and the quantity of nanoparticles introduced. Capsules ranging from 10 μm to 50 μm were obtained using an Ultraturrax. Capsules' shell is very thin (approximately 50 nm) (Figure 4), which results in very low mechanical strength (the capsules crush on themselves or break very easily).

The textural properties, size and thickness of the capsules have an influence on diffusion, so it's important to master them.

References

- [1] Zhang, X.; Hou, Y.; Ettelaie, R.; Guan, R.; Zhang, M.; Zhang, Y.; Yang, H. Pickering Emulsion-Derived Liquid–Solid Hybrid Catalyst for Bridging Homogeneous and Heterogeneous Catalysis. *J. Am. Chem. Soc.*, 141, 5220–5230 (2019).
- [2] Jiang, H.; Hong, L.; Li, Y.; Ngai, T. All-Silica Submicrometer Colloidosomes for Cargo Protection and Tunable Release. *Angew. Chem. Int.*, 57, 11662 – 11666 (2018).
- [3] Zhang, M.; Ettelaie, R.; Yan, T.; Zhang, S.; Cheng, F.; Binks, B. P.; Yang, H. Ionic Liquid Droplet Microreactor for Catalysis Reactions Not at Equilibrium. *J. Am. Chem. Soc.*, 139, 17387–17396 (2017).
- [4] Zhang, L.; D'Acunzi, M.; Kappl, M.; Auernhammer, G. K.; Vollmer, D.; van Kats, C. M.; van Blaaderen, A. Hollow Silica Spheres: Synthesis and Mechanical Properties. *Langmuir*, 25, 2711–2717 (2009).
- [5] Brinker, C.J., Drotning, W.D. & Scherer, G.W. A Comparison between the Densification Kinetics of Colloidal and Polymeric Silica Gels. *MRS Online Proceedings Library* 32, 25 (1984).
- [6] Landry M. R., Thermoporometry by differential scanning calorimetry: experimental considerations and applications. *Thermochimica Acta*, 433, 27-50 (2005).

Session
Modélisation numérique
des écoulements en milieux poreux

A finite element solver for modeling coupled heat transfers in architected porous media up to very high temperature

S. Ouchtout^a, L. Cangemi^a, Y. Favennec^b, B. Rousseau^b

^a*IFPEN, 92852 Rueil-Malmaison, France.*

^b*Nantes Université, CNRS, Laboratoire de Thermique et Energie de Nantes, 44306 Nantes, France.*

Keywords: Architected Porous Media, Convective-Conductive-Radiative Heat Transfers, Darcy-Brinkmann-Forchheimer law, Finite Element Analysis.

1. Introduction

Concentrated solar power systems constitute today a promising route to produce industrial heat at $T = 800\text{-}1500^\circ\text{C}$ for strategic high temperature applications (cement production, steam cracking, hydrogen production). The same free-carbon heat can be used for producing electricity in 100 MW power plants according to the solar-to-heat conversion technologies. During the last few years, increasing attention has been given to employ architected porous ceramics with prescribed textural features for designing volumetric solar receivers likely to deliver hot air at $T = 1000^\circ\text{C}$. These receivers are installed on the top part of an high-temperature solar tower. However improvements must still be made to reach conversion efficiencies higher than 85% at $T = 1000^\circ\text{C}$ for considering massive industrial developments [1]. To reach such efficiencies, it is fundamental to understand how heat is distributed in the volume of the porous receiver.

In reason of the elevated operating temperatures, heat transfers involved within the porous media include the three modes of heat transfer, namely conduction, convection, and radiation. The balance between these modes is influenced by the operating conditions (incident solar flux distribution) as well as by the textural parameters such as porosity or mean cell size, and also the physical properties, such as the thermal conductivity, the volume radiative properties among others. There are two main approaches to numerically model the problem where convection, conduction and radiation are combined. The first one is the discrete-scale approach (or the pore-scale approach) in which two phases are considered, namely the void phase in which radiation, conduction and flow occurs, and the solid phase in which only conduction exist (if the ligament are opaque). The transfer between these three physics takes place on the void phase and on the internal boundary between both domains. The second one is continuous-scale approach based on the pre-knowledge of effective physical properties which feed homogenized transport equations. For volumetric solar receivers, mains studies dealing with the modeling of the coupled heat transfers are mainly focused on what happens at the macroscopic scale, which makes the continuous-scale approach very suitable and the most used, since it also requires much less computational effort in comparison to the discrete-scale approach [2, 3].

2. Numerical methodology and results

In this work, we present and study a nonlinear coupled integro-PDEs model combining both the phenomena of convection, conduction and radiation in a porous medium, representing the volumetric solar receiver. The coupled model is governed by 4 subproblems. The first is an integro-differential equation representing the phenomenon of radiation (absorption and scattering processes). The second and the third are nonlinear partial differential equations representing the heat conduction equation of the solid and the fluid phase respectively. The fourth one is composed of two nonlinear equations (momentum equation and continuity equation), describing the fluid flow, and modeled by the Darcy-Brinkmann-Forchheimer equations, representing the convection phenomenon. We carry out the analysis and the

numerical approximation of the model within a variational framework and we perform the full discretization of the problem based on the discrete ordinate method for the angular discretization and the finite element method (standard FE, vectorial FE, Mixed FE and SUPG-FE) for the spatial discretization. All non-linearities are handled using a fixed-point method coupled with a Newton–Raphson linearization method. We consider a three-dimensional geometry (cube or cylinder) in order to represent the volumetric solar receiver. We start the numerical results by investigating the coupling problem of all physics as well as the troublesome obstacle of several nonlinearities. To do that, we present and compare, in terms of convergence and computational cost, different possible strategies for solving such a proposed coupled problem. In addition, the effectiveness of our solver’s numerical strategy is based on a parallel distribution, developed using domain decomposition. Then, we proceed to study the coupled problem of convective, conductive and radiative heat transfers within the volumetric solar receiver, and we perform several numerical simulations of all the variables involved. The results are discussed regarding the effect of different parameters (initial velocity, porosity, mean cell size diameter, etc.) on the thermal efficiency of the volumetric solar receiver. Moreover, it will allow us to better understand the role of each mode of heat transfer on the volume distribution of all the thermal quantities (temperature, flux) involved. Our FEM-solver is also important for designing afterwards porous architected ceramics using a topology optimization route.

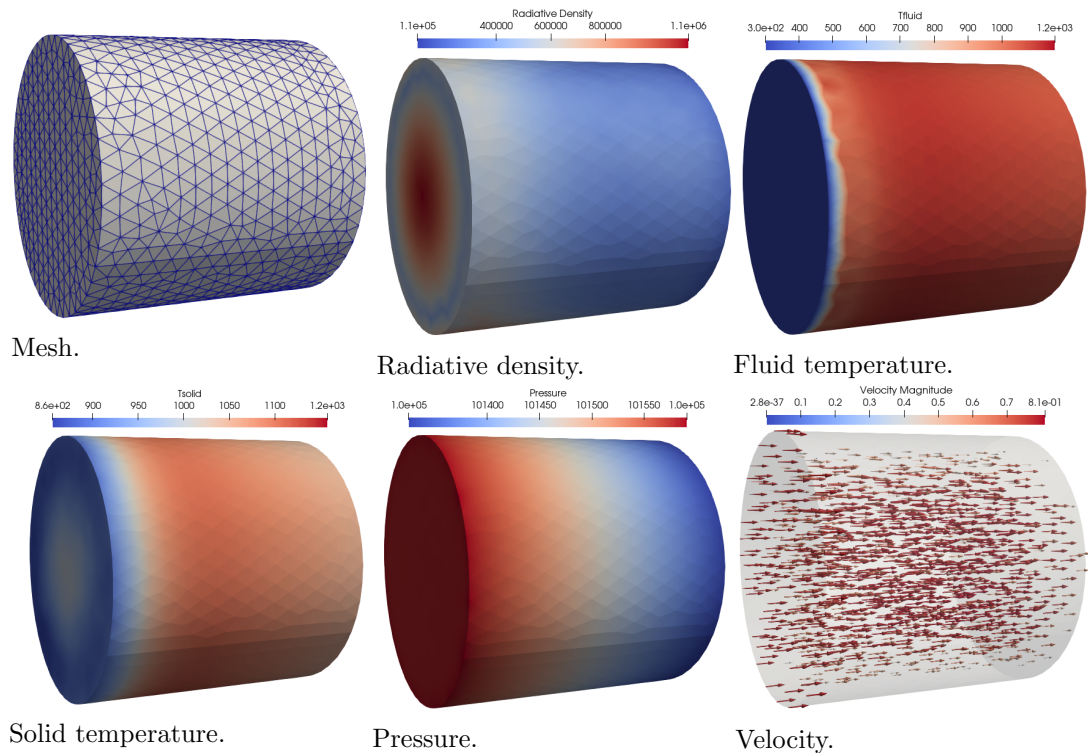


FIGURE 1: Simulation of the coupled model of convection, conduction and radiation in the volumetric solar receiver.

Références

- [1] Patil, V. R., Kiener, F., Grylka, A., & Steinfeld, A. Experimental testing of a solar air cavity-receiver with reticulated porous ceramic absorbers for thermal processing at above 1000 C. *Solar Energy*, 2021, vol. 214, p. 72-85.
- [2] Ouchtout, S., Rousseau, B., & Favennec, Y. Finite element framework for modeling conducto-radiative transfers within heterogeneous media at both discrete and continuous scales. *International Journal of Heat and Mass Transfer*, 2022, vol. 197, p. 123274.
- [3] Barreto, G., Canhoto, P., & Collares-Pereira, M. Three-dimensional CFD modelling and thermal performance analysis of porous volumetric receivers coupled to solar concentration systems. *Applied Energy*, 2019, vol. 252, p. 113433.

Physics-informed neural networks for modelling groundwater flow in unconfined aquifers

Adhish Guli Virupaksha ^{a,b}, François Lehmann^a, Marwan Fahs^a, Hussein Hoteit^c, Thomas Nagel^b

^a*Institut Terre et Environnement de Strasbourg, Université de Strasbourg, CNRS, ENGEES, Strasbourg, France*

^b*Geotechnical Institute, Technische Universität Bergakademie Freiberg, Freiberg 09599, Germany*

^c*Physical Science and Engineering Division, King Abdullah University of Science and Technology, Thuwal, Saudi Arabia*

Keywords: PINNs, Porous Media, Unconfined Aquifer, Darcy's law

1 Introduction

Physics-informed neural networks (PINNs) are a class of machine learning models that incorporate physical laws or principles into the neural network architecture [1]. These models aim to combine the power of data-driven approaches, like neural networks, with the governing equations of physical processes to improve accuracy and generalization, particularly in scenarios with limited or noisy data.

PINNs are receiving increasing interest in simulating flow in porous media [2]. However, to the best of our knowledge, it has never been used to simulate flow in unconfined aquifers. In this work, we show how PINNs can be used in such a case. We suggest a time scaling approach to normalize the space and time domains.

2 Material and method

The flow processes in unconfined aquifers are governed by Darcy's law and the continuity equation with the Dupuit approximation, given as follows:

$$S \frac{\partial H}{\partial t} - \frac{\partial}{\partial x} \left(kH \frac{\partial H}{\partial x} \right) - \frac{\partial}{\partial y} \left(kH \frac{\partial H}{\partial y} \right) = Q \quad (1)$$

where $S[-]$ represents the storativity, $H[L]$ represents the pressure head, $k[L.T^{-1}]$ represents the hydraulic conductivity, and $Q[L.T^{-1}]$ is the source/sink term.

With PINNs, H is approximated using a deep neural network. The network is trained to satisfy the governing partial differential equation (PDE) on a given number of collocation points. Since PINNs do not utilize any predefined datasets, the neural network is trained by creating data points in line with the initial and boundary conditions. The loss function is defined by the mean square error, as follows:

$$\text{MSE} = \text{MSE}_{\text{PDE}} + \text{MSE}_{\text{BC}} + \text{MSE}_{\text{IC}} \quad (2)$$

Where MSE_{PDE} , MSE_{BC} , and MSE_{IC} represent the errors related to the PDE, the boundary conditions and the initial conditions, respectively.

The three components of the loss function are defined as follows:

$$\text{MSE}_{\text{PDE}} = \frac{1}{N_f} \sum_i^{N_f} f(t_i, x_i, y_i)^2 \quad (3)$$

$$\text{MSE}_{\text{BC}} = \frac{1}{N_b} \sum_i^{N_b} (H^b(t_i, x_i, y_i) - H_i^b)^2 \quad (4)$$

$$\text{MSE}_{\text{IC}} = \frac{1}{N_I} \sum_i^{N_I} (H^I(t_i, x_i, y_i) - H_i^I)^2 \quad (5)$$

Here $H^I(t_i, x_i)$ and $H^b(t_i, x_i)$ represent the initial and boundary conditions, N_f , N_b and N_I are the number of collocation points used to impose the physical equations, the boundary and initial conditions, respectively.

The function f used in MSE_{PDE} is defined as the residual form of Eq. (1):

$$f = S \frac{\partial H}{\partial t} - \frac{\partial}{\partial x} \left(kH \frac{\partial H}{\partial x} \right) - \frac{\partial}{\partial y} \left(kH \frac{\partial H}{\partial y} \right) - Q \quad (6)$$

The partial derivatives of H are obtained using automatic differentiators.

3 Results and discussions

As a first step, the PINN-based method has been applied to a 1D case. The application to 2D problems is under development. A sample of the results obtained with PINNs in a 1D scenario is presented in Figure 1. It concerns flow in unconfined aquifer with imposed head charges at the left and right sides. The aquifer is homogenous and isotropic. The hydraulic conductivity of the aquifer is assumed to be 10^{-5} m/s. The storativity (i.e. specific yield) S is considered to be 0.2. The length of the aquifer is 20 m. The head at the right boundary is linearly increasing from 1 m to 5 m in 7 days, while the left side is imposed at a constant head of 5 m.

Several runs have been performed to select the parameters used for the NN and the optimizer. The results presented in the figure are obtained with 2^{15} collocation points in the spatial and temporal domain and 2^8 points for the initial conditions. The NN model is a 4-layer feed-forward deep neural network with hyperbolic tangent activation function. The network utilizes two optimizers. The model is initially trained using Adam optimizer and then followed by LBFGS optimizer for further reducing and stabilizing the loss function. The Adam optimizer works with a learning rate of 0.001 over 30,000 epochs while the LBFGS optimizer operates over 300 epochs with a learning rate of 0.1. PINNs cannot provide good results without normalizing the space and time domains. In our case, this is done by defining a new variable for the time (t^*) that is equal to the time divide by 1000 ($t^* = t/1000$). The results of PINNs have been compared with the results of the finite element model COMSOL. The figure below shows good agreement. The training loss has been 8.6×10^{-5} .

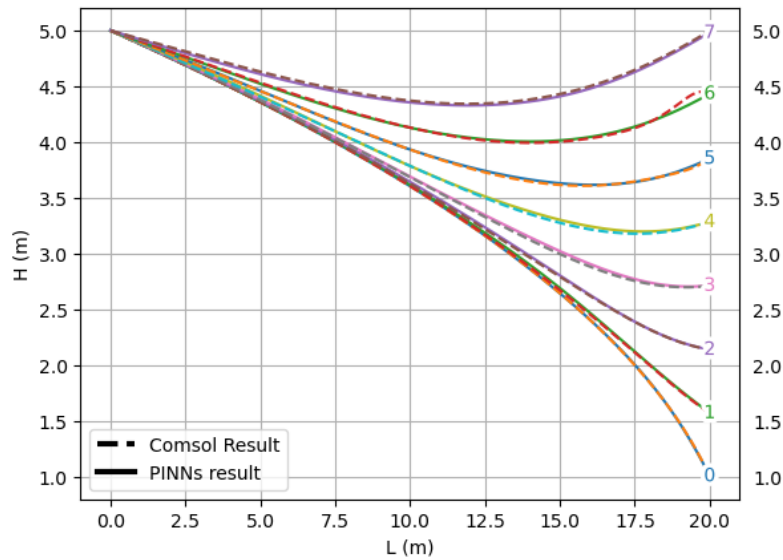


Figure 1: Pressure head distribution at different time steps in an unconfined aquifer: Comparison of PINNs and COMSOL

References

- [1] M. Raissi et. Al, Physics-informed neural networks: A deep learning framework for solving forward and inverse problems involving nonlinear partial differential equations, *Journal of Computational Physics*, Volume 378, Pages 686-707 (2019).
- [2] Lal Dangi et al. Predicting flow in porous media: a comparison of physics-driven neural network approaches,” *Mathematical Models in Engineering*, Vol. 9, No. 2 (2023).

Sensitivity analysis for rainfall-induced landslide models

Rashad Abbasov^{1,*}, Marwan Fahs¹, Anis Younes¹, Renaud Toussaint^{1,2}

¹*Institut Terre et Environnement de Strasbourg, Université de Strasbourg, CNRS, ENGEEES, UMR 7063, Strasbourg, France*

²*PoreLab, The Njord Centre, Department of Physics, University of Oslo, Oslo, Norway.*

Keywords: Rainfall-induced landslides, slope stability, Local Factor of Safety, uncertainty analysis

Landslide is the mass movement of soil and rocks down slopes. Landslides are geological processes that occur when a slope becomes unstable. Natural and anthropogenic activities can cause mechanical imbalance in which shear stress exceeds shear strength and initiates landslides [1]. Intense rainfall events are one of the main causes of slope instability. In particular, rainfall infiltration increases water saturation and body load on soil, which locally increases the shear stress, and can also negatively affect shear strength [2].

As a result of climate change, rainfall-induced landslides (RILS) are becoming frequent. This naturally occurring geologic hazard is unavoidable in the context of climate change. But, it is possible to reduce potential serious risks by developing warning systems via modeling. Modeling RILS requires integrating a hydro-mechanical model with landslide susceptibility indicators [3]. The hydromechanical processes can be described with the Richards and local equilibrium equations [3]. The Mohr-Coulomb failure criterion-based local factor of safety (LFS) concept helps to calculate and visualize slope stability as a landslide susceptibility indicator [4].

$$LFS = \frac{\cos(\varphi') \cdot (c' + \sigma_{eff}^I \cdot \tan(\varphi'))}{\sigma_{eff}^{II}} \quad (1)$$

Where $\sigma_{eff}^I [M.L^{-1}.T^{-2}]$ and $\sigma_{eff}^{II} [M.L^{-1}.T^{-2}]$ are the largest and second largest principal values of the effective, respectively. Parameters $c' [M.L^{-1}.T^{-2}]$ and $\varphi' [-]$ represent effective soil cohesion and effective friction angle, accordingly.

Model input parameters can be uncertain because they are gathered by calibration with observations with limited data. These uncertainties can go through the model and affect the outputs. The influence of uncertainty on model outputs can result in unreliable predictions. For this reason, an uncertainty analysis (UA) should be performed for predictions on RILS. However, UA is not an easy task because it demands dealing with several challenges such as model nonlinearities, high CPU time, high dimensionality of the model, relevant metrics, and verifications. The main aim of this work is to suggest an appropriate strategy for UA of RILS.

We developed an advanced COMSOL® model to deal with nonlinearities and to optimize the computational cost for data generation, required for UA. Implementation of sensitivity analysis (SA) is a fundamental aspect of solving high-dimensionality obstacles. We suggest an appropriate SA that consists of 2 main steps: the first step is applying the screening technique (ST), and the second is implementing a global sensitivity analysis (GSA). ST uses folded Plackett–Burman (PB) screening design to eliminate insignificant parameters. The second step is GSA. It helps in ranking the remaining major parameters by order of importance. In this study, GSA relies on the surrogate model-based polynomial chaos expansion (PCE) technique. PCE technique computes polynomial coefficients that allow the forward evaluation of the Sobol indices. In turn, Sobol indices characterize the importance of parameters by ranking them. According to the results of our study case, the Poisson ratio is the most impacting parameter on the output. The area of the failure zone is a relevant metric (output) and helps to decipher relations with input parameters in an efficient way. Analytical expressions of LFS, in simple cases where it can be obtained, match very well the results of our study, which validates our approach.

References:

- [1] Haque U, Blum P, da Silva PF, Andersen P, Pilz J, Chalov SR, et al. Fatal landslides in Europe. *Landslides* 2016;13:1545–54. <https://doi.org/10.1007/s10346-016-0689-3>.
- [2] Travelletti J, Delacourt C, Allemand P, Malet J-P, Schmittbuhl J, Toussaint R, et al. Correlation of multi-temporal ground-based optical images for landslide monitoring: Application, potential and limitations. *ISPRS Journal of Photogrammetry and Remote Sensing* 2012;70:39–55. <https://doi.org/10.1016/j.isprsjprs.2012.03.007>.
- [3] Moradi S, Huisman J, Class H, Vereecken H. The Effect of Bedrock Topography on Timing and Location of Landslide Initiation Using the Local Factor of Safety Concept. *Water* 2018;10:1290. <https://doi.org/10.3390/w10101290>.
- [4] Lu N, Şener-Kaya B, Wayllace A, Godt JW. Analysis of rainfall-induced slope instability using a field of local factor of safety. *Water Resour Res* 2012;48:2012WR011830. <https://doi.org/10.1029/2012WR011830>.

Numerical study and inverse analysis of a non destructive measurement method for oxygen diffusivity in partially carbonated concrete

O. Ouïjdane^a, B. Huet^a, P.Turcry^b, A. Aït-Mokhtar^b, R.A. Patel^c, F.Dehn^c

^aHolcim Innovation Center. – Lyon, France

^bUniversity of La Rochelle- CNRS. – La Rochelle, France

^cKarlsruhe Institute of Technology. – Karlsruhe, Germany

Keywords: Durability of structures, Gas diffusivity, Heterogenous concrete, Gas transport modeling, Leakage, Inverse analysis.

1 Introduction/Abstract:

Gas diffusivity in cementitious materials plays a crucial role in their durability analysis. This study aims to validate a non-destructive method for measuring oxygen diffusivity in cementitious materials using numerical modeling and experiments [Figure 1]. This research provides improved understanding on the impact of various factors on gas diffusivity in heterogenous concrete, including the re-equilibration time, purge duration, leakage effects, and the presence of different layers.

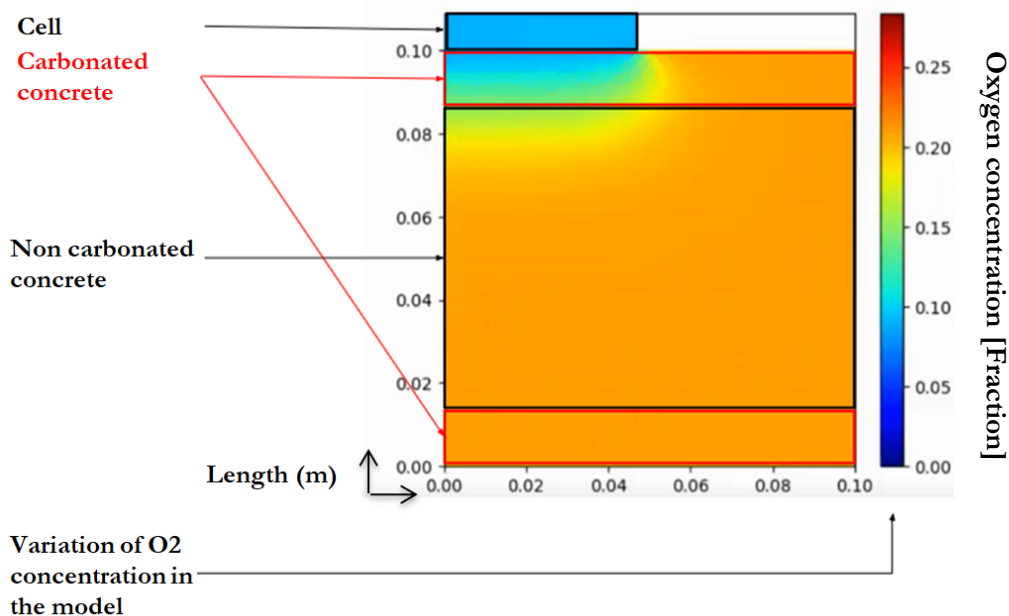


Figure 1: Oxygen concentration variation in a symmetrical 2D numerical model of a partially carbonated concrete.

The diffusion measurement method we develop uses a cell with a specific volume that is placed in contact with a cementitious material. The cell is purged and we observe how it gradually fills with oxygen that passes through the material. Assessing the gas permeability of cementitious materials using the diffusion

measurement method can help evaluating their long-term durability by providing, for example, insights into their ability to resist deterioration caused by corrosion.

We optimize the dimensions and geometry of the measurement cell using numerical model. Diffusion is modeled using Fick's second law, which states that the rate of diffusion is proportional to the concentration gradient and the diffusion coefficient of the material. We solve this theoretical diffusion equation in 1D geometry analytically and numerically and in 2D geometry numerically. We define the optimal geometry of measurement cell as the one giving the minimum relative error between the analytical solution and the 2D numerical solution for a wide range of material properties (diffusion coefficient and layers size). The error quantification and fitting process involve comparing the numerical models to the analytical solution.

With numerical models, we quantify oxygen diffusivity and the accuracy of the measurement considering both the leakage through the measurement cell and the lateral leakage through the concrete. We analyze the effect of the presence of different layers in heterogeneous cementitious materials [Figure 2].

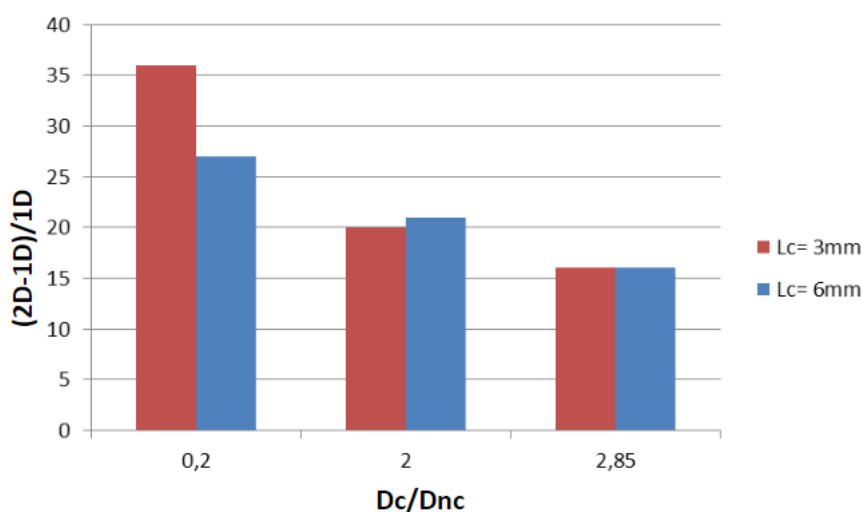


Figure 2: Variation of the difference between the 1D and 2D curves as a function of the ratio of the diffusion coefficients for concretes where the min (D_c, D_{nc}) = $0.3 \text{ [e-8 m/s}^2]$ for a cell height $h_m = 3 \text{ mm}$.

The results we obtain through numerical modeling provide validation for a non-destructive measurement method applied on a defined range of commonly used cementitious materials for both onsite and laboratory materials. We then conduct an experimental validation using laboratory samples.

The purpose of experiments is to verify in real conditions the accuracy of the method. By comparing the experimental results with the numerical simulations, we can evaluate the error between the two and check if our measurement technique works. In this validation process, we compare various aspects of the experiments and numerical simulations, such as the measurement time, the purge time, the time between two successive experiments and the characteristic lengths associated to the parameters mentioned earlier. By comparing these parameters with the corresponding values obtained from the numerical simulations, we can determine the accuracy of the experimental measurements. Inverse analysis is applied to experimental results to estimate parameters and validate the model using experimental data.

This new method for oxygen diffusivity testing for cementitious materials contributes to a better understanding of gas diffusivity in cementitious materials in real field conditions. It also offers a valuable complementary tool for assessing the durability of concrete structures.

References

- [1] V. Dutzer, W. Dridi, S. Poyet, P. Le Bescop, X. Bourbon, "The link between gas diffusion and carbonation in hardened cement pastes," *Cement and Concrete Research*, 123, 105795 (2019). <https://doi.org/10.1016/j.cemconres.2019.105795>
- [2] A. Leemann, P. Nygaard, J. Kaufmann, R. Loser, "Relation between carbonation resistance, mix design and exposure of mortar and concrete," *Cement and Concrete Composites*, 62, 33–43 (2015). <https://doi.org/10.1016/j.cemconcomp.2015.04.020>
- [3] I.-S. Yoon, "Comprehensive Approach to Calculate Oxygen Diffusivity of Cementitious Materials Considering Carbonation," *International Journal of Concrete Structures and Materials*, 12, 16 (2018). <https://doi.org/10.1186/s40069-018-0242-y>
- [4] H. Zhang, C. Romero Rodriguez, H. Dong, Y. Gan, E. Schlangen, B. Šavija, "Elucidating the Effect of Accelerated Carbonation on Porosity and Mechanical Properties of Hydrated Portland Cement Paste Using X-Ray Tomography and Advanced Micromechanical Testing," *Micromachines*, 11 (2020). <https://doi.org/10.3390/mi11050471>

Weakly monotone finite volume scheme for parabolic equations in strongly anisotropic porous media

Aberrah Moha^a, El-Houssaine Quenjel^b, Patrick Perré^b, Rhoudaf Mohamed^a

^a*Moulay Ismaïl University, Faculty of Sciences, B.P. 11201 Zitoune 50 500 Meknès, Morocco.
moha.aberrah@edu.umi.ac.ma*

^b*Université Paris-Saclay, CentraleSupélec, Laboratoire de Génie des Procédés et Matériaux, Centre Européen de Biotechnologie et de Bioéconomie (CEBB), 3 rue des Rouges Terres 51110 Pomacle, France.*

Keywords: monotonicity, finite volume method, parabolic equation, anisotropy, mass transfer, wood.

1. Abstract

Parabolic equations appear frequently in the modeling of many everyday life applications. For example, they form part of complex systems such as flows in porous media, fluid dynamics models, as well as mass and heat transfer problems. In terms of numerical resolution of these equations by the finite volume method, several schemes have been developed, mostly focused on preserving certain properties like positivity and maximum principle. However, the monotony is quite difficult question.

In this work, we present an original approach allowing to preserve the weak monotonicity of a finite volume discretization in the case of highly anisotropic parabolic equations. In other words, the computed numerical solution honors the physical ranges of the initial condition. The main idea lies in devising a nonlinear damping parameter eliminating the problematic fluxes when they occur. We check that the structure of the scheme naturally ensures the weak monotonicity of the approximate solutions. We also establish energy estimates, which leads to a proof of existence of the numerical solutions.

Several numerical test cases demonstrate the proposed approach's ability to maintain the physical ranges of the solution, as well as to provide good accuracy and robustness with respect to the mesh and high ratios of anisotropy. Finally, we apply this novel methodology to simulate mass transfer in hygroscopic media, focusing on mass diffusion inside within wood.

Références

- [1] Yuan, G., Sheng, Z. : Monotone finite volume schemes for diffusion equations on polygonal meshes. *J. Comput. Phys.* 227(12), 6288-6312 (2008)
- [2] P. A. Forsyth. A control volume finite element approach to napl groundwater contamination. *SIAM Journal on Scientific and Statistical Computing*, 12(5) :1029-1057, 1991.
- [3] R. Eymard, C. Guichard, and R. Herbin. Small-stencil 3D schemes for diffusive flows in porous media. *ESAIM : Mathematical Modelling and Numerical Analysis*, 46(2) :265-290, 2012.
- [4] C. Guichard and E. H. Quenjel. Weighted positive nonlinear finite volume method for dominated anisotropic diffusive equations. *Advances in Computational Mathematics*, 48(6) :1-63, 2022.
- [5] E. H. Quenjel, P. Perré. : Computation of the effective thermal conductivity from 3D real morphologies of wood. *Heat Mass Transf.* 58, 219-2206 (2022)
- [6] M. Aberrah, E. H. Quenjel, P. Perré, and M. Rhoudaf. Weakly monotone finite volume scheme for parabolic equations in strongly anisotropic media. *Journal of Applied Mathematics and Computing*, <https://doi.org/10.1007/s12190-023-01883-7>, 2023.

NaCl Salt Crust Dynamics Diagram

Glad Licsandru^a, Catherine Noiriell^b, Paul Duru^a, Sandrine Geoffroy^c, Ariane Abou-Chakra^c and Marc Prat^a

^a*Institut de Mécanique des Fluides de Toulouse (IMFT), Toulouse, FRANCE.*

^b*Géosciences Environnement Toulouse (GET), Toulouse, FRANCE*

^c*Laboratoire Matériaux et Durabilité des Constructions, Toulouse, FRANCE*

Keywords: Dissolution, Evaporation, Precipitation, Porous Medium, Salt Crust

Abstract

The impact of salt crust formation on water evaporation from a porous medium is an important issue in relation with the water cycle, agriculture, building sciences and more. Salt crusts have been found to have great impact on the evaporation rates of porous media as well as to show big morphological changes. These changes can be seen in nature and in laboratory experiments. One here can mention doming [1], impressive recurring patterns as seen in salt deserts (Uyuni in Bolivia) while usually in laboratory experiments, they are split in uniform or cauliflower type crusts. This type of uniform and cauliflower crusts have been previously related to the initial pore size of the supporting porous media. The study shows that this support porous media is not needed in order to obtain the changes in its structure. Here it can be seen that salt crusts are not a simple accumulation of salt crystals at the porous medium surface, in the form of efflorescence, but undergo complex dynamics. These types of dynamics present a point of interest in the scientific community as they are still not fully understood. The work shows that by manipulating the saturation of a salt crust the topology of the crust can change dramatically. We report on the experiments from [2]–[4] in the form of a study that allows the identification of various crust evolution regimes depending on the competition between evaporation and vapor condensation. All the preformed experiments are done in Hele-Shaw cells. This technique allows for observations to be made directly on suspended salt crusts that have been previously detached from a porous media. The full spectrum of the various regimes is summarized in a NaCl salt crust dynamics diagram. These findings provide in-depth insights into the salt crust dynamics while showing how one can change between different morphologies by modifying key factors. This new data paves the way for the better understanding of the efflorescent salt crusts impact on evaporation and the factors leading to its final forms.

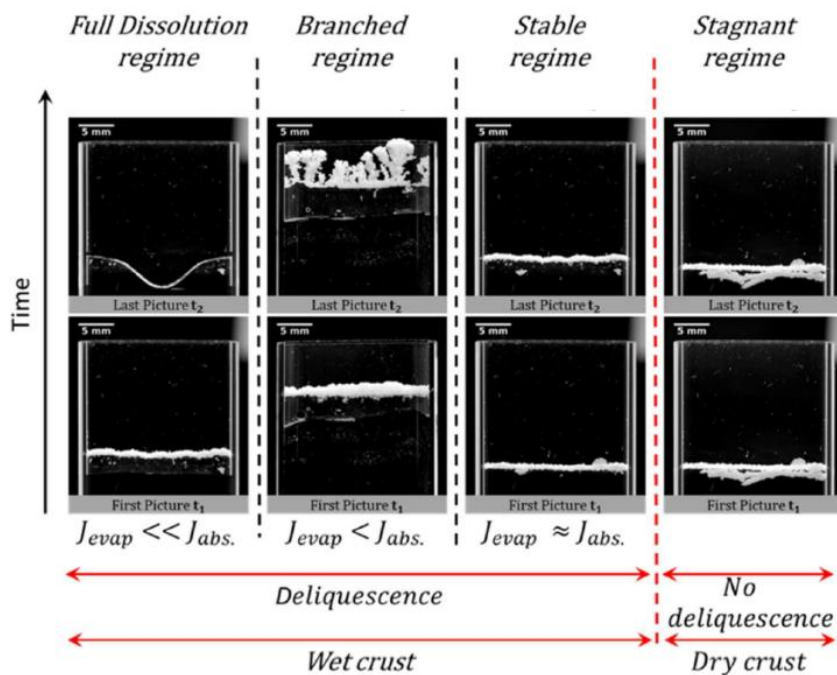


Figure 1: NaCl salt crust dynamics diagram (adapted from [4])

References

- [1] U. Nachshon, N. Weisbrod, R. Katzir, and A. Nasser, “NaCl Crust Architecture and Its Impact on Evaporation: Three-Dimensional Insights,” *Geophysical Research Letters*, vol. 45, no. 12, pp. 6100–6108, 2018, doi: 10.1029/2018GL078363.
- [2] G. Licsandru, C. Noiriél, P. Duru, S. Geoffroy, A. A. Chakra, and M. Prat, “Dissolution-precipitation-driven upward migration of a salt crust,” *Phys. Rev. E*, vol. 100, no. 3, p. 032802, Sep. 2019, doi: 10.1103/PhysRevE.100.032802.
- [3] G. Licsandru, C. Noiriél, S. Geoffroy, A. Abou-Chakra, P. Duru, and M. Prat, “Detachment mechanism and reduced evaporation of an evaporative NaCl salt crust,” *Sci Rep*, vol. 12, no. 1, Art. no. 1, May 2022, doi: 10.1038/s41598-022-11541-w.
- [4] G. Licsandru, C. Noiriél, P. Duru, S. Geoffroy, A. Abou-Chakra, and M. Prat, “Evaporative destabilization of a salt crust with branched pattern formation,” *Sci Rep*, vol. 13, no. 1, Art. no. 1, Mar. 2023, doi: 10.1038/s41598-023-31640-6.

Analysis of carbon brush seals with long bristles

A. Souissi^{a,b}, M. Arghir^a, D. Lasseux^b L. Amami^c

^aInstitut P', GMSC Department-TriboLab, University of Poitiers - Poitiers

^bI2M, TREFLE Department, University of Bordeaux – Bordeaux

^cCETIM, FST Department, Nantes

Keywords: brush seal, carbon fiber bristles, theoretical model, experimental validation.

1 Introduction

The present work introduces the analysis of a dynamic seal (a brush seal) employed in rotating machinery to limit gas leakage between high and low-pressure zones. The seal is comprised of a carbon brush consisting of closely serrated, long bristles of small diameter. The bristles free length exceeds the radial clearance between the rotor and the stator of the device in which the seal is installed. The brush flexes in the axial direction along the rotor and fills the radial rotor-stator clearance. Thus, a porous barrier is formed, impeding the flow of leakage.

Theoretical estimation of the leakage flow rate is particularly challenging due to the complexity of the seal properties characterization, in particular its porosity and permeability. The brush behavior do not only depends on the density defined as the number of bristles per circumferential length, but also on its deformation. This is accounted for by considering the bristles as beams that undergo large deformations. Contact interactions occur between the bristles and the rotor, as well as between the bristles themselves. Bristles experience deformations not only due to contacts but also due to fluid forces acting upon them. By achieving a state of equilibrium between the flow forces and the deformed brush structure, a constant permeability is then established.

2 Objective and methods:

The objective of this study is the prediction of the leakage flow rate through the brush seal. A simplified model is employed by considering only the contacts of a first row of bristles with the rotor and by neglecting the contacts between bristles. The distance between bristles varies between zero at their clamped end and an imposed spacing at their free end. Darcy's law is employed locally to describe the flow through the heterogeneous bundle of bristles. The permeability coefficients are estimated from homogeneous representative unit cells orthogonal to and along the deformed bristles. The theoretical model predictions are compared with experimental results obtained on a dedicated test rig.

2.1 Macroscopic model and bristle deformation:

The bristles have a very large length (over 1.9mm) to diameter ($d=5 \mu\text{m}$) aspect ratio and are submitted to large non-linear deformations. A Kirchhoff beam theory is therefore employed to describe the deformed beam together with a finite element approach using third order Hermitian functions. A penalty formulation is used to take into account the contact with the rotor. The first row of bristles is kept in contact with the rotor whereas the free end of the next rows is progressively shifted to larger radial values. The spacing between the free ends of the bristles (D_p) is a parameter of the model. The resulting form of the deformed characteristic brush section is depicted in Figure 1.

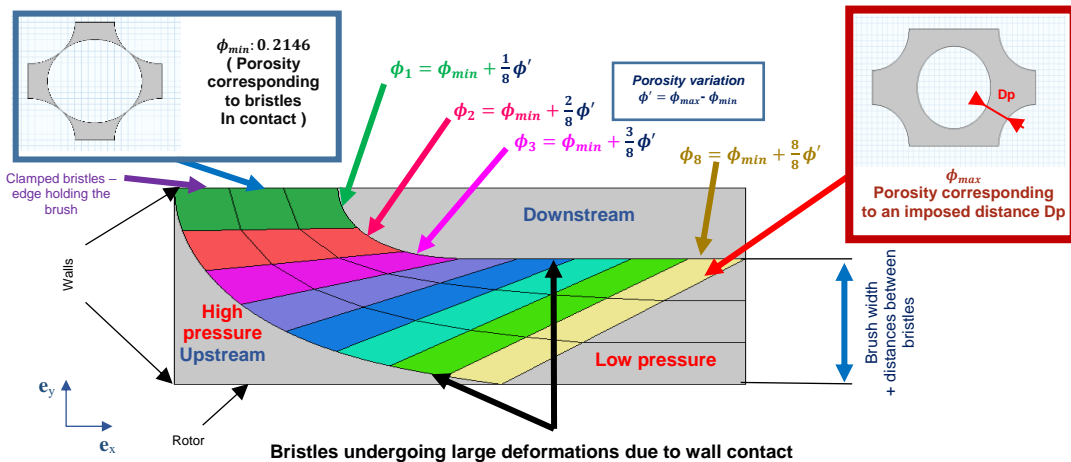


Figure 1: Macroscopic model domain

A boundary fitted curvilinear coordinate system is then associated to the deformed bristles. It follows the first upstream, the last downstream bristle and the local normal direction. The porosity then varies along the coordinate system from its lowest value at the clamped end to its largest value at its free end. Two local problems are then solved for each grid block of the brush (colored area in Figure 1) yielding the permeability components along and normal to the bristle. These values are then computed from the local curvilinear coordinate system aligned with the bristles to the global Cartesian coordinate system (e_x, e_y). A heterogeneous Darcy problem is then solved in a domain encompassing the upstream high pressure zone, the porous brush and the downstream low pressure zone. A test rig was also developed as depicted in Figure 2. It consists of a rotor deprived of rotation and enables testing carbon brush seals with five different interferences between the bristles and the rotor. Results of measured leakage flow rates are reported in Figure 3. Comparisons between the theoretical model and experimental results obtained for Position 3 are represented in Figure 4. Numerical values of D_p , ranging from $0.1d$ to $0.15d$, show consistency with the experimental results. However, the variation of the experimental leakage flow rate with the applied pressure difference (between upstream and downstream zones) cannot be closely matched by the present approach for two important reasons. First, the deformation of the bristles considers only the rotor interference and disregards the influence of fluid forces. Second, the present approach assumes constant distance between deformed bristles, which is proportional to D_p . These are strong assumptions that must be reviewed in future developments of the model.

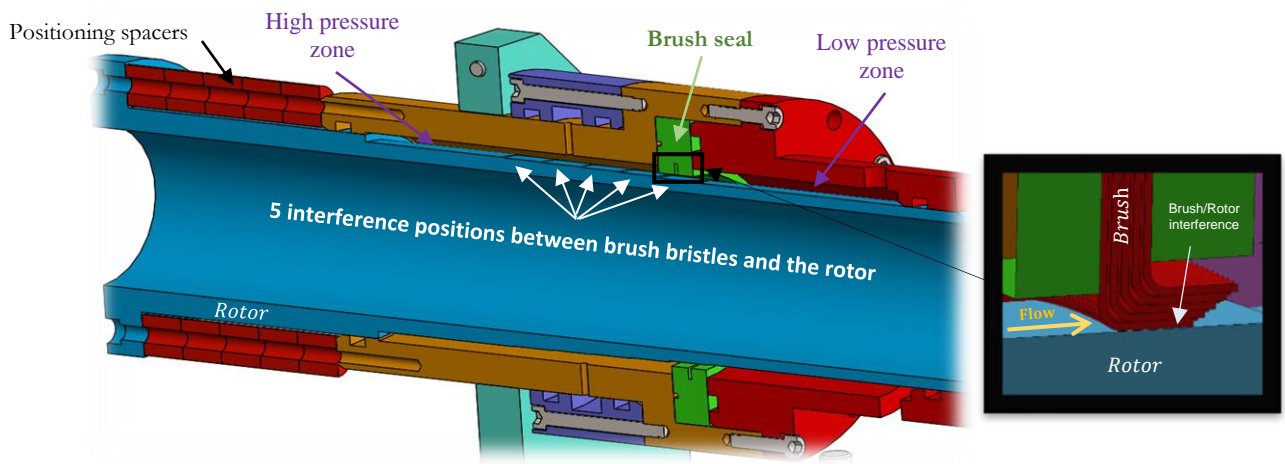


Figure 2: Test rig

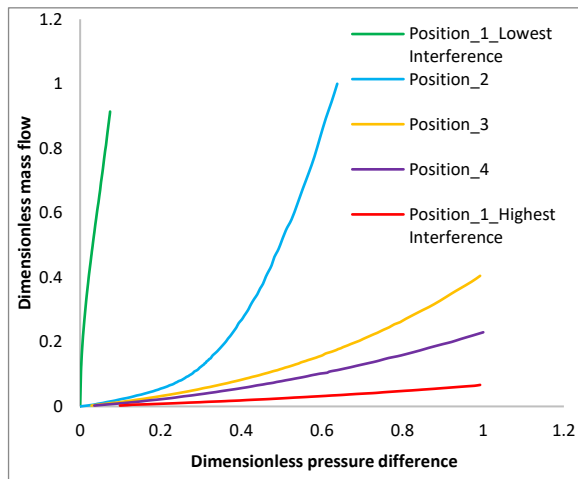


Figure 3: Experimental mass flow rate

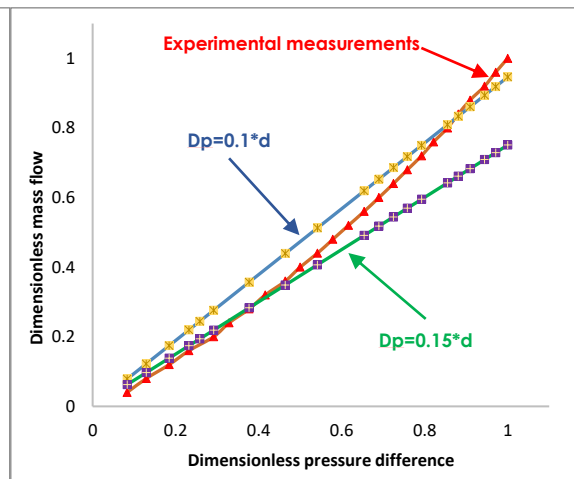


Figure 4: Comparisons between theoretical and experimental results

References

- [1] Lasreux, D., J.Valdés-Parada, F., "Upscaling techniques in continuum mechanics", June 2022. (s.d.)
- [2] Meier, C., Wall, W.Popp, A. "A Locking Free Finite Element Formulation and Reduced Models for Geometrically Exact Kirchhoff_Rods", Computer Methods in Applied Mechanics and Engineering, March 2019, DOI: 10.1016/j.cma.2016.05.12. (s.d.)

Inertial flow in porous media : effect of pressure gradient orientation

Yanis Bendali^{*1,2}, Morgan Chabanon¹, Quentin Holka², Ephraïm Toubiana², and Benoit Goyeau¹

¹Laboratoire d'Énergétique Moléculaire et Macroscopique, Combustion – CentraleSupélec, Université Paris-Saclay, Centre National de la Recherche Scientifique, Centre National de la Recherche Scientifique : UPR288 – France

²Energy and Propulsion Department – Safran Tech, Rue des Jeunes Bois, Châteaufort, CS 80112, 78772 Magny-Les-Hameaux, FRANCE – France

Résumé

Upscaling inertial flows is important for many engineering applications where pressure drops and velocity distribution need to be predicted in porous systems. The most classical model used is the Forchheimer equation that links the superficial velocity with the macroscopic pressure gradient using a global permeability tensor. The latter differs from the intrinsic permeability tensor by taking into account inertial effects of the flow. The Volume Averaging method then allows to write closure problems in order to determine the value of the global permeability tensor (1). However an important challenge is the treatment of the non-linear terms remaining in the closure problems. As a consequence of these non-linearities, closure problems are themselves dependent on the local averaged flow parameters such as the value and orientation of the macroscopic pressure gradient of the flow (2). First, the influence of the pressure gradient orientation for the characterisation of the global permeability tensor is assessed through the study of test cases. A fully developed laminar flow entering a 2D porous elbow is considered in order to enforce a change of flow direction in the porous medium. The global permeability tensor is characterised using the non-linear closure problems provided by the Volume Averaging method. This approach is compared with diagonal permeability formulations prescribed by commercial CFD softwares that do not take into account flow orientation. The macroscopic simulations are then compared with volume-averaged direct numerical simulations of the fluid flow in the resolved porous domain. Results show that, the general macroscopic model correctly predicts the flow within the porous media, while the diagonal model significantly under-predicts the pressure variation along the elbow with increasing pore Reynolds numbers.

Then, to facilitate the resolution of the non-linear closure problems, a linearised approach for small pore Reynolds number is proposed. One of the main advantages of this method is that it does not require to solve the full closure problems for each value and orientation of the macroscopic pressure gradient (3). The validity of this approach is assessed for various unit cell geometries against numerical solutions of the corresponding non-linear problems, showing excellent agreement for pore Reynolds number up to about one. Finally, generalisation of this linearisation methodology to other types of non-linear flows such as compressible flows is examined.

*Intervenant

References

- (1) S. Whitaker, 'The Forchheimer equation: A theoretical development', *Transport in Porous Media*, vol. 25, pp. 27–61, Sep. 1996
- (2) D. Lasseux, A. A. Abbasian Arani, and A. Ahmadi, 'On the stationary macroscopic inertial effects for one phase flow in ordered and disordered porous media', *Physics of Fluids*, vol. 23, no. 7, p. 073103, Jul. 2011
- (3) M. Pauthenet, Y. Davit, M. Quintard, and A. Bottaro, 'Inertial Sensitivity of Porous Microstructures', *Transport in Porous Media*, vol. 125, Nov. 2018

Physics informed neural network for modelling flow in porous media: First order formulation

F. Lehmann^a, M. Fahs^a, A. Alhubail^b, H. Hoteit^b

^a*Institut Terre et Environnement de Strasbourg, University of Strasbourg, CNRS, ENGEES, Strasbourg, France*

^b*Physical Science and Engineering Division, King Abdullah University of Science and Technology, Saudi Arabia*

Keywords: Physics informed neural network, flow in porous media, heterogeneous domains

1 Introduction

Physics Informed Neural Networks (PINNs) is a promising application of the techniques of deep learning neural networks in modeling physical processes (Raissi et al., 2019). PINNs can be used for solving the governing equations and for developing parametric solutions. PINNs can be also used for solving inverse problems and for metamodeling. However, current implementations of PINNs for flow in heterogeneous porous media are facing convergence issues (Zhang et al. 2023). Indeed, automatic differentiation is used for PINNs to evaluate spatial derivatives. Automatic differentiation cannot be applied for evaluating the spatial derivatives of the hydraulic conductivity field as this field can be discontinuous. The main objective of this work is to develop an accurate implementation of PINNs that avoids this problem.

2 First order formulation

Accurate implementation of PINNs for modeling flow in heterogeneous porous media is developed in this work. This is achieved by using the mixed pressure head-velocity form of the governing equation. This allows for avoiding the evaluation of the spatial derivatives of the discontinuous permeability field. The mixed formulation is also called first order formulation because it allows for avoiding the evaluation of second derivatives. This allows for improving the performance of the PINNs because evaluation of the second derivatives with the automatic differentiation is time consuming (Gladstone et al. 2022).

Several structures of PINNs are investigated in this work and numerical experiments are performed to find the best way to simulate flow in heterogeneous domains. The results show that implementation dealing with the mixed form of the governing equations and individual neural networks for the pressure and the velocity components provides the highest accuracy at equivalent learning time with other implementation. The new implementation of PINNs can be applied to simulate flow in porous media, regardless of the type and level of heterogeneity. The proposed methodology presents a novel approach to broaden the scope of PINNs in modeling fluid flow in porous media, while preserving the precise representation of the domain's discontinuous features.

References

- [1] Raissi, M., Perdikaris, P., Karniadakis, G.E., 2019. Physics-informed neural networks: A deep learning framework for solving forward and inverse problems involving nonlinear partial differential equations. *Journal of Computational Physics* 378, 686–707. <https://doi.org/10.1016/j.jcp.2018.10.045>
- [2] Zhang, Z., Yan, X., Liu, P., Zhang, K., Han, R., Wang, S., 2023. A physics-informed convolutional neural network for the simulation and prediction of two-phase Darcy flows in heterogeneous porous media. *Journal of Computational Physics* 477, 111919. <https://doi.org/10.1016/j.jcp.2023.111919>
- [3] Rini J. Gladstone, Mohammad A. Nabian, Hadi Meidani, 2022. FO-PINNs: A First-Order formulation for Physics Informed Neural Networks. <https://doi.org/10.48550/arXiv.2210.14320>

Session
Structures poreuses réactives

Development of 3D and functionalised electrodes to metal decontamination of polluted water: application to the uranium recovery

F.Belnou^a, M.L.Schlegel^a, H.Maskrot^a, T.Proslie^b

^aUniversité Paris-Saclay, CEA, Service de Recherche en Matériaux et procédés Avancés (SRMA), 91191 Gif-sur-Yvette, France

^bUniversité Paris-Saclay, CEA, Laboratoire d'intégration et de développement des cavités et des cryomodules (LIDC2), 91191 Gif-sur-Yvette, France

Keywords: Electrochemistry, Additive manufacturing, Metal recovery, Thin films

1 Abstract

The depletion of the worldwide reserves of conventional mining ores [1], [2] calls for developing alternative methods to collect strategic materials from non-conventional resources. The extraction of dissolved elements from natural waters is promising in view of the huge amounts possibly available. For example, there is more than 4.5 billion tons of uranium dissolved in oceans and seas [1]–[3]. Several techniques can be used to extract dissolved elements. Among them, electrochemical extraction is an interesting approach because it combines chemical sobriety, reversibility, and limited impact on water quality after extraction [3]. Currently, electrochemical metal collection is limited by the electrode surface and reactivity. In contrast, the development of additive manufacturing allows the fabrication of complex structures with a controlled porosity and a high surface area [4], thereby improving the flow and interaction of the electrolyte with the electrode surface. Moreover, the hybridization of additive manufacturing with Atomic Layer Deposition (ALD), which is a thin coating deposition technique, permits to functionalize the surface of the electrodes, enhancing the reactivity of the surface and increasing the electrode durability [5].

Laser-Power Bed Fusion (L-PBF) was used to fabricate porous, 3D and architected electrodes, with a large reactive surface and a lattice structure for improved solution stirring and mixing in a flow-by electrochemical system (Figure 1 a-b). The electrode was coated with Atomic Layer Deposition (ALD), which allows to deposit coatings even in the smallest pores of the electrode.

Electrochemical study of a hexacyanoferrate solution was performed to characterize and optimize the system. Hexacyanoferrate was chosen because its electrochemical behavior is well known. Then, electrochemical tests were carried out with a uranium solution, the solution of interest. First, electrochemical characterization is a cyclic voltammetry to characterize the behavior of the electrodes (Figure 2) between -0.5 and 0.5 V. Subsequently, chronoamperometric analysis was used to study uranium recovery, at a fixed potential and pH. The outgoing electrolyte is characterized by Inductively Coupled Plasma (ICP) to quantify the U(VI) reduced to U(IV) by electrodes. The results are compared to those of a flat and polished electrode made by L-PBF (Figure 1 c), used as a reference, to show the benefits of architected and/or functionalized electrodes.

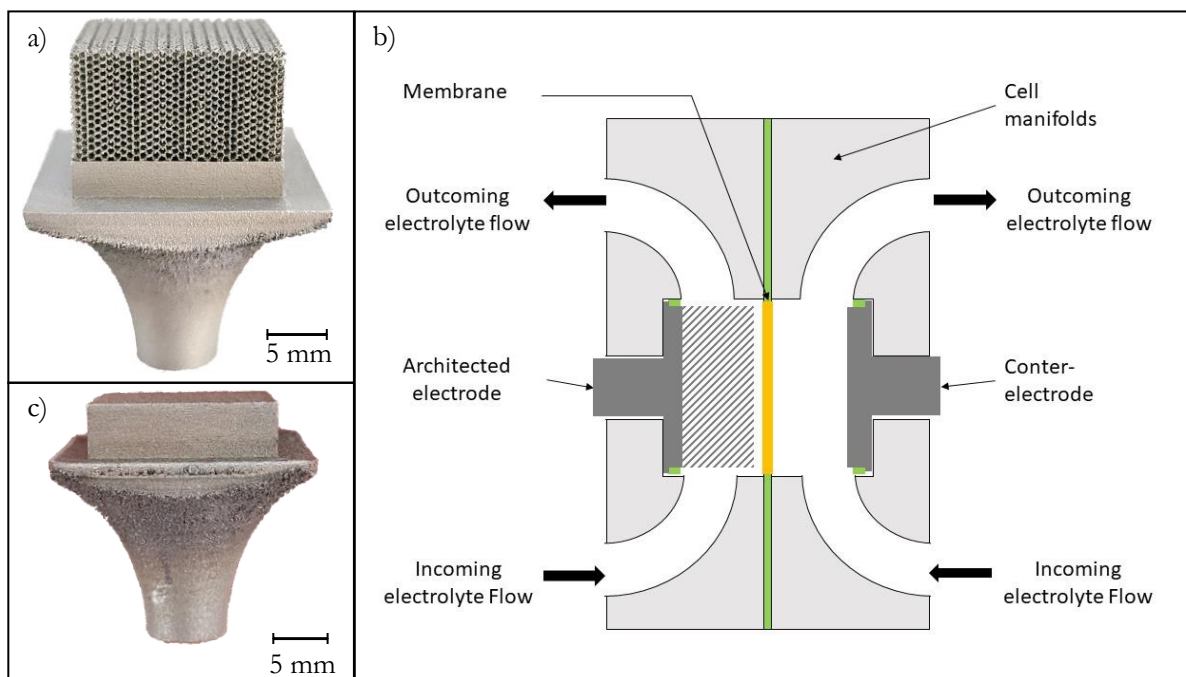


Figure 1: a) architected uncoated electrode b) Scheme of the electrochemical flow cell c) flat uncoated electrode

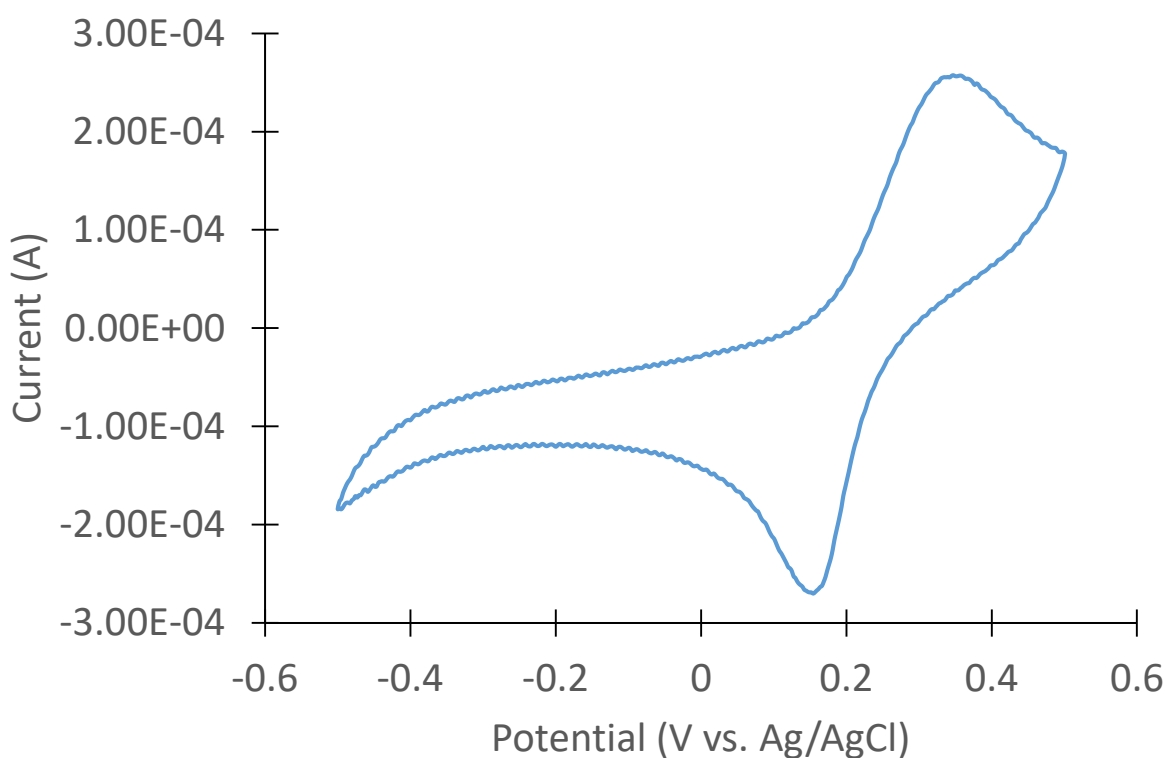


Figure 2: Cyclic voltammetry on a polished flat uncoated electrode with a $K_3Fe(III)(CN)_6$ 1 mM and KCl 0,1 M solution, $0,04 \text{ mL}\cdot\text{s}^{-1}$ flow rate and $10 \text{ mV}\cdot\text{s}^{-1}$ scan speed

References

- [1] C. Tsouris, Uranium extraction: Fuel from seawater, *Nat. Energy*, 2 (2017)
- [2] NAE, Uranium 2020: Resources, Production and Demand, 484 (2020)
- [3] C. Liu *et al.*, A half-wave rectified alternating current electrochemical method for uranium extraction from seawater, *Nat. Energy*, 8 (2017)

- [4] Y. Wang *et al.*, Hip Implant Design With Three-Dimensional Porous Architecture of Optimized Graded Density, *J. Mech. Des.*, 13 (2018).
- [5] N. Schneider and F. Donsanti, Atomic Layer Deposition (ALD) - Principes généraux, matériaux et applications, *Innov. Technol.*, 12 (2016).

Development of macroporous geopolymer foams functionalized by a photocatalyst.

S. Benkhirat^a, G. Plantard^{b*}, K. Nouneh^a

^a*PROMES-CNRS UPR 8521, PROcess Material and Solar Energy, Rambla de la Thermodynamique, 66100, Perpignan, France.*

^b*University Ibn Tofail, Faculty of sciences, Laboratory of Materials Physics and Subatomics LPMS, Kenitra, Maroc.*

Keywords: Foam, Geopolymer foam, Macroporous foam, Photocatalysis.

1 Introduction

Heterogeneous photocatalysis is one of the advanced oxidation processes for treating a wide range of pollutants in water [1]. Driven by the advancement of technologies based on the use of the solar resource, this technique has gained ground in recent years and has proven to be very effective in removing toxic compounds from water in an economical and clean way, as it uses a renewable energy source and semiconductor materials with limited cost [2]. These technologies are based on the production of highly reactive oxidizing species such as the hydroxyl radical, to degrade recalcitrant organic pollutants. It consists of using a photocatalyst under UV irradiation to oxidize the pollutants present in the water.

This work is part of the development of innovative supported materials. Photocatalytic materials dedicated to a solar application must meet the constraint of radiation management for the production of radicals. It is essential that the catalyst is homogeneously distributed in order to capture the radiation in the volume of the photoreactor which is the site of photo-oxidation. In the literature, macroporous supports, such as metal foams, are a prime candidate [3]. They develop a macroporosity allowing the distribution of radiation in the volume, their photocatalytic performance is close to that of nanometric powders, which are the reference in this field, but which require a separation step [4]. To overcome the high cost of producing metallic foams, it is proposed to design geopolymer foams based on the development technology developed in civil engineering. In a first step, the method of elaboration of the geopolymeric material classically used in the literature will be presented [5]. To confer porosity to the material, hydrogen peroxide is added during the polycondensation in order to generate bubbles. Thus, fly ash and metakaolin, the basic constituents of a geopolymer, are mixed, then an alkaline solution based on NaOH and Na₂SiO₃ is added to activate the polycondensation process [6]. The porosity is generated by the production of O₂ from the decomposition reaction of hydrogen peroxide which was chosen as the foaming agent. The volume expansion of the foam is monitored during its formation over time. The difficulty lies in the fact that the growth of gas bubbles can become limiting if the polycondensation rate of the geopolymer is faster than the decomposition rate of

H₂O₂. The amount of hydrogen peroxide and the operating conditions allowed to modulate the porosity of the material. The foam was then dried (35°C, 24h) and calcined (800°C, 2 h) to obtain a mechanically resistant material. The structural properties of the material will be studied (composition, crystallinity, morphology) using scanning and X-ray microscopy techniques. Tensile tests will be used to define the mechanical characteristics (Young's modulus). The pore size distribution of the foams was determined by image analysis of digital micrographs using image analysis software (Image J). The pore size of the geopolymeric foams ranged from 0.01 to 3.5 mm. Several parameters such as H₂O₂ concentration, surfactant nature, viscosity will be optimized in order to confer macroporosity and to define the experimental conditions allowing to control the material characteristics.

References

- [1] A Galvez J., Malato Rodríguez S., Solar detoxification, United Nations Educ. Sci. Cult. Organ., (2003), 237.
- [2] Malato S., Fernández-Ibáñez P., Maldonado M.I., Blanco J., Gernjak W., Decontamination and disinfection of water by solar photocatalysis: Recent overview and trends, *Catal. Today*, 147, (2009), 1–59.
- [3] Plesch G., Gorbar M., Vogt U.F., Jenesak K., Vargova M., Reticulated macroporous ceramic foam supported TiO₂ for photocatalytic applications, *Materials Letters*, 63, (2009), 461-463.
- [4] Plantard G., Goetz V., Correlations between optical, specific surface and photocatalytic properties of media integrated in a photo-reactor, *Chem. Eng. J.*, 252, (2014), 194–201.
- [5] Rangan, B. Vijaya. Geopolymer concrete for environmental protection. *The Indian Concrete Journal*. 88 (4) 2014, 41-59.
- [6] Zhang, Zuhua; Provis, John L.; Reid, Andrew; Wang, Hao). Geopolymer foam concrete: An emerging material for sustainable construction. *Construction and Building Materials*, 56 (2014), 113–127.

Reactive transport modelling in porous fractured media: contribution to the understanding of weathering processes

S. Favier^a, F. Golfier^a, Y. Teitler^a, M. Cathelineau^a

^a *Université de Lorraine, CNRS, GeoRessources, 54000 Nancy, France*

Keywords: reactive transport, Discrete fracture matrix model, dual-porosity model

1 Introduction

Weathering processes are involved with many of the current challenges of the geoscience community such as climate regulation, the critical zone formation and the supergene deposits formation of highly demanded metals (e.g., Co, Ni, Sc, U). Yet, understanding the different processes controlling the weathering remains a major challenge. Recent studies have highlighted fractures' critical impact in controlling the dissolution and redistribution processes by creating preferential fluid flow pathways [1]. However, the impact of physical and chemical heterogeneities on the weathering front progression is still not totally understood.

Due to the complexity of the mechanisms involved in the weathering, reactive transport models (RTMs) are a powerful tool to understand, quantify and predict the coupling effect of chemical and physical processes at different scales and across large temporal scales on weathering [2][3]. The study of the Ni heterogeneous distribution in New Caledonia is an excellent case study to shed light on the impact of fractures on the formation of weathering heterogeneities. In New Caledonia, indeed, Ni-laterite supergene deposits result from the weathering of the peridotite by the downward progression of rainwater. The dissolution/precipitation process leads to the progressive enrichment in Ni at the interface between the saprolite and the oxide horizon. Therefore Ni distribution can be used as a proxy of the weathering front progression

In this study, we investigate the impact of fracture networks as chemical and hydrological heterogeneities on the weathering front migration in fractured rock mass through different models of increasing complexity. First, a global approach with a 1D dual-porosity model is developed to highlight their impact on weathering pattern by comparing the results with an unfractured porous domain (single porosity model). Then, a discrete approach is presented, where fractures are explicitly defined as 1D interfaces embedded in a 2D porous rock matrix. The effect of the connectivity of the fracture network on the redistribution of metals of interest is thus studied, and potential hotspots of interest are identified. The results are discussed considering field observations from Ni-laterite deposits in New Caledonia.

2 Numerical models

The weathering of an unfractured peridotite column, i.e., a single porosity model (S.P. Model) is compared with the weathering of a fractured peridotite rock mass modelled by a dual porosity formulation (D.P. Model). The two different geochemical fractures and matrix sub-domains, corresponding to the different characteristic times of processes at stake, are coupled with an exchange term, which controls the diffusive exchange of the solutes. These mass transfer functions, however, cannot fully capture the complex flow behaviour in fractured media, and the application to reactive transfer processes is also delicate.

In addition, a discrete fracture matrix model (DFM Model) is built to study the impact of the fracture connectivity on the weathering. The DFM or hybrid models divide the domain into regions for which an explicit fracture formulation is coupled with a continuum representation of the matrix, adding more resolution to the description, albeit at the cost of heavier numeric simulations. The modelling is performed through the iCP (interface Comsol- PhreeqC) formulation to couple the complex fluid flow with the geochemistry.

3 Results and Discussion

The typical mineralogical and geochemical profiles are obtained for both S.P., D.P. and DFM models. DFM results are illustrated in Figure 1. Globally, three different geochemical zones are observed. At the bottom of the profile, the saprolite zone (region 1), characterized by the dominance of Mg-Ni phyllosilicates. The Mg and Si grades are still high, while Ni and Fe are low. At the top of the profile, the oxide zone (region 3) characterized by the dominance of goethite. The model is depleted in Mg and Si. Fe is high and Ni is controlled by the goethite. At the transition (region 2) between the saprolite and the oxide horizon, the Ni-phyllosilicates are the most present, so is the case for the Ni enrichment. A smoother transition is observed for the D.P. model.

In the D.P. model, mineralogical heterogeneities are observed between the matrix and the fractures. The saprolite zone is deeper in the fractures, meaning that the weathering is more intense. The transition area is also much thicker in the fractures where the Ni-phyllosilicates are the dominant species. These heterogeneities successfully recreate the Ni heterogeneities observed between the fractures (between 20 to 30 wt.%) and the matrix (up to 5wt.%) in the field.

Integrating explicitly the geometry of the fracture network with the DFM model allows to successfully recreate Ni heterogeneities (and thus weathering heterogeneities) observed on the field. Ni preferentially migrates in the fractures before diffusing in the matrix creating boulders with concentration zonation.

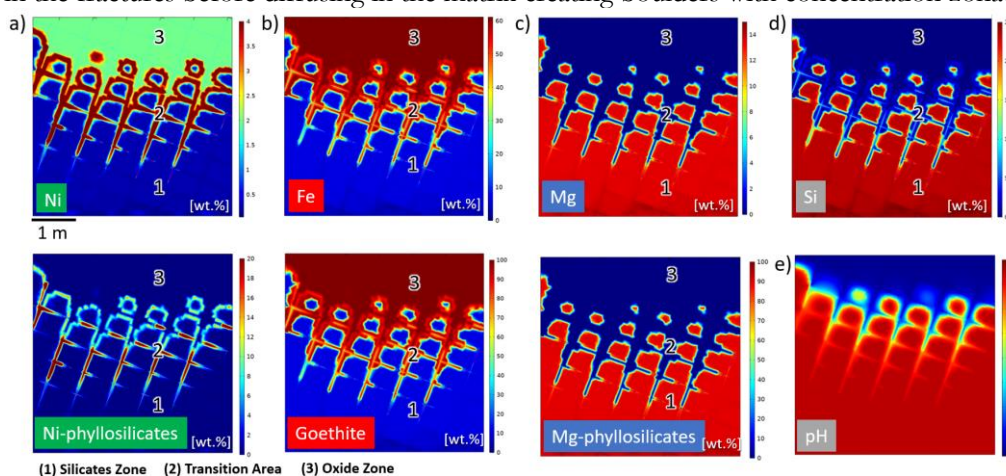


Figure 1 – Geochemical and mineralogical distribution in DFM model of a) Ni and Ni-phyllosilicates, b) Fe and Goethite, c) Mg and Mg-phyllosilicates, d) Si and e) pH.

4 Conclusions

The dual porosity modelling of a fractured rock mass under weathering successfully recreates geochemical heterogeneities observed in the field. They originate from the physico-chemical differentiation of the fractured rock mass into interconnected sub-domains. The fractured bedrock acts as a kind of filtering mechanism for the newly formed phyllosilicates: Ni phyllosilicates precipitate more likely in fractures, while Mg phyllosilicates remain trapped in the matrix because of the differences in residence time and liquid-to-solid ratio.

The DFN modelling allows to go deeper in the understanding of the impact of a complex fracture network on the weathering front progression. Depending on its geometry and permeability, the fracture network controls the fluid flow, hence favouring the formation of geometrical weathering heterogeneities.

References

- [1] Favier S., Teitler Y., Golfier F., Cathelineau, M. Multiscale physical–chemical analysis of the impact of fracture networks on weathering: Application to nickel redistribution in the formation of Ni-laterite ores, New Caledonia. *Ore Geology Reviews*, 147, 104971. (2022)
- [2] Myagkiy A., Golfier F., Truche L., Cathelineau M. Reactive Transport Modeling Applied to Ni Laterite Ore Deposits in New Caledonia: Role of Hydrodynamic Factors and Geological Structures in Ni Mineralization. *Geochemistry, Geophysics, Geosystems*, 20(3), 1425–1440 (2019).
- [3] Myagkiy A., Truche L., Cathelineau M. Golfier F. Revealing the conditions of Ni mineralization in the laterite profiles of New Caledonia: Insights from reactive geochemical transport modelling. *Chemical Geology*, 466, 274–284. (2017).

Porous On-Demand Wafers for Energy, Environment and a Resilient supply chain

G. Dakroub^a, H. Maskrot^a, B. Jousselme^b, F.Oswald^b, R.Bazin^b

^aUniversité Paris-Saclay, CEA, Service de recherches sur les matériaux et les procédés avancés,
91191, GIF-surYvette, France

^bUniversité Paris-Saclay, CEA, CNRS, NIMBE, LICSEN, 91191, Gif-sur-Yvette, France

Contact: ghadi.dakroub@cea.fr

Keywords: Low carbon energy, porous structures, additive manufacturing, thin films.

1 Introduction

The global energy demand is increasing with the development of technologies and population growth. Therefore, the scientific community is bent on replacing fossil energy sources with new and renewable ones, and on developing efficient systems of energy storage.

In this context, the **POWE²R** (Porous On-Demand Wafers for Energy, Environment and a Resilient supply chain) project aims at developing on-demand innovative 3D structures for energy and environment, in an eco-responsible spirit and a resilient supply chain.

Additive manufacturing such as Laser Powder Bed Fusion (L-PBF) is a powerful technology for the elaboration of complex 3D structures and is widely used in different domains such as aerospace, biomedical and green energy [1]. It can produce complex porous and dense metal structures in an eco-responsible spirit, minimizing material waste and environmental pollution [2].

This project aims to demonstrate the relevancy of functionalized porous structures, developed by coupling additive manufacturing processes and surface treatment such as thin films deposition techniques, in the field of low-carbon energy and environment.

2 Results

2.1 Porous structures for Proton Exchange Membrane Fuel Cell (PEMFC)

Highly porous frits have been manufactured using L-PBF process as gas diffusion layer (GDL) for the Proton Exchange Membrane Fuel Cell (PEMFC). These porous structures exhibit good material integrity and display an open porosity of 70%, enabling easy diffusion of water and gas through the filter (Figure 1a and 1b). The porosity level of these frits falls within the range of commercial Gas Diffusion Layers (GDL) (50-90%) usually made of carbon fiber. Furthermore, other complex structures were tested in a PEMFC assembly. The polarization curve (Figure 1c) of the 316L structure coated with gold reveal good performances similar to commercial graphite bipolar plates.

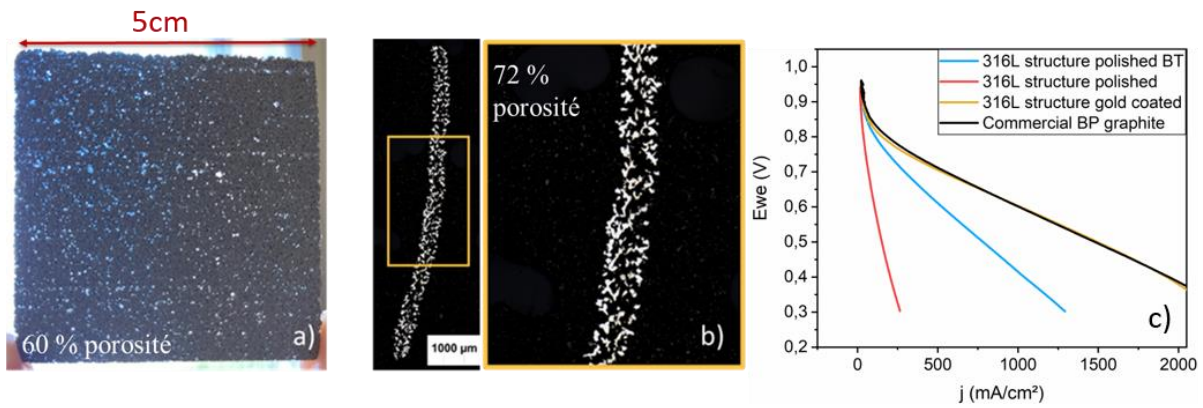


Figure 1: a) Gas diffusion Layer (GDL) printed by L-PBF. b) Cross-sectional images of the GDL using optical microscopy. c) Polarization curves representing the performances of the 316L structures in the PEMFC compared to graphite.

2.2 Porous structures for nuclear waste storage

316L stainless steel cylindrical filters with a diameter of 50 mm and a thickness of 3 mm have been manufactured by L-PBF processes for potential use as aerosol-retaining vents for nuclear waste containers (Figure 2a). Multiple filters were produced by varying the fabrication parameters i.e. the energy provided by the laser source. The optical microscope images show clearly the influence of the parameters on creating porosity in the filters structure (figure 2b). In addition, figure 2c shows a consistency in the evolution of the filters porosity percentages and mass with the increase of the energy density.

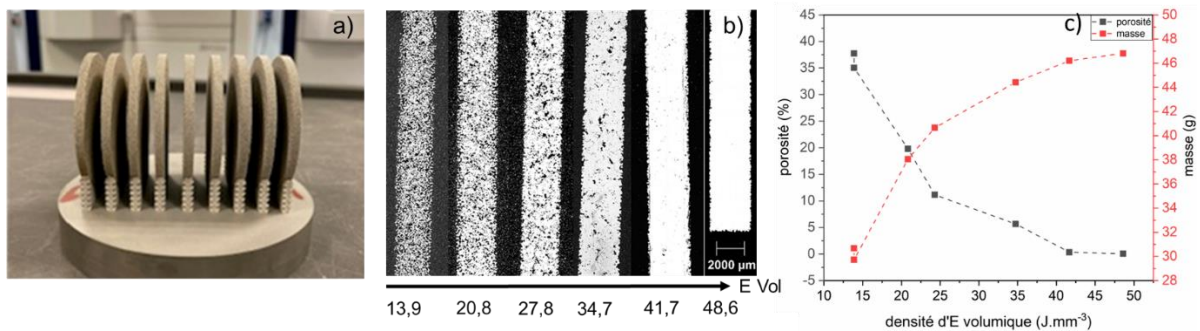


Figure 2: a) Cylindrical filters plate printed by L-PBF. b) Cross-sectional images of the filters using optical microscopy. c) Variation of the filters porosity and mass as a function of the energy density.

3 Reference

- [1] P. Huang *et al.*, « Stainless steel bipolar plate fuel cell with different flow field structures prepared by laser additive manufacturing », *Int. J. Heat Mass Transf.*, vol. 183, p. 122186, févr. 2022, doi: 10.1016/j.ijheatmasstransfer.2021.122186.
- [2] H. Heidary, M. J. Kermani, et B. Dabir, « Influences of bipolar plate channel blockages on PEM fuel cell performances », *Energy Convers. Manag.*, vol. 124, p. 51-60, sept. 2016, doi: 10.1016/j.enconman.2016.06.043.

Session

Mécanique des milieux poreux :
déformation, rupture, endommagement

Geothermal induced seismicity: Understanding the 2019 earthquake crises of Strasbourg

Arezou Dodangeh^{*1}, Renaud Toussaint^{2,3}, Marwan Fahs², and Eirik Flekkøy³

¹ITES, CNRS – University of Strasbourg, CNRS, ENGEES, Institut Terre et Environnement de Strasbourg UMR7063, Strasbourg, France, University of Strasbourg, CNRS, ENGEES, Institut Terre et Environnement de Strasbourg, UMR 7063, Strasbourg, France – France

²ITES, CNRS – University of Strasbourg, CNRS, ENGEES, Institut Terre et Environnement de Strasbourg UMR7063, Strasbourg, France, University of Strasbourg, CNRS, ENGEES, Institut Terre et Environnement de Strasbourg, UMR 7063, Strasbourg, France – France

³PoreLab, University of Oslo – SFF PoreLab, Njord, Physics Department, University of Oslo, Norway – France

Abstract

Geothermal energy is an alternative renewable and green potential energy source. But it has several drawbacks, the most important of which is the risk of seismicity. Two kinds of seismicity are related to well operations: the induced one and the triggered one.

Alsace is one of the most important regions in Europe in geothermal resources. Geoven was a geothermal plant pilot situated in the commune of Vendenheim at the north of Strasbourg city. It aimed at exploiting the geothermal energy by circulating fluid at depth along the Robertsau fault.

In this site two clusters of earthquake, one of them close to the site and other one at the Robertsau area, 5km south, were observed in 2019. The idea of a physical connection between earthquakes at the Robertsau area and the pumping at the Geoven site has been formed. The large distance between the injection well and the cluster and the fact that no earthquake was observed between them, have caused some polemics between scientists and the company in charge of Geoven.

The main goal is to evaluate a possible link, through a simple methodology based on fluid/solid deformation and mechanical coupling, with numerical modeling.

The methodology follows:

1. Identifying the geometry of the fault by extracting the angles and tectonic stresses along the main faults.
2. Modeling pressure perturbation in the area due to water injection by solving a quasi 2D pressure diffusion equation with the proper injection parameters, permeability, and porosity.
3. Evaluating the stress on the fault and analyzing the risk of earthquake triggering by

*Speaker

using a Mohr-coulomb failure criterion and activation by fluid pore pressure rise.

We find out that, in the northern cluster, the fault is strong and a large activation pressure is needed for slip to occur. This slip of microcracks in the vicinity of the injection well is required to improve the reservoir. Indeed, the increase in pore pressure in this area close to the well is very high, and micro-earthquakes occur – this sliding is the objective of stimulation. On the other hand, around the southern cluster, the pressure required for sliding drops sharply: the fault is weak at this point. This means that slip occurs even with a small increase in pressure. We show that, at this point, the pore pressure increases enough to trigger earthquakes. But between these two clusters, the fault is resistant due to its orientation, and the increase in pore pressure is not large enough for sliding. For this reason, there is a distance of 5km between the two clusters, without earthquakes.

It can be concluded that the fault geometry corresponds to a weak configuration around the southern cluster. That leads to an activation pressure required for sliding at this point, much lower than in other locations. We show that mechanically, the pressure perturbation resulting from Geoven operation, even if tiny in this distant location, can be enough to trigger earthquakes in that zone.

Induced seismicity due to fluid injection in geological reservoirs: influence of pumping strategies

B er enice Vallier^{*1}, Renaud Toussaint^{2,3}, Marwan Fahs⁴, Cl ement Baujard⁵, Albert Genter⁶, Eirik Grude Flekk oy⁷, and Knut J orgen M al oy⁷

¹ITES, CNRS – University of Strasbourg, CNRS, ENGEES, Institut Terre et Environnement de Strasbourg UMR7063, Strasbourg, France, University of Strasbourg, CNRS, ENGEES, Institut Terre et Environnement de Strasbourg, UMR 7063, Strasbourg, France – France

²ITES, CNRS – University of Strasbourg, CNRS, ENGEES, Institut Terre et Environnement de Strasbourg UMR7063, Strasbourg, France, University of Strasbourg, CNRS, ENGEES, Institut Terre et Environnement de Strasbourg, UMR 7063, Strasbourg, France – France

³PoreLab, University of Oslo – Norv ege

⁴ITES, CNRS – University of Strasbourg, CNRS, ENGEES, Institut Terre et Environnement de Strasbourg UMR7063, Strasbourg, France, University of Strasbourg, CNRS, ENGEES, Institut Terre et Environnement de Strasbourg, UMR 7063, Strasbourg, France – France

⁵ES G eothermie – ES G eothermie, 5 rue Amp ere, Mundolsheim, FRANCE – France

⁶ES G eothermie – ES G eothermie, 5 rue Amp ere, Mundolsheim, FRANCE – France

⁷PoreLab, University of Oslo – Norv ege

R esum e

In the context of deep exploitation (gas storage, deep geothermal energy or wastewater disposal), there is the necessity to enhance the reservoir permeability before exploitation. To enhance the permeability, one way is to conduct stimulations by fluid injection which increase the pore pressure. However, this method can generate an increase of the seismic risk on distant faults. This is due to the fact that the overpressure provokes an effective normal stress decrease, leading to a potential rupture of critically stressed distant faults, known as induced seismicity. Induced seismicity potentially related to well operations has been observed in zone of oil and gas production, mining exploitation, fluid sequestration or in deep geothermal reservoirs.

The main goal of this work is to prevent induced seismicity from critically stressed distant faults by minimizing the pressure disturbances at distance of the well due to underground industrial operations while maintaining important pore pressure close to the well. Thus, we numerically study the diffusion of pressure disturbances due to well injection in a poro-elastic reservoir. We then use the diffusion of pressure disturbances to understand the evolution of the effective stress and to investigate the risks of induced seismicity.

A numerical model based on the finite difference method is developed to solve the pressure diffusion equation. The domain is assumed to be isotropic and homogeneous. The 2D domain represents the fault plane and permeable damaged zone embedded in a less permeable rock in 2D. We also perform simulations in the homogeneous sedimentary reservoir

*Intervenant

using 3D modeling.

The numerical model is validated by comparing the numerical distant pressure disturbances (at 5km from the injection/production wells) to analytical solutions developed from the Green's function of diffusion equation. The numerical model is then used to investigate the influence of a different fluid injection/production strategy (time-dependent injection) on the near-well and distant pressure disturbances. The performances of different pumping strategies are compared at an equivalent level of pressure close to the well in the region targeted for simulation. The results show that the oscillating pumping strategy has a significant potential in reducing the induced seismicity on distant faults. Further works including models of increasing complexity with more realistic fault geometries and operational conditions will be conducted for mitigation strategies.

Numerical study of the effect of the boundary conditions in DEM modelling on the mechanical behavior of a cemented granular media: application to biocalcified sand

T. Dumas^a, M. Sarkis^a, A. Naillon^a, B. Chareyre^a

^aUniversité Grenoble Alpes, CNRS, Grenoble INP, 3SR, F-38000, Grenoble, France

Keywords: DEM modelling, numerical simulation, boundary conditions, triaxial test, granular matter, biocalcification

1 Introduction

Microbially induced calcite precipitation (MICP) is a recent technique used to reinforce soil, structures and materials. It uses bacteria to precipitate calcite in a medium to improve its strength by creating bonds between the grains. It has been shown that only a small percentage of calcite is needed to considerably increase the strength of sand [1], and that the mechanical properties of the materials depend on the micromechanical properties of the contact [2].

In order to predict the mechanical behaviour of this cemented sand, a first numerical model has been developed [3] using the open-source code Yade [4] based on the discrete elements method (DEM). In particular, the goal was to simulate a triaxial test on biocalcified sand, using micromechanical parameters determined by experiments [5]. This first numerical model allows to describe, with good accuracy, the macroscopic response of lightly cemented samples when the volume fraction of calcite is lower than 4%. However, the peak stress was generally underestimated with the numerical model, whereas the dilatancy of the sample was overestimated for higher volume fraction of calcite. The three main limitations identified in this model were the low average numerical coordination number, the use of rigid boundary conditions and a parallelepipedic sample, whereas triaxial test are performed with cylindrical samples with a high average coordination number surrounded by an elastic membrane.

2 Numerical model

To tackle these limitations, a numerical development has been done to model cylindrical samples with a flexible membrane. The membrane model uses a topological object called *a-shape* [6], which extends the notion of convex hull to non-convex envelopes [7]. To compare indicators between samples with different boundary conditions, a method to compute the internal values of porosity and volumetric strain have been developed with the use of Voronoi cells. Cemented interactions are assigned in the initial state to match the experimental coordination number. Simulated triaxial compression with such model shows a significant increase of the strength compared to uncemented sand, and the post-peak response is much more fragile, as expected for cemented sand.

The model is used to study the effect of the boundary conditions on the mechanical behavior of a cemented granular media. Triaxial tests are simulated under three different confining pressures, three different density (loose, intermediate and dense), different geometries (cylindrical and parallelepipedal) and different boundary conditions (rigid walls and membrane). Overall, these simulations showed good stress-strain reproduction with almost no differences between different boundary conditions. The main difference is observed for the volumetric strain, which is reduced by around 40% for membrane boundary condition in comparison to rigid wall. The 3D shapes of the samples and the associated strain fields produce results much closer to those observed experimentally with the membrane. More specifically, it has been shown that the friction angle on the piston used for the test has a great impact on the final shape of the samples, going

from barrel deformation to lateral displacement of the sample with a shear band. The initial geometry of the specimen was found to have little influence on the numerical macroscopic response.

Finally, a comparison with triaxial experiment performed under X-Ray microtomography is being carried out to quantify our ability to predict the macroscopic behavior of biocemented sand.

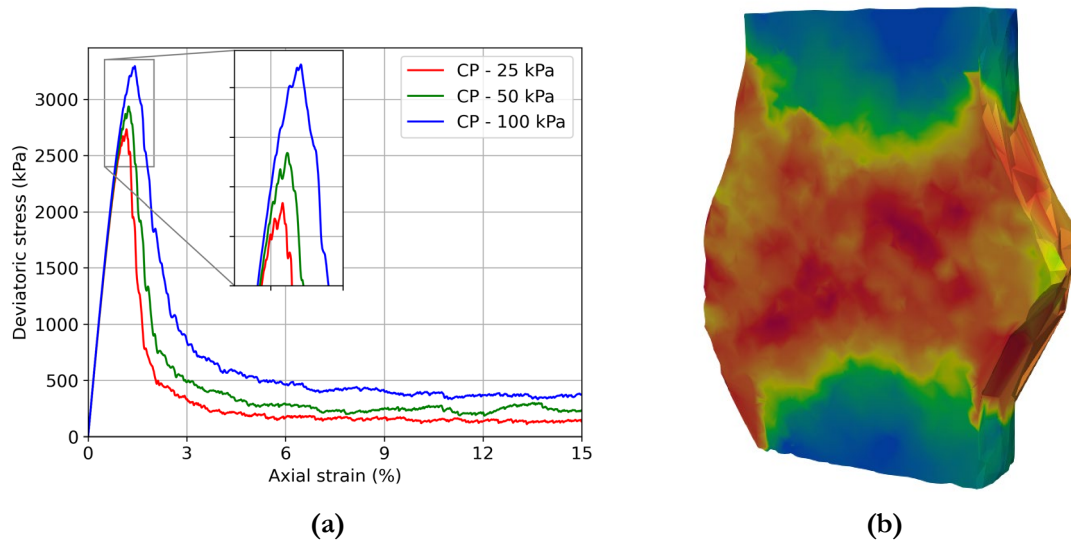


Figure 1: (a) Numerical behaviour of high-cemented sand under different triaxial loading, (b) Associated deformation field of the cylindrical sample at the end of loading

References

- [1] D. Terzis and L. Laloui, “A decade of progress and turning points in the understanding of bio-improved soils: A review,” *Geomechanics for Energy and the Environment*, vol. 19, p. 100116, 2019.
- [2] A. Dadda, C. Geindreau, F. Emeriault, A. Esnault Filet, and A. Garandet, “Influence of the microstructural properties of biocemented sand on its mechanical behavior,” *International Journal for Numerical and Analytical Methods in Geomechanics*, vol. 43, no. 2, pp. 568–577, 2019.
- [3] M. Sarkis, M. Abbas, A. Naillon, F. Emeriault, C. Geindreau, and A. Esnault-Filet, “Computers and Geotechnics D . E . M . modeling of biocemented sand : Influence of the cohesive contact surface area distribution and the percentage of cohesive contacts,” *Computers and Geotechnics*, vol. 149, no. June, p. 104860, 2022.
- [4] Šmilauer V. et al. (2021). Yade Documentation 3rd ed. The Yade Project. <http://yadedem.org/doc/>.
- [5] M. Sarkis, A. Naillon, F. Emeriault, and C. Geindreau, “Tensile strength measurement of the calcite bond between biocemented sand grains,” *Accepted in Acta Geotechnica*, 2023.
- [6] Tran Kai Frank Da and Sébastien Loriot and Mariette Yvinec. 3D Alpha Shapes. In *CGAL User and Reference Manual*. CGAL Editorial Board, 5.5.2 edition, 2023.
- [7] Pekmezi, G., Littlefield, D., and Chareyre, B. (2020). Statistical distributions of the elastic moduli of particle aggregates at the mesoscale. *International Journal of Impact Engineering*, 139.

Transmissivité d'une fracture et perméabilité d'un milieu poreux en régime glissant

T. Zaouter^a, D. Lasseux^b, F. J. Valdés-Parada^c, M. Prat^d

^aCEA, DES, ISEC, DPME, SEME, Laboratoire d'Étanchéité, Univ. Montpellier, Marcoule, France

^bI2M, UMR 5295, CNRS, Univ. Bordeaux, 351, Cours de la Libération, 33405 Talence CEDEX, France

^cDivisión de Ciencias Básicas e Ingeniería, Universidad Autónoma Metropolitana-Iztapalapa, Av. Ferrocarril San Rafael Atlixco 186, Col. Leyes de Reforma, 09310, CDMX, Mexico

^dInstitut de Mécanique des Fluides de Toulouse (IMFT), Université de Toulouse, CNRS, Toulouse, France

Keywords: Fracture, Milieux Poreux, Écoulement glissant, Changement d'échelle

Résumé

Les écoulements de gaz en régime raréfié se rencontrent dans de nombreuses applications en fracture rugueuse (étanchéité) ou en milieux poreux (stockage géologique, extraction gazière dans des roches très peu perméables). Lorsque la raréfaction est modérée (nombre de Knudsen inférieur à 0,1), l'écoulement à l'échelle microscopique est modélisé par les équations de Navier-Stokes et une condition de glissement, typiquement du premier ordre [1], pour la vitesse aux parois. À l'échelle macroscopique, la signature de l'effet du glissement se retrouve de manière implicite dans le tenseur de transmissivité apparente dans le cas d'une fracture [2], ou, de façon analogue, dans le tenseur de perméabilité pour un milieu poreux [3, 4]. Un développement en série selon les puissances du nombre de Knudsen moyen permet de scinder la contribution visqueuse de celle du glissement, tous les coefficients étant alors intrinsèques, celui devant chaque monôme d'ordre supérieur ou égal à un étant le tenseur de correction de glissement à l'ordre donné. Chaque tenseur de correction est alors obtenu à partir de la solution d'un problème de fermeture qui lui est propre, séquentiellement couplé avec ceux aux ordres inférieurs néanmoins [2, 3, 4].

Dans ce travail, on propose une méthode efficace permettant de réduire d'un facteur deux le nombre de problèmes de fermeture à résoudre pour obtenir le tenseur de correction à l'ordre souhaité [6, 7]. En particulier, on montre que l'approximation de Klinkenberg [5], communément employée et qui correspond à la troncature de la série au premier ordre, est obtenue uniquement à partir de la solution donnant la transmissivité intrinsèque (resp. la perméabilité intrinsèque dans le cas du milieu poreux). En d'autres termes, la solution du problème de fermeture intrinsèque sans glissement (de type Reynolds en fracture, et Stokes en poreux) obtenue à l'aide d'un solveur standard, permet également de déterminer le tenseur de correction de premier ordre. Ce résultat montre le lien direct qui existe entre ces deux premiers coefficients, souvent observé en pratique. Les développements réalisés permettent également d'établir la symétrie des différents tenseurs ainsi que de statuer sur leur positivité ou négativité selon l'ordre. Enfin, la solution des deux premiers problèmes de fermeture permet d'obtenir suffisamment de tenseurs de correction pour construire un approximant de Padé reproduisant de manière très satisfaisante la dépendance fonctionnelle entre transmissivité (resp. perméabilité) et nombre de Knudsen moyen.

References

- [1] E. Lauga, M. P. Brenner & H. A. Stone, *Microfluidics: The no-slip boundary condition*, Springer, (2007).
- [2] T. Zaouter, D. Lasseux & M. Prat. Gas slip flow in a fracture: local Reynolds equation and upscaled macroscopic model. *Journal of Fluid Mechanics*, 837, pp. 413-442, (2018).
- [3] D. Lasseux, F. J. Valdés Parada, J. A. Ochoa Tapia & B. Goyeau. A macroscopic model for slightly compressible gas slip-flow in homogeneous porous media. *Physics of Fluids*, 26(5), (2014).
- [4] D. Lasseux, F. J. Valdés Parada & M. L. Porter. An improved macroscale model for gas slip flow in porous media. *Journal of Fluid Mechanics*, 805, pp. 118-146, (2016).
- [5] L. Klinkenberg. The permeability of porous media to liquids and gases. *Drilling and Production Practice*, pp. 200-213, (1941).
- [6] T. Zaouter, F. J. Valdés-Parada, M. Prat & D. Lasseux. Effective transmissivity for slip flow in a fracture. *Journal of Fluid Mechanics*, soumis.
- [7] D. Lasseux, T. Zaouter & F. J. Valdés-Parada. Determination of Klinkenberg and higher-order correction tensors for slip flow in porous media. *Physical Review Fluids*, 8, 053401, (2023).

Towards a DFT approach to the Mechanical Properties of Nanoporous Materials

Akli Kahlal, Vitor M. Sermoud, Gilles Pijaudier-Cabot, David Grégoire, Christelle Miqueu

Université de Pau et des Pays de l'Adour, E2S UPPA, CNRS, LFCR, Anglet, France

Keywords: Classical density functional theory, Nanoporous materials, mechanical properties

1 Introduction

Nanoporous materials exhibit unique properties due to their intricate structure, making them promising candidates for various applications. Understanding the mechanical behavior of the solid skeleton within these materials is crucial for their practical utilization. In this study, we aim at the implementation of classical density functional theory (cDFT) to explore the mechanical properties of nanoporous materials and to investigate the deformation of the solid skeleton. Classical density functional theory (cDFT) has been primarily employed for determining the structural and thermodynamic properties of inhomogeneous fluids while its application to solid phases has been explored in limited studies [1,2]. Notably, prior research in this field has heavily depended on the Gaussian approximation to characterize the density distribution [3].

2 Towards a solid phase

Two distinct approaches are employed in this study to obtain a stable solid phase within the context of classical density functional theory (cDFT). The first approach involves implementing Gaussian parametrization (equation (1)), which enables us to model a face-centered cubic (FCC) solid phase. By utilizing this approach, we were able to compute the phase diagram of a Lennard-Jones gas-liquid-FCC system, providing valuable insights into the equilibrium behavior of our system.

$$\rho_g(\alpha, c, r) = (1 - c) \left(\frac{\alpha}{\pi}\right)^{3/2} \sum_i \exp(-\alpha(r - R_i)^2) \quad (1)$$

In this equation, the summation is performed over all lattice points, “ $\alpha^{-1/2}$ ” represents the mean peak width of the gaussians, and “ c ” denotes the vacancy concentration in a unit cell.

In the second approach, we draw inspiration from the recent work of Lutsko and Lam [3] and explore an alternative method of spontaneous crystallization without imposing a specific structure for the solid phase. Lutsko and Lam introduced a novel free energy functional that incorporates a non-local hard-sphere contribution, which exhibits improved stability when simulating a solid compared to the widely used tensorial White-Bear II (WBII) functional. Additionally, a density approximation scheme using trilinear interpolation [4] is implemented. The combination of this new free energy functional and the density approximation scheme enhances the overall, leading to spontaneous crystallization. Moreover, to investigate the deformation of nanoporous solids, we adopt the canonical ensemble instead of the conventional grand canonical one. We also test various dispersive contributions based on different potentials, including VR-Mie and WCA. As an example, Figure 1 illustrates the spontaneous localization of the density in a 2D system with VR-Mie potential obtained by using cDFT at a fixed number of particles.

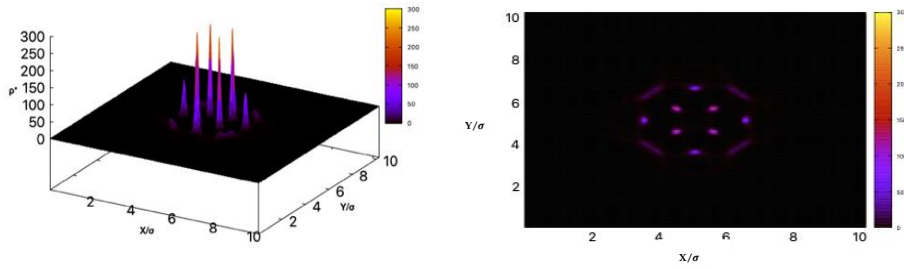


Figure 1: Spontaneous localization of the density field obtained by using cDFT at fixed number of particles in a 2D system at $T^*=0.4$ (VR-Mie potential)

By combining the cDFT approach with Gaussian parametrization and the exploration of spontaneous crystallization, this research aims to establish a solid foundation for investigating various mechanical properties associated with the solid skeleton of nanoporous materials.

References

- [1] P. Tarazona, A density functional theory of melting, *Molecular physics* 52.1 (1984).
- [2] T. Neuhaus, A. Härtel, Density functional theory of heterogeneous crystallization, *Eur. Phys. J. Special Topics* 223 (2014).
- [3] M. Oettel, Description of hard-sphere crystals and crystal-fluid interfaces: A comparison between density functional approaches and a phase-field crystal model, *Physical review E* 86.2 (2012).
- [4] J. Lutsko, J. Lam, Classical density functional theory, unconstrained crystallization, and polymorphic behavior, *Phys. Rev. E* 98 (2018).
- [5] J. Lutsko, C. Schoonen, Classical density-functional theory applied to the solid state, *Phys. Rev. E* 102.6 (2020).

Session
Milieux poreux biologiques

Mechanical properties and durability of a sand cemented by microbially-induced calcite precipitation (MICP)

Michela La Bella*¹, Marilyn Sarkis¹, Theo Dumas¹, Fabrice Emeriault¹, Christian Geindreau¹, Catherine Noiriél², and Antoine Naillon¹

¹Université Grenoble Alpes, CNRS, Grenoble INP, 3SR, F-38000, Grenoble, France – , University of Grenoble Alpes (UGA) – France

²Géosciences Environnement Toulouse, Observatoire Midi-Pyrénées, Université Paul Sabatier, CNRS, IRD, CNES, Université de Toulouse, 31400 Toulouse, France – Université de Toulouse Paul Sabatier – France

Abstract

Microbially-induced calcite precipitation (MICP) is a recent technique which represents a promising tool for soil improvement and remediation mediated by bacterial activity. More specifically bio-induced precipitation of calcium carbonate (CaCO_3) can be used to transform a non-cohesive sand into a cohesive medium, creating CaCO_3 crystal bridges between the sand grains(1). This application of MICP presents many advantages compared to the commonly used soil-reinforcement techniques that may involve high carbon footprint, use of toxic materials and high-energy consumption. On the contrary, bio-cementation would represent an environmentally friendly solution.

The mechanical properties of bio-cemented sands have been extensively characterized at the macroscale and microscale in our group. Synchrotron X-ray microtomography measurements (2) and triaxial tests on bio-cemented column samples permitted to understand that the macroscopic mechanical response of bio-cemented samples mostly depends on the micromechanical properties of the cohesive contact, the percentage of these cohesive contacts and their surface area distribution (3). Then, micromechanical characterization (4) (tensile and shear strength) of single agglomerates of two cemented sand grains have been performed in order to obtain input parameters in computation using D.E.M. (Discrete Elements Method) to predict the mechanical behaviour of bio-cemented samples (5).

In the optic of the application of bio-cemented materials, the durability becomes a key point. When exposed to aggressive environments, such as weakly acidic water, CaCO_3 crystals dissolve triggering the degradation of the bio-cemented material and its potential strength decrease (6). The variation of pH and concentration of the solution influences the dissolution behaviour of CaCO_3 crystals resulting in changes also on the morphology and contact properties of the crystals. Microfluidics represent a promising tool to study the behaviour of dissolution of CaCO_3 crystals. In particular, it permits the possibility to perform in-situ experiments monitoring several parameters, such as flow rate, pH and concentration

*Speaker

of the solution simultaneously.

The understanding on the evolution of the cemented contact surface areas measured at the local scale in the 2D porous media will be integrated in the D.E.M. model to gain multi-scale insights on the evolution of the mechanical properties of bio-cemented materials when exposed to acidic conditions.

References

- (1) D. Terzis and L. Laloui, "A decade of progress and turning points in the understanding of bio-improved soils: A review," *Geomechanics for Energy and the Environment*, vol. 19, p. 100116, (2019).
- (2) A. Dadda, C. Geindreau, F. Emeriault, A. Esnault Filet, and A. Garandet, "Influence of the microstructural properties of biocemented sand on its mechanical behavior," *International Journal for Numerical and Analytical Methods in Geomechanics*, vol. 43, no. 2, pp. 568–577, (2019).
- (3) A. Dadda, F. Emeriault, C. Geindreau, A. Esnault-filet, and A. Garandet, "Amélioration des propriétés mécaniques des sols par biocimentation: étude mécanique et microstructurale," *Revue Française de Géotechnique*, vol. 160, no. 4, (2019).
- (4) M. Sarkis, A. Naillon, F. Emeriault, and C. Geindreau, "Tensile strength measurement of the calcite bond between bio-cemented sand grains," *Accepted in Acta Geotechnica*, (2023).
- (5) M. Sarkis, M. Abbas, A. Naillon, F. Emeriault, C. Geindreau, and A. Esnault-Filet, "Computers and Geotechnics D . E . M . modeling of biocemented sand: Influence of the cohesive contact surface area distribution and the percentage of cohesive contacts," *Computers and Geotechnics*, vol. 149, no. June, p. 104860, (2022).
- (6) C. Geindreau, F. Emeriault, A. Dadda, O. Yaba, L. Spadini, A. Esnault Filet, A. Garandet, "Mechanical and Microstructural Changes of Biocemented Sand Subjected to an Acid Solution," *International Journal of Geomechanics*, vol. 22, no. 3, (2022).

Insight into the mechanism of malachite green dye adsorption on porous media: Characterization, modeling, and effects of adsorption affinity.

Fatima Zahra Falah^{*1}, Mouna Latifa Bouamrani , M'hammed El Kouali , Mohammed Talbi , and Samia Yousfi

¹Laboratory of analytical and molecular chemistry, Faculty of Sciences Ben Msik Hassan II University of Casablanca, BP 7955,Casablanca 20660, Morocco. – Maroc

Résumé

The transport of contaminated particles in porous media is an important pathway for wastewater treatment. Dye wastewater typically exhibits elevated levels of colored organic compounds and inorganic salts, making it challenging for biological processes to effectively treat (1). Adsorption is a cost-effective and efficient technology that can be utilized to eliminate dyes from water (2). Biochar, which is produced through the oxygen-limited pyrolysis of biomass and consists of carbon-rich residues, has garnered significant interest as a highly promising option for adsorption processes. This is primarily due to its numerous advantages such as its porous structure, cost-effective production, natural availability, exceptional stability, and abundance of functional groups(3). Our objective is to evaluate the feasibility of using biochar derived from soybean meal (SMB) as a cost-effective, porous biological media, for removing malachite green dye (MG) from wastewater. The biochar was characterized using the Fourier transform infrared spectroscopy (FTIR), scanning electron microscopy (SEM). In addition, the point of zero charge pH (pzc) was determined by potentiometric pH titration, enabling us to predict the adsorption behavior of our biochar under different pH conditions. The adsorption behavior of MG was successfully fitted using the pseudo-second-order kinetic model and Langmuir isotherm model, revealing a maximum adsorption capacity of 189.99 mg/g, allowing us to say that adsorption is mainly due to chemical interactions between the adsorbent and the adsorbate and that it occurs according to an ideal process, with monomolecular adsorption on specific adsorption sites. The thermodynamic studies indicated that the adsorption of MG was an endothermic and spontaneous process at all temperatures (25-55°C). Hence, these results suggest that SMB as a porous media has promising prospects and offers significant advantages in terms of pollutant adsorption in applications for treating wastewater and contaminated soils. Its use not only enables waste from the agri-food industry to be recycled but also contributes to sustainable and effective solutions for cleaning up the environment. Keywords: Porous Media; Adsorption; Agri-food waste recovery; Biochar; Malachite Green (MG).

*Intervenant

Dynamics and upscaling of porous biofilms with heterogeneous rheology

Jean-Matthieu Etancelin¹, Marlène Murriss-Espin², Sarah Perez¹, and Philippe Poncet^{*1}

¹Laboratoire de Mathématiques et de leurs Applications [Pau] – Université de Pau et des Pays de l'Adour, Centre National de la Recherche Scientifique – France

²Adult Cystic Fibrosis Center of Toulouse (CRCM), Department of Pneumology and Allergology – CHU Toulouse – France

Résumé

Our focus lies on operational applications and novel numerical approaches for modeling the heterogeneous mucus biofilm in the human lungs, specifically for monitoring cystic fibrosis (CF) therapies. At an operational level, our goal is to predict the impact of a therapy on mucociliary clearance, which refers to the functional ability of respiratory mucus to move along with the surrounding cells. Conversely, non-functional mucus fails to sufficiently clear the lung wall of allergens, toxins, viruses, bacteria, and their byproducts such as DNA filaments and altered mucoïd elements.

In this biological configuration, the mucus itself acts as a porous medium composed of Newtonian periciliary fluid (PCL) and highly concentrated mucins produced by goblet cells. The interaction between mucins and PCL, facilitated by their motion within the biofilm, results in the formation of a polymerized mucus with distinct rheological properties. Among various rheological features like viscoelasticity, viscoplasticity, yield stress, and shear-thinning, we specifically focus on the latter, as it has been identified as the primary characteristic leading to non-functional mucus (4,5).

The results presented here are twofold. Firstly, we present the modeling based on the superficial velocity formulation, that we approximate numerically by a well-chosen coupling between particle methods (2), PSE schemes (1) and Stokeslets methods. The keypoint is the connexion between the equations governing the biofilm and the reactive flows involved in Digital rock Physics (DRP), as described in (3). Secondly, we use this efficient numerical method for the upscaling of the diffusion in the biofilm: the upscaled tortuosity index is practically quantified (which defines the relationship between the effective diffusion and the molecular diffusion of chemical species with respect to the local porosity). Finally, we show that these numerical results are compatible with clinical resume of the patients whose sputum rheology has been characterized (5).

This work is funded by French National Agency of Research, project MucoReaDy ANR-20-CE45-0022-01, and by Carnot Institute ISIFoR project MicroMineral P450902ISI.

References:

*Intervenant

- (1) S. Perez, P. Poncet, *Particle-Strength-Exchange methods for Lagrangian 3D DNS of rheological and reactive fluids with evolving interfaces at the pore-scale*, InterPore 2022 - MS09, Abu Dhabi, EAU, 2022.
- (2) J.M. Etancelin, P. Moonen, P. Poncet, *Improvement of remeshed Lagrangian methods for the simulation of dissolution processes at pore-scale*, *Advances in Water Resources*, 146:103780, 2020. DOI: 10.1016/j.advwatres.2020.103780
- (3) David Sanchez, Laurène Hume, Robin Chatelin, Philippe Poncet. *Analysis of 3D non-linear Stokes problem coupled to transport-diffusion for shear-thinning heterogeneous microscale flows, applications to digital rock physics and mucociliary clearance*. ESAIM: Mathematical Modelling and Numerical Analysis, EDP Sciences, 2019, 53 (4), pp.1083-1124. DOI:10.1051/m2an/2019013
- (4) Dominique Anne-Archard, Robin Chatelin, Marlène Murriss-Espin, David Sanchez, Marc Thiriet, Alain Didier, Philippe Poncet. *Modeling Cystic Fibrosis and Mucociliary Clearance*. Modeling of microscale transport in biological processes, Academic Press, pp.113-154, 2017, 978-0-12-804595-4. DOI: 10.1016/B978-0-12-804595-4.00005-5
- (5) Robin Chatelin, Dominique Anne-Archard, Marlene Murriss-Espin, Marc Thiriet, Philippe Poncet. *Numerical and experimental investigation of mucociliary clearance breakdown in cystic fibrosis*. Journal of Biomechanics, 2017, 53, pp.56-63. DOI:10.1016/j.jbiomech.2016.12.026

Can we control biofilm-induced clogging in porous media?

C. Toulouze^a, C. Papadopoulos^a, C. Coudret^b, D. Ciuculescu-Pradines^b, P. Swider^a, Y. Davit^a

^aInstitute of fluid mechanics (IMFT), 2 Allée du Professeur Camille Soula – 31400 Toulouse

^bLaboratory of molecular interaction chemical and photochemical reactivity (IMRCP), 118 route de Narbonne – 31062 Toulouse

Keywords: Bacterial biofilms, 3D-printed porous media, permeability, control

Bacterial biofilms are sessile communities that develop on surfaces and represent the dominant form of life for bacteria [1][4] [Figure1.A]. Biofilms play a key role in a variety of engineering problems found in porous media sciences, ranging from soils bioremediation to bioreactors for the production of proteins of interest or for filtering wastewater [2]. On the other hand, uncontrolled growth can induce clogging and loss of efficiency in technical systems, biofouling in industrial and medical devices, or even resistant contaminations [3][6] [Figure1.B]. Developing approaches to regulate the development of the biomass in porous structures could pave the way towards a new field in control engineering, aiming at controlling the permeability of porous media colonized by biofilm [5].

In particular, it has been observed recently that a competition between growth and detachment leads to large amplitude fluctuations of the pressure drop [6]. For example, in a bioreactor system for the filtration of wastewater or the production of a protein of interest, such fluctuations could induce important changes of yield [2][3]. In this work, we ask the question of whether we can avoid such fluctuations and more generally control the permeability of porous structures colonized by biofilms. We hypothesized that a closed loop control could be implemented to reach a target permeability in a demonstration microfluidic device.

We will first present a novel experimental technology that allows us to measure the dynamics of the pressure drop across a porous structure, while working in a microfluidic system with accurate control of environmental conditions. The core of the system is a 3D printed microbioreactor containing a porous structure, where biofilms develop. The porous structure is printed by stereolithography and composed of 300 μm wide/700 μm long channels, with a connectivity of 3. This system is adapted for control because we can: precisely define and change the structure and the material of the porous media; change nutrient types, concentrations and flow rate through programmable gear pumps; impose temperature to favour or not growth with a thermostat cell, while measuring the effect of those different parameters through a pressure sensor and oxygen sensor [Figure2]. The system can also be imaged via X-ray microtomography with a newly developed contrast agent based upon gold nanoparticles.

We will show a simple example of how pressure fluctuations can be controlled for a biofilm of *Pseudomonas aeruginosa* and discuss the implications in terms of the definition of a cost function. We will further present our global strategy for control, which relies on feedback control of four environmental conditions [Figure2.A]: nutrient concentrations, temperature, flow and the presence of bacterial predators-in particular *Bdellovibrio bacteriovorus* [8].

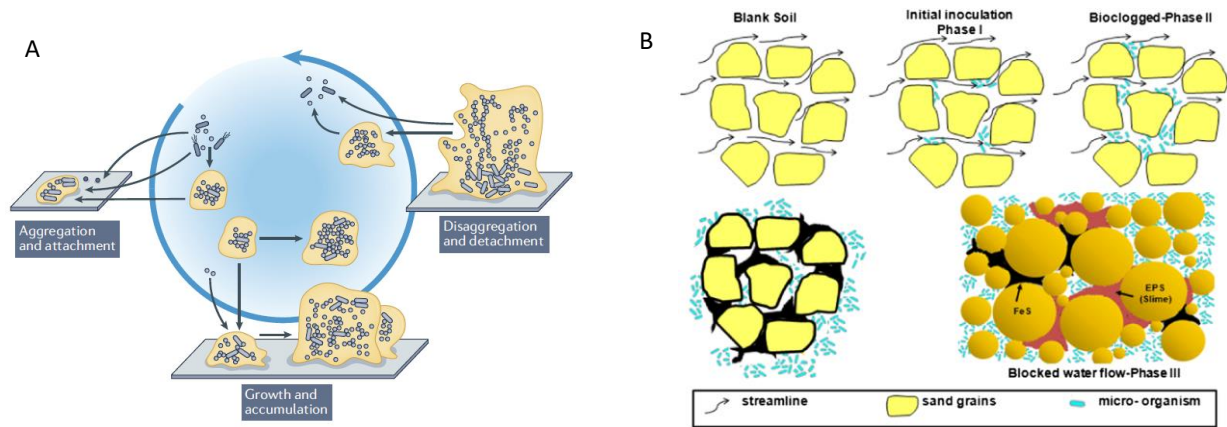


Figure 1: A) Expanded conceptual model of biofilm formation [4], B) Bioclogging process from the initial inoculation of the porous medium which does not alter the flow pattern (Phase I) to the increase in microcolonies density causing bioclogging of the pores and change of the flow pattern (Phases II and III) [7]

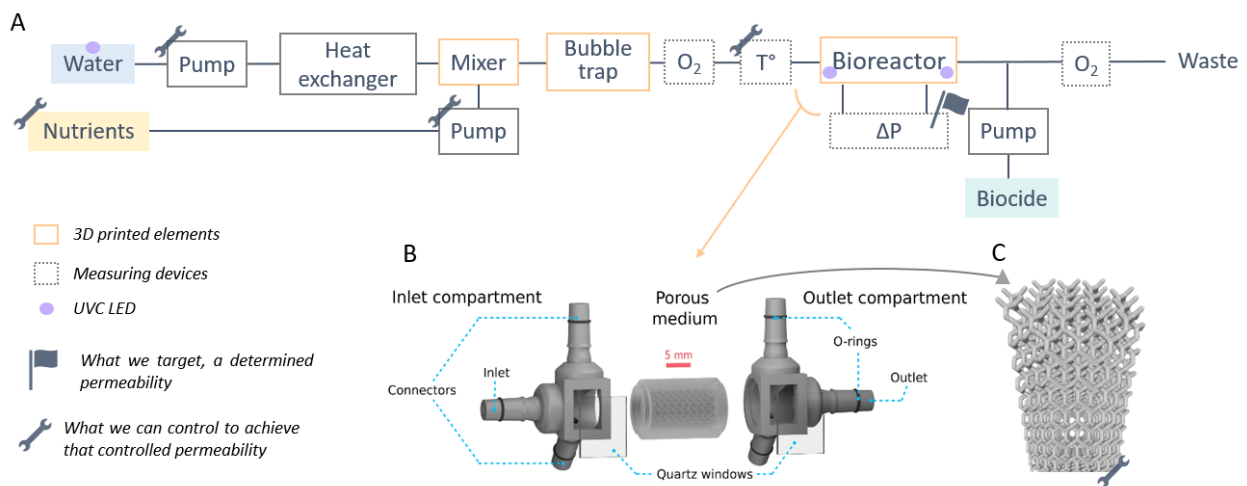


Figure 2: A) Setup scheme for the study of biofilm grown in 3D porous media, B) detailed 3D model of the bioreactor, C) representation of the bioreactor's channels

References

- [1] Flemming HC, Wuertz S. Bacteria and archaea on Earth and their abundance in biofilms. *Nat Rev Microbiol*, 17(4):247-260. (2019 Apr)
- [2] Lemke, P., Zoheir, A. E., Rabe, K. S., & Niemeyer, C. M, *Biotechnology and Bioengineering*, Microfluidic cultivation and analysis of productive biofilms. V118, Pages 3860-3870 (2021).
- [3] Iliuta, Ion and Faiçal Larachi. "Dynamics of cells attachment, aggregation, growth and detachment in trickle-bed bioreactors." *Chemical Engineering Science* 61 (2006)
- [4] K Sauer, P Stoodley, D M Goeres, L Hall-Stoodley, M burmole, P S Stewart, T Bjarnsholt, The biofilm life cycle: expanding the conceptual model of biofilm formation, *Nat Rev, Microbio*, vol20 p609-620, 2022
- [5] A. Brovelli, F. Malaguerra, D.A. Barry, Bioclogging in porous media: Model development and sensitivity to initial conditions, *Environmental Modelling & Software*, Volume 24, Issue 5, Pages 611-626, 2009
- [6] D L. Kurz, E. Secchi, F J. Carrillo, I C. Bourg, R. Strocker, J Jimenez-Martinez, Competition between growth and shear stress drives intermittency in preferential flow paths in porous medium biofilms, *PNAS*, 2022, V119
- [7] . Souli, Hanène & Farah, tahani & Fleureau, Jean-Marie & Kermouche, Guillaume & Fry, Jean-Jacques & Girard, Benjamin & Aelbrecht, Denis & Lambert, John & Harkes, M.P. Durability of Bioclogging Treatment of Soils. *Journal of Geotechnical and Geoenvironmental Engineering*. (2016). 142. 10.1061.
- [8] Fereshteh Heidari Tajabadi, Sayed Morteza Karimian, Zeinab Mohsenipour, Sahar Mohammadi, Mohammadreza Salehi, Mahboubeh Sattarzadeh, Sima Fakhari, Mahnoush Momeni, Mohammad Dahmardehei, Mohammad Mehdi Feizabadi, Biocontrol treatment: Application of *Bdellovibrio bacteriovorus* HD100 against burn wound infection caused by *Pseudomonas aeruginosa* in mice, *Burns*, Volume 49, Issue 5, Pages 1181-1195, 2023

Nonlocal dynamics of biofilm clogging in a porous microfluidic device

G. Ramos^{a,b,c}, M. Benbelkacem^a, T. Desclaux^a, O. Liot^a, P. Duru^a, F. El Garah^b
Y. Davit^a

^a*Institut de Mécanique des Fluides de Toulouse, UMR 5502, Toulouse, France*

^b*Laboratoire de Génie Chimique, Université de Toulouse, CNRS, INPT, UPS, Toulouse, France*

^c*FERMAT, Université de Toulouse, CNRS, INPT, INSA, UPS, Toulouse, France*

Keywords: Biofilms, Microfluidics, Porous networks

Bacteria constitute about 15% of the global biomass on Earth [1]. The success of bacteria in colonizing a wide range of ecosystems is mainly due to biofilms, a sessile form of microbial life [2]. Biofilms are communities of interacting microbes that adhere to each other and to structures in their environment [3], making them more resistant to stress. Biofilms regulate critical processes in porous ecosystems [4], such as soils and groundwater systems, and are also key actors in bioengineering applications, such as biofilters [5]. These porous systems generally have a complex architecture, with structures that are connected, heterogeneous and exhibit strong couplings between flow and transport phenomena. Understanding the fundamental mechanisms of the colonization process in such systems may provide important insight into environmental processes and yield new approaches to bioengineering.

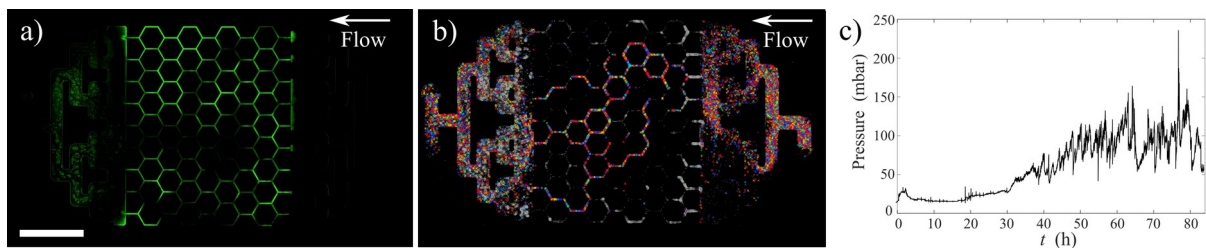


Figure 1: Bacterial biofilm in a porous microfluidic device under flow: a) Fluorescence image showing a biofilm of *Pseudomonas aeruginosa*. Each channel in the network has a cross section of $100 \times 100 \mu\text{m}$. Scale bar 5 mm. The arrow indicates the direction of the flow. b) Trajectories of the main flow paths obtained by Particle Tracking Velocimetry (PTV). These flow paths fluctuate in time due to constant reorganization of the biofilm inside the network. a) and b) modified from [6]. c) Pressure signal of the microfluidic device. Fluctuations on the pressure signal are also a signature of the constant reorganization of the biofilm.

In this work, we study biofilm growth in porous media using microfluidics [6]. The setup consists in a glass/PMDS honeycomb channel network, colonized by *Pseudomonas aeruginosa*, a known biofilm model bacteria [3]. Using microscopy techniques, image analysis and particle tracking velocimetry (PTV), we obtain both the distribution of biomass and the velocity field within the network. This allows us to study the coupling mechanisms between flow and biofilm growth. We further study how this evolves over a range of flow rates. Results show a spatial

distribution of biofilm that is strongly correlated to the flow rate within each channel. We observe that clogging of channels due to biofilm creates preferential flow paths. These paths are unstable with cycles of clogging/declogging due to a competition between growth and flow-induced detachment. Signal analysis of pressure and fluorescence intensity show that these events have a characteristic frequency, and we propose a model taking into account the stress on the biofilm that reproduces these cyclic detachments. Furthermore, we show that bacterial communication (Quorum Sensing) can also play a role in controlling the frequency of detachments.

References

- [1] Y. Bar-On, R. Phillips, R. Milo: The biomass distribution on earth. *PNAS* **115**, 6506-6511 (2017)
- [2] H. Flemming, S. Wuertz: Bacteria and archaea on earth and their abundance in biofilms. *Nat. Rev. Microbiol.* **17**, 247-260 (2019)
- [3] V. Gordon, M. Davis-Fields, K. Kovach, C. Rodesney: Biofilms and mechanics: a review of experimental techniques and findings. *J. Phys. D: Appl. Phys.* **50**, 223002 (2017)
- [4] D. Scheidweiler, H. Peter, P. Pramateftaki, P. de Anna, T.J. Battin: Unraveling the biophysical underpinnings to the success of multispecies biofilms in porous environments. *ISME J* **13**, 1700-1710 (2019)
- [5] C. A. Rolph, R. Villa, B. Jefferson, A. Brookes, A. Choya, G. Icton, F. Hassard: From full-scale biofilters to bioreactors: Engineering biological metaldehyde removal. *Science of the Total Environment* **685**, 410-418 (2019)
- [6] G. Ramos, C. Toulouze, M. Rima, O. Liot, P. Duru, & Y. Davit: Ultraviolet control of bacterial biofilms in microfluidic chips. *Biomicrofluidics*, **17**, 024107 (2023).

Session

Systèmes multiphases - multicomposants

Non-Fickian dispersion in unsaturated porous media, influence of the Peclet number

E. Ollivier-Triquet^{a,b}, Daniela Bauer^a, Benjamin Braconnier^a, Souhail Youssef^a
Laurent Talon^b

^a IFP Energies nouvelles, 1 et 4 avenue de Bois-Préau, 92852 Rueil-Malmaison, France

^b FAST, Université Paris-Saclay, Rue André Rivière
91405 Orsay cedex, France, France

Keywords: Vadose zone, transport, saturation, non-Fickian dispersion, multiphase flow, Peclet, micromodel, Lattice-Boltzmann simulations, Multiple-Point Statistics algorithm.

1 Introduction

Human activity has a significant impact on the vadose zone, an area located below the land surface and above the water tables, only partially saturated with water. The vadose is susceptible to pollution from agricultural or industrial activities, posing a threat to water resources. Plus, saturation levels vary greatly, especially with the increasing frequency of droughts due to climate change. Hence, predicting contaminant transport in unsaturated conditions is crucial. However, the understanding of dispersion in unsaturated porous media remains limited, due to the complex interaction of multiphase non-miscible flows with the porous medium. Traditional models such as the Fickian model, described by the Advection-Diffusion Equation, fail to accurately capture dispersion in unsaturated porous media. The objective is to address the issue of transport in unsaturated porous media by identifying relevant properties at the pore scale to understand dispersion at a larger scale. One of the goals is to determine whether dispersion follows Fickian or non-Fickian behavior, as this understanding is crucial for predicting the spreading of pollutant in the vadose zone. To investigate transport in unsaturated porous media, a dual approach is being employed: pore-scale transport experiments and Lattice Boltzmann simulations. Direct visualization of fluid structure in porous media is challenging. Thus, we use micromodels, transparent interconnected porous networks, to enable optical visualization at the pore scale. First, a micromodel experimental set-up was established and optimized to study multiphase flow and transport. Analysis methods were developed, along with techniques for characterizing dispersion through spatial moment analysis.

A series of experiments were conducted to obtain initial results on multiphase flow and dispersion. The evolution of saturation and phase distributions with the capillary number was characterized. Transport experiments were performed for the entire range of saturations, showing that dispersion increases as saturation decreases. However, analyzing low saturations was challenging due to the significant increase in dispersion and limitations imposed by the micromodel size, preventing the study of long-term dispersion. To overcome this limitation, Lattice Boltzmann simulations were used for flow and transport, as there is no size limitation except for computational time. However, simulating the distribution of two phases after a multiphase flow in a complex porous medium remains challenging. Generating large-scale images of unsaturated porous media based on experimental data was then crucial for observing late-time dispersion. Machine learning techniques, specifically the Multiple Point Statistic algorithm, were employed to generate images of wider unsaturated porous media and a large dataset of smaller images to increase the statistical significance of the study. Flow and transport simulations were conducted using the generated image dataset to explore the influence of saturation on flow and transport. This involved examining flow properties under saturated and unsaturated conditions. The nature of transport, specifically whether it exhibited Fickian or non-Fickian behavior was investigated. Furthermore, the effect of the Peclet number (a measure of the balance between advection and diffusion) on dispersion for different saturation levels was analyzed.

Results

This study revealed that decreasing saturation significantly increases flow heterogeneity, leading to increased dispersion. Notably, the non-Fickian nature of flow tends to be more pronounced with low saturations (Fig. 1). Plus, the transition from Fickian to non-Fickian depends on the Peclet number (Fig.2). There is a competition between advection and diffusion in saturated conditions, resulting in a diffusive Fickian regime for low Peclet numbers. However, transport in unsaturated conditions is mainly advective, even at low Peclet, and thus displays a non-Fickian behavior.

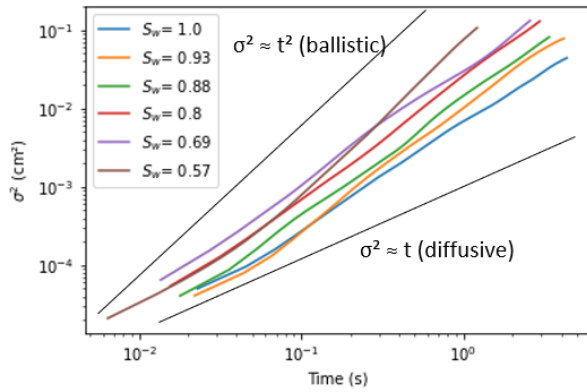


Figure 1: Lattice-Boltzmann transport simulations in 2D unsaturated images. Second moment of the concentration profiles as a function of time for different saturations values ($Pe=100$).

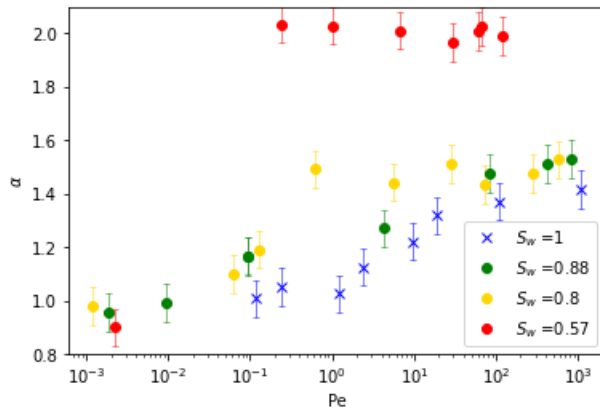


Figure 2 Power law index α of the second moment evolution with time as a function of the Peclet number for different saturations. α is obtained through a power law fit, $\sigma^2 = D_{\text{frac}} t^\alpha$, with D_{frac} a fractional dispersion coefficient. α deviation from 1 indicates the non-Fickian nature of dispersion.

References

- [1] M., Bromly, C., Hinz (2004). Non-Fickian transport in unsaturated repacked sand. Water Ressources, 40(7).
- [2] J., Jimenez-Martinez, A., Alcolea, J., Straubhaar, and P., Renard. (2020) Impact of phases distribution in mixing and reactions in unsaturated porous media. Adv Water Resour, 144:103697.

Fragmentation and coalescence dynamics of non-wetting blobs during immiscible two-phase flows in porous media

L. Talon^a, R. Bouguemari^a, A. Yiotis^b, D. Salin^a

^aUniversité Paris-Saclay, CNRS, FAST, 91405, Orsay, France

^bSchool of Mineral Resources Engineering, Technical University of Crete, 73100 Chania, Greece

Keywords: Two Phase Flow, Blob distribution, Population Balance Equation

We study experimentally the dynamics of non-wetting blobs flowing simultaneously with a wetting fluid in a quasi-two-dimensional porous medium consisting of random obstacles Fig. 1. The blobs continuously merge forming larger ones (coalescence) and breakup into smaller ones (fragmentation) leading to an overall dynamic equilibrium between the two processes (see Fig. 2). We develop a clustering algorithm for the identification of fragmentation and coalescence events that records the size of the blobs prior and immediately after each event from high-resolution videos of the immiscible flow experiments. The results provide significant insight on the main physical features of these two processes, such as blob size distributions, breakup and coalescence frequency as a function of total flow rate, and the size distributions of the blobs formed by either the fragmentation or coalescence of other ones. One of the salient features of the fragmentation process in our study is that blobs smaller than the typical pore size exhibit a higher probability of producing two almost identical children (in size), whereas larger blobs breakup into two children of different sizes. In the latter case, one of children is found to have a dimension practically equal to the typical pore size. Our experimental results are also interpreted in the framework of a mean-field approach, where the dynamics of the blob sizes is expressed through an integro-differential population balance equation (PBE) that comprise terms for the description of the rates of size gains and losses by either fragmentation or coalescence. We recover appropriate expressions for the relevant coalescence and fragmentation kernels, as functions of the blob sizes that participate in each event. A rather surprising result is that for a given blob size population, we obtain an equilibrium between the gains by fragmentation and the losses by coalescence. Furthermore, the opposite is also true, as the population gains by coalescence are found to be equal to the losses by fragmentation.

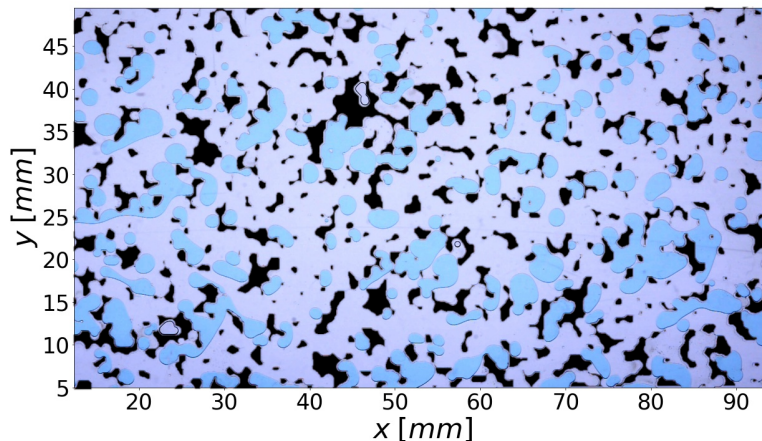


FIGURE 1: Close-up snapshot of a section of the cell during an immiscible flow experiment. The non-wetting blobs are shown in blue, while the wetting phase is totally transparent. While solid obstacles are also transparent, we represent them here in black color.

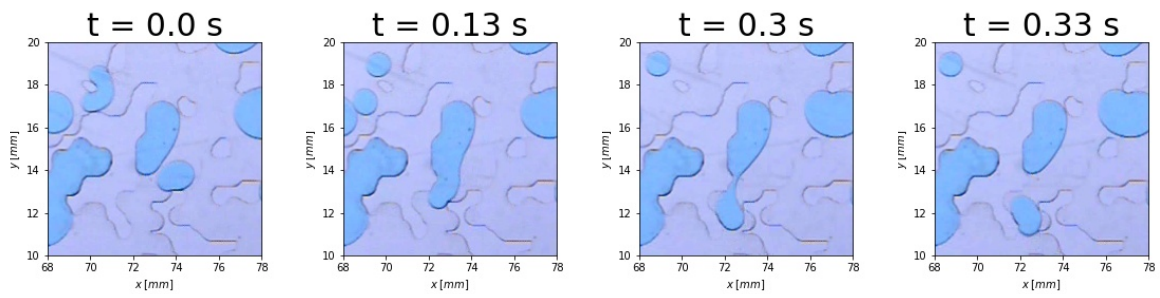


FIGURE 2: Time sequence of a coalescence event (between $t = 0$ and $t = 0.13\text{ s}$) followed by a fragmentation event between $t = 0.3\text{ s}$ and $t = 0.33\text{ s}$

Impact of initial air and subsequent H₂ gas migration in a radioactive waste repository

M. H. Bahlouli (a,b), Z. Saadi (a), R. Ababou (b)

^aIRSN, 31 avenue de la Division Leclerc - 92260 Fontenay-aux-Roses

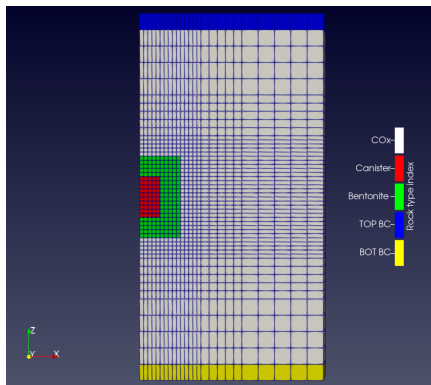
^bInstitut de Mécanique des Fluides de Toulouse, 2 Allée du Professeur C. Soula, 31400 Toulouse

Keywords: Radioactive waste, Two-phase flow, Multi-component transport, TOUGH code

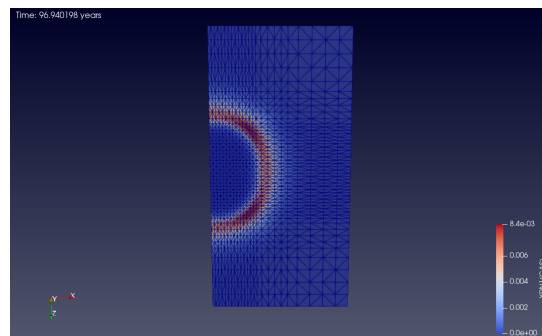
In a geological repository for high-level radioactive waste, corrosion of steel and water radiolysis leads to generation and accumulation of hydrogen gas which may significantly affect long-term safety of the repository. Numerical modeling can be used to predict the hydraulic and hydromechanical evolution of such a disposal facility and to estimate the influence of excavation and generated gas on host clay rock and sealings. While several modelling teams have studied gas migration [1], very few have considered the initial presence of air and its impact on later hydrogen migration. Note that, during excavation, the CO₂ around the tunnels is disturbed, which creates an Excavation Disturbed Zone (EDZ), both hydraulically (rock desaturation) and mechanically (fracturing, redistribution of stresses, natural convergence).

In our study, we have compared results obtained from TOUGH [2] modules (Equations Of States): EOS5 for modeling two-phase flow with only water and hydrogen, and EOS7R for modeling a more complex multi-component two-phase system with water, brine, air, and two radionuclides able to volatilize and dissolve. This EOS7R model is tuned to attribute non-radioactive hydrogen gas properties to the 1st radionuclide (brine and the 2nd radionuclide are turned off). The van Genuchten (1980) relative permeability and capillary pressure functions are used.

The model is then run at the scale of a waste cell: Figure 1a. One challenge is to estimate the peak gas pressure around the cell and check whether it exceeds lithostatic pressure at depth 630m. If that is achieved, the mechanical stability of the engineered system and natural barriers may be affected. The results indicate that hydrogen gas plume migration is impeded by the bentonite seal around the canister. However, the migration of dissolved H₂ away from the container is less impeded, as indicated by Figure 1b. In future, this model will be extended to take into account hydromechanical coupling.



(a) Preliminary axi-symmetric model of CIGEO waste cell: Finite Volumes mesh



(b) EOS7R TOUGH2 simulation: H₂ Mass Fraction XH₂GAS in the Gas mixture ($t = 97$ years)

References

- [1] Talandier, Jean. *Couplex-Gaz Benchmark: Synthesis of results for case 1*. (Workshop Couplex-Gaz, 4 avril 2007).
- [2] Pruess, Karsten, Curtis M. Oldenburg, and G. J. Moridis. *TOUGH2 user's guide version 2. No. LBNL-43134*. Lawrence Berkeley National Lab.(LBNL), Berkeley, CA (United States), 1999.

Impact of initial air and subsequent H₂ gas migration in a radioactive waste repository

M. H. Bahlouli^{a,b}, Z. Saadi^a, R. Ababou^b

^aIRSN, 31 avenue de la Division Leclerc - 92260 Fontenay-aux-Roses

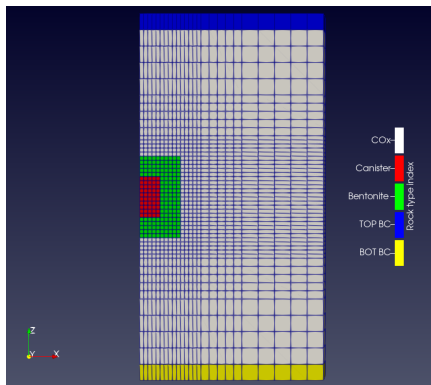
^bInstitut de Mécanique des Fluides de Toulouse, 2 Allée du Professeur C. Soula, 31400 Toulouse

Keywords: Radioactive waste, Two-phase flow, Multi-component transport, TOUGH code

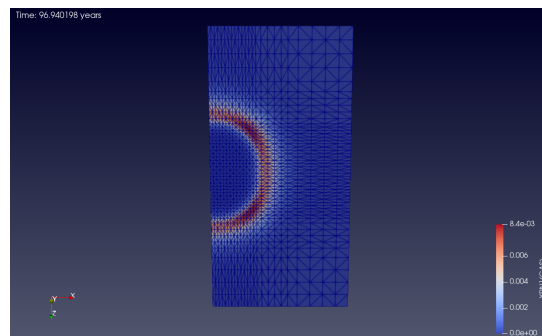
In a geological repository for high-level radioactive waste, corrosion of steel and water radiolysis leads to generation and accumulation of hydrogen gas which may significantly affect long-term safety of the repository. Numerical modeling can be used to predict the hydraulic and hydromechanical evolution of such a disposal facility and to estimate the influence of excavation and generated gas on host clay rock and sealings. While several modelling teams have studied gas migration [1], very few have considered the initial presence of air and its impact on later hydrogen migration. Note that, during excavation, the CO₂ around the tunnels is disturbed, which creates an Excavation Disturbed Zone (EDZ), both hydraulically (rock desaturation) and mechanically (fracturing, redistribution of stresses, natural convergence).

In our study, we have compared results obtained from TOUGH [2] modules (Equations Of States): EOS5 for modeling two-phase flow with only water and hydrogen, and EOS7R for modeling a more complex multi-component two-phase system with water, brine, air, and two radionuclides able to volatilize and dissolve. This EOS7R model is tuned to attribute non-radioactive hydrogen gas properties to the 1st radionuclide (brine and the 2nd radionuclide are turned off). The van Genuchten (1980) relative permeability and capillary pressure functions are used.

The model is then run at the scale of a waste cell: Figure 1a. One challenge is to estimate the peak gas pressure around the cell and check whether it exceeds lithostatic pressure at depth 630m. If that is achieved, the mechanical stability of the engineered system and natural barriers may be affected. The results indicate that hydrogen gas plume migration is impeded by the bentonite seal around the canister. However, the migration of dissolved H₂ away from the container is less impeded, as indicated by Figure 1b. In future, this model will be extended to take into account hydromechanical coupling.



(a) Preliminary axi-symmetric model of CIGEO waste cell: Finite Volumes mesh



(b) EOS7R TOUGH2 simulation: H₂ Mass Fraction XH₂GAS in the Gas mixture ($t = 97$ years)

References

- [1] Talandier, Jean. *Couplex-Gaz Benchmark: Synthesis of results for case 1*. (Workshop Couplex-Gaz, 4 avril 2007).
- [2] Pruess, Karsten, Curtis M. Oldenburg, and G. J. Moridis. *TOUGH2 user's guide version 2*. No. LBNL-43134. Lawrence Berkeley National Lab.(LBNL), Berkeley, CA (United States), 1999.

Gas migration through water-saturated bentonite: laboratory experiments and microstructural analysis

M. Zaidi^{a*}, N. Mokeni^a, M. Dymitrowska^a

^aInstitut de Radioprotection et de Sûreté Nucléaire (IRSN), PSE-ENV/SEDRE/LETIS, Fontenay-aux-Roses, 92260, France

Keywords: Bentonite, Breakthrough pressure, Gas permeability, X-ray Computed Tomography

1 Introduction

France's nuclear waste repository is located 500 meters underground within a Callovo-Oxfordian clay formation, which acts as a natural barrier for containment [1]. The repository is further protected by engineered barriers, such as MX80 bentonite plugs, which are designed to seal the repository [2]. However, due to the expected significant production of hydrogen within the repository, this gaseous phase could modify the flows and mechanical conditions of the rock and bentonite plugs and therefore potentially impact the transport of radionuclides [3]. The aim of this study was to investigate the properties of gas migration in a water-saturated bentonite-based material. For that, laboratory-scale experiments were conducted for gas injection in constant-volume cell filled with saturated MX80. X-ray computed microtomography (x-ray μ CT) was used to analyse the microstructure and identify the preferential pathways for gas migration within the material.

2 Materials and Methods

The experimental setup involved using an X-ray transparent constant volume cell with dimensions of 22.8 mm in diameter and 22.1 mm in height. The cell was filled with MX80 bentonite prepared at a dry density of 1.4 g/cm³ and an initial degree of saturation of 4.37%. The MX80 sample was subjected to long-term hydration under low-pressure conditions. After the hydration stage, nitrogen gas was injected into the (saturated) specimen at controlled pressures ranging from 0.25 to 3 MPa. At regular intervals, the specimen was subjected to X-ray μ CT imaging scans to monitor and observe changes in the microstructure occurring within the specimen over time.

3 Results

Preliminary results of this study indicate that gas breakthrough occurred after 30 days of injection, when the pressure reached 3 MPa. The measured gas permeability was 9.74.10⁻²⁰ m². 3D X-ray μ CT images obtained at the end of gas injection showed the development of a network of porosity and microcracks, allowing the gas the migration of gas within the sample (Figure1).

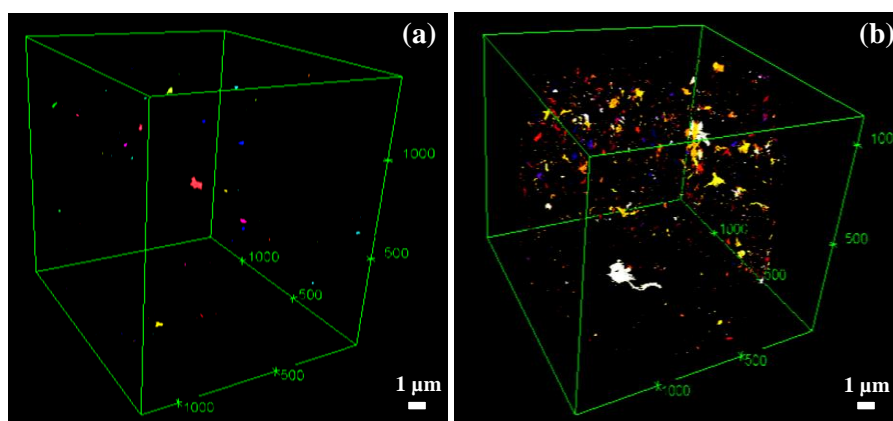


Figure1 : Evolution of the porosity in the MX80. (a) Before gas injection, and (b) after gas breakthrough

References

- [1] Delay, J., Vinsot, A., Krieguer, J.-M., Rebours, H. and Armand, G. Making of the underground scientific experimental programme at the Meuse/Haute-Marne underground research laboratory, northeastern France. *Physics and Chemistry of the Earth*, 32, 2–18 (2007).
- [2] ANDRA. Architecture and management of a geological repository, France (2005).
- [3] Horseman, S. T., Harrington, J. F., & Sellin, P. Gas migration in Mx80 buffer bentonite. *MRS Online Proceedings Library (OPL)*, 465, 1003 (1996).

Surfactant-enhanced remediation of LNAPL contaminated porous medium

D. Kerimbekova^{a,b}, I. Panfilov^a, A. Pereira^a, D. Stemmelen^a, S. Leclerc^a,
G. Kalenov^b, D. Sapobekova^c

^aUniversité de Lorraine, CNRS, LEMTA, F-54000 Nancy, France

^bAl-Farabi Kazakh National University, Almaty, Kazakhstan

^cSatbayev Kazakh National Technical University, Almaty, Kazakhstan

Keywords: LNAPL, porous medium, surfactant-enhanced remediation (SER), magnetic resonance imaging (MRI)

1. Introduction

Currently, the remediation of groundwater from contamination with petroleum products is one of the most important areas of the global water protection. Mainly, it is occurred due to improper disposal of petroleum-containing wastes [1] after the oil processing, leads to a long-term source of groundwater contamination. In accordance with [2], the technology of surfactant-enhanced remediation (SER) is characterized by high efficiency of non-aqueous phase liquid (LNAPL) removal in porous media compared to pump-and-treat method, that because of action of capillary forces can leave a considerable amount of residual petroleum contaminants within aquifers.

In [1] the authors consider the SER technology of contaminated groundwater, as it can lead to damage the tailing and rebound effects occurred due to action of capillary forces. Surfactant is heterogeneous molecule represented as monomer, which consists of hydrophilic (head) and hydrophobic (tail) groups composed of a long chain hydrocarbon [3]. According to [4] solubilization and mobilization are two main mechanisms of surfactants, allowing to enhance the removal of non-aqueous phase liquid (LNAPL) in the porous medium. When increasing the number of surfactants monomers in considered solution, containing two immiscible fluids «LNAPL-Water», system becomes saturated that leads to forming the surfactants micelles, under action of which the solubilization of non-aqueous phase is observed. It should be noted that during surfactant injection to contaminated porous medium the mobilization effect of light non-aqueous phase liquids (LNAPLs) is increased. This effect is occurred due to the decreasing in interfacial tension between two immiscible fluids contributes to reduction of capillary forces, which act to retain significant amount of LNAPLs as ganglia within porous medium of aquifers.

In this paper, the SER process of LNAPL contaminated porous medium is considered using magnetic resonance imaging (MRI). The main objective of this work is carrying out of experimental research of LNAPL displacement in vertical model of porous medium in two ways: by simple water flooding and by surfactant injection to evaluate the impact of surfactant on residual LNAPL removing from contaminated zones.

2. Results and discussions

From Figure 1 it was shown that surfactant-enhanced remediation method after water injection to porous medium in experiment №1 is more effective for residual LNAPL displacement compared to experiment №2 when surfactant water solution was injected at the beginning. In the case of experiment №1, approximately 11% of residual LNAPL from initial residual saturation was displaced. As for experiment №2, SER method is effective at the initial time moment and demonstrates more effects in area of higher saturation of LNAPL.

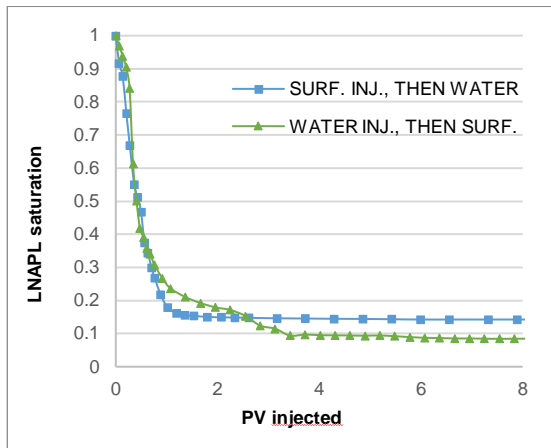


Figure 1: Comparisons of results between two experiments: green curve – experiment №1, blue curve – experiment №2.

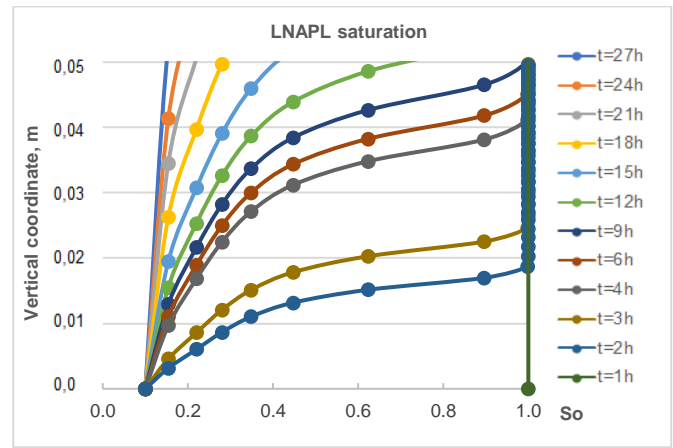


Figure 2: Changes in LNAPL saturation along vertical coordinate.

In experiment №1, at the beginning 100 ml of water solution was flooded to porous media that is corresponded to 3 pore volume (PV). After the end of water flooding 200 ml of surfactant water solution was injected for residual NAPL displacement in porous media. This case is corresponded to green curve from Figure 1. As for experiment №2, at the beginning 180 ml of surfactant water solution was used for immiscible fluid displacement in porous media that is corresponded to blue curve on Figure 1. The injection rate for two experiments was similar and equaled 0.16 ml/min.

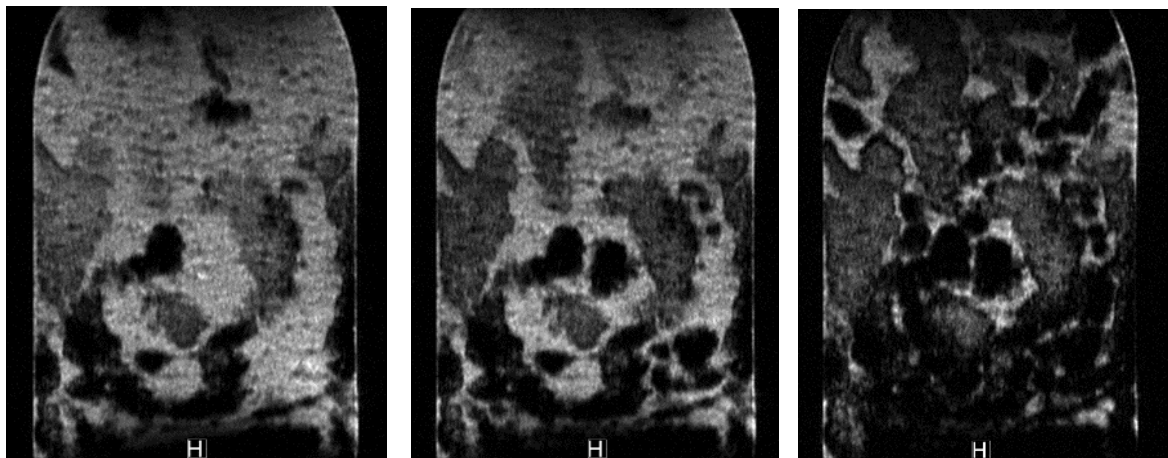


Figure 3: Consecutive MRI images of immiscible phase displacement.

As it was shown on Figure 2 the changes of LNAPL saturation along vertical coordinate approximately similar with changes in saturation of non-wetting phase without acting capillary forces. It is observed, that after surfactant water injection the residual LNAPL saturation decreases due to reducing of interfacial tension between two immiscible phases that leads to decreasing of capillary force value. Thus, experimental observations and compiled numerical model show the effectiveness of SER of LNAPL contaminated porous medium.

Reference

- [1] Liu, J., Wei, K., Xu, Sh., Cui, J., Ma, J., Xiao, X., Xi, B., He, X. Surfactant-enhanced remediation of oil-contaminated soil and groundwater: A review. *Science of the Total Environment*, Vol. 756, p. 1-19 (2021).
- [2] Huo, L., Liu, G., Yang, X., Ahmad, Z., Zhong, H. Surfactant-enhanced aquifer remediation: Mechanisms, influences, limitations and the countermeasures. *Chemosphere*, Vol. 252, p. 1-16 (2020).
- [3] Beshia, A.T., Bekele, D., Naidu, R., Chadalavada, S. Recent advances in surfactant-enhanced In-Situ Chemical Oxidation for the remediation of non-aqueous phase liquid contaminated soils and aquifers. *Environmental Technology and Innovation*, Vol. 9, p. 303-322 (2018).
- [4] Paria, S. Surfactant-enhanced remediation of organic contaminated soil and water. *Advances in Colloid and Interface Science*, Vol. 110, p. 75-95 (2004).

Use of Oil-in-Water Emulsions to achieve Stable Displacement of Soil Pollution

S. Wang^a, A. Rodríguez de Castro^a, A. Ahmadi-Sénichault^a, A. Omari^b

^aI2M, Arts et Métiers Institute of Technology, CNRS, Esplanade des Arts et Métiers, 33405 Talence Cedex, France

^bI2M, Bordeaux-INP, CNRS, Esplanade des Arts et Métiers, 33405 Talence Cedex, France

Keywords: Soil remediation; Emulsion flooding; Porous media; Multiphase flow; Microfluidics.

1 Introduction

Soil pollution is undeniably a global problem that impacts the lives of many people and affects biodiversity [1]. Contamination by non-aqueous phase liquids (NAPLs) is particularly difficult to treat or remove because of their high viscosity and low aqueous solubility [2]. At present, waterflooding is commonly used to obtain in situ remediation of the NAPLs-polluted sites. However, the generation of preferential fluid paths as a consequence of soil heterogeneity leads to low efficiency of this method. Emulsions are colloidal systems of two immiscible liquids, where one liquid is dispersed in the other one, stabilized by emulsifiers such as surfactants, solid particles or polymers [3]. Emulsions develop high viscosity and can be used to enhance the mobility of the pollutant during their flow through micron-sized pores. In the present study, oil-in-water emulsions with high viscosity were used to displace a model pollutant in a microfluidic device, obtaining significant reduction in residual pollutant saturation as compared to water-flooding. Moreover, the emulsions distributed evenly over the whole porous medium. This provided good contact with the pollutant, which is suitable for the prospective use of emulsions as carrier fluids to deliver reagents that reduce pollutant toxicity in soils.

2 Materials and experimental methods

The porous medium was a transparent microfluidic chip having a permeability of 1.73 Darcy. The pores had a size distribution with mean diameter of 157 μm and minimum and maximum value of 10 μm and 940 μm respectively. Monodisperse oil-in-water emulsions with average size of 10 μm and water were used as displacing fluids and light mineral oil was used as model organic pollutant. The fluids were injected with a pressure-controlled pump. An optical microscope equipped with a high-resolution camera was used to monitor the position of all phases in the micromodel. The fluids were dyed with different colours to improve visualization in the microchip. A four-step strategy was devised to emulate real conditions: water saturation, oil drainage, water imbibition and emulsion flooding. Pressure drop in the microchip and flow rate were continuously measured in order to evaluate relative permeabilities of the liquid phases. Images of the phase distribution at the end of each stage were acquired. Post-treatment and analysis of the acquired images was conducted using ImageJ open software, allowing for the quantification of residual pollutant saturation.

The distribution of the different phases in the micromodel after each stage are shown in Figure 1. The residual oil saturation (S_{OR}) after water imbibition experiment was 42% while it was only 15% after emulsion displacement. In addition, the emulsion was evenly distributed throughout the medium and displacement was stable. This is a consequence of the higher dynamic viscosity of the emulsion as compared to light mineral oil, producing favourable displacement conditions. Moreover, the emulsion-water interfacial tension was lower than that the interfacial tension between oil and water. This increased the value of capillary number and resulted in a better mobilization of the pollutant.

3 Conclusions and prospects

Under the present experimental conditions, oil-in-water emulsions proved to be efficient mobility control agents offering a better performance than water for flooding-based remediation. These results must now be extended to other emulsion formulations and boundary conditions. Although the invasion front was homogeneous, some ganglia of trapped pollutants were still present after emulsion injection. Based on the present experiments, the use of stable emulsions as carrier fluids to deliver reagents capable of reducing

the toxicity of the remaining ganglia seems a promising remediation strategy. Indeed, the emulsion was efficiently put in contact with the pollutant throughout the sample, with no unswept zones.

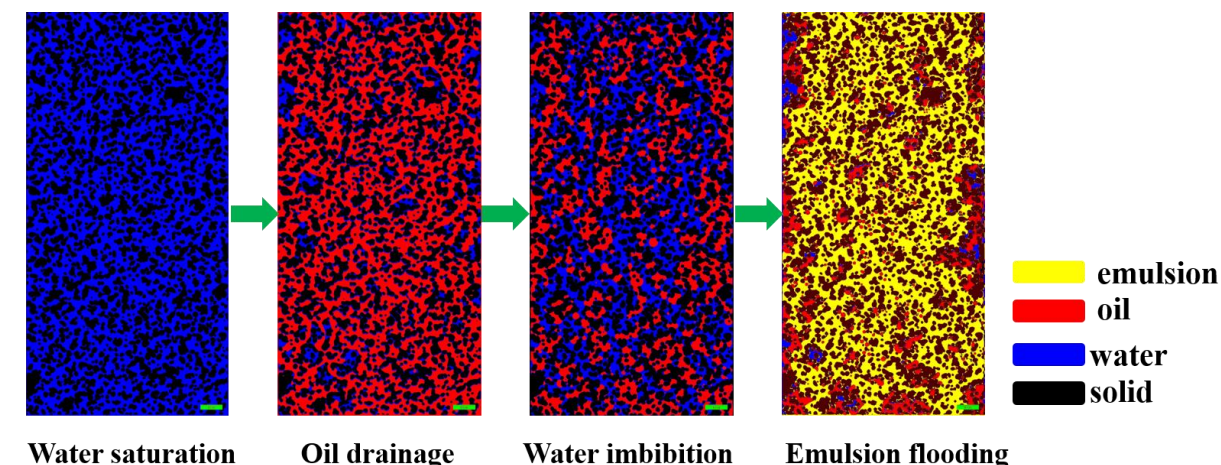


Figure 1: Post-treated images of microchip after water saturation, oil drainage, water imbibition and emulsion flooding experiments, showing the position of the different phases. The scale bar was 1000µm long.

References

- [1] Renji Zheng, Xuezhen Feng, Wensong Zou, Ranhao Wang, Dazhong Yang, Wenfei Wei, Shangying Li, and Hong Chen. Converting loess into zeolite for heavy metal polluted soil remediation based on “soil for soil-remediation” strategy, *Journal of Hazardous Materials*, 412, 125199 (2021).
- [2] Pramod Kumar Pant, Diffusion equations for fluid flow in porous rocks, *SAMRIDDHI: A Journal of Physical Sciences, Engineering and Technology*, 9(01), 05–13 (2017).
- [3] Fernando Leal-Calderon, Véronique Schmitt, and Jerome Bibette, *Emulsion science: basic principles*, 225. Springer Science & Business Media, France (2007).

Imbibition dynamics including corner film flow in a spiral-grooved channel

C. Kankolongo^{a,b}, D. Lasseux^a, M. Prat^c, T. Zaouter^b, F. Ledrappier^d

^a Université de Bordeaux, CNRS, Bordeaux INP, I2M, UMR 5295, F-33400 Talence, France.

^b CEA, DES, ISEC, DPME, SEME, Laboratoire d'Étanchéité, Univ. Montpellier, Marcoule, France.

^c Université de Toulouse, INPT, UPS, IMFT, Avenue Camille Soula, 31400 Toulouse, France.

^d TECHNETHICS Group France, Laboratoire d'Étanchéité Maestral F 26700 Pierrelatte, France.

Keywords: imbibition, corner flow, sealing

1. Introduction

In the field of sealing, mechanical assemblies commonly consist of two flanges made of hard metallic material and a seal made of soft metallic material as shown in figure 1a. These flanges have surface defects due to the manufacturing process, *e.g.*, face-turning, which produces a characteristic spiral-grooved profile as shown in figure 1b. The residual opening defects thus constitute leak paths for the fluid to be sealed and the modeling of fluid flow in the resulting connected aperture field between the high and low pressure zones is essential in order to predict seal efficiency. To help understand the flow

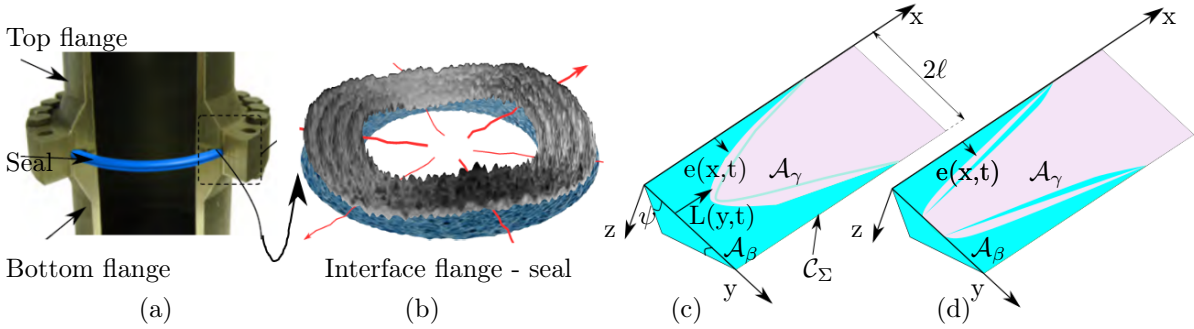


FIGURE 1: Flange - seal interface.

within the connected channels, in particular under two-phase flow conditions, (*i.e.*, when the fluid to be sealed invades the contact initially saturated by air), it is of interest to analyze the case of a rather simple situation made of single spiral-grooved channel, taking into account the presence of sharp corners as shown in figure 1c. In this context, liquid films can develop in the corners of the channel in the case of imbibition, as studied in [1, 2]. Indeed, the presence of the corner films may significantly modify the overall imbibition kinetic and can explain, for instance, capillary instabilities leading to gas trapping. For instance, Dong and Chatzis [3] studied the imbibition of a wetting liquid film in the corner without liquid invasion in the whole channel as shown in figure 1d. By making use of similarity solutions, they showed that the extension of the liquid film and the leak volume in the corner of a rectilinear channel of square cross-section are proportional to the square root of time when flow is triggered by the capillary pressure. Amyot [2] made a similar study in a rectilinear channel of triangular cross-section (figure 1d) with a flow rate imposed at the channel inlet. In accordance with experimental observations, it was shown that the dynamics of the central meniscus is disturbed by that of the liquid film in the corner. The present work reports on analytical solutions for the dynamics of the central meniscus, including that of the liquid film in the corners of a spiral-grooved channel, complementing the analysis reported in the latter reference.

2. Model

The interest is focused on imbibition of a liquid (the β -phase) in a spiral-grooved channel of triangular cross-section as schematized in figure 1c, initially saturated by a gas (the γ -phase). It is assumed that

$\tan \psi \ll 1$ and the gas phase remains at constant pressure. Under these assumptions and on the basis of the lubrication theory, the Reynolds' equations describing mass and momentum conservation for the β -region occupying the region \mathcal{A}_β , are given by

$$\frac{\partial q_{\beta i}}{\partial x_i} = 0, \quad q_{\beta i} = -\rho_\beta \frac{h(y)^3}{12\mu_\beta} \frac{\partial p_\beta}{\partial x_i}, \quad i = 1, 2, \quad (1)$$

In addition, assuming that the capillary number is small enough ($Ca = \mu_\beta u / \sigma < \tan \psi$, u being a characteristic velocity in the β -phase), the boundary condition at the fluid-fluid interface can be shown to reduce to the Young-Laplace relationship

$$p_\gamma - p_\beta = \sigma \kappa, \quad \text{at } x = L(y, t). \quad (2)$$

In these equations, q_β is the lineic mass flow-rate, p_β and p_γ are the liquid and gas pressure, respectively, ρ_β is the liquid density, μ_β is the liquid dynamic viscosity, $h(y)$ is the aperture, κ is the double mean curvature and σ is the surface tension. For completeness, the kinematic condition at the fluid-fluid interface parametrized by $y = e(x, t)$ must be considered, *i.e.* $\frac{\partial e}{\partial t} + \frac{q_{\beta x}(e)}{\rho_\beta h(e)} \frac{\partial e}{\partial x} - \frac{q_{\beta y}(e)}{\rho_\beta h(e)} = 0$.

By integration of the above equations, considering an imposed volume flow rate, Q_0 , at the channel inlet, the expression of the liquid film extension as a function of time, $L_f(t)$, can be obtained, as in [2], by making use of similarity solutions. It is given by

$$L_f(t) = \left(\frac{5}{12}\right)^{1/5} \tan(\psi)^{1/5} Q_0^{1/5} \left(\frac{\sigma \cos \theta_e}{\mu_\beta}\right)^{2/5} t^{3/5}. \quad (3)$$

A more detailed solution can be derived, that reads

$$L_f(t) = \left(\frac{5}{6}\right)^{1/5} \left(\frac{\cos^2(\theta_e + \psi/2) \cos^2(\psi/2)}{A}\right)^{1/5} Q_0^{1/5} \left(\frac{\sigma \cos \theta_e}{\mu_\beta}\right)^{2/5} t^{3/5}. \quad (4)$$

In equations (3) and (4), θ_e is the equilibrium contact angle and A is a constant which depends of ψ and θ_e .

The evolution of the liquid film extension, $L_f(t)$, is reported in Figure 2a according to the two solutions given in equations (3) (ST) and (4) (SA) using values of the different parameters given in [2]. Note that the two solutions are very close to each other. This is confirmed by the ratio, $R_{ST/SA}$, of the two expressions given in equations (3) and (4), represented in Figure 2, which remains close to unity for an angle of the corner, ψ such that $\tan \psi < 0.5$.

Coupling between the dynamics of the liquid film flow in the corner and that of the central meniscus ($L(y, t)$ in figure 1c) will be further discussed in our presentation.

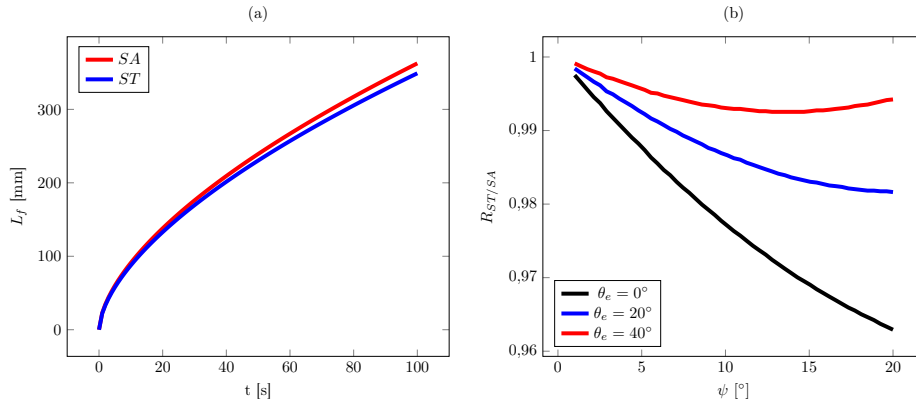


FIGURE 2: (a) Evolution of the film extension for an imposed volume flow rate; (b) Ratio of liquid film extensions as a function of ψ .

Références

- [1] Dong, M. and Chatzis, I., The Imbibition and flow of a wetting liquid along the corners of a square capillary tube, *Journal of Colloid and Interface Science*, 172, 278–288 (1995).
- [2] Amyot, O., Contribution à l'étude des écoulements diphasiques à travers un contact rugueux, *Thèse de doctorat de l'Université de Poitiers* (2004).

Pollutant transport in shallow aquifers

C. Bourel^a, J. Carrayrou^b, C. Rosier^a, R. Awada^a

^aLMPA, Université du Littoral Côte d'Opale, France.

^bMIA, Université de La Rochelle, France.

Keywords: Fluid flow modeling, Saturated and unsaturated porous media, Numerical simulations, Asymptotic analysis, Vertical Richards equations, Dupuit Hypothesis

1. Presentation of the models

We present two new efficient models to describe water flow in shallow aquifers (see [3], [2]). The aim is to provide alternatives to the classical 3d-Richards model, which is known to be very difficult to handle numerically, especially in the considered situation of a large geometry and over long time periods. To avoid these difficulties, we exploit the shallow geometry of the aquifer. These models are tuned to have exactly the same (dominant) behavior as the 3d-Richards model when the ratio $\varepsilon = \text{thickness over longitudinal length of the aquifer}$ is small. Thanks to a formal asymptotic analysis when $\varepsilon \rightarrow 0$, these dominant components of the flow have been obtained in several time scales :

- **Fast component of the flow.** This component of the flow is dominant on a small time scale. It is described by a collection of vertical 1d-Richards problems parameterized by the horizontal position ;
- **Slow component of the flow.** This component of the flow corresponds to a large time scale, where the vertical flow appears instantaneous. The corresponding evolution of the hydraulic head is independent of the vertical variable and becomes a 2d-horizontal problem (corresponding to the so-called Dupuit hypothesis).

The new models are obtained by mimicking and coupling these two particular behaviors.

1.1. A first model : splitting the domain

The strategy is to introduce an artificial interface $l = l(t, x)$ between the two different types of flow (possibly depending on the other unknowns of the problem). Model 1 consists in finding the pressure head $P = P(t, x, z)$ and an auxiliary hydraulic head $\tilde{H} = \tilde{H}(t, x)$ such that :

Flow in the upper part of the aquifer. In this part, only the fast component of the flow is described. We choose a collection of 1D-Richards equations parameterized by $x \in \Omega_x$:

$$\begin{cases} \frac{\partial s(P)}{\partial t} + \frac{\partial u_3}{\partial z} = 0, & u = -k(P) \frac{\partial H}{\partial z} e_3, & \text{for } l < z < h_{\text{soil}}, \\ \alpha(P, u \cdot n) = 0 & & \text{for } z = h_{\text{soil}}, & P = \tilde{H} - l & \text{for } z = l, \end{cases} \quad (1)$$

where u is the flow velocity, $H := P + z$ is the hydraulic head, $s(P)$ is the soil saturation, $k(P)$ is soil conductivity, e_3 is the unit vector in the vertical direction and α a given function describing the boundary condition at the top of the aquifer.

Flow in the lower part of the aquifer. In the lower part of the aquifer, below the level $z = l(t, x)$, the vertical flow is assumed to be instantaneous. The corresponding hydraulic head \tilde{H} is constant with respect to z . We have, for $\tilde{k}(\tilde{H})$ being an averaged conductivity tensor,

$$\begin{cases} P(t, x, z) = (\tilde{H}(t, x) - z) & \text{for } h_{\text{bot}} < z < l, \\ \int_{h_{\text{bot}}}^{h_{\text{soil}}} \frac{\partial s(P)}{\partial t} dz - \text{div}_x (\tilde{k}(\tilde{H}) \nabla_x \tilde{H}) = 0. \end{cases} \quad (2)$$

We obtain a new class of models, parameterized by the interface l (under the constraint $h_{\text{bot}} \leq l < h_{\text{bot}}$). Roughly speaking, this type of model can be seen as the coupling of 1d-vertical Richard models with a 2d-horizontal flow under the classical Dupuit hypothesis (first equation of (2)). The same kind of models can be found in [1] and [4] in a situation of a water table remaining far from the ground level (and treated from a numerical point of view).

1.2. A second model : splitting the velocity

The principle is to impose the effective behaviors described above not on different parts of the domain, as in [3], but on each direction (horizontal and vertical) of the velocity field, in the entire domain. We introduce $l = l(t, x)$ the saturated/unsaturated interface of the aquifer. Model 2 consists in finding the pressure P such that :

$$\frac{\partial s(P)}{\partial t} + \text{div } v = 0, \quad v = w + u e_3, \quad P = H + z, \quad (3)$$

$$u = -k(P) \frac{\partial H}{\partial z}, \quad w := -k(Q) \nabla \tilde{H}, \quad Q(t, x, z) = l(t, x) - z, \quad \tilde{H} = \int_{h_{\text{bot}}}^l H. \quad (4)$$

Horizontal component of the velocity w . It mimics the *slow* effective behavior. It is associated with an auxiliary hydraulic head \tilde{H} (average of the physical hydraulic head H) which is constant with respect to the vertical variable. The explicit dependence on the vertical variable is based on the auxiliary pressure Q so that w is constant in the water table and is small in the upper part (above l).

Vertical component of the velocity u . It mimics the *fast* effective behavior. The first equation of (3), written as $\frac{\partial s(P)}{\partial t} + \text{div } u = -\text{div } w$, roughly corresponds to a 1d-Richards problem on each vertical column associated with the source term $(-\text{div } w)$ which accounts for the amount of water flowing horizontally into or out of each of these columns. As w is small in the upper part, we recover in particular a 1d-vertical flow.

2. Conclusion

Models 1 and 2 are good approximations of the original 3d-Richards model in shallow aquifers. In particular, it is formally proved that they admit the same effective problems on any time scale when the ratio ε introduced above is small.

Moreover, even in aquifers that are not infinitely shallow, the models 1 and 2 approximate the flow well. They accurately describe the infiltration between the soil surface and the water table. This is crucial when studying the transport of chemical constituents in the aquifer, especially since many chemical reactions are expected in the first meters of the subsurface, where oxygen is still very present.

Model 1 is tunable thanks to the choice of l . Model 2 is even better because it approximates the velocity field very well and avoids the drawback of model 1 where the velocity jumps from purely vertical to purely horizontal at the interface l .

From a numerical point of view both models can be solved using a scheme that alternately solves a 2d problem and a collection of 1d-vertical problems. The computational cost is greatly reduced compared to solving the 3d-Richards problem directly.

Références

- [1] MB Abbott, JC Bathurst, JA Cunge, PE O'connell, and J Rasmussen. An introduction to the european hydrological system - systeme hydrologique europeen,"SHE", 2 : Structure of a physically-based, distributed modelling system. *Journal of Hydrology*, 87(1) :61–77, 1986.
- [2] Christophe Bourel. Shallow aquifers without dupuit hypothesis. *Submitted*, 2023.
- [3] Christophe Bourel, Catherine Choquet, Carole Rosier, and Munkhgerel Tsegmid. Modeling of shallow aquifers in interaction with overland water. *Appl. Math. Model.*, 81 :727–751, 2020.
- [4] Mary F Pikul, Robert L Street, and Irwin Remson. A numerical model based on coupled one-dimensional Richards and Boussinesq equations. *Water Resources Research*, 10(2) :295–302, 1974.

Hydrodynamic dispersion in porous media enhances reaction in spherical fronts

Pratyaksh Karan^{1,a}, Uddipta Ghosh^{2,b}, Yves Méheust^{1,c} and Tanguy Le Borgne^{1,d}

¹Geosciences Rennes, UMR 6118, CNRS, Université de Rennes 1, Rennes, 35042, France

²Department of Mechanical Engineering, IIT Gandhinagar, 382055, Gujarat, India

Keywords: Reaction Front, Spherical Injection, Remediation

1 Introduction

Reaction fronts, characterized as the region in which two miscible fluids, one of which displaces the other one, react with each other, are typically sustained by fluid mixing and play a central role in a large range of porous media systems and applications [1,2], an important example being remediation of aquifers by injecting biological entities (microbes) that consume the contaminant by reacting with it to form a less-toxic or potentially neutral product [3]. In many cases, point-wise continuous injection of a reactant that displaces a resident reactant in three dimensions leads to a growing spherical reaction front. While such configurations have until now been studied under the assumption of a constant diffusion coefficient, in porous media the dominant diffusive process at the continuum scale is hydrodynamic dispersion, which depends linearly on the flow velocity.

2 Physical Description

Hydrodynamic dispersion is the Darcy scale manifestation of the interaction between molecular diffusion and advection by the heterogeneous pore scale velocity field. The Dispersion coefficient is expressed by a second rank tensor that is customarily taken to be a linear function of the local discharge rate [4]. In most practical cases, it dominates pure molecular diffusion by several orders of magnitude. Due to its dependence on the local Darcy velocity, hydrodynamic dispersion may strongly influence the dynamics of reactive fronts, and thus significantly alter the local and global reaction rates. However, its effect on spherical reaction fronts is so far unknown.

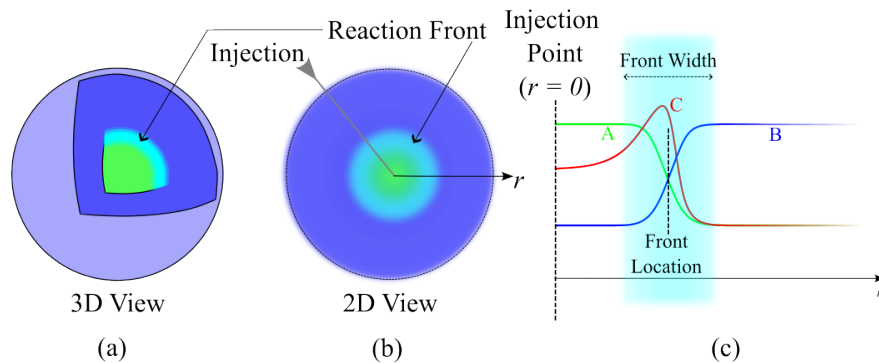


FIG. 1. Illustrative representations of the spherical reaction front; the plot cartoon in panel c demonstrates a typical reaction front and the typical radial concentration profiles for the reactants (A and B) and the product (C) in the front's vicinity.

Here, we analyze the impact of this non-uniform and time-varying hydrodynamic dispersion on reactive transport occurring in such a spherically-advected reaction front under point injection and at constant flow rate. This physical setup is illustrated in Fig. 1. We develop a mathematical framework considering the Advection-Dispersion-Reaction Equation (ADRE) and an irreversible bimolecular $A+B \rightarrow C$ reaction, the reactant A being continually injected at a point into a porous medium that is initially saturated with the species B. To unveil the essential physics of the impact of hydrodynamic dispersion on the dynamics of the reaction fronts and in order to maintain focus on the exclusive contributions of hydrodynamic dispersion, the medium's permeability is assumed to be uniform. We carry out numerical simulations and derive new asymptotic analytical solutions, which show good agreement with the numerical results.

3 Results

At early and intermediate times, hydrodynamic dispersion qualitatively alters the transient front properties (front location, width and global reaction rate). During this initial transient regime, dispersion leads to a

more advanced reaction front and a larger global reaction rate than when molecular diffusion is the only mixing process apart from advection, as well as to different temporal scalings for the reaction front properties. On the other hand, at sufficiently large times, the reaction front reaches a steady state, characterized by a static position and time-independent reactant concentrations and reaction rate, regardless of the presence and strength of dispersion. When dispersion is weak, the steady state front is positioned in a region where dispersion is negligible compared to diffusion. Conversely, when dispersion is large, the steady state front is positioned in the transition zone where dispersion and diffusion are comparable. In this second scenario, hydrodynamic dispersion permanently affects the reaction front's transport by altering the steady state itself and augmenting the global reaction rate. We establish the quantitative threshold strength of dispersion for this second scenario to exist, which is found to depend on the flow characteristics.

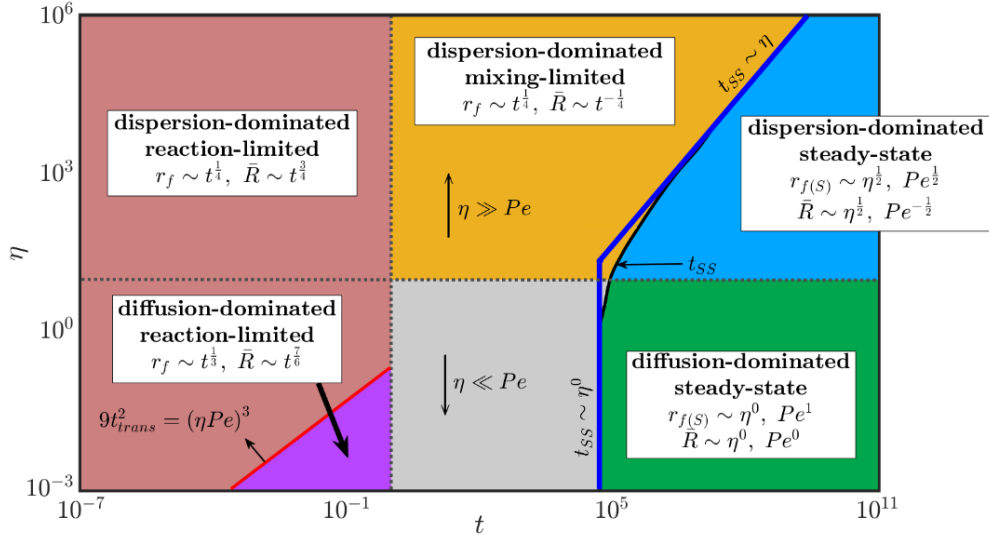


FIG. 2. Phase diagram for the reactive transport regimes of spherically-advected reaction fronts for $Pe = 10$, as a function of time and η .

The different regimes that are recovered for a spherical reaction front are summarized in the regime diagram of Fig. 2. The variables r_f and \bar{R} represent the front's radial location and the global reaction rate (i.e. the pointwise reaction rate integrated over the entire volume) respectively, whereas t is time, all three variables being dimensionless (the non-dimensionalization scheme is presented in tab. 1). The parameters Pe and η represent the Péclet number (corresponding to the typical ratio of the strength of advection to that of molecular diffusion) and the normalized dispersion length. As a consequence, the factor ηPe quantifies the overall strength of dispersion. Evidently, for a strong enough dispersion, apart from the early time front location and reaction rate scaling being different from a dispersion-free scenario, the steady state is reached at a comparatively later time and exhibits a different scaling in terms of η and Pe , and indeed exhibits a larger magnitude for both the front's radial location and the global reaction rate.

Variable	Characteristic Scale	Remarks
Concentration (c_c)	c_0	Injection concentration of species A (same as ambient concentration of B)
Time (t_c)	$(k_R c_0)^{-1}$	Reaction time scale
Coordinate length (r_c)	$((Q_0/\phi_0)/(k_R c_0))^{1/3}$	Volume flow rate is $4\pi Q_0$
Velocity (v_c)	$(Q_0/\phi_0)/r_c^2$	$Pe = \frac{r_c^2/D_M}{r_c/v_c} = \frac{(Q_0/\phi_0)}{r_c D_M} \quad \eta = \frac{\ell_L}{r_c}$
Hydraulic head (h_c)	Q_0/Kr_c	

TAB. 1. Characteristic scales of relevant variables.

References

- [1] M. Dentz, T. Le Borgne, A. Englert, and B. Bijeljic. *J. Contam. Hydrol.* **120**, 1 (2011).
- [2] A. J. Valocchi, D. Bolster, and C. J. Werth. *Transp. Porous Media* **130**, 157 (2019).
- [3] S. Canak, L. Berezljjev, K. Borojevic, J. Asotic, S. Ketin. *Fresen. Environ. Bull.* **1(28)**, 3056-64 (2019).
- [4] Bear J. *Modeling phenomena of flow and transport in porous media*. Springer (2018).

Analysis of the surface/subsurface coupled evaporation for an energetic system

T.Doury^{a,b}, P. Horgue^a, R.Guibert^a, G.Debenest^a

^aIMFT, Allée Camille Soula, Université de Toulouse, INPT, UPS - 31400 Toulouse, France

^bCarneau Energies et Ressources Développements, 22 chemin de la Passerelle - 31770, Colomiers, France

Keywords: Multiphase flow, Porous Media, Evaporation, Drying

1 Introduction

Dealing with environmental flows may lead to major challenges in geosciences such as the coupling of porous medium and free flows to analyze the influence between them.

To simulate this configuration, one should develop a complete description of the flow in both domains in order to be accurate on the drying process quantification. As a first step, we focus on the modeling of all the phenomena involved in the porous medium. The numerical model is developed from an implicit pressure/ explicit saturation [4] open-source code based on the OpenFOAM software.

2 Mathematical and Numerical model

The multiphase flow in porous media is usually modeled using the generalized Darcy's law system of equations. When drying occurs, it is necessary to consider the evaporation and handle it correctly in the momentum equation by implementing a new term to the existing set of equations. Contrary to the initial model in which saturation is solved considering water in the wetting phase only the saturation equation is modified based on an existing Darcy generalized model [1]. The component mass transfer in the non-wetting phase is considered, allowing water transfer from a phase to another following the variation of water mass fraction in the non-wetting phase and its diffusivity under those conditions.

To drive this mass transfer process and challenge our new set of equation, we use a boundary condition based on an evaporation rate [3] dependant on user determined parameters of a non-simulated free flow at the interface with porous medium.

3 Results

To validate our new model, we must confront it to several experimental studies from the literature. The figure (1) shows the comparison between numerical results and an experimental work [4]. On the left, we can see the evolution of the evaporation rate over time for different free flow average velocities and in the right sub-figure the associated total mass evaporated.

It can be seen that a good agreement between experimental and numerical studies is reached for 3 of the 4 velocities (3.5m/s, 2.5m/s and 1.5m/s). All numerical results show the same global tendency of a constant evaporation rate for a few days followed by a sudden decrease and then another level seems to be reached. This evolution appears to be coherent with the observed results in the experimental study. The cumulative evaporation also shows good agreement between numerical and experimental. Nevertheless, for a small free flow velocity ($u=0,75\text{m/s}$), it seems that the initial evaporation rate is lower than expected seeing the experimental study, resulting in a total evaporation significantly smaller. This limitation needs to be furtherly studied.

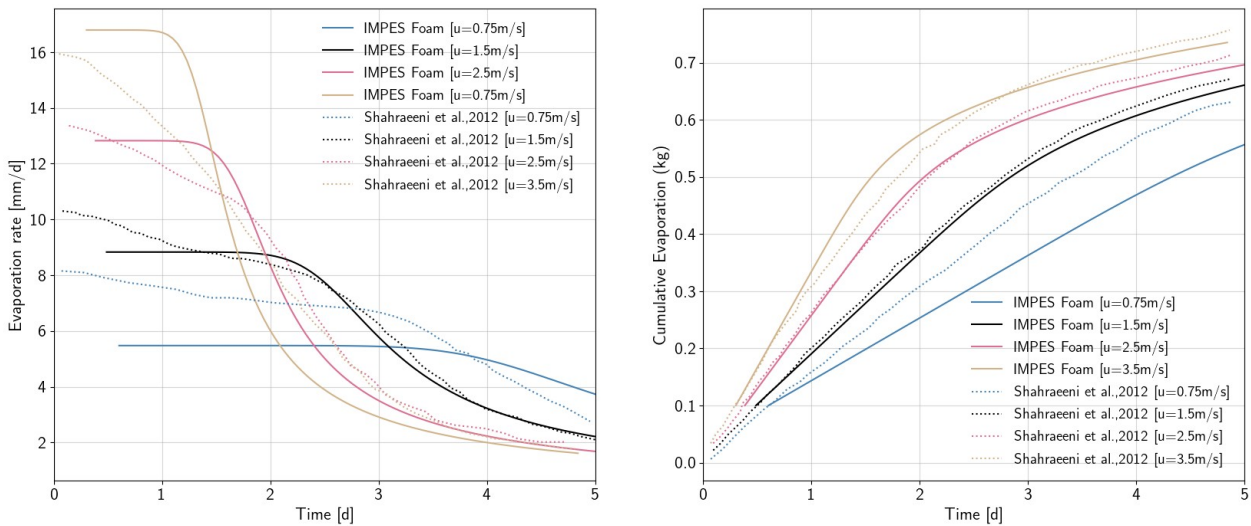


Figure 1: Comparison of numerical and experiment evaporation results.

4 Conclusion

Based on several studies, we find a good agreement between our porous-only modeling approach and experimental litterature. The isothermal model is thus validated and adding the energy equation is the next step to have a full representation and understanding of the phenomena occuring in our case study.

References

- [1] Horgue, P., Soulaire, C., Franc, J., Guibert, R., Debenest, G., (2015), An open-source toolbox for multiphase flow in porous media, *Comput. Phys. Commun.* 187, 217–226
- [2] Mosthaf, K., Helmig, R., and Or, D. (2014), Modeling and analysis of evaporation processes from porous media on the REV scale, *Water Resour. Res.*, 50, 1059–1079
- [3] Smits, K. M., Ngo, V. V., Cihan, A., Sakaki, T., and Illangasekare, T. H. (2012), An evaluation of models of bare soil evaporation formulated with different land surface boundary conditions and assumptions, *Water Resour. Res.*, 48
- [4] Shahraeeni, E., Lehmann, P., and Or, D. (2012), Coupling of evaporative fluxes from drying porous surfaces with air boundary layer: Characteristics of evaporation from discrete pores, *Water Resour. Res.*, 48

Model of water drop infiltration in amphiphilic porous media

F. Cajot^{a,b}, A. Bérard^a, C. Doussan^a, P. Beltrame^b

^aINRAE - UMR1114 EMMAH INRAE-AU - F84000 Avignon - FRANCE

^bAvignon Université - UMR1114 EMMAH INRAE-AU - F84000 Avignon - FRANCE

Keywords: wettability, water transfer, amphiphilic, porous media

Abstract

Under the current climate change, assessing water transfer and infiltration in soil, considered as complex porous medium, is a crucial point for estimating consequences of either heavy rain on runoff or of drought on plant water uptake. In both cases, variations in soil wettability due to amphiphilic materials is an overlooked point, but can greatly affect the infiltration and water transfer, such as water repellency in soil [1, 2, 3]. A macroscopic model of the infiltration of a water drop into a porous medium is developed and applied to a soil containing amphiphilic molecules such as Exopolysaccharides (EPS) found in soil near plant roots [4]. These molecules present a hydrophobic or hydrophilic property depending on the water content in soil. Experiments found in literature [5, 6] or performed in our laboratory show two main behaviors :

i) When the soil is sufficiently moist, imbibition is immediate and rapid as in hydrophilic soils.

ii) In contrast, for a dry soil, the drop does not infiltrate immediately and the subsequent imbibition is slower and depending on the soil hydrophobicity, the drop may never infiltrate.

Models based on Richards Equation [7] in the soil and its variants [8, 9] can only reproduce the rapid infiltration of regime i). We propose here to derive new equations describing the hydrophilic and hydrophobic interactions both in the soil and on the soil surface in contact with the water drop to describe all water infiltration regimes. In place of a contact angle to characterize the wettability of the soil surface, we introduce a free energy term which includes attractive and repulsive interactions, derived from the modeling of drop dynamics on a substrate [10] and include the dependence of the surface wettability on the water saturation in the porous matrix [1]. Concerning the soil, we recently developed a water-dependent hydrophobicity model [11] which has been extended to the case of amphiphilic molecules. In order to reproduce to interactions between water at soil surface and in the soil volume, and to be consistent with thermodynamic principles, we show that it is necessary to add a term inside the porous matrix that depends on both the saturation and the film height at the surface. The resulting equation system is a fourth order PDE system similar to the lubrication model with wettability. To our knowledge, it is the first time that wettability, both in the soil and on the soil surface, is accounted for to represent water infiltration. The numerical simulation of developed coupled equations is in agreement with the experiments of the infiltration of a drop on a thin layer of sand containing EPS. We retrieve the dependence of the Water Drop Penetration Time (WDPT) test with the concentration of amphiphilic molecules and soil moisture. Moreover, we are able to reproduce the two regimes of the infiltration dynamics: instantaneous infiltration and progressive and slow infiltration depending on the initial water saturation of the soil.

References

- [1] Doerr, S. H., Shakesby, R. A., and Walsh, R. P. D., Soil water repellency: its causes, characteristics and hydrogeomorphological significance, *Earth-Science Reviews*, 51(1):33–65 (2000).
- [2] Bens, O., Wahl, N. A., Fischer, H., and Huttli, R. F., Water infiltration and hydraulic conductivity in sandy cambisols: impacts of forest transformation on soil hydrological properties, *EurJ Forest Res*, 126(1):101–109 (2007).
- [3] Orfánus, T., Zvala, A., Ciernikova, M., Stojkovicova, D., Nagy, V., and Dlapa, P., Peculiarities of Infiltration Measurements in Water-Repellent Forest Soil, *Forests*, 12(4):472 (2021).
- [4] Bérard, A., Clavel, T., Le Bourvellec, C., Davoine, A., Le Gall, S., Doussan, C., and Bureau, S., Exopolysaccharides in the rhizosphere: A comparative study of extraction methods. Application to their quantification in Mediterranean soils, *Soil Biology and Biochemistry*, 149:107961 (2020).

FICPM - Rueil-Malmaison, France - October 17-19, 2023.

- [5] Liu, H., Ju, Z., Bachmann, J., Horton, R., and Ren, T., Moisture-Dependent Wettability of Artificial Hydrophobic Soils and Its Relevance for Soil Water Desorption Curves, *Soil Science Society of America Journal*, 76(2):342–349 (2012).
- [6] Hapgood, K. P., Litster, J. D., Biggs, S. R., and Howes, T., Drop Penetration into Porous Powder Beds, *Journal of Colloid and Interface Science*, 253(2):353–366 (2002).
- [7] Richards, L. A., CAPILLARY CONDUCTION OF LIQUIDS THROUGH POROUS MEDIUMS, *Physics*, 1(5):318–333 (1931).
- [8] Beljadid, A., Cueto-Felgueroso, L., and Juanes, R., A continuum model of unstable infiltration in porous media endowed with an entropy function, *Advances in Water Resources*, 144:103684 (2020).
- [9] Landl, M., Phalempin, M., Schluter, S., Vetterlein, D., Vanderborght, J., Kroener, E., and Schnepf, A., Modeling the Impact of Rhizosphere Bulk Density and Mucilage Gradients on Root Water Uptake, *Frontiers in Agronomy*, 3 (2021).
- [10] Thiele, U., Recent advances in and future challenges for mesoscopic hydrodynamic modelling of complex wetting, *Colloids and Surfaces A: Physicochemical and Engineering Aspects*, 553:487–495 (2018).
- [11] Beltrame, P. and Cajot, F., Model of hydrophobic porous media applied to stratified media: Water trapping, intermittent flow and fingering instability, *EPL*, 138(5):53004 (2022).

Analysis of evaporation in a hydrophobic micro-model

M.A.Ben Amara^a, N. Sghaier^a, M. Prat^b

^a *Laboratoire d'Etudes des Systèmes Thermiques et Energétiques de Monastir, Tunisia*

^b *Université de Toulouse, INPT, UPS, IMFT, Avenue Camille Soula, F-31400 Toulouse, France and CNRS, IMFT, F-31400 Toulouse, France*

Keywords: Evaporation pattern, micro-model, drying, image processing.

1 Introduction

Numerous engineering and environmental applications involve evaporation from a porous medium. In the present work, evaporation is studied in a quasi-two-dimensional micro-model composed of spherical hydrophobic beads of 1 mm in diameter sandwiched between two hydrophobic glass plates with the lower plate coated by a polymeric film (RTV). The study is based on two visualization experiments. In the first experiment, the micro-model is held horizontally and filled with a NaCl aqueous solution at 5% in NaCl mass fraction. In the second experiment, the micromodel is vertical and filled with a solution at 25%. The consideration of a saline solution is motivated by the study of salt crystallization induced by the evaporation process. However, the focus here is on the drying pattern prior to the occurrence of crystallization.

2. Results

As illustrated in Fig.1, the micromodel orientation, i.e. vertical or horizontal, leads to two markedly different drying patterns. In the horizontal case, invasion by the air as the result of evaporation occurs preferentially in the central region of the micromodel with a well-defined boundary between the gaseous region and the liquid region. In the vertical case, the pattern is characterized by an almost flat travelling front separating the gas region (on top) from the liquid region.

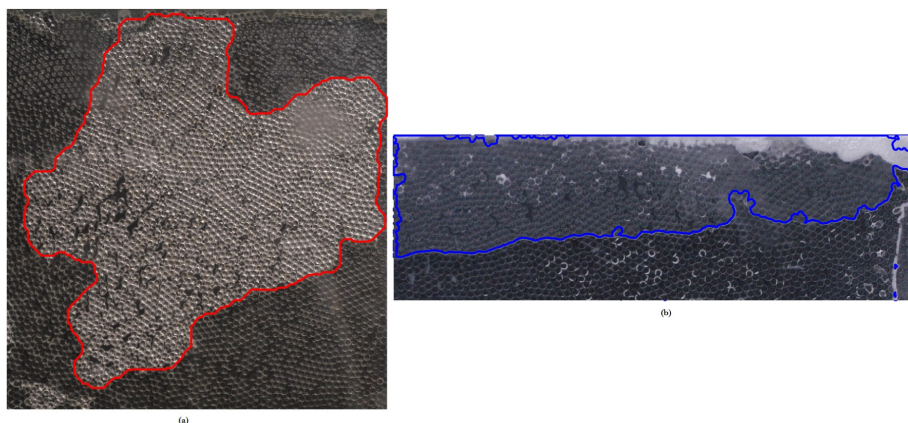


Figure 1: Drying pattern: on the left: horizontal micro-model (gas region in light grey, liquid region in dark grey, the red line corresponds to the boundary between both regions), on the right: vertical micro-model (the blue line corresponds to the boundary between the gas region (lighter grey) and the liquid region (darker grey)).

2 Analysis

The almost flat front in the vertical case is consistent with the expected combined effects of capillarity and gravity in a hydrophobic system. The puzzling pattern is the one observed in the horizontal case. From previous works on drying in hydrophobic systems [1, 2], it is indeed expected that an almost flat travelling front also forms in the horizontal case. In order to explain the observed unexpected pattern, the micromodel is partitioned in eight regions of interest. The porosity, pore body distribution (PSD) and pore

throat distribution (TSD) are determined in each region of interest thanks to image processing techniques based on the identification of the Delaunay and Voronoi diagram from the centres of the beads in the micro-model (Fig.2).

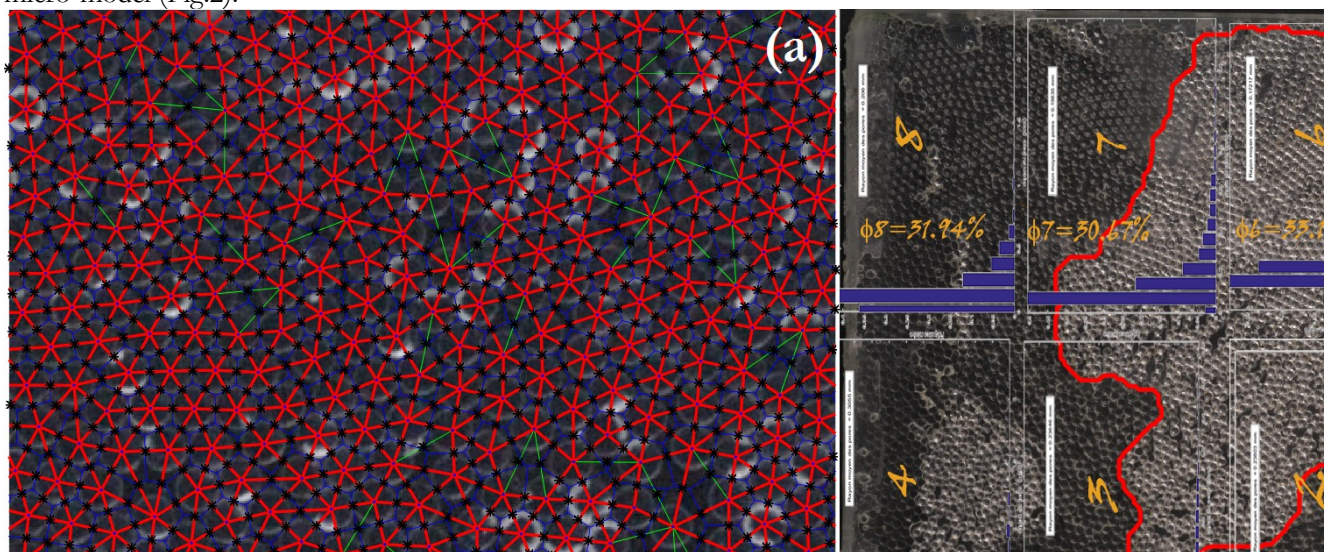


Figure 2: (a) Zoom of Voronoi tessellation (in blue) and Delaunay triangulation (in red) from beads centres in the micromodel. (b) PSD in the eight regions of interest in the micromodel.

3 Conclusion

This investigation leads to the conclusion that the preferential invasion seen in the experiment is due to a different arrangement of the beads in the region preferentially invaded leading to different pore body and throat size distribution compared to the adjacent regions. In other words, a heterogeneity at larger scale than the bead scale disorder is responsible for the observed pattern in the horizontal case. Thus, the present investigation sheds light on the combined effects of hydrophobicity, gravity, capillarity and large scale disorder on evaporation in porous media. This situation is currently further investigated from pore network simulations on a two-dimensional network.

References

- [1] O.Chapuis, M.Prat, Influence of wettability conditions on slow evaporation in two-dimensional porous media, Phys. Rev. E, 75, 046311 (1-11)(2007)
- [2] H.Chraïbi, M.Prat, O.Chapuis, Influence of contact angle on slow evaporation in two dimensional porous media, Phys. Rev. E, 79, 026313 (2009)

Session
Poster

Identification and understanding of colloidal destabilization mechanisms in geothermal processes

I. Raies^{a,b}, E. Kohler^a, M. Fleury^a, B. Ledésert^b

^a IFP Energies nouvelles, 1 et 4 avenue de Bois-Préau, 92852 Rueil-Malmaison, France

^b Laboratoire Géosciences et Environnement Cergy, 1 rue Descartes, 95000 Neuville-sur-Oise, France

Keywords: Geothermal energy, reinjection, clays, colloids, retention, porosity, permeability decline, clogging, characterization, XRD, SEM-EDS, STEM, DLS, NMR, coreflooding experiments.

1 Introduction

In this work, the impact of clay minerals on formation damage of sandstone reservoirs is studied to provide a better understanding of the problem of deep geothermal reservoir permeability reduction due to fine particle dispersion and migration. In some situations, despite the presence of filters in the geothermal loop at the surface, particles smaller than the filter size ($<1 \mu\text{m}$) may surprisingly generate significant permeability reduction affecting in the long term the overall performance of the geothermal system.

2 Results

Type of particles and stability study

Our study is carried out on cores from a Triassic reservoir in the Paris Basin (Feigneux, 60 km Northeast of Paris). Our goal being to first identify the clays responsible for clogging, a mineralogical characterization of these natural samples was carried out by coupling X-Ray Diffraction (XRD), Scanning Electron Microscopy (SEM) and Energy Dispersive X-ray Spectroscopy (EDS). The results show that the studied stratigraphic interval contains mostly illite and chlorite particles (Figure 1). Moreover, the spatial arrangement of the clays in the rocks as well as the morphology and size of the particles suggest that illite is more easily mobilized than chlorite by the flow in the pore network. Thus, based on these results, illite particles were prepared and their aggregation kinetic measured using Dynamic Light Scattering (DLS) technique. Their hydrodynamic radius is around 100 nm. Significant differences are observed with increased salt concentration which accelerates illite aggregation kinetics and promotes interparticle attraction and consequently the formation of larger particles (Figure 2).

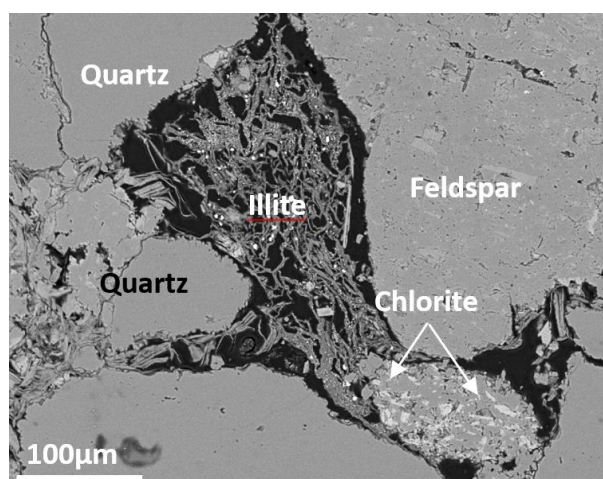


Figure 1: Backscattered Electron SEM image of an example of sites of interest selected due to the presence of likely clayey aggregates.

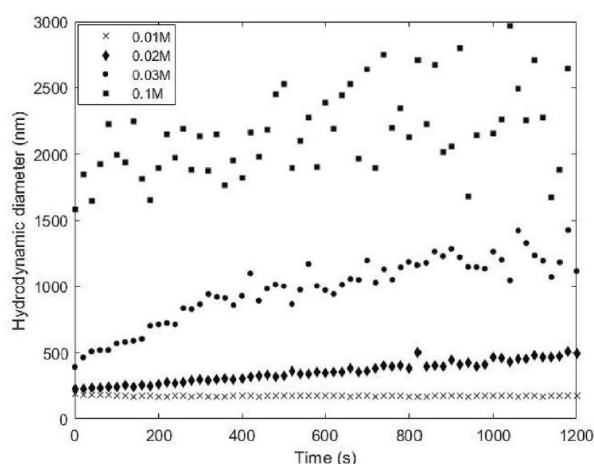


Figure 2: Aggregation kinetic curves for different NaCl concentrations ranging from 0.01 M to 0.1 M. $T = 30 \text{ }^\circ\text{C}$; $\text{pH} = 7.3$; Cillite = 500 ppm

Core flooding experiments.

Core-flooding experiments were carried out using sand columns to mimic the permeability decline due to the injection of illite-containing fluids in sandstone reservoirs. In particular, the effects of ionic strength, temperature, particle concentration and flowrate of the injected fluid were investigated [1]. When the ionic strength increases, a permeability decline of more than a factor of 2 could be observed for pore velocities representative of in-situ conditions (Figure 3). Further details of the retention of particles in the columns were obtained from Magnetic Resonance Imaging and X-ray Tomography techniques [2], showing that the particle deposition is non uniform along the column (Figure 4).

It is clearly shown that very fine particles as small as 100 nm can generate significant permeability reduction under specific conditions in high permeability porous media representative of the Triassic reservoirs of the Paris basin. These retention mechanisms are explained in the general framework of the DLVO theory. More details can be found in references 1 and 2.

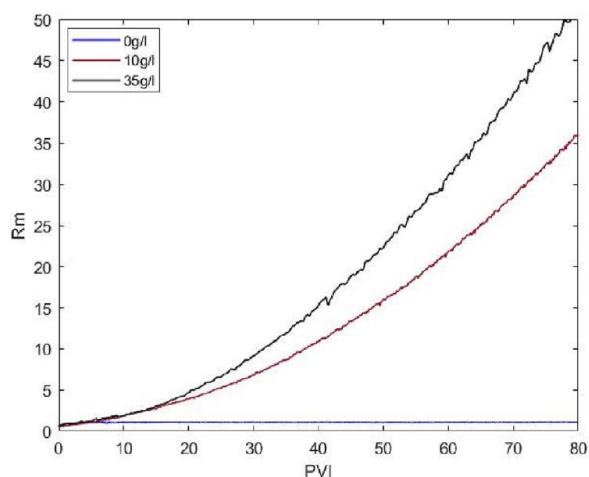


Figure 3: Evolution of mobility reduction factor R_m as a function of the number of pore volumes injected (PVI) for different brine salinities. Increasing salt concentration leads to greater damage due to the formation of large aggregates blocking pore throats.

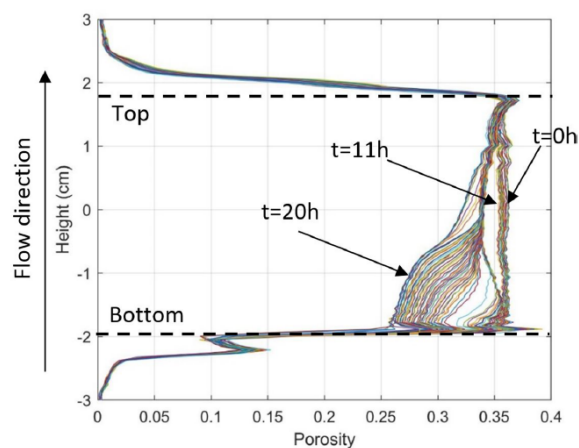


Figure 4: Porosity profiles of the sand column during illite injection showing an initial slight uniform decrease of the porous medium porosity followed by a significant porosity reduction in the cell's inlet reflecting an increasing particle accumulation and blockage.

References

- [1] Raies, I., Kohler, E., Fleury, M., Pédel, N., & Ledésert, B. (2023). Formation damage induced by clay colloids deposition in Triassic clastic geothermal fields: Insights from an experimental approach. *Applied Clay Science*, 234, 106868.
- [2] Raies, I., Fleury, M., Kohler, E., Pédel, N., & Ledésert, B. (2023). Clay-induced permeability decline in sandstone reservoirs: Insights from a coupled NMR-SEM experimental approach. *Geothermics*, 114, 102784.

Understanding Water Transfers in Hygroscopic Fiber Stacks: Bound Water vs Vapor Transport

Yuliang Zou, Benjamin Maillet, Laurent Brochard, Philippe Coussot

Laboratoire Navier (Ecole des Ponts Paris Tech-Univ Gustave Eiffel-CNRS), Champs-sur-Marne, France

Keywords: NMR, MRI, Bound water transfer, Vapor diffusion, Cellulose

Abstract

Cellulose and fibers, as the primary constituents of textiles, paper and bio-based building materials, play a crucial role in our daily lives by influencing the comfort and functionality of clothing and building, as well as paper products due to their hygroscopic nature. In addition, vapor diffusion is commonly believed to drive water transfers. However, the water absorbed (inside the cell walls, forming nanopores between cellulose microfibrils), known as bound water in this study, and which can exchange with vapor via sorption-desorption processes, can account for up to 30% of the dry mass of cellulose fiber, but the diffusion of bound water remains poorly understood. To optimize the design and manufacturing processes of these materials, a comprehensive understanding of water transfers within cellulose is necessary. However, quantitative investigation of this phenomenon is challenging due to the limited availability of simple and effective methods for measuring water distribution within the materials.

This study presents an innovative experimental technique that combines Magnetic Resonance Imaging (MRI) and macroscopic measurements to simultaneously monitor water transfers in cellulose samples with varying porosities. By employing Nuclear Magnetic Resonance (NMR), the bound water diffusion was measured by drying cellulose fibers with a pore network filled with olive oil to prevent vapor diffusion. Surprisingly, our findings indicate a continuous diffusion of bound water through the cellulosic solid skeleton, allowing for the direct measurement of its diffusion coefficient.

Subsequently, specific tests were conducted under controlled boundary conditions (relative humidity) to estimate the vapor diffusion coefficient using macroscopic measurements. The constant mass flux, encompassing both vapor and bound water transfers, was determined once a steady state was reached. By subtracting the bound water diffusion flux from the overall diffusion flux, the vapor diffusion flux and its corresponding diffusion coefficient were obtained.

Furthermore, a simple diffusion model based on the conservation of water-vapor mass was employed to describe the transient water transfer process, incorporating both fluxes. By comparing the model predictions, utilizing the obtained diffusion coefficients, with the saturation profiles measured by MRI at different time intervals, we achieved excellent agreement across a broad range of sample porosities.

This original experimental protocol holds great potential for characterizing fabric properties and offers valuable insights for the textiles and paper manufacturing industries. By mastering the mechanisms of water transfers, advancements can be made in enhancing comfort, energy efficiency, and functional properties of textiles and paper products and bio-based building materials.

References

- [1] Ma, Xiaoyan, et al. Vapor-sorption coupled diffusion in cellulose fiber pile revealed by magnetic resonance imaging, *Physical Review Applied* 17.2 (2022): 024048.
- [2] Zou, Yuliang, et al. Fast diffusion of bound water in cellulose fiber network, *Cellulose* (Under revision).

Water diffusion through hygroscopic cotton layers

Luoyi Yan^{*1}, Benjamin Maillet¹, Rahima Sidi-Boulenouar¹, Yuliang Zou¹, Laurent Brochard¹, and Philippe Coussot¹

¹Navier, École des Ponts ParisTech, Univ Gustave Eiffel, CNRS – Navier, École des Ponts ParisTech, Univ Gustave Eiffel, CNRS – France

Résumé

As a typical biobased material, cotton is globally used for textiles. As a consequence, its hygrothermal behaviour is of vital significance since it can greatly affect the comfort or discomfort they procure due to the resulting wetness or heat loss along the skin. However, our current knowledge of water transfers through such materials is still limited (2). The major problem is the lack of information and proper description of water transport and phase changes inside the porous structure. Measurements remain challenging, in particular considering that the materials are not transparent and different states of water (free water, bound water, vapor) can coexist. The most difficult point is bound water, i.e., water absorbed inside the molecular structure of cell walls, which can hardly be detected with standard microscopy techniques, whereas it can represent a water mass of up to 30% of the dry mass of the material. In this study, cotton fibre stacks are prepared at different porosities (0.2 to 0.9), to identify whether the water can transfer through the fibre network instead of the pores, the sample is filled with oil, only leaving one surface to diffuse (evaporation). Thanks to the NMR (nuclear magnetic resonance), we discover that bound water can diffuse through the fibre network up to the free surface of the sample. Correspondingly, the diffusion coefficient of bound water can be deduced from the water saturation vs time data with the help of a simple diffusion model properly taking into account the boundary conditions. This diffusion coefficient increases with the porosity due to the variation of compression, resulting in a different fiber orientations. In addition to the bound water diffusion, we also give a direct determination of diffusion coefficients of vapor. To achieve this, a series of experiments of steady-state water transport were carried out through the cotton sample. Using the value of the diffusion coefficient of bound water determined as above, combining the boundary conditions under steady state, the fraction of transport due to vapor diffusion coefficient through the fibre stack were deduced. These results allow a full description of water transfers (in the hygroscopic domain) through cotton clothes or insulation materials for construction.

*Intervenant

Ammonia removal with activated carbon/metal oxides nanocomposites

Ali Djellali^{*1}, Juliette Blanchard¹, and Leticia Fernández Velasco²

¹Laboratoire de Réactivité de Surface – Institut de Chimie du CNRS, Sorbonne Université, Centre National de la Recherche Scientifique, Centre National de la Recherche Scientifique : UMR7197 – France

²Ecole Royale Militaire / Koninklijke Militaire School – Belgique

Résumé

One of the main industrial air pollutants is ammonia (NH₃) which damages ecosystems by eutrophication, making them acidic, and contaminating groundwater and soil, it can potentially be harmful for human beings (1). Several methods have been investigated to reduce ammonia emission, but thanks to its high activity at low temperature, low energy consumption and simplicity of use, adsorption garnered much interest (2).

In this work, we will investigate the removal of ammonia using nanocomposites elaborated from activated carbon and titanium oxide nanoparticles AC/TiO₂. To do that, two activated carbons were made from Algerian olive waste through chemical activation. The precursor was dried after being washed with water. It was then crushed and a grain size ranging between 0.3 and 1.0 mm was selected by sieving. For activation, ZnCl₂ and H₃PO₄ are used in two different mass ratios 1:1 and 1:3, respectively. The mixtures were carbonized at 450°C for 1h with a heating rate of 10°C/min. The resulted materials were washed thoroughly with distilled water until neutral pH (3). These two samples, named ACZn and AC3P have specific surface area over 1400 m².g⁻¹. Moreover, AC3P contains a significant fraction of mesopores. AC/TiO₂ nanocomposites with different TiO₂ loadings (1, 5, 10 and 15wt%) were successfully prepared by performing the hydrothermal synthesis of TiO₂ NPs (4) in presence of AC: effective loadings (estimated based on TGA) are close to theoretical values; TiO₂ crystalline phase are not detected (based on XRD), which indicates that the TiO₂ NPs are well dispersed in the AC (including inside the pores).

These samples were tested for NH₃ adsorption by measuring their breakthrough curves for this gas. The results showed that the presence of TiO₂ significantly increased the ammonia uptake in the case of ACZn (17.03 mg/g) sample where it doubled for ACZn-15%TiO₂ (30.49 mg/g). However, it had a slightly negative effect for AC3P (45.30) mg/g sample. Other characterizations will be performed to understand the difference in these two series of samples.

*Intervenant

Microfluidic investigation of the impact of colloidal transport on two-phase flow in geological porous media.

Walid Okaybi*¹

¹Institut des Sciences de la Terre d'Orléans - UMR7327 – Observatoire des Sciences de l'Univers en région Centre, Institut National des Sciences de l'Univers, Université d'Orléans, Centre National de la Recherche Scientifique – France

Résumé

Microfluidic investigation of the impact of colloidal transport on two-phase flow in geological porous media.

Walid OKAYBI, Sophie ROMANI, Cyprien SOULAINÉ

walid.okaybi@cnrs-orleans.fr

¹Institut des Sciences de la Terre d'Orléans, Université d'Orléans/CNRS/BRGM UMR7327, 1A Rue de la Ferrollerie, 45100 Orléans, France

Colloidal particles show potential in facilitating the movement and extraction of trapped contaminants from porous media, which has implications for various energy and water-related applications. To achieve this target, most studies focus on optimizing surface activity of colloidal particles to freely move along the solid matrix with less depositions as possible until they arrive, and bind at the immiscible fluid interface (1). However, few studies focus on how particle depositions (2) and pore-clogging leading to the redirection of local streamlines aid in mobilizing immiscible fluids. In order to assess their impact on the enhanced recovery of trapped contaminants, it is necessary to downscale to the pore scale (order of micrometers). Therefore, an experimental approach using microfluidics combined with CFD simulations has been deployed. These phenomena are directly visualized and tracked using microfluidic devices that mimic the porous structure of rocks. In this study, we will investigate particle depositions, pore-clogging and transport of colloidal particles in both saturated and un-saturated porous medium in microfluidic chips.

We find that during the injection of the suspension in a simplified systems made of a single-grain collector, most particles are deposited mainly in the front part of the grain facing the flow at higher hydrodynamic forces and salt concentrations. However, at lower salt concentrations and Péclet numbers we find more depositions downstream the grain. In complex saturated porous media, we integrate the observed patterns of deposition, the distribution of clogged pores, and the measured variations in flow rate with a digital twin relying on the Darcy-Brinkman-Stokes model. This approach accounts for the actual pore-clogging distribution observed in experiments. It allows us to investigate the variation in the local velocity

*Intervenant

profiles at different stage of the medium clogging, and establish the relationship between $K()$ (permeability) and the experimental conditions. Similar workflow and tools are used in unsaturated condition to find the optimal physical, electrical and hydrodynamic parameters leading to the maximum recovery of trapped contaminants.

References:

Hendraningrat et al. (2013), Schneider et al. (2021).

Ionomer Reconstruction in Three-dimensional Digital Images of Catalyst Layer Microstructure of PEM Fuel Cells

M. Ahmed-Maloum^a, L. Guetaz^b, T. David^b, A. Morin^b, J. Pauchet^b, M. Quintard^a, M. Prat^a

^a*Institut de Mécanique des Fluides de Toulouse (IMFT), Université de Toulouse, CNRS, 31400 Toulouse, France*

^b*Atomic Energy and Alternative Energies Commission (CEA), Laboratory of Innovation on Technologies for new Energies and Nanomaterials (LITEN), University Grenoble Alpes, F-38054 Grenoble, France*

Keywords: Fuel cells, Hydrogen, CCL, FIB-SEM, Ionomer distribution, 3D imaging

1 Introduction

Proton exchange membrane fuel cells (PEMFCs) have emerged as a promising alternative energy source, offering clean and efficient power generation for various applications. A crucial component of PEMFCs is the catalyst layers (CL), where electrochemical reactions take place, converting hydrogen and oxygen into water and electricity. Within the CL, the complex interplay of catalyst, ionomer, and carbon support, governs the overall performance and durability of the fuel cell.

Among these components, the ionomer plays a pivotal role by enabling the transport of protons while simultaneously ensuring the necessary mechanical stability and water management within the CL. Understanding the spatial distribution and behaviour of the ionomer within the CL is of utmost importance for optimizing the fuel cell performance and improving its design.

In this work, we present a numerical approach to reconstruct the ionomer distribution in three dimensional images of the CL microstructure obtained by FIB-SEM imaging.

2 Methodology

The CCL used in this study is a TEC10E50E with high surface area (HSA) carbon from Tanaka. To analyse its structure, 3D FIB-SEM data was collected using a Zeiss Crossbeam 550 microscope. The imaged volume had dimensions of 13.2 μm by 10.95 μm by 5.24 μm , with a spacing of 5 nm between slices and a pixel size of 5 nm, resulting in cubic voxels measuring 5 nm³. The process of segmenting the three-dimensional image into solid voxels and void voxels uses a combination of techniques described in references [1] and [2].

However, the current segmentation procedure does not allow for the separation of the ionomer (I) from the carbon black and platinum (Pt/C). Consequently, a numerical approach that incorporates several algorithms is developed to identify the distribution of the ionomer within the image consistently with high resolution TEM images ([3], [4]). In particular, a local size filtering of the solid phase inclusions, and a coverage model based on the computation of the 3D local curvature of the solid phase are developed to identify the ionomer in two forms: filament ionomer that partially occupies the pore space, and ionomer thin films that coat the platinum-loaded carbon phase.

3 Results

An illustrative example of the computed ionomer distribution is shown in figure.1. The reconstruction leads to an ionomer distribution forming a well-connected percolating network across the thickness of the cathode catalyst layer. The obtained reconstructed images are currently used to compute effective transport properties of the considered CL.

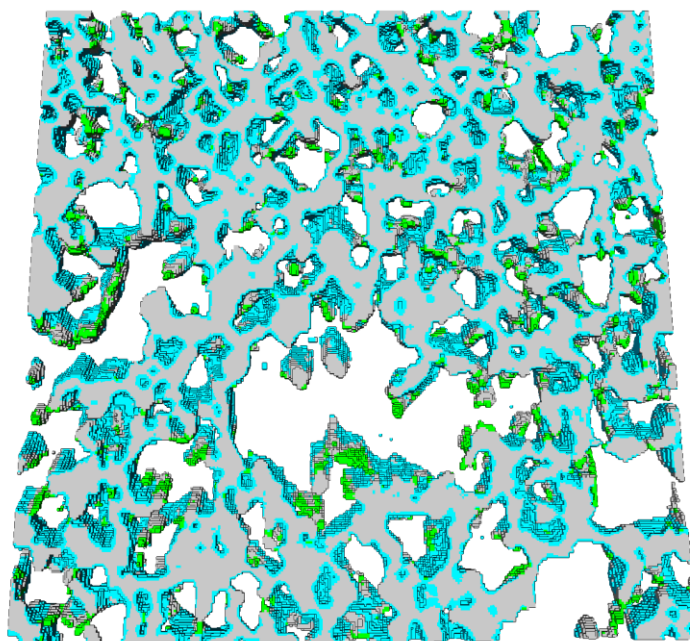


Figure 1: Computed ionomer distribution represented in a 75 nm wide and 1500 nm laterally extended slice of a CCL for a ionomer coverage of 0.82 with the coating ionomer in blue, the filament ionomer in green and the carbon phase in grey.

Acknowledgements: This project has received funding from the Fuel Cells and Hydrogen 2 Joint Undertaking (now Clean Hydrogen Partnership) under Grant Agreement No 875025. This Joint Undertaking receives support from the European Union's Horizon 2020 Research and Innovation program, Hydrogen Europe and Hydrogen Europe Research

References

- [1] M. Ahmed-Maloum et al., Computation of oxygen diffusion properties of the gas diffusion medium-microporous layer assembly from the combination of X-ray microtomography and focused ion beam three three dimensional digital images, *J. of Power Sources* 561, 232735 (2023)
- [2] M. Ahmed-Maloum et al., Reconstruction of ionomer coating in high resolution three-dimensional digital images of catalyst layer microstructure of PEM fuel cells, to be submitted.
- [3] M. Lopez-Haro, T. Printemps et al. Three-dimensional analysis of Nafion layers in fuel cell electrodes. *Nat Commun* 5, 5229 (2014).
- [4] R. Girod et al., Three-dimensional nanoimaging of fuel cell catalyst layers. *Nat Catal* (2023).

Sedimentological control on permeability heterogeneity: case study of the Middle Buntsandstein sandstones, East France

L. Bofill^a, G. Schäfer^a, P. Ackerer^a, G. Bozetti^a, M. Schuster^a, J. Ghienne^a, C. Scherer^b, E. Souza^c, G. Armelenti^b

^a*Institute Terre et Environnement de Strasbourg
Université de Strasbourg, Strasbourg, 67000*

^b*Instituto de Geociencias, Universidade Federal do Rio Grande do Sul, Porto Alegre, Brazil*

^c*Universidade Federal do PAMPA, Caçapava do Sul, Brazil*

Keywords: Sedimentology, permeability, heterogeneity, sandstone

1 Introduction

Sedimentological studies of sandstones provide information about permeability and porosity distribution, as well as variations in geobodies' geometries, which can have a significant impact on predictions of flow models. Sandstone heterogeneities are characterized by the physical processes acting to transport, deposit and bury sediments and are present in all scales [4], from the control of grain size and sorting, sedimentary facies distribution and bedding patterns, up to stratigraphic cycles that affect the reservoir in a regional scale.

The present study focusses on the Middle Buntsandstein sandstones, more specifically on the Lower Grès Vosgien Formation (LGV), which is widely used for geothermal water exploration, groundwater public supply, and more recently recognized as hosting the most promising lithium deposits in Europe [3]. The LGV is dominated by sandstones interpreted as been deposited by fluvial processes, intercalated with aeolian deposits. The scientific objective is to understand to which extent sedimentological and stratigraphic processes generate significant heterogeneities to heat transfer and mass transport models, using outcrops of the Buntsandstein Group at the Vosges mountains as analogues to the Middle Buntsandstein aquifer.

2 Methodology

The study applies a high-resolution sedimentological characterisation coupled with handheld air permeameter data to identify correlations between sedimentary characteristics and permeability response. The sedimentological dataset consists of 260 meters of rock descriptions from twelve different outcrops, along with eleven thin sections for petrographic analysis. The petrographic analysis aims to understand the controlling factors of permeability at a porous scale. Outliers in the permeability data were identified using the IQR method and removed, which resulted in a dataset composed of 1045 measurements linked to sedimentological characteristics. To quantify the correlation between permeability and sedimentology, the rank correlation coefficient Kendall's Tau (τ) is applied [1][2]. Additionally, a digital outcrop model (DOM) generated using an unmanned aerial vehicle (UAV) drone is used to measure the lateral extent of sedimentary facies and bounding surfaces. The DOM serves as a reference to create realistic geocellular models, with the resolution of cell size determined by permeability variograms range.

3 Results

Three facies associations have been recognized: fluvial channel fill, wet aeolian sand sheet and aeolian dune. The results reveal the necessity to differentiate sandstones deposited at the different facies associations, as well as the predominant sedimentary facies within them, in order to generate realistic hydrogeological conceptual models. Permeability contrasts of more than one order of magnitude are present at different scales, including within a single sedimentary facies, between facies and among facies associations (Figure 1). The distribution of these heterogeneities is controlled by the dynamics of the fluvial system, associated with sediments compaction that affected differently the fluvial and the aeolian facies. The rank correlation coefficient (τ) demonstrates a strong correlation between permeability and sedimentary facies. In terms of diagenetic processes, the amount of early eodiagenetic quartz overgrowth controls the

degree of grains compaction, which is the primary factor responsible for macroporosity preservation (Figure 2).

4 Outlook

Further work is underway and is focused on (1) creating 3-D geologic models to represent the distribution of the Buntsandstein permeability heterogeneities and (2) defining the best approaches for using geologic models in flow and transport models. Based on this, targeted simulations using the flow and transport models are planned.

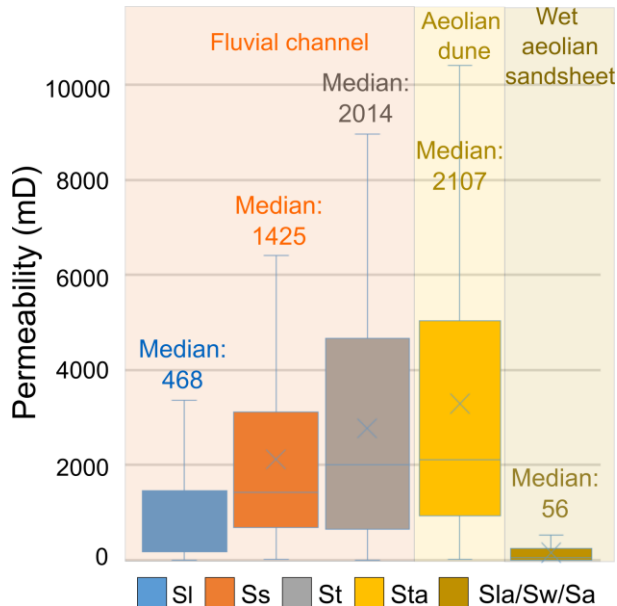


Figure 1 Permeability data related to different facies and facies associations. Sedimentary facies code: Sl, Low-angle cross-bedding; Ss, Sigmoidal cross-bedding; St, Trough cross-bedding; Sta, Aeolian trough cross-bedding; Sla, Aeolian translated strata; Sw, Wa

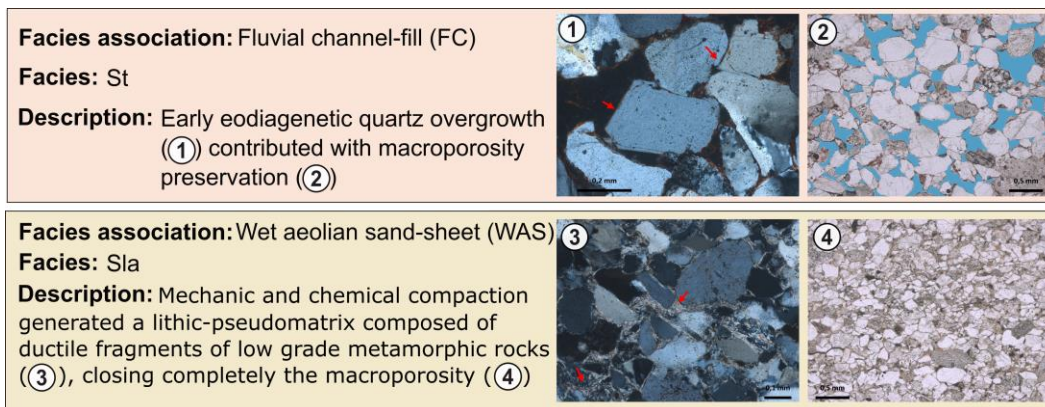


Figure 2 Different petrographic characteristics between facies.

References

- [1] AKOGLU, H., User's guide to correlation coefficients. Turkish Journal of Emergency Medicine, 18, 91-93. (2018)
- [2] KENDALL, M. G., A New Measure of Rank Correlation, Biometrika, 30, 81-93. (1938).
- [3] SANJUAN, B.; GOURCEROL, B.; MILLOT, R.; RETTENMAIER, D.; JEANDEL, E.; ROMBAUT, A., Lithium-rich brines in Europe: An up-date about geochemical characteristics and implications for potential Li resources. Geothermics, 101, 18 p. (2022).
- [4] SHULTZ, M.R.; CRAMER, R.S.; PLANK, C.; LEVINE, H.; EHMAN, D., Best Practices for Environmental Site Management: A Practical Guide for Applying Environmental Sequence Stratigraphy to Improve Conceptual Site Models. *Groundwater Issue*, EPA/600/R-17/293, 18 p. (2017).

Enhancing Remediation of Residual DNAPL in Multilayer Systems: Injection of Alcohol-Surfactant-Polymer Mixtures

Amir Alamooti ^{a,b,c}, Stéfan Colombano ^a, Azita Ahmadi-Sénichault ^b, Fabien Lion ^a, David Cazaux ^d, Cédric Marion ^d, Jérôme Lagron ^d, Dorian Davarzani ^a

^a BRGM (French Geological Survey), Orléans 45000, France

^b Institut de Mécanique et Ingénierie de Bordeaux (I2M), Arts et Métiers Institute of Technology, CNRS, Talence, 33405, France

^c ADEME (Agence de la transition écologique), ANGERS, 49004, France

^d INOVYN, 39500 Tavaux, France

Keywords: DNAPL, biopolymer, alcohol, multilayer, mobilization, solubilization

1 Introduction

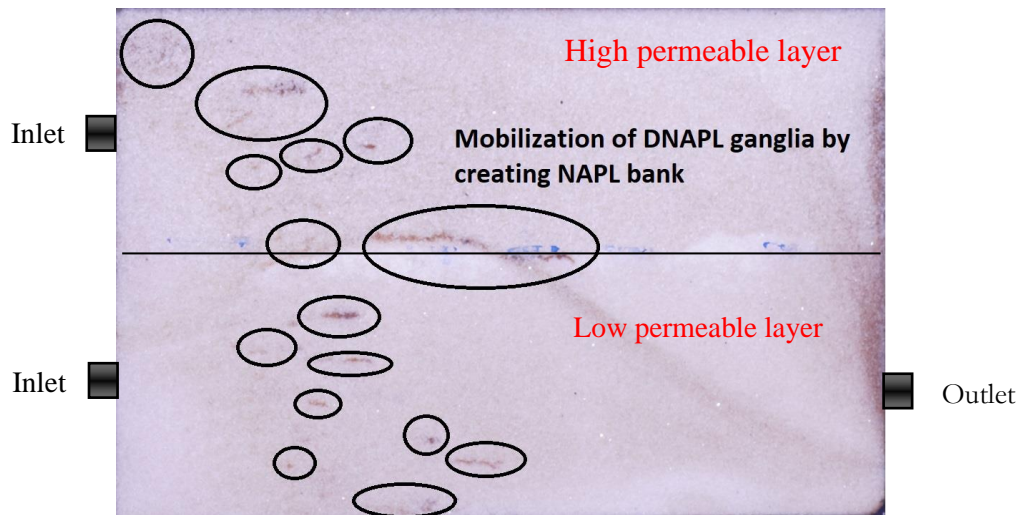
For the remediation of DNAPL polluted soils, a well-known technique consists in the flushing of the contaminated aquifer by a polymer or surfactant solution [1]. However, even after the initial flushing using these methods, there will remain some trapped DNAPL that cannot be further mobilized [2]. Post-injection of alcohol-surfactant emulsion can result in higher recovery of DNAPL by solubilization or mobilization mechanisms [3]. In the case of a multilayer system, recovering residual DNAPL from all layers after primary flushing can be challenging. In this study, we demonstrate how the injection of a mixture comprising alcohol, surfactant, and polymer can enhance the recovery of residual DNAPL in a multilayer system.

2 Methodology

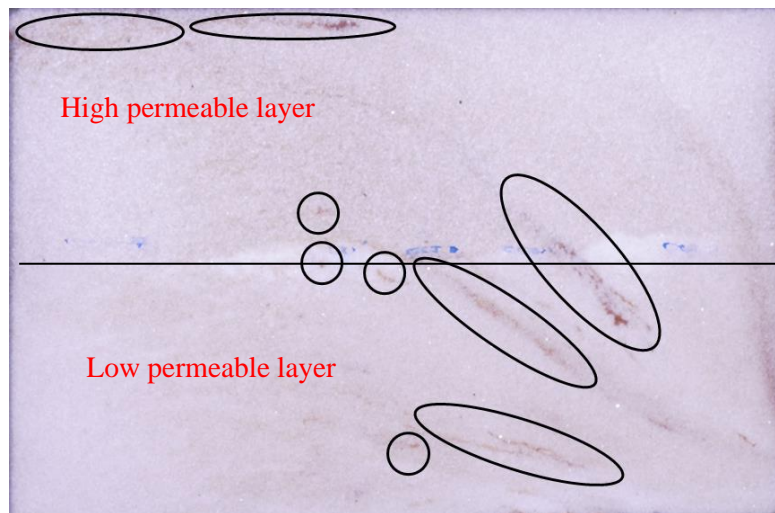
The mixture employed consisted of two alcohols, 1-propanol and 1-hexanol. Xanthan, a biopolymer known for its non-Newtonian behavior in solution, and Sodium dodecylbenzene sulfonate (SDBS), a surfactant for stabilizing the mixture were used. Batch experiments were carried out with varying concentrations of the surfactant and volume fractions of alcohols, water, and DNAPL. To assess the effectiveness of the alcohol/polymer mixtures in recovering residual DNAPL, 1D-columns were used. Furthermore, the performance of these mixtures in improving multicomponent DNAPL recovery in multilayer systems was evaluated using a confined 2D tank of decimetric scale.

3 Results

The analysis of batch experiments reveals that the use of only 1-propanol as the remediating fluid leads to a decrease in the volume of DNAPL, indicating that solubilization is the primary washing mechanism. Conversely, the addition of 1-hexanol, regardless of the presence of 1-propanol, results in an increase in the volume of DNAPL. This demonstrates that the presence of 1-hexanol in the mixture influences the partitioning behavior of 1-propanol, leading to a mobilization mechanism. Density analysis of the samples obtained from displacement experiments in column and the tank shows that the mobilization mechanism can improve the recovery efficiency from 91% (achieved by primary flushing) to 99%, and from 86% to 94% for single-layer experiments in 1D column and multilayer experiments in 2D tank, respectively. The images obtained from 2D experiments demonstrate that in the case of the mobilization mechanism, a contaminant bank forms in front of the injected mixture in the flushed zone of the soil, as depicted in Figure 1.



(a)



(b)

Figure 1: Mobilization of DNAPL ganglia by creating NAPL bank in the two-layer sand packed 2D tank. a) 20 minutes after the start of alcohol emulsion injection, b) 40 minutes after start if alcohol emulsion injection

References

- [1] A. Alamooti, S. Colombano, S. Omirbekov, A. Ahmadi, F. Lion, and H. Davarzani, "Influence of the injection of densified polymer suspension on the efficiency of DNAPL displacement in contaminated saturated soils," *J Hazard Mater*, vol. 440, p. 129702, 2022.
- [2] K. D. Pennell, M. Jin, L. M. Abriola, and G. A. Pope, "Surfactant enhanced remediation of soil columns contaminated by residual tetrachloroethylene," *J Contam Hydrol*, vol. 16, no. 1, pp. 35–53, May 1994.
- [3] C. St-Pierre, R. Martel, U. Gabriel, R. Lefebvre, T. Robert, and J. Hawari, "TCE recovery mechanisms using micellar and alcohol solutions: phase diagrams and sand column experiments," *J Contam Hydrol*, vol. 71, no. 1–4, pp. 155–192, Jul. 2004.

Potential of Mean Force between Silica Particles in Aqueous Solutions from Molecular Simulations: Effect of Inter-Particle Distance and Salinity

K. Ariskina^a, C. Soulaine^a, J. Puibasset^b

^aEarth Sciences Institute of Orléans (ISTO) UMR 7327, University of Orléans, CNRS – Orléans, 45100

^bInterfaces, Confinement, Materials and Nanostructures (ICMN) UMR 7374, University of Orléans, CNRS - Orléans, 45100

Keywords: colloids, free energy, non-DLVO interactions, umbrella sampling

1 Introduction

Colloidal interactions within saturated porous media have attracted increasing attention in recent decades due to the remarkable ability of colloids to capture and transfer non-aqueous phases. This capability allows them to control the physico-chemical characteristics of the solution and affect the poromechanical properties of the media. Understanding and predicting colloidal behaviour within geological formations requires first studying inter-particle couplings at the nanometer level. The underlying mechanisms of colloidal interactions have been well described using the Derjaguin-Landau-Verwey-Overbeek (DLVO) theory, accounting for Van der Waals forces and osmotic repulsion across a broad range of spatio-temporal scales [1,2]. Nevertheless, this approach has proven to be inadequate at inter-particle separations below 3 nm, since phenomena such as electrostatic attraction in electrical double layers, contact and hydration repulsion dominate hydrodynamic interactions [3]. While the nature of colloidal couplings at such ultra-small scales plays a key role in geological processes, such as enhanced oil recovery and groundwater remediation, it remains poorly investigated.

2 Results and Discussion

In this work, an umbrella sampling molecular dynamics technique has been applied to characterize the free energy landscapes of a pair of spherical silica nanoparticles in various aqueous solutions as a function of inter-particle distance. First of all, it has been shown that the ultra-thin fluid layer affects the fluctuations of the interparticle potential of mean force. Particular attention is paid to couplings at distances less than 3 nm. It has been illustrated that non-DLVO forces become important at small inter-particle separations. The limitations of the conventional theory in describing colloidal interactions have been confirmed at close proximity of colloids for different salinity conditions. The present study of the interplays among aqueous silica nanoparticles at the atomistic level needs further investigations to advance the understanding of colloidal phenomena within porous structures.

References

- [1] Derjaguin, B; Landau L., Theory of the stability of strongly charged lyophobic sols and of the adhesion of strongly charged particles in solutions of electrolytes, *Acta Physicochim. USSR*, 14, 633 - 662 (1941).
- [2] Verwey, E.J.W., Overbeek, J.Th.G., *Theory of the Stability of Lyophobic Colloids: The Interaction of Sol Particles Having an Electric Double Layer*, 205 p., Elsevier, Amsterdam (1948).
- [3] Shen X., Bourg I. C., Interaction between Hydrated Smectite Clay Particles as a Function of Salinity (0–1 M) and Counterion Type (Na, K, Ca), *Journal of Physical Chemistry C*, 126, 20990–20997 (2022).

EOR on-chip experiments: on the effect of the viscosity ratio on tertiary oil recovery

Haohong PI^a, Abdelaziz Omari^a, Giuseppe Sciumè^a

^a*Institute of Mechanics and Mechanical Engineering, Building A11, University of Bordeaux - TALENCE Cedex, 33405*

Keywords: EOR, two-phase flow, porous medium model, fluid mechanics.

1 Introduction

In enhanced oil recovery (EOR), tertiary oil recovery after the water-flooding period is less studied than secondary flooding technique. Moreover, core-flood experiments at the darcy scale are the usual method used to study the efficiency of the chosen lever to increase the recovery rate of the original oil in place (OOIP) [1,2]. However beside reproducibility aspects, a significant drawback is that with these black box experiments, we cannot observe and capture key phenomena at the pore scale, including interfacial interactions and details about mobilization of the trapped oil (*e.g.* size and distribution of residual ganglia). This is why microfluidic micromodel devices are now extensively used in lab EOR experiments. They preserve the structural details of the rock while offering advantages such as easy cleaning and repeatability. Visual tracking of fluids displacement is particularly important as it can provide more details about the behavior of wetting and non-wetting phases in porous media, aiding in targeted strategies to enhance oil recovery rates.

A typical strategy to enhance the recovery of OOIP is to modify the properties of the injected fluids [3]. This same approach is followed here where the size distribution of the ganglia of the non-wetting fluid trapped in the porous medium as well as their trapping mechanisms are also analysed. This contribution focuses in particular on the effect of the ratio of injected fluid viscosity over the oil viscosity and of the Capillary number (Ca) on the oil mobilization trends, non-wetting fluid trapping and characteristics and becoming of oil ganglia.

2 Experimental procedure and results

Before water-flooding experiments, the oil was injected into a water-wet microfluidic chip to reach the irreducible water saturation. Microscopic imaging techniques were used to capture the distribution of wetting and non-wetting phases during the drainage and imbibition processes. After the drainage process to irreducible water saturation, the analysis of the residual water location in the porous medium revealed that it was trapped in small pores as expected. During the subsequent imbibition process, a noticeable viscous fingering phenomenon was observed. After the completion of waterflooding, in addition to the unswept areas, residual oil ganglia were trapped due to capillary forces. More than 40% recovery rate of OOIP was obtained at the end of this water-flooding step. To further enhance the oil recovery, especially by mobilizing the trapped residual oil ganglia in the porous medium, we inject therefore a sweeping aqueous fluid of higher viscosity. In this tertiary EOR experiments, we focus on the impact of viscosity ratio on the oil mobilization ability. Several water-glycerol mixtures corresponding to different viscosity ratios were injected at the same flow rate. It was notably observed that the mobilization of trapped oil ganglia and the oil in the unswept regions was significantly improved, leading to a decrease of the residual oil saturation (S^{or}). The relationship between S^{or} and Ca will be also discussed.

Typical results of our experiments are depicted in the figure below. In the top of the figure a simplified representation of the presence of wetting phase (aqueous) and non-wetting phase (oil) in the chip at different stages is provided as well as the value of flow rate. The saturation of the wetting phase in the chip is tracked and analysed during the three stages of the experiment (*i.e.* drainage phase, secondary and tertiary recovery). The irreducible water saturation during drainage reached 0.1, which is consistent with common reported values and corroborates the findings of core experiments. During imbibition, the breakthrough occurs after injecting almost 0.2 V_p (pore volume) of water. The impact of Ca was studied in the secondary recovery stage by steeply increasing the flow rate until reaching a plateau, where the oil recovery was

approximately 50% of the original oil in place. Then a glycerol-water mixture at various proportions was used to increase the viscosity of the wetting phase; the changes in the saturation of the wetting phase reflected its impact on the oil recovery rate. These results will be presented and discussed later in detail.

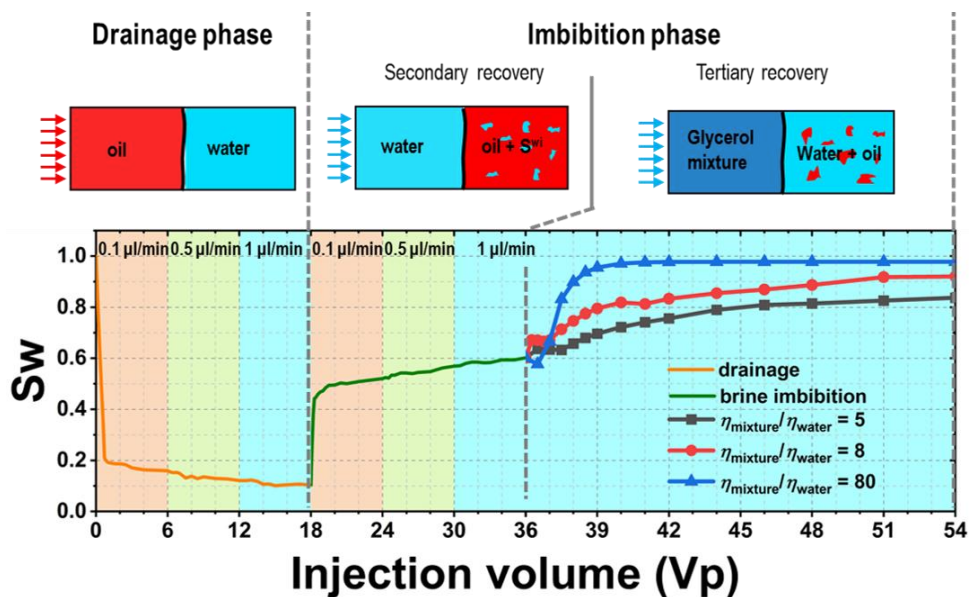


Figure 1: EOR on-chip schematic, and saturation of the wetting phase at each stage.

References

- [1] Pini R, Krevor S, Krause M, et al. Capillary heterogeneity in sandstone rocks during CO₂/water core-flooding experiments. *Energy Procedia*, 37, 5473-5479 (2013).
- [2] Karambeigi M S, Abbassi R, Roayaei E, et al. Emulsion flooding for enhanced oil recovery: interactive optimization of phase behavior, microvisual and core-flood experiments. *Journal of Industrial and Engineering Chemistry*, 29, 382-391 (2015).
- [3] Saadat M, Tsai P A, Ho T H, et al. Development of a microfluidic method to study enhanced oil recovery by low salinity water flooding. *Acs Omega*, 5, 17521-17530 (2020).

Bacterial communication in porous media flows

D. Anastasopoulou^{a,b}, G. Ramos Peroni^a, Y. Abidine^a, Y. Davit^a, T. Le Borgne^b,

^aInstitut de Mécanique des Fluides (IMFT), UMR 5502 CNRS and Toulouse INP, 31400 Toulouse, France

^bGeosciences Rennes, UMR 6118, CNRS, Université de Rennes 1, Rennes, France

Keywords: Biofilms, Fluorescence Microscopy, Microfluidics, Porous media, Quorum Sensing

In many environmental, biological and engineered systems, bacteria live in sessile communities termed biofilms. In these multi-cellular groups, coordinated behaviors can emerge. Bacteria are highly interactive and communicate via chemical signaling, what is known as quorum sensing (QS). QS regulates gene induction and relies on the synthesis and group-wide detection of small molecules, called autoinducers, which diffuse in and out of the bacterial cell [1]. When biofilms are exposed to fluid flow, advective transport can transport autoinducers, thus leading to a spatially distributed QS response [2]. While this phenomenon has been studied in simple microfluidics channels, little is known about how communications develop in more complex structures, such as porous media. This could play an important role in medical devices such as prosthetic parts and implants which are primarily porous [3]. QS under flow likely also influences soil ecology, nutrient cycling and the overall condition of the soil ecosystem [4].

QS activation plays a critical role in bacterial detachment [6]. For instance, in the case of *Staphylococcus aureus*, it has been reported that activation of quorum sensing leads to degradation of the biofilm extracellular matrix and as consequence detachment and dispersal [2] [7]. In porous media, complex couplings develop between biofilm growth, flow and detachment. Growth leads to pore clogging, which can control flow channels, solute transport and microbial competition [5]. In such systems, QS-induced detachment will unclog some pores, change the flow paths through the structure and may play a central role in regulating bacterial communities. We thus hypothesize that QS-induced detachment is a fundamental component of biofilm dynamics in porous media (Fig.1).

To test this hypothesis, we used *S. aureus* equipped with a dual-labeling system, which can be tracked by fluorescence imaging for viability and communication. First, we examined the effect of flow on QS in a single pore microfluidic chip. We observed that under sufficient flow rate, QS is activated close to the solid/biofilm interface but not at the flow/biofilm interface. This is because advection can wash away the autoinducers, thus prohibiting communications, whereas autoinducers can accumulate when transport is diffusion dominated (Fig.2), a phenomenon that has been already observed previously [2]. We further proceeded with the use of a complex network in a microfluidic device (Fig.3). We observed a rich spectrum of dynamics where clogging and communication phenomena alternate between pores through time. To understand the basic mechanisms driving these dynamics, we considered a simpler T junction geometry. We will use these results to discuss the interplay between flow, biofilm growth, communication and detachment in porous media (Fig.1).

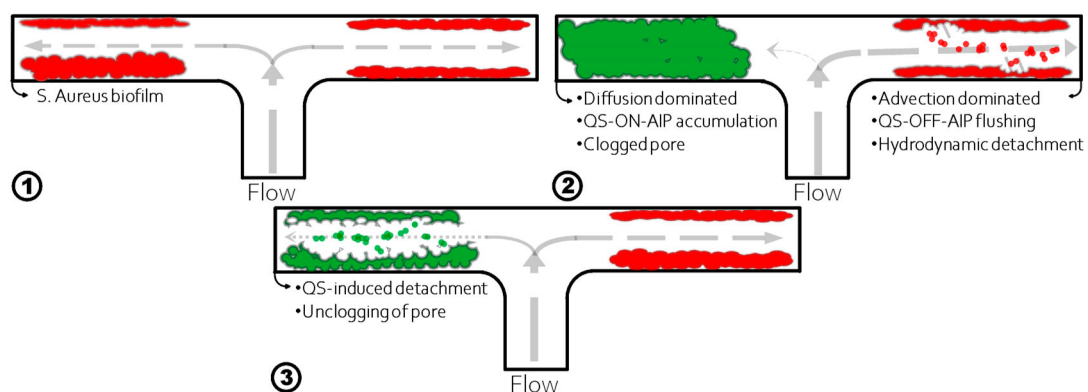


Figure 1: Schematic representation of hypothetical evolution of growth, communication, detachment and clogging in a T shaped microfluidic chip. The red color indicates the viable *S. aureus* cells/ biofilm, while the green corresponds to the communicating ones.

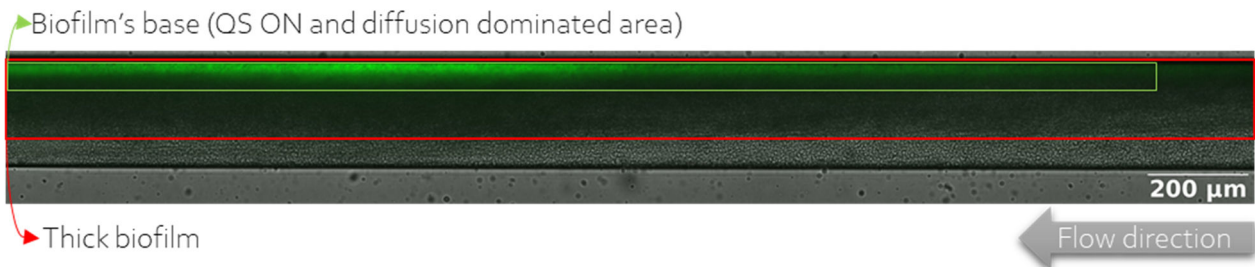


Figure 2: Biofilm of *S. aureus* after 61hr of growth under flow rate of 1 μ l/ min. Green fluorescence indicates the bacterial communication, only in the base of the biofilm, where diffusion governs the transport of the autoinducers.

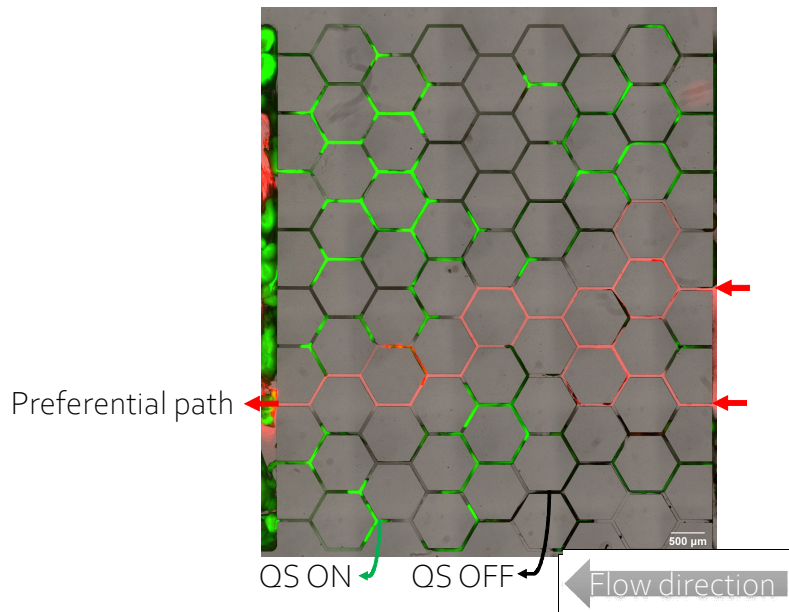


Figure 3: Biofilm of *S. aureus* after 118,5hr of growth under flow rate of 2 μ l/ min. Green fluorescence indicates the bacterial communication while red corresponds to beads, of 1nm, to mark the preferential path of flow the present moment.

References

- [1] J. E. González and N. D. Keshavan, "Messing with bacterial quorum sensing," *Microbiology and Molecular Biology Reviews*, vol. 70(4), pp. 859-875, 2006.
- [2] M. K. Kim and et al., "Local and global consequences of flow on bacterial quorum sensing," *Nature Microbiology*, vol. 1, pp. 1-5, 2016.
- [3] A. Srivastava and et al., "The role of biofilms in medical devices and implants.," in *Biofilms in Human Diseases: Treatment and Control*, Springer, 2019, pp. 151-165.
- [4] H. C. Flemming and S. Wuertz, "Bacteria and archaea on Earth and their abundance in biofilms," *Nature Reviews Microbiology*, vol. 17, no. 4, pp. 247-260, 2019.
- [5] K. Z. Coyte and et al., "Microbial competition in porous environments can select against rapid biofilm growth," *Proceedings of the National Academy of Sciences*, vol. 114, no. 2, pp. E161-170, 2017.
- [6] C. Solano and et al., "Biofilm dispersion and quorum sensing," *Current opinion in microbiology*, vol. 18, pp. 96-104, 2014.
- [7] B. R. Boles and A. Horswill, "Agr-mediated dispersal of *Staphylococcus aureus* biofilms," *PLoS pathogens*, vol. 4, no. 4, p. 1000052, 2008.

Modelling a Li-ion battery separator using effective properties: is an invariant scalar value of tortuosity appropriate?

Isaac Paten^a, Martin Petitfrère^b, Olivier Liot^a, Céline Merlet^c, Romain de Loubens^b, Michel Quintard^a, Yohan Davit^a

^a*Institut de Mécanique des Fluides (IMFT), CNRS & Université de Toulouse, 31400 Toulouse, France*

^b*TotalEnergies - OneTech R&D, Palaiseau, 91120*

^c*CIRIMAT, CNRS and Université de Toulouse, Toulouse, 31062*

Keywords: Li-ion battery, battery separator, volume averaging, effective properties, tortuosity

1 Abstract

When simulating lithium-ion batteries, the separator is often homogenised and modelled using a single scalar value of tortuosity. However, real separator materials can be highly anisotropic, thus using a scalar tortuosity value may lead to large errors – Lagadec’s dataset for a Celgard PP1615 separator has a tortuosity tensor with diagonal components differing by over an order of magnitude [1]. In this work, we calculate a full tortuosity tensor for this dataset, using a Bamberger method [2]. Then, we compare cell simulations with two different effective separators: the first uses a single scalar value for tortuosity, and the second uses a diagonal tensor for tortuosity.

Additionally, heterogeneities in the separator structure may cause some distributions of mass and charge flux, which would be overlooked in a model with an invariant tortuosity tensor. In this work, a “semi-homogenised” model is presented, which strives to capture flux distributions whilst not requiring the large computational resources of direct numerical simulations (DNS). The method can serve as an intermediate between DNS and simplified homogenised models. In essence, a tomographic image of a real separator structure [1] is divided into small blocks (see Figure 1), and effective property tensors are calculated for each block - these are determined by solving three steady-state diffusive transport simulations (one for each axis) [3]. The result is a spatial field of effective properties, as opposed to the invariant properties used in a fully-homogenised model. Simulations of the fully-homogenised model, semi-homogenised model, and the DNS are compared by taking several slices of the domain. Average positive ion flux and the L2 norm are calculated for these slices, to evaluate how well flux distributions are represented.

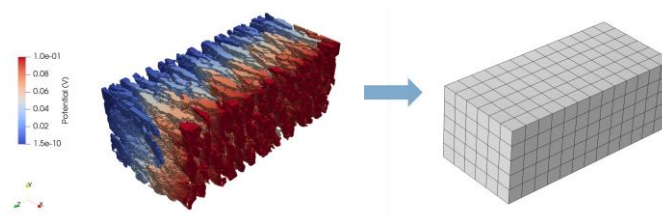


Figure 1: Illustrating the construction of the semi-homogenised model

References

- [1] M. Lagadec, Microstructure of Celgard PP1615 Lithium-Ion Battery Separator, (2016).
- [2] R. Guibert, A Comparison of Various Methods for the Numerical Evaluation of Porous Media Permeability Tensors from Pore-Scale Geometry, *Maths. Geosci.*, 48(3), (2016).
- [3] S. Cooper, TauFactor: An open-source application for calculating tortuosity factors from tomographic data, *SoftwareX*, 5, 203-210 (2016).

Comparative Analysis of Electrical Conductivity and Tensiometry Methods for Measuring Critical Micelle Concentration (CMC) of Surfactants CAHS and SDS: Impact of Water Type on CMC Measurements

A. Shoker^{a,b,c}, P. Kessouria, A. Ahmadi-Sénichault^b, A. Mainault^c

^a BRGM (French Geological Survey), 45060 Orléans, France

^b Institut de Mécanique et Ingénierie de Bordeaux (I2M), Arts et Métiers Institute of Technology, CNRS, Talence, 33405, France

^c L'Unité Mixte de Recherche METIS, Sorbonne Université, 75252 Paris Cedex 05, France

Keywords: surfactants, CMC measurement, surface tension, electrical conductivity, porous media.

1 Introduction

Surfactant foams play a crucial role in different operations in porous media, like soil remediation. Surfactants have the ability to reduce the surface tension between two immiscible phases, such as oil and water, and act as major foaming agents [1]. This work is part of the ANR project BBFOAM aiming to characterize the foam flow in a porous medium, in the presence of pollutants. For surfactant analysis, determining the critical micelle concentration (CMC) is of paramount importance. The CMC is the concentration at which surfactant molecules begin to self-assemble and form micelles, which significantly affect their surface tension and electrical properties [2]. In this study, we assess two commonly used methods for measuring the CMC of surfactants: conductimetry (electrical conductivity measurement), and tensiometry (surface tension measurements) [3]. Two different types of water: tap, and deionized water, used in laboratory and field applications were employed to investigate the influence of water type on CMC measurements. Two types of surfactants were used: Sodium Dodecyl Sulfate (SDS), an anionic surfactant, and Cocamidopropyl hydroxysultaine (CAHS), a zwitterionic surfactant.

2 Experiments

2.1 Conductimetry

This method measured the fluid electrical conductivity of both surfactant solutions in tap and deionized water, with different concentrations, using a conductivity meter. The conductivity measurement was carried out for various concentrations of solutions, with min 0.1g/L to max 3g/L, in triplicate and the mean value was calculated. The surfactant concentration was plotted against the electrical conductivity (see Figure 1). We fit the data with a linear fit, in order to identify the CMC, as the point on the plot corresponding to a change of slope.

2.2 Tensiometry

We measured the surface tension of SDS and CAHS solutions with different concentrations as above. It is performed by using the Drop Shape Analyzer system (DSA-100 from Kruss). The Interfacial tension (IFT) is calculated from the shadow of the digital image captured by the camera using the drop shape analysis [3]. The IFT was plotted, following the same principle as in previous method.

3 Discussion and Results

3.1 Deionized water

Using conductimetry, the measured CMC for CAHS is 0.48 g/L and 0.85 g/L for SDS (Figure 1b). In tensiometry, the measured CMC is 0.55 g/L for CAHS and 0.79 g/L for SDS (Figure 2b). The variations in the calculated values are expected among different techniques, as they measure different physical properties associated with the surface absorption or aggregation behavior of the micelles.

3.2 Tap water

Using the conductimetry, we were not able to determine the CMC of the tested surfactants, because no detectable change in the slope of the line was detected (Figure 1a). For tensiometry, the measured CMC is 0.59 g/L for CAHS, and 0.42 g/L for SDS. The difference in values raised between the deionized and tap aqueous solutions referred to the effect of ions exist in the tap water solution. The results are in Table 1.

Table 1. CMC values for the surfactants (CAHS and SDS) by different techniques and in different water types.

Method \ Water type	CMC CAHS by conductimetry	CMC CAHS by tensiometry	CMC SDS by conductimetry	CMC SDS by tensiometry	CMC SDS literature	CMC CAHS literature
Deionized water	0.48 g/L	0.55 g/L	0.85 g/L	0.79 g/L	2.2 g/L [4]	0.7 g/L [5]
Tap water	invalid	0.59 g/L	invalid	0.42 g/L	-	-

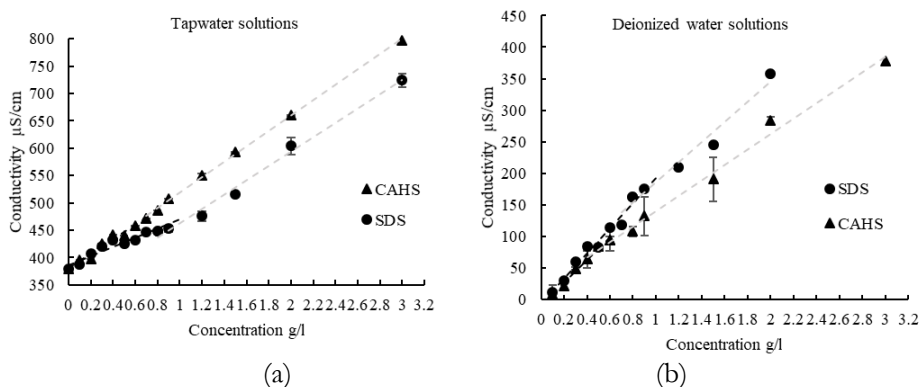


Figure 1. Conductivity vs. concentration for surfactants in tap water (a) and deionized water (b) solutions

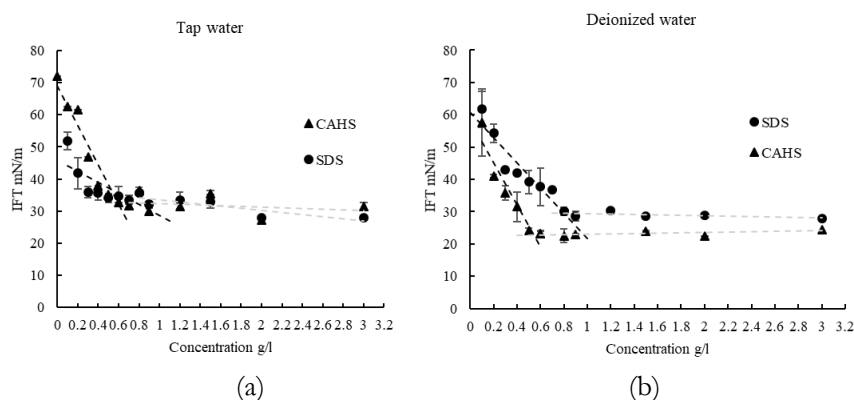


Figure 2. Surface tension (IFT) vs. concentration for surfactants in tap water (a) and deionized water (b) solutions.

4 Conclusion

The results underline the influence of the water type on choosing the CMC determination method, with a recommendation to use both methods when working with deionized water, and the unfeasibility of the conductimetry when using tap water. The results also showed that the tensiometry method expresses higher sensitivity to micelle formation than conductimetry. Further chemical analysis is needed to better understand the effect of these ions on the CMC.

5 Acknowledgements

This work is part of the ANR project BBFOAM (<https://anr.fr/Project-ANR-21-CE04-0004>).

6 References

- [1] Mulligan, Catherine N., R. N. Yong, and B. F. Gibbs. "Surfactant-enhanced remediation of contaminated soil: a review." *Engineering geology* 60.1-4 (2001): 371-380.
- [2] R.J. Pugh, Foaming, foam films, antifoaming and defoaming, *Elqvier*, 64, 67-142(1996).
- [3] Perinelli, D. R., Cespi, M., Lorusso, N., Palmieri, G. F., Bonacucina, G., & Blasi, P., Surfactant self-assembling and critical micelle concentration: one approach fits all?. *Langmuir*, 36(21), 5745-5753. (2020).
- [4] Rharbi, Y., & Winnik, M. A. Salt effects on solute exchange in sodium dodecyl sulfate micelles. *Journal of the American Chemical Society*, 124(10), 2082-2083. (2002).
- [5] Mouton, J. Procédé simultané de traitement de sols contaminés par des HAP et du plomb (Doctoral dissertation, Ph. D. thesis, INRS-ETE, Université du Québec, Québec, QC, Canada). (2008).

Flow barriers and channels in heterogeneous porous media: Detection and visualization by viscous energy dissipation

I. Colecchio^a, J. Gonzalez Litardo^{b,d}, C. Picighelli^{b,d}, A. Boschan^{b,d}, B. Noetinger^a, A. D. Otero^d

^aIFP Energies Nouvelles 1 & 4, avenue de Bois-Préau, 92852 Rueil-Malmaison Cedex - France

^bGMP, Facultad de Ingeniería, Universidad de Buenos Aires, Paseo Colón 850, Buenos Aires, Argentina

^cCONICET, Buenos Aires, Argentina

^dCentro de Simulación Computacional, CSC - CONICET, Godoy Cruz 2390, Buenos Aires, Argentina

Keywords: Viscous dissipation, Heterogeneous porous media, Connectivity

Abstract

Flow and transport in heterogeneous porous media strongly depend on the connectivity of the high conductivity component. Frequently, small critical regions determine the overall flow behavior. Energy dissipation approaches make it possible to detect these regions, yielding more accurate effective properties [1].

We have simulated flow in a synthetic binary medium (b) with a high conductivity ($k_{high} = 100m/day$) and a low one ($k_{low} = 0.01m/day$). No flow boundary conditions are applied in the vertical boundaries while a pressure gradient exists between the inlet (bottom) and the outlet (top). The resulting energy dissipation maps are shown in (a) (with k_{high} : ■, k_{low} : □), and in (c) (with k_{high} : □, k_{low} : ■). Zooms over a small critical region are shown in the bottom row (d, e, f).

When k_{high} paths connect inlet and outlet (i.e. when percolation of the k_{high} component occurs) energy dissipation is distributed mostly along flow channels (a, d). Otherwise, channelization is absent and energy dissipation is distributed along barriers (c, f).

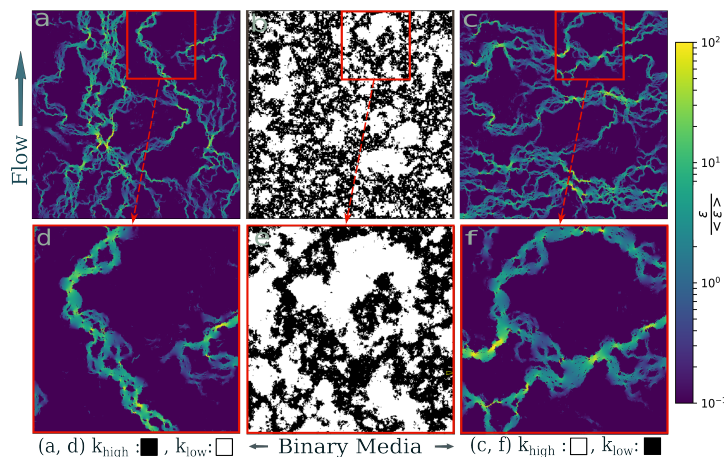


Figure 1: When k_{high} (■) paths connect inlet and outlet, energy dissipation (ε) is distributed along flow channels (a, d). To obtain the energy dissipation shown in (c,f) the conductivity values in the binary medium were swapped before the simulation of flow. Thus, channelization is absent and energy dissipation is distributed along barriers.

References

- [1] I. Colecchio and A. Boschan and A. D. Otero and B. Noetinger, "On the multiscale characterization of effective hydraulic conductivity in random heterogeneous media: A historical survey and some new perspectives", *Advances in Water Resources*, 140, 103594 (2020).

Strain localization patterns during hole fluid pressurization of an anisotropic Vosges Sandstone under true triaxial conditions

M. Mukherjee^a, P. Bésuelle^b, Y. Meheust^a

^aUniv. Rennes, CNRS, Geosciences Rennes, UMR6118, 35042 Rennes, France

^bUniv. Grenoble Alpes, CNRS, Grenoble INP, 3SR, 38000 Grenoble, France

Keywords: Rock Mechanics, DIC, True triaxial, hole pressurization, strain localization

Tensile fracturing of porous rocks induced by fluid pressure is an important process, encompassing both natural and artificial phenomena, including the formation of dike, vein growth and subsequent mineralization; the extraction of hydrocarbon through hydraulic fracturing or gas outbursts in underground mines. A particular concern during engineered tensile fracturing of rock mass through fluid pressure (such as hydraulic fracturing) is generating passive seismic events. Hence, it is necessary to monitor the evolution of this kind of engineered deformation and localization pattern of the deformation to demarcate the damage zone of the subsurface.

In this study, fluid driven tensile fracturing experiments were performed on anisotropic Vosges sandstone blocks retrieved from a quarry near the city of Hangviller,. Prismatic samples of volume $50 \times 50 \times 30 \text{ mm}^3$ were prepared. A hole of diameter 10 mm and length 30 mm was then bored within the samples, with its axis intersecting the centre of the $50 \times 50 \text{ mm}^2$ face. A white and black random speckled pattern was then applied on the $50 \times 50 \text{ mm}^2$ face of the specimen. The high pressure true triaxial apparatus (TTA) used for the loading experiment has been designed at Laboratory 3SR, Grenoble with the unique feature of a transparent sapphire glass window in contact with the specimen's speckled surface allowing to photograph the face of the specimen during deformation so as to a posteriori reconstruct the surface strain field using Digital Image Correlation (DIC) [1]. DIC computation was performed in the SPAM [2] software by computing the correlation function between many subset (correlation windows) of corresponding images taken at two successive time steps. DIC algorithm includes rigid displacement and rotation and linear distortion of the correlation windows.

Specimen is prevented from fluid invasion thanks to an external soft jacket all around the specimen and by an internal one inside the cylindrical hole. Loading experiments were conducted in the specimens with two different orientations; one in which the applied axial load was perpendicular to the bedding plane of the sandstone and another in which the axial load was applied parallel to the bedding plane. In either of the situations, isotropic loading was applied with a rate of 0.4 MPa/min to 8 MPa followed by the application of vertical load at a rate of 0.2 MPa/min to 10 MPa. Internal fluid pressurization in the circular cavity was achieved by injecting water with a pump at a rate of 0.2 MPa/min until visible fracture occurred in the specimen.

The evolution of the volumetric and deviatoric component of surfacic strain tensor with loading and fluid pressurization up to post failure was correlated with macroscopic stress-strain curves. Local zones of compaction and dilatancy around and away from the cavity are presented. Monitoring the advancement of strain concentration from early stages to failure, and how these high deformation zones control the post failure behavior is reported. The study thus establishes a correlation between the mechanical response with the development and evolution of kinematic structures during fracturing of porous sandstone with fluid pressure.

References

- [1] P. Bésuelle and P. Lanatà, "A new true triaxial cell for field measurements on rock specimens and its use in the characterization of strain localization on a Vosges sandstone during a plane strain compression test," *Geotechnical Testing Journal*, vol. 39, no. 5, pp. 879–890, Sep. 2016, doi: 10.1520/GTJ20150227.
- [2] O. Stamati *et al.*, "spam: Software for Practical Analysis of Materials," *The Journal of Open Source Software*, vol. 5, no. 51, p. 2286, Jul. 2020, doi: 10.21105/joss.02286.

A pore-constriction network model considering different preferential infiltration strategies for fine injection analysis

Fan Chen^{??}, Antoine Wautier^{??}, Pierre Philippe^{??}

^aINRAE, Aix Marseille Université, RECOVER, Aix-en-Provence, France

Keywords: Fine infiltration, PFV-DEM, Pore-network model

Suffusion is a phenomenon commonly observed in gap-graded soils that involves the detachment and transport of the finest grains under the action of an internal fluid flow. This can have detrimental effects, as the significant loss of fines may trigger mechanical instabilities in the material, posing a potential risk of catastrophic failure for hydraulic structures, possibly in the form of static liquefaction. To address this risk, an innovative approach is being considered – the injection of fines back into the remaining granular skeleton, primarily comprised of coarse sand grains. This remediation technique draws inspiration from recent numerical findings, which indicate that the inclusion of weakly loaded grains can substantially enhance the mechanical stability of granular materials [1, 2]. In this work we aim to study the infiltration behavior using numerical and analytical methods to assess the potential of this mitigation method against adverse impacts of suffusion.

In this work, we propose to use the discrete element method (DEM) to analyze the fine infiltration process into the suffused coarse material. Both dry and flow driven infiltration are considered with the simultaneous release of a small number of fine grains above a gravity-deposited coarse sand column following the grading of the Hostun sand used in the laboratory. For the flow case we use the Pore scale Finite Volume (PFV) scheme introduced by Chareyre et al. (3). Besides, different fine/coarse size ratios (D_{50}/d from 3.4 to 11.3) and different void ratios (from loose to dense) of sand column are considered. Both the lateral and vertical displacements of fine grains are analyzed to understand the infiltration behaviors of injected fines in term of infiltration depth and lateral diffusion. Similarly to previous experiments, the distribution of fine grains penetration depth in both dry and immersed cases are fitted by exponential decay curves to determine characteristic length of infiltration.

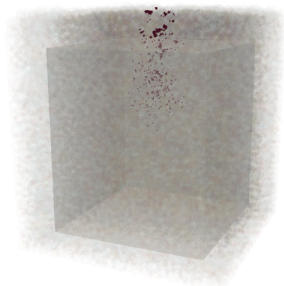


FIGURE 1: Infiltration process using coupled PFV-DEM

To further analyse the numerical results, an analytical pore-constriction-based network model is used to predict the infiltration depths without running DEM simulations with both coarse and fine grains (4, 5). By utilizing the Delaunay tessellation method, we describe a coarse assembly of grains as a network of interconnected pores, which allows us to precisely identify and study pore constrictions, crucial points where fine particles may get clogged during infiltration. The analytical nature of the model enables us to simulate various infiltration scenarios, examining the influences of different parameters, such as grain size distribution, pore connectivity, and hydraulic gradients. Consequently, we gain valuable insights into the intricate mechanisms governing fine infiltration processes within the sand column.

Références

- [1] Antoine Wautier, Stéphane Bonelli, and François Nicot, Rattlers' contribution to granular plasticity and mechanical stability, *International Journal of Plasticity*, 112 :172–193,(2019).
- [2] Tao Wang, Antoine Wautier, Sihong Liu, and François Nicot, How fines content affects granular plasticity of under-filled binary mixtures, *Acta Geotechnica*, 1–15,(2021).
- [3] Chareyre, B., Cortis, A., Catalano, E. et al. Pore-Scale Modeling of Viscous Flow and Induced Forces in Dense Sphere Packings. *Transp Porous Med*, 92, 473–493 (2012).
- [4] Wautier, A, Bonelli, S, Nicot, F. DEM investigations of internal erosion : Grain transport in the light of micromechanics. *Int J Numer Anal Methods Geomech*, 43 : 339– 352, (2019).
- [5] Wautier, A., Bonelli, S. & Nicot, F. Scale separation between grain detachment and grain transport in granular media subjected to an internal flow. *Granular Matter* 19, 22 (2017).

Characterizing Multiphase Flow Behavior for Residual Trapping of CO₂ in Rock Fractures using a Versatile Fracture Flow Cell

Amin Rezaei^{*1,2}, Francesco Gomez¹, Insa Neuweiler², and Yves Meheust¹

¹Université de Rennes, CNRS, Géosciences Rennes, UMR 6118, Rennes, 35042, France – Université de Rennes, CNRS, Géosciences Rennes, UMR 6118, Rennes, 35042, France – France

²Institute of Fluid Mechanics and Environmental Physics in Civil Engineering, Leibniz University Hannover, Hannover, 30167, Germany – Allemagne

Résumé

While research on multiphase flow in porous media has been very extensive in the last 40 years, at both the pore and continuum scales, comprehensive understanding of how the phenomenology of two-phase flow in geological fractures is impacted by both the flow conditions (capillary number Ca and viscosity ratio M) and the geometry (fracture closure), remains elusive. We investigate residual trapping of CO₂ in fractured reservoirs at the fracture scale, exploring the complex interplay between fracture surface roughness and the displacement of fluid-fluid interfaces. Our systematic approach explores the phenomenology of two-phase flow in fractures, taking into meticulous consideration the fluid properties, flow conditions, and fracture geometry. To this aim, we have developed a transparent fracture flow cell with self-affine rough-walled surfaces and precisely-controlled mean aperture, which can be varied. The fracture wall geometry is generated from numerical models that are consistent with the well-known stochastic geometric properties of geological fractures. A camera allows recording the dynamics of the fluid phases' spatial distribution within the fracture plane. The displacement patterns are characterized as functions of Ca , M , the density difference of the fluids, and the fracture's geometrical parameters. We thus aim to characterize the amount of supercritical CO₂ trapped in fractured aquifers as a function of those controlling parameters.

*Intervenant

PoroS : a Software Suite for the Prediction of Permeability of Anisotropic Multi-Scale Porous Structures

P.D. Mulye^a, E. Syerko^a, A. Leygue^a, C. Binetruy^a

^aNantes Université, École Centrale Nantes, CNRS, GeM, UMR 6183, Nantes, F-44000, France

Keywords: fibrous medium, permeability, anisotropy, 3D flow, numerical computation

1. Introduction

Permeability is one of the key properties of porous materials in general. This work focuses on the permeability of *fibrous* materials used as reinforcements of structural composites that represent the most general and complex case of porous media properties due to their multi-scale and anisotropic character. The permeability measurement of fibrous engineering textiles is not a trivial task. This is due to their anisotropic multi-scale character (the finest scale characteristic size is several μm) and their inherent natural variability. Virtual characterization of permeability using numerical methods has important advantages over experimental measurement. It does not require a specialized and often costly measurement equipment, it reduces material waste, allows to analyze the influence on permeability of material micro-structural parameters, while being capable of addressing the material variability. However, at present there is no widely accepted numerical approach for permeability prediction due to modeling challenges such as the choice of the RVE (representative volume element), boundary conditions, numerical approximation, permeability identification technique, as revealed in the international virtual permeability benchmark [1].

2. PoroS : a numerical solver for the prediction of saturated permeability

A novel scientific software named ‘PoroS’ [2] has been developed, which contains a set of numerical solvers specifically designed for anisotropic multi-scale materials for the prediction of permeability. The objective of the development of this scientific software is to calculate the saturated permeability of a porous material based on the real 3D images of the micro/meso structure. Alternatively, digital twins of the material, built, for example, using an open-source TexGen software [3] in case of textile structures, can also be used as input to PoroS. The first version of the software PoroS 1.0 has been developed to compute the permeability of the materials with single-scale porosity. The Stokes flow problem is solved using the Finite Element Method and specially designed matrix-free iterative solvers. The voxel-based discretization was used with hexahedral Taylor-Hood elements [4] that satisfy the LBB condition. The pseudo-compressibility formulation was employed, and the full-field homogenization method [5] then allowed the full 3D permeability tensor to be calculated using only the computed velocity fields, giving the advantage of reducing the number of degrees of freedom without having to compute the pressure field.

3. Results and discussion

After validating the flow solvers using a set of conventional test-cases from the literature, PoroS was compared with the results obtained in the first stage of the virtual permeability benchmark [1]. The input geometry was a 3D segmented microscopic image (Fig. 1) of $1003 \times 973 \times 124$ voxels with a nominal resolution of $0.52 \mu\text{m}/\text{voxel}$ (available on the repository at <https://doi.org/10.5281/zenodo.6611926>). It can be seen that the results obtained using PoroS fall within the cluster of the results reported by the participants of the benchmark (Fig. 2) and are close to the mean value defined after eliminating the benchmark outliers.

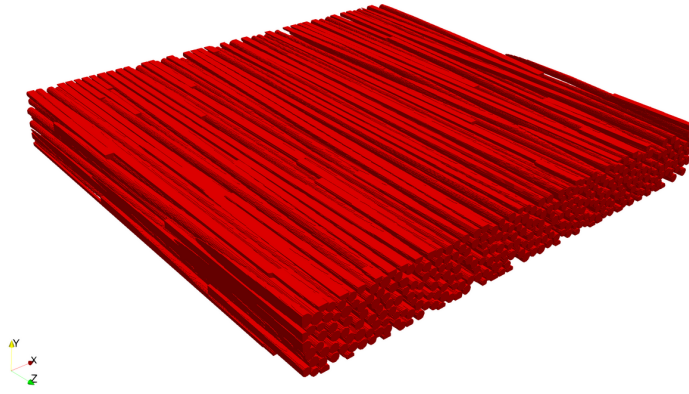


FIGURE 1: 3D microscopic volume image (segmented) showing fibres used as input

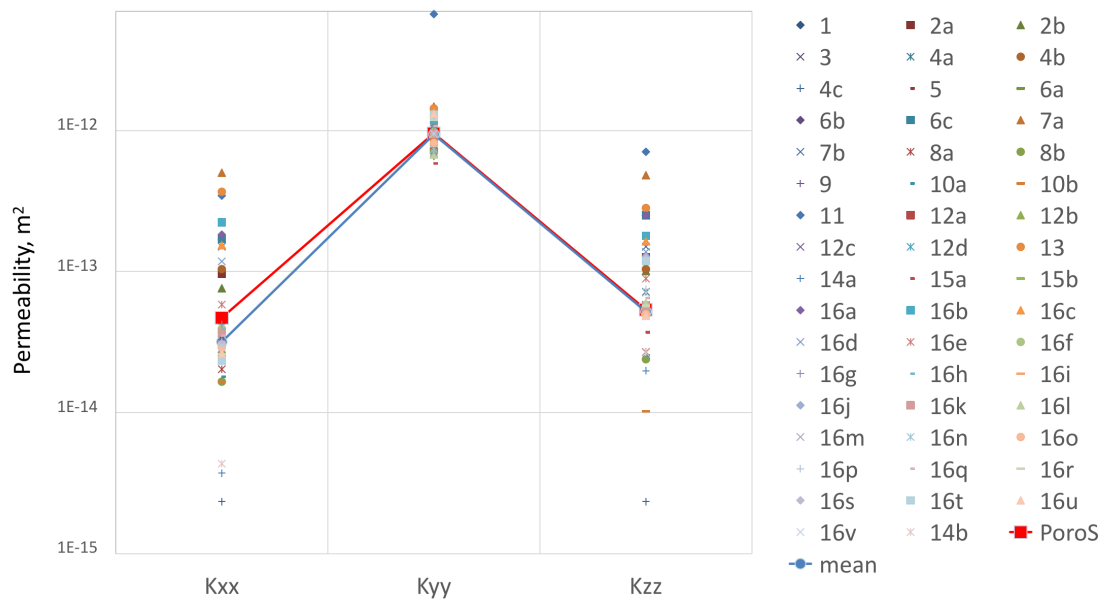


FIGURE 2: Comparison of permeability tensor main components computed using PoroS with the results of all participants of the virtual permeability benchmark [1]

Références

- [1] E. Syerko, T. Schmidt, D. May, C. Binetruy, S. G. Advani, S. Lomov, L. Silva et al, Benchmark exercise on image-based permeability determination of engineering textiles : Microscale predictions, *Composites Part A : Applied Science and Manufacturing*, 167, 107397, (2023).
- [2] Agence pour la Protection des Programmes, PoroS 1.0 *IDDN.FR.001.400009.000.S.P.2022.000.20600*, (2022).
- [3] L. Brown, mike-matveev, georgespachman, *louisepb/TexGen : TexGen v3.12.1*, Zenodo <http://doi.org/10.5281/zenodo.4537855>, (2021).
- [4] J. Donea, A. Huerta, *Finite element methods for flow problems*. John Wiley & Sons, (2003).
- [5] E. Lopez, E. Abisset-Chavanne, F. Lebel, R. Upadhyay, S. Comas, C. Binetruy, F. Chinesta, Flow modeling of linear and nonlinear fluids in two and three scale fibrous fabrics, *International Journal of Material Forming*, 9, 215-27 (2016).

Numerical simulation of the forced convective flow in a channel partially filled with an anisotropic porous medium

S. Ben Aoua^{a,b}, F. Mechighel^{a*}, R. Kibboua^b

^aLR3MI Laboratory, Mechanical engineering department, Faculty of Technology, BP 12, University of Annaba

^bUniversity of Sciences and Technologies Houari Boumediel USTHB, LTPMP/FGMGP, BP 32 El Alia, Algiers 16111, Algeria.

*Corresponding authors: farid.mechighel@etu.unilim.fr

Keywords: Porous media, Convection, Darcy-Brinkman-Forchheimer equation

Abstract

A numerical study of a laminar stationary forced convection inside a flat horizontal channel partially filled with a porous medium has been carried out. The porous medium is assumed to be anisotropic and its walls are maintained at a constant heat flux. The Darcy-Brinkman-Forchheimer model is used to describe the flow in the porous medium. The governing equations of conservation of mass, momentum and energy, and the associated boundary conditions are solved using a numerical code based on the finite volume method. The objective of this work is to specify the nature of convective flows in anisotropic porous medium. The results highlighted the influence of the anisotropic permeability ratio K^* (with K^* in the range between 0.1 and 10), the anisotropy angle θ (with θ in the range 0 and 90°), the dimensionless thickness E^* of the porous layer (between 0 and 1), the Darcy number Da (with Da in the range between 10^{-4} and 10^{-1}), and the thermal conductivity ratio Rc ($Rc = 1$ and $Rc = 10$) on both the Nusselt number and the pressure drop.

Development of macroporous geopolymer foams functionalized by a photocatalyst.

Sara Benkhirat*¹, Gael Plantard^{2,3}, Khalid Nouneh⁴, and Enrique Ribeiro³

¹Université de Perpignan Via Domitia – Gael PLANTARD – France

²Université de perpignan via domitia – Gael PLANTARD – France

³laboratoire PROMES – Université de Perignan Via Domitia – France

⁴Université Ibn Tofail – Maroc

Résumé

Heterogeneous photocatalysis is one of the advanced oxidation processes for treating a wide range of pollutants in water (1). Driven by the advancement of technologies based on the use of the solar resource, this technique has gained ground in recent years and has proven to be very effective in removing toxic compounds from water in an economical and clean way, as it uses a renewable energy source and semiconductor materials with limited cost (2). These technologies are based on the production of highly reactive oxidizing species such as the hydroxyl radical, to degrade recalcitrant organic pollutants. It consists of using a photocatalyst under UV irradiation to oxidize the pollutants present in the water. This work is part of the development of innovative supported materials. Photocatalytic materials dedicated to a solar application must meet the constraint of radiation management for the production of radicals. It is essential that the catalyst is homogeneously distributed in order to capture the radiation in the volume of the photoreactor which is the site of photo-oxidation. In the literature, macroporous supports, such as metal foams, are a prime candidate (3). They develop a macroporosity allowing the distribution of radiation in the volume, their photocatalytic performance is close to that of nanometric powders, which are the reference in this field, but which require a separation step (4). To overcome the high cost of producing metallic foams, it is proposed to design geopolymer foams based on the development technology developed in civil engineering. In a first step, the method of elaboration of the geopolymeric material classically used in the literature will be presented (5). To confer porosity to the material, hydrogen peroxide is added during the polycondensation in order to generate bubbles. Thus, fly ash and metakaolin, the basic constituents of a geopolymer, are mixed, then an alkaline solution based on NaOH and Na₂SiO₃ is added to activate the polycondensation process (6). The porosity is generated by the production of O₂ from the decomposition reaction of hydrogen peroxide which was chosen as the foaming agent. The volume expansion of the foam is monitored during its formation over time. The difficulty lies in the fact that the growth of gas bubbles can become limiting if the polycondensation rate of the geopolymer is faster than the decomposition rate of H₂O₂. The amount of hydrogen peroxide and the operating conditions allowed to modulate the porosity of the material. The foam was then dried (40°C, 24h) and calcined (800°C, 2 h) to obtain a mechanically resistant material. The structural properties of the material will be studied (composition, crystallinity, morphology) using scanning and X-ray microscopy techniques. Tensile tests will be used to define the mechanical characteristics (Young's modulus). The pore size distribution of the foams was

*Intervenant

determined by image analysis of digital micrographs using image analysis software (Image J). The pore size of the geopolymeric foams ranged from 0.01 to 3.5 mm. Several parameters such as H₂O₂ concentration, surfactant nature, viscosity will be optimized in order to confer macroporosity and to define the experimental conditions allowing to control the material characteristics.

Session
Stockage du CO₂

Rayleigh-Taylor convection in a granular porous medium: An experimental study

Shabina Ashraf^{a??}, Jayabrata Dhar^{a??}, François Nadal^{b??}, Patrice Meunier^{c??}, Yves Méheust^{a1}

^aUniversity of Rennes, CNRS, Géosciences Rennes (UMR 6118), 35042 Rennes, France

^bCEA, Bordeaux

^cIRPHE, Aix-Marseille University, CNRS, Centrale Marseille, Marseille, France

Keywords: Rayleigh-Taylor convection, CO₂ storage, optical measurement

A large fraction of greenhouse gases (about 60%) released into the atmosphere are due to CO₂ emissions from industrial processes and the burning of fossil fuels [1]. One of the strategies employed to reduce the emissions is trapping them securely in the subsurface [2, 3, 4]. Dissolution trapping, in particular, involves injecting the CO₂ into a deep aquifer where the supercritical CO₂ (sCO₂) partially dissolves in the aquifer brine beneath it, forming a CO₂ enriched layer within the aqueous phase. The density contrast between the CO₂-enriched brine at the top of the liquid domain and the ambient aquifer brine below results in natural convection of CO₂ [2, 3, 4]. This makes the ambient brine come up, thereby accelerating further dissolution of the sCO₂ into the fresh brine.

The study of Brouzet et al. shows that traditional continuum scale, Darcy law-governed, models underestimate the timescales of this convective dissolution's dynamics, owing to pore scale coupling between convective flow and dissolved CO₂ transport [5]. We present here a 2D experimental study using miscible analog fluids with a contrast in densities to understand the convective transport of the dissolved sCO₂. The fluids and the granular medium are refractive index matched, which renders the medium transparent and allows measuring the pore scale concentration field at various Rayleigh (Ra) and Darcy numbers (Da). This is done by changing the density of the fluids and the size of the solid grain. Darcy scale simulations, run with the same continuum scale parameters as the experiments, are compared to the experimental dynamics. They underpredict the experimental findings by several orders of magnitude, which is consistent with the findings of Brouzet et al. This holds true even when the number $Ra\sqrt{Da}$, which quantifies the size of the most unstable wavelength with respect to the inverse of the typical pore size, is much smaller than 1, i.e., when obvious causes for the failure of the continuum scale description can be excluded.

References

- [1] International panel on climate change (IPCC), Tech. Rep., IPPCC Secretariat, Geneva, Switzerland (2014).
- [2] G. Pau, J. Bell, K. Pruess, A. Almgren, M. Lijewski, and K. Zhang, *Adv. Water Res.* **33**, 443 (2010).
- [3] H. Emami-Meybodi, H. Hassanzadeha, C. Green, and J. Ennis-King, *Int. J. Greenhouse Gas Control* **40**, 238 (2015).
- [4] P. Meunier and F. Nadal, *J. Fluid Mech.* **855**, 1 (2018).
- [5] C. Brouzet, Y. Méheust, and P. Meunier, *Phys. Rev. Fluids* **7**, 033802 (2022).

Wettability alteration of microfluidic devices using plasma and its influence on trapping mechanisms in geological reservoirs

Viktor Gredičák^{*1,2,3}, Claire Douat³, Aneta Slodczyk^{1,2}, Lionel Mercury¹, and Sophie Roman¹

¹ISTO – UMR 7327, Univ. Orléans, CNRS, BRGM, F-45071, Orléans, France – France

²CEMHTI – CNRS UPR 3079, Université d’Orléans, Orléans Cedex 2, France – France

³GREMI – UMR 7344, CNRS, Univ. Orléans, Orléans Cedex 2, France – France

Abstract

Geological storage of carbon dioxide (CO₂) in saline aquifers is one of the prominent approaches within the carbon capture utilization and storage (CCUS) framework. CO₂ storage in geological reservoirs is a multi-fluid flow problem where properties of the rock matrix, the fluids, and the injection define the efficiency of the storage. Wettability, as an influential parameter, seems to be left out from macro-scale models of CO₂ trapping mechanisms. In order to assess the impact of porous media wettability on capillary and solubility trapping, we decided to approach the topic by downscaling to pore scale (order of micrometers to nanometers). Therefore, an experimental approach using microfluidics, plasma jet and Raman spectroscopy has been deployed. We designed microfluidic chips to mimic simple porous rock structures and enable direct visualization and tracking of the physical trapping and solubilization process. Properties of plasma are utilized to change the wettability of micromodels by injecting plasma jet inside the microchannels. On top of that, we utilized the μ -Raman setup to track the evolution of CO₂ dissolution in water during microfluidic experiments. Overcoming technical challenges, we discovered the positive impact of plasma on the hydrophilic properties of microchannels, however, the wettability aging of micromodels still portrays a challenge. Increased hydrophilicity of micromodel surfaces after plasma treatment acts favorably on the dissolution of CO₂ in water due to the increased interfacial area, however, negatively affects physical trapping of CO₂ bubbles. Preliminary Raman spectrometry results indicate possible analysis of dissolved CO₂ even at close to atmospheric pressure despite the large fluorescence coming from the micromodel material (borosilicate glass). More work is needed for quantitative analysis of the CO₂ signal, however, it has been confirmed that gaseous CO₂ signal intensity (Fermi diad) scales with increasing pressure.

*Speaker

Capillary trapping mechanisms for CO₂ geological storage : experimental and computational microfluidic

Nathan Bernard^{*1}, Cyprien Soullain¹, and Sophie Roman¹

¹Institut des Sciences de la Terre d'Orléans - UMR7327 – Bureau de Recherches Géologiques et Minières (BRGM), Observatoire des Sciences de l'Univers en région Centre, Institut National des Sciences de l'Univers, Université d'Orléans, Centre National de la Recherche Scientifique – France

Résumé

Keywords: Carbon capture and storage, porous media, two-phase flow, microfluidics, pore-doublet

1.Introduction

Carbon Capture and Storage, or CCS, is one of the solution proposed by the Paris agreement to keep the global warming under the 2°C threshold. This technique relies on 4 main mechanisms to trap the CO₂ underground : the structural trapping, the solubility trapping, the mineralization and last but not least the capillary or residual trapping, where the CO₂ is trapped by the capillary forces in the rock matrix of a reservoir. But before implementing this technology at the industrial scale, we need to correctly asses the amount of CO₂ that can be trapped in the targeted geological formations. In this work, we study the residual trapping, which relies on complex interactions between the two fluids (brine and supercritical CO₂) and the porous media. To tackle this task, we need to study the phenomenon at the pore-scale (order of micrometers). This is done by reproducing the two-phase flows at the pore scale, using both microfluidics devices and numerical models. This allows us to study the wetting layers forming in porous media during drainage and the impact they may have on the flow.

2.Method

Microfluidics devices, also called micromodels or aquifer-on-chips, are designed to mimic the porous media and to allow for the direct observation of the fluid flow and interfacial dynamics thanks to their transparent nature. In this work, particular interest is given to pore-doublets, whose geometry is composed of two parallel channels linked together at the inlet and the outlet. These pore-doublet are widely used to study two-phase flow in porous media (1) . Their particular structure allow us to experimentally reproduce the complex phenomenons occuring during flow (snap-off, Haine's jump) (2) , while keeping a geometry simple enough to describe the flow using analytical equations. We couple the experimental approach with numerical models derived from the Stoke's equations.

^{*}Intervenant

3.Results

The methodology developed allows us to experimentally demonstrate theoretical results describing an instability occurring during the drainage of a symmetrical pore doublet (3) . We also present a new way to take into account the wetting layers forming in porous media during a drainage, and their impact on the interfacial dynamics during two phase flows. Our study shows that neglecting these effects, as most studies do, can lead to significant errors in the models.

JEMP 2023 – IFPEN, Rueil-Malmaison, France –17-19 October 2023References

(1)Mahdi Mansouri-Boroujeni, Cyprien Soulaïne, Mohamed Azaroula, Sophie Roman, How interfacial dynamics controls drainage pore-invasion patterns in porous media, *Advances in Water*

Ressources, 171, (2023).

(2)Sophie Roman, Moataz O. Abu-al-Saud, Tetsu Tokunaga, Jiamin Wan, Anthony R. Kovescek, Hamdi

A. Tchepi, Measurements and simulation of liquid films during drainage displacements and snap-

off in constricted capillary tubes, *Journal of Colloid and Interface Science*, 507, (2017)

(3)Talal T. Al-Housseiny, Jesus Hernandez, and Howard A. Stone , Preferential flow penetration in a

network of identical channels, *Physics of Fluids*, 26, (2014).

Microwave Treatment of Shales for Carbon Capture and Enhanced Oil Recovery

Anuka Agnes*¹, Sean Rigby*¹, David Large*¹, and Mohamed Adam*¹

¹University of Nottingham – Royaume-Uni

Résumé

Global trends keep indicating the need to mitigate the effect of CO₂ emissions through carbon storage and, thence, reservoir cap rocks with good sealing efficiency are vital. Microwaves are often used to enhance hydrocarbon recovery before carbon sequestration so their impact on reservoir permeability and seal efficiency needs to be studied. This study aims to determine the effect of microwave treatment on the Sleipner seal-rock, Nordland shale, thereby assessing whether it is still an appropriate sealing rock for carbon storage, and gas accumulation, after microwave treatment. Gas adsorption was used to characterise the pore structure of shales, while scanning electron microscopy and X-ray diffraction methods were used to determine the mineralogy of shale samples before and after microwave treatments. The fractal dimensions of the rock were determined from the nitrogen adsorption isotherms. The specific surface areas were also determined using the Langmuir and BET models. After microwave treatments, the quantity of gas adsorbed increased with increasing pressure thereby indicating the presence of larger pores, while the values of fractal dimensions, over all length-scales probed, were seen to increase following microwave treatments indicating increased rock heterogeneity. Gas uptake experiments also showed the impact of the evolved pore structure on transport properties, while SEM, and XRD analysis showed the impact of mineralogical changes on the pore structure of the Nordland Shales. High values of specific surface areas were observed after microwave treatments. Increasing heterogeneity of shale samples, as indicated by an increase in fractal dimensions after microwave treatments, is found significant for the changes to fluid migration rates following microwave treatment. A corresponding increase in porosity of shales is also important for oil and gas accumulation and subsequently an increased oil and gas recovery. This study therefore shows that microwave treatment of shales is useful for both carbon storage and enhanced oil recovery.

*Intervenant

CO₂ Hydrate Kinetics for CO₂ Storage in Depleted Gas Reservoirs through Microfluidic Experiments

P. Dehghani^{a,b}, A. Sinquin^a, N. Gland^a, A. Minh Tang^b

^aIFP Energies nouvelles, 1-4 Avenue de Bois-Préau, 92852 Rueil-Malmaison, France.

^bNavier, Ecole des Ponts, Université Gustave Eiffel, CNRS, Marne-la-Vallée, France.

Keywords: CO₂ Storage, Depleted reservoir, CO₂ hydrate, Nucleation, kinetics, Microfluidic, Salinity effect.

1 Introduction

Carbon dioxide (CO₂) storage in depleted oil and gas reservoirs offers a promising approach for addressing greenhouse gas emissions and mitigating climate change. Depleted oil and gas reservoirs, along with deep saline aquifers and coal seams, can be used for CO₂ storage. These structures possess distinct properties and demand diverse injection strategies to ensure efficient CO₂ storage. [1-3]. The success of geological storage of carbon dioxide (CO₂) in depleted reservoirs depends on various factors, including the efficiency of CO₂ injection, particularly in the near-wellbore region where flow rates are high. In this area, static effects, and dynamic effects such as Joule-Thomson can lead to the formation of CO₂ hydrates (Fig.1a) [4, 5]. Hydrate formation can significantly reduce injectivity and impair well operations on-site (Fig.1b).

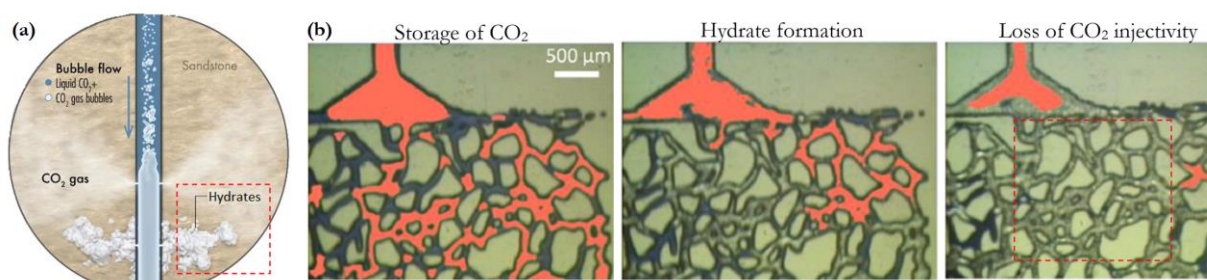


Figure 1.(a) CO₂ storage in depleted reservoirs [6] (b) Hydrate formation leading to loss of injectivity at the pore scale [7].

A IFPEN microfluidic platform called High Pressure Low Temperature (HPLT) was used to investigate the formation of CO₂ hydrates (liquid/gas) under pressure and temperature conditions relevant to the near-wellbore region during CO₂ storage in depleted reservoirs (Fig.2a). CO₂ liquid droplets and gas bubbles in a continuous water phase were generated successfully using a “Y-junction” microfluidic chip. These micron droplets and bubbles were then stored in a serpentine channel under pressure, with each isolated droplet serving as a separate reactor. The temperature was precisely controlled using a Peltier module set to low temperature to induce hydrate nucleation (Fig.2b, Fig.2c).

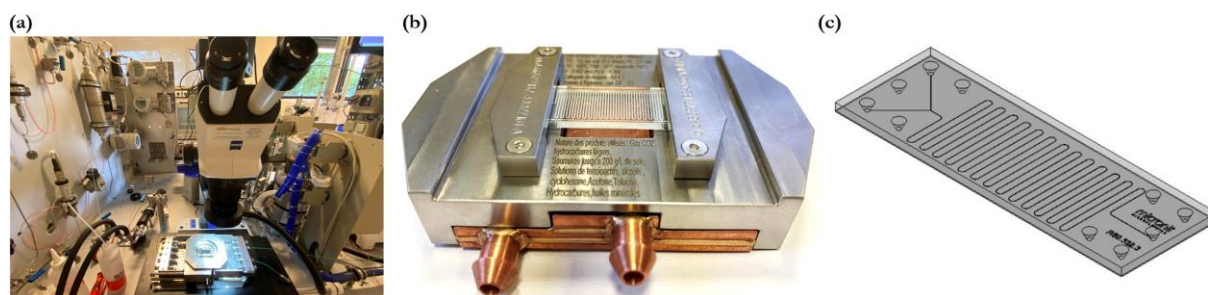


Figure 2. (a) IFPEN microfluidic platform/High Pressure Low Temperature (HPLT) (b) IFPEN holder and temperature control system (c) Micronit© “Y-junction” microfluidic chip.

Figure 3b depicts the progression of crystallization in one pure water droplet in Cyclopentane as part of our preliminary work [8]. In Figures 3b the onset of crystallization is localized with an arrow. The nucleation

and growth processes of CO₂ hydrates can be determined similarly to previous studies by monitoring the onset of crystallization over time and temperature/pressure (Fig. 3a). CO₂ hydrate onset will be detected at various NaCl concentrations and on a much broader range of subcooling [9, 10].

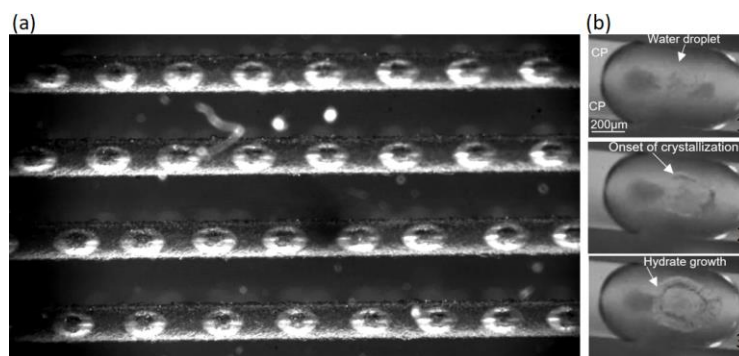


Figure 3. (a) Serpentine canals: overview of immobile CO₂ liquid droplets in water (b-1) Serpentine tube: water droplet in Cyclopentane (b-2) Onset of Cyclopentane hydrate crystallization (b-3) Cyclopentane hydrate growth.

Overall, this microfluidic experimental approach allows for a detailed investigation of CO₂ hydrate formation in similar conditions to those found in the near-wellbore region during CO₂ storage in depleted reservoirs. The insights gained from this study can contribute to a better understanding of the risks associated with CO₂ hydrate formation, help to introduce a more realistic hydrates crystallization kinetics in the reservoir models and develop strategies for improved CO₂ injection and storage in geological formations.

References

- [1] Withey P, Johnston C, Guo J, *Quantifying the global warming potential of carbon dioxide emissions from bioenergy with carbon capture and storage*. *Renew. Sustain. Energy*, 115, 109408 (2019).
- [2] Nikoosokhan S, Brochard L, Vandamme M, Dangla P, Pellenq R.J.-M, Lecampion B, Fen-Chong T, *CO₂ Storage in Coal Seams: Coupling Surface Adsorption and Strain*. *Geomech. CO2 Storage Facil*, 115–132 (2013).
- [3] IPCC. *Special report on carbon dioxide capture and storage*. New York: Cambridge University Press, ISBN:92-9169-1190-4 (2005).
- [4] Oldenburg CM, *Joule-Thomson cooling due to CO₂ injection into natural gas reservoirs*. *Energy Conversion and Management* 48(6): 1808–1815. doi: 10.1016/j.enconman.01.010 (2007).
- [5] Gao M, Wang L, Chen X et al., *Joule-Thomson Effect on a CCS-Relevant (CO₂ + N₂) System*. *ACS omega* 6(14): 9857–9867. doi: 10.1021/acsomega.1c00554 (2021).
- [6] Haratian A, *A comprehensive review on Carbon capture storage in geological structures and emerging technologies*, 7th International Conference on Applied Research in Science & Engineering (2023).
- [7] Gautepluss J, Almenningen S, Erslund G, *Multiscale investigation of CO₂ hydrate self-sealing potential for carbon geo-sequestration*, *Chemical Engineering Journal* Volume 381, 122646 (2020).
- [8] Dehghani P, Siquin A, Gland N, Tang A.M, Audrey E, *Investigating cyclopentane hydrates nucleation and growth using microfluidics*, *Science and Technology for Energy Transition* (Paper accepted in 2023).
- [9] Le Goff T.H, Lagarde F, Bousqué M, Santanach-Carreras E, *A Microfluidic Experimental Approach to Assess CO₂ Hydrate Risk for CO₂ Storage into Depleted Gas Reservoirs*, *GHGT-16* (2022).
- [10] Siquin A, Betro B, Wender A, Defiolle D, Karimi K, Gland N, Estublier A, Le Goff T.H, Lagarde F, Pauget L, *CO₂ Hydrate Stability Zone: Effect of Salinity, Measurements and Models*, *GHGT-16* (2022).

Microwave Assisted CO₂ Desorption from Solvent Flowing into Hollow Fiber Membrane

A. HAJJ^{1,3}, E. SAVARY³, T. HAUVILLER², S. CURET², P. PRÉ¹

1 : IMT Atlantique, GEPEA, UMR CNRS 6144, 44307 Nantes, France

2 : Oniris, Nantes Université, CNRS, GEPEA, UMR 6144, F-44000 Nantes, France

3 : SAIREM, 82, rue Elisée Reclus, 69150 Decines Charpien, France

e-mail : ali.hajj2@imt-atlantique.fr

Keywords: EM modelling, separation process, Amine scrubbing, CO₂ capture, Gas absorption, Microwave regeneration, process intensification.

A Promising Alternative for Carbon Capture

Chemical absorption is considered as one of the most mature technologies for carbon capture from flue gases, it is composed of the absorption stage where CO₂ is dissolved chemically into the solvent and the desorption stage where the latter is regenerated at high temperatures. Despite its technological maturity it suffers from several drawbacks most noticeably the large equipment footprint and the high operating cost of the desorption stage. This is presented by the intensive steam consumption that provides heat for the desorption reaction of CO₂ and acts as a sweeping gas. Lately, application of microwave technology (MW) to chemical absorption has been receiving increasing attention owing to increased operational flexibility, small footprint, and most notably its intensification potential [2], [3]. Successful scale-up of the process depends on the choice of the gas-liquid contactor. Hollow fiber membrane modules can be used in MW assisted CO₂ desorption due to their inertness to MW irradiation. In addition, they provide a further potential for process intensification thanks to their high surface area in comparison to packed columns[4], [5]. This original research aims at studying the potential of MW technology for improving the chemical desorption of CO₂ from aqueous ethanolamine solution, while using hollow fiber membrane modules as a gas-liquid contactor.

MW-Assisted Solvent Regeneration: Experimental Investigation at the Scale of a Single Fiber

The MW assisted regeneration of the solvent was first studied at the single fiber scale, this was done to examine the effect of the local temperature/concentration gradients and hydrodynamic conditions on the CO₂ desorption flux at steady state. To this end, a single hollow fiber (PTFE), was placed in a microwave cavity, in a concentric manner relative to a quartz tube as shown in Figure 1. A CO₂-rich solvent and an N₂ stream were circulated through the fiber lumen and the annular area between the fiber and quartz tube respectively. Incident MW irradiation bypasses the inert membrane material and are dissipated in the solvent, this increases the latter's temperature and reverses the absorption reaction to release gaseous CO₂. The released CO₂ diffuses through the unwetted gas-filled pores of the membrane only to be swept by an N₂ flow on the annular side similar to a "sweeping gas membrane distillation" mode. Experimental campaigns focused on characterizing the response of the system with respect to:

1. Solvent flow rate: set to similar hydrodynamic conditions as in a membrane module unit
2. Solvent CO₂ loading: varied over the range of operating conditions of a classical stripping column
3. MW power: controlled to achieve different average outlet liquid temperatures
4. Sweeping gas flow rate

Results show the increase of the desorption flux with respect to all tested parameters.

MW-Assisted Solvent Regeneration: Numerical Modeling at the Scale of a Single Fiber

Considering the multitude of the involved coupled physical phenomena, a progressive step-by-step approach was applied in accounting for all physical phenomena. COMSOL® Multiphysics 6.0 software was used to solve the Maxwell's equations to obtain E-field maps throughout the MW cavity and solvent. Afterwards, heat transfer and Naviers-Stokes equations were coupled with Maxwell's equations and solved over the fiber domain to generate spatial temperature maps in the solvent. Numerical results show that strong radial temperature gradients exist in the solvent, most notably at the stagnant film region near solvent-fiber boundary, this is contrary to the liquid bulk where the temperature is somewhat homogenous (figure 2). In parallel, a 1D mass-transfer model for reversible isothermal absorption of gases in reactive liquids proposed by Weiland[6] was coded using MATLAB® using finite different method. Mass-transfer is modeled using the film theory [7] by considering liquid film with membrane thickness, while

neglecting gas side resistance. The transfer mechanism in the membrane was described by combined molecular/Knudsen diffusion. The desorption reaction was accounted for through an enhancement factor assuming an instantaneous reaction regime [8]. The temperature map latterly obtained was transformed into two longitudinal 1D T-profiles, representative of the liquid bulk and film regions respectively. Incorporating the obtained T-profile pair into the 1D transfer model permits the desorption to be simulated at non-isothermal conditions. Simulation results show that local desorption flux J increases as a function of the temperature along the fiber length (figure 3). The average flux showed considerable deviation existed with the experimental results, but perfect agreement was achieved through application of partial wetting condition on the membrane where the wetted fraction was varied to minimize the gap with experimental data.

Conclusion and Perspectives

The MW assisted CO_2 desorption was investigated experimentally on the scale of a single hollow fiber to validate a model simulating desorption rates function of different operating parameters. Future challenges will focus on upscaling the modeling approach from the scale of a single fiber to that of a membrane module containing a bundle of fibers in a non-uniform E-field, or even different desorption configurations such vacuum decompression stripping.

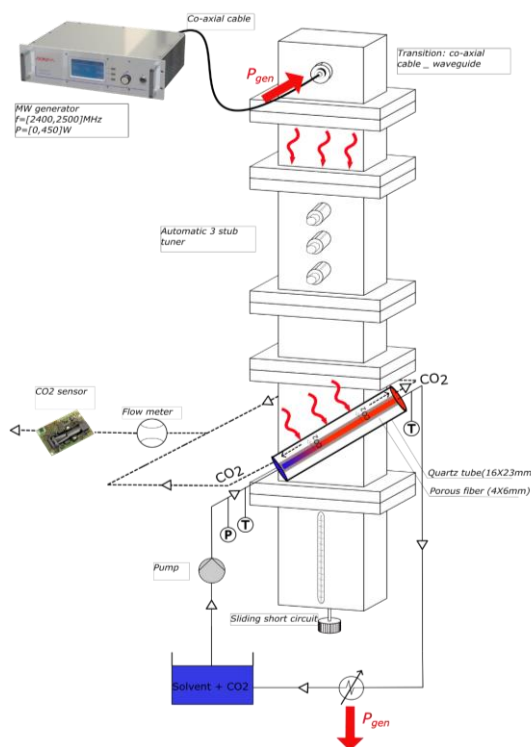


Figure 1: MW assisted regeneration of CO_2 rich solvents at the scale of a single hollow fiber.

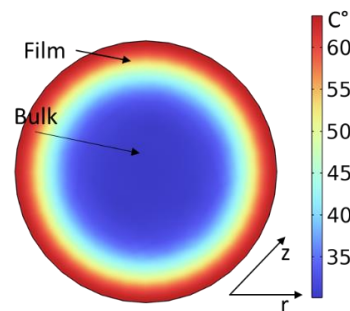


Figure 2: Radial temperature map of solvent under MW irradiation

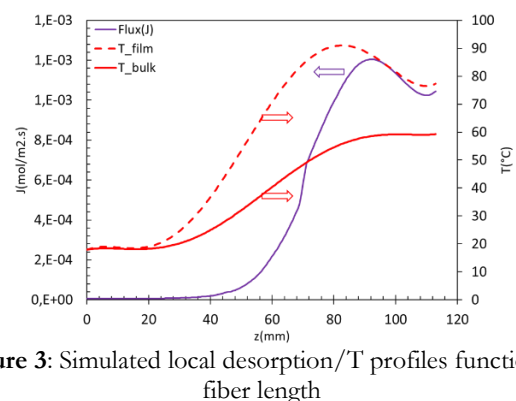


Figure 3: Simulated local desorption/T profiles function of fiber length

References:

- [1] S. Ziaii, G. T. Rochelle, and T. F. Edgar, "Dynamic Modeling to Minimize Energy Use for CO_2 Capture in Power Plants by Aqueous Monoethanolamine," *Ind. Eng. Chem. Res.*, vol. 48, no. 13, pp. 6105–6111, Jul. 2009, doi: 10.1021/ie801385q.
- [2] Z. Ji, J. Wang, D. Hou, Z. Yin, and Z. Luan, "Effect of microwave irradiation on vacuum membrane distillation," *J. Membr. Sci.*, vol. 429, pp. 473–479, Feb. 2013, doi: 10.1016/j.memsci.2012.11.041.
- [3] F. Bougie and X. Fan, "Analysis of the Regeneration of Monoethanolamine Aqueous Solutions by Microwave Irradiation," *Energy Procedia*, vol. 142, pp. 3661–3666, Dec. 2017, doi: 10.1016/j.egypro.2017.12.259.
- [4] H. Kreulen, C. A. Smolders, G. F. Versteeg, and W. P. M. van Swaaij, "Microporous hollow fibre membrane modules as gas-liquid contactors. Part 1. Physical mass transfer processes," *J. Membr. Sci.*, vol. 78, no. 3, pp. 197–216, Apr. 1993, doi: 10.1016/0376-7388(93)80001-E.
- [5] N. Nishikawa *et al.*, " CO_2 removal by hollow-fiber gas-liquid contactor," *Energy Convers. Manag.*, vol. 36, no. 6–9, pp. 415–418, Jun. 1995, doi: 10.1016/0196-8904(95)00033-A.
- [6] R. H. Weiland, M. Rawal, and R. G. Rice, "Stripping of carbon dioxide from monoethanolamine solutions in a packed column," *AIChE J.*, vol. 28, no. 6, pp. 963–973, Nov. 1982, doi: 10.1002/aic.690280611.
- [7] W. G. Whitman, "The two film theory of gas absorption," *Int. J. Heat Mass Transf.*, vol. 5, no. 5, pp. 429–433, May 1962, doi: 10.1016/0017-9310(62)90032-7.
- [8] G. Astarita and D. W. Savage, "Gas absorption and desorption with reversible instantaneous chemical reaction," *Chem. Eng. Sci.*, vol. 35, no. 8, pp. 1755–1764, 1980, doi: 10.1016/0009-2509(80)85011-1